UQAC
Université du Québec
à Chicoutimi

Origine et migration des eaux souterraines du Bouclier Canadien révélées à partir de la modélisation numérique et des traceurs géochimiques

Par
Othniel Glodie Dominique Ngombe

Thèse présentée à l'Université du Québec à Chicoutimi dans le cadre d'un programme conjoint avec l'Université du Québec à Montréal en vue de l'obtention du grade de philosophiae doctor (Ph. D.) en Sciences de la Terre et de l'Atmosphère

Québec, Canada

RÉSUMÉ

La compréhension des processus hydrogéochimiques qui modifient la qualité de l'eau souterraine est un élément clé pour évaluer et protéger cette ressource face aux problèmes de salinisation. Ces processus sont contrôlés par le parcours et le temps de résidence des eaux souterraines. Dès leur infiltration dans l'aquifère, les eaux souterraines sont en constante évolution de leur chimie à travers le temps, tendant, dans certains cas, naturellement vers des pôles salins. Cette évolution naturelle peut conduire à la formation de saumures continentales, lesquelles sont généralement rencontrées à de grandes profondeurs (> 500 m). L'état saumuré peut être défini comme le stade final d'évolution des processus de salinisation continentale. L'origine et la mobilité des saumures continentales, essentielles à la gestion et la protection des aquifères, demeurent controversées en raison de leur long temps de résidence en milieu profond, qui favorise la superposition de processus hydrogéochimiques et conduit à des interprétations parfois contradictoires.

Dans la région du Saguenay-Lac-Saint-Jean, plusieurs études suggèrent la présence d'un membre dilué de saumures continentales profondes et des vestiges d'une eau de mer ancienne à moins de 100 m de profondeur. L'origine de cette salinité et les conditions hydrodynamiques de la migration des saumures profondes constituent un enjeu majeur pour la ressource en eau souterraine. Dans ce contexte, il est essentiel de préciser l'origine de ces eaux anciennes, de comprendre leur évolution à travers le temps, de caractériser les processus de mélange entre les eaux souterraines anciennes et récentes, et d'évaluer leur participation au cycle de l'eau. Ainsi, ce projet doctoral a visé à approfondir la compréhension des processus de salinisation continentale en tenant compte des contextes géologiques, de l'histoire hydrogéologique, et du rôle des fluides profonds dans la salinisation des aquifères de subsurface.

En premier lieu, une approche combinée d'analyses isotopiques et de modélisation numérique 2D d'écoulement et du transport advectif-dispersif de l'âge a été développée afin d'explorer les conditions hydrodynamiques expliquant la présence à de faibles profondeurs d'eaux anciennes et d'origines profondes. Les résultats indiquent un mélange d'eaux météoriques et de saumures profondes Précambriennes du Bouclier Canadien, pouvant, sous les conditions aux limites imposées au modèle, remonter vers la surface grâce au fort gradient topographique régional (hautes-terres vs basses-terres). L'âge simulé des eaux souterraines profondes, d'une centaine de millions d'années, cohérent avec les interprétations isotopiques, est similaire à celles des saumures identifiées à de grandes profondeurs ailleurs dans le Bouclier Canadien. Les résultats numériques démontrent également que les failles du graben agissent comme voies préférentielles, favorisant la circulation ascendante de ces eaux très anciennes. En second lieu, à l'aide de la base de données mondiale de 308 échantillons de saumures continentales profondes, cette étude a permis de comparer l'évolution des saumures trouvées dans des roches sédimentaires et l'évolution des saumures trouvées dans des roches cristallines. Les résultats montrent que les deux types de saumures continentales convergent vers un membre Ca-Cl enrichi en Br^- et Sr^{2+}. En troisième lieu, la compréhension de l'évolution hydraulique et géochimique des saumures continentales associée à une approche multi-traceurs a permis d'identifier les pôles compositionnels régionaux et de proposer un modèle conceptuel hydrogéologique régional. Les résultats révèlent trois sources principales de salinité peu profonde : une eau marine Holocène, une saumure marine Paléozoïque et une saumure Précambrienne du Bouclier Canadien (> 100 Ma) contenant 1-5% d'hélium mantellique provenant du manteau lithosphérique sub-continental. La présence d'eaux glaciaires Wisconsiniennes (entre 8.2 et 25.5 Ka BP) et de saumures profondes (entre 7.5 et 12.5 km) circulant via les failles du graben est également confirmée par cette approche multi-traceurs. Les signatures isotopiques montrent que ces fluides ont été significativement modifiés par des processus de cryo-concentration durant la dernière glaciation, soulignant l'influence d'événements paléohydrogéologiques sur le système hydrogéologique actuel. Ce projet doctoral a aussi permis de déterminer un ensemble de marqueurs géochimiques (Li/Br, B/Br et Rb/Sr) discriminant les saumures sédimentaires des saumures cristallines.

Ce projet doctoral met en évidence le rôle des eaux anciennes, des événements paléohydrogéologiques et des failles profondes dans la salinisation continentale des eaux souterraines contenues dans les aquifères régionaux, et fourni un premier aperçu des mécanismes hydrodynamiques profonds en contexte de graben. Ces résultats constituent une base utile pour mieux comprendre les dynamiques hydrogéologiques locales et éclairer les réflexions sur la gestion durable de la ressource en eau, en identifiant un ensemble de traceurs géochimiques, et les zones les plus vulnérables à la salinisation des nappes d'eau fraiche superficielle.

TABLE DE MATIÈRES

LISTE DES FIGURES

LISTE DES TABLEAUX

LISTE DES ABRÉVIATIONS

- TSD : Total des solides dissous
- IME : Indice de maturation de l'eau
- Shieldbrine : Saumures caractéristiques des socles cristallins
- Sedbrine : Saumures caractéristiques des bassins sédimentaires
- LMW : Eau météoritique local
- RW : Eau de recharge
- HMW : Eau marine datant de l’Holocène
- WGM : Eau de fonte glaciaire datant du Wisconsinien
- PMB : Saumures Marine Paléozoïque
- PSB : Saumures du Bouclier Précambrien
- SW : Eau de mer
- LSJAS : Suite anorthositique du Lac Saint-Jean
- SLSJ : Saguenay-Lac-Saint-Jean

DÉDICACE

À toi papa, mon modèle et ma source de motivation. Je ne porte pas que ton prénom et nom, monsieur Dominique Ngombe, mais également toutes les valeurs que tu incarnais, le travail, la résilience, la patience, la détermination, le courage, le goût de l'effort. Certes tu n'es plus là physiquement pour voir le résultat de ton œuvre, mais tes paroles, tes valeurs et ton travail continuent de vivre au travers tes enfants. De là où tu es, je te dédie ce travail, mon très cher papa.

À toi maman, celle qui a toujours cru en moi. Tu n'as jamais cessé de me porter dans tes prières. Je ne pense pas que j'y serais arrivé sans ton soutien et tes encouragements sans failles. Tu as fortement contribué à ma stabilité émotionnelle et intellectuelle, grâce à toi j'ai toujours su garder les pieds sur terre. Cet accomplissement est aussi le tien.

REMERCIEMENTS

Au moment d'écrire ces lignes, je mesure l'ampleur du chemin parcouru. Tout a commencé lors d'une rencontre Zoom. Depuis ce premier échange jusqu'à l'achèvement de ce manuscrit, j'ai vécu une aventure incroyable, rythmée par des pleurs, des fous rires, des échecs, des réussites, du stress, de l'excitation, des moments de grands doutes et de satisfaction du travail accompli.

Je tiens avant tout à remercier le professeur Julien Walter, mon directeur de thèse, pour la confiance accordée, votre patience à chaque étape de mon cheminement et la qualité de nos discussions scientifiques. J'ai énormément appris à vos côtés. Les discussions constructives dans votre bureau, vos nombreux commentaires sur mes travaux, vos encouragements tout au long de ces quatre années, sans oublier ces moments conviviaux, les cinq à sept chez vous, nos parties de tennis, ont contribué de façon significative à l'achèvement de ce projet. Vous avez su me communiquer cette passion pour l'hydrogéochimie.

Merci aux professeurs Romain Chesnaux et John Molson, mes co-directeurs, pour votre confiance et votre patience à mon égard. Professeur Romain, merci pour vos conseils précis. Votre attention portée à l'humain et au bien-être émotionnel m'a profondément touché. Je n'oublierai jamais ces soirées à votre chalet, ou encore ces bleuets et ces champignons collectés, que de bons souvenirs... Professeur John, votre rigueur m'a particulièrement marqué et a été très formatrice pour moi. Merci pour le partage d'expérience en modélisation, pour tout le soutien technique, pour toutes ses rencontres Zoom et toutes les heures passées à travailler sur le modèle numérique avec moi.

J'adresse aussi mes remerciements à plusieurs collègues et enseignants qui ont accompagné différentes étapes de cette aventure. Notamment, le professeur Daniele L. Pinti, professeur à l'UQAM et co-auteur du troisième article de cette thèse, pour ses suggestions concernant l'interprétation des gaz rares et son implication remarquable dans l'amélioration de ce papier ; le professeur Pierre Cousineau (UQAC) pour ses conseils et orientations ; la professeure Sarah Dare (UQAC) pour ses conseils et ressources concernant l'interprétation des isotopes de strontium, ainsi que pour ses encouragements. Je remercie également Laura-Pier Perron Desmeules, professionnelle de recherche, pour sa rigueur, ses conseils et notre collaboration sur le terrain. Ces longues journées partagées sur le terrain avec toi m'ont rappelé l'importance et les implications sociales de la science que nous faisons. Je tiens à exprimer ma reconnaissance à mes amis, les docteurs Adoubi Vincent de Paul Adombi et Daouda Méité, pour leur aide précieuse dès mes premiers moments de doute, leurs explications patientes sur les bases de la modélisation, ainsi que pour leur soutien moral ; ces soirées « atiéké » resteront des moments marquants de cette aventure. Mes collègues de la team hydro, Philip-Alex, Maha, et Alireza, je vous remercie également pour ces discussions, ces partages et ces sorties de terrain.

Je tiens à remercier ma famille, en particulier ma maman Josée, mes sœurs Mignonne, Lydia, Grâce, Dorine et Eunice, ainsi que mon frère Emmanuel, pour le soutien moral, émotionnel et spirituel inestimable que vous m'avez apporté, merci pour tout.

J'adresse également mes remerciements à mes amis Mélina et Yves, pour plus de vingt ans d'amitié et de soutien. Nous avons traversé de nombreuses expériences, tant positives que négatives, et votre présence a été constante. Jonathan et Chris, vous avez toute ma gratitude. Votre soutien a été essentiel tant sur le plan académique que personnel.

Réelle, je ne peux pas terminer ce chapitre sans mettre à l'honneur et remercier l'un de mes plus fervents soutiens. Un énorme merci pour ta patience, ton soutien, pour les moments d'équilibre indispensables et le courage que tu me donnes.

Je ne peux cependant pas citer tout le monde. Que celles et ceux que je n'ai pas cités, celles et ceux qui étaient là au tout début ou à une étape donnée de cette aventure, qui ont contribué, de près ou de loin, à l'aboutissement de cette thèse trouvent ici l'expression de ma profonde gratitude. Je n'y serais pas arrivé sans vous.

Chapitre 1 : INTRODUCTION

1.1. Mise en contexte

Comprendre comment le mélange entre les eaux souterraines anciennes et récentes, et comment l'évolution hydrogéochimique à l'échelle des temps géologiques influencent le renouvellement, la qualité et la disponibilité à long terme des eaux souterraines, demeure un défi majeur. L'interdépendance de ces facteurs (mélange des eaux et évolution géochimique) conduit, dans certains cas, à la salinisation continentale des aquifères, enjeu important au Saguenay-Lac-Saint-Jean. Des études antérieures ont mis en évidence la présence d'eaux salées d'origine naturelle sur l'ensemble de ce territoire, faisant de la région un laboratoire naturel de premier plan pour répondre à la problématique de la salinisation continentale. De plus, cette région bénéficie de plusieurs informations sur les modèles d'évolution hydrogéochimique, et des données hydrogéologiques et hydrogéochimiques, offrant des outils supplémentaires pour l'étude de la salinisation continentale.

La première phase introductive de ce projet doctoral a consisté à définir le cadre conceptuel de l'étude, construit sur une synthèse des théories et modèles issus de la littérature scientifique existante. Tout d'abord, la variabilité hydrogéochimique des eaux souterraines a été mise en évidence (Section 1.2.1). Ensuite, l'accent a été mis sur l'état des connaissances sur les modèles d'évolution de la chimie des eaux souterraines (Section 1.2.2) expliquant entre autres la variabilité hydrogéochimique des eaux souterraines et l'influence des contextes géologiques. Ces deux premières parties ont permis d'émettre des hypothèses quant aux processus à l'origine des saumures continentales (Section 1.2.3) et de poser une problématique générale au projet d'étude (Section 1.3). Certaines de ces hypothèses peuvent expliquer la présence des eaux salées dans la région d'étude (Section 1.4).

1.2. Cadre conceptuel de l'étude

1.2.1. Variabilité hydrogéochimique

La chimie des eaux souterraines varie en fonction de plusieurs facteurs, tels que la géochimie des roches, les événements climatiques passés et présents, la connectivité hydraulique entre

aquifères, la perméabilité et la topographie. Ces facteurs conditionnent la nature, l'intensité et la durée des interactions eau-roche, contrôlant les processus hydrogéochimiques qui expliquent l'essentiel de cette variabilité (Chebotarev, 1955). La variabilité hydrogéochimique s'exprime également à travers le contenu minéral, aussi appelé total des solides dissous (TSD, Tableau 1-1). Le TSD qui représente la concentration totale des substances dissoutes dans l'eau, est couramment utilisé comme indicateur de la salinité et dans certains cas du temps de résidence (Tóth, 1999). Usuellement, la salinité permet de distinguer différents types d'eaux : les eaux douces, saumâtres, salines et les saumures (Tableau 1-1). Les saumures correspondent alors aux eaux ayant un TSD supérieur à 35 g/L et définissent l'état final de l'évolution des eaux souterraines (Kharaka et Dorsey, 2005). La Figure 1-1 présente une classification de 1 800 échantillons d'eau souterraine, provenant de différents endroits à travers le monde, tels que les boucliers Canadien, Fennoscandien, Ukrainien, les socles cristallins de l'Europe (Casanova et al., 2004). Cette étude met en évidence que le chemin d'évolution naturel des eaux souterraines vers les saumures est caractérisé par une eau de recharge dont l'anion dominant est le bicarbonate (HCO_3^-) vers des pôles salins dont l'anion dominant est le chlore (Cl^-). Tel que la salinité et le temps de résidences, les ions chlorures augmentent aussi avec le TSD (Boumaiza et al., 2022b). Cette évolution décrivant la salinisation vers les saumures continentales, est observée dans les socles cristallins et les bassins sédimentaires (Gascoyne et Kamineni, 1994; Yardley et Bodnar, 2014). En effet, ces deux contextes géologiques représentent les deux plus importants réservoirs de saumures continentales au monde.

Tableau 1-1: Regroupement qualitatif des eaux naturelles, modifié de Chebotarev (1955)

Groupe d'eaux naturelles		TSD approximatif (mg/L)
Groupes majeurs	Subdivisions	
Eaux douces	Potable	Moins de 500
	Fraîche	Moins de 700
	Assez fraîche	700 – 1 500
	Passablement fraîche	1 500 – 2 500
Eaux saumâtres	Légèrement saumâtre	2 500 – 3 200
	Saumâtre	3 200 – 4 000
	Assurément saumâtre	4 000 – 5 000
Eaux salées	Légèrement salée	5 000 – 6 500
	Salée	6 500 – 7 000
	Très salée	7 000 – 10 000
	Extrêmement salée	10 000 – 35 000
	Saumure	Plus de 35 000

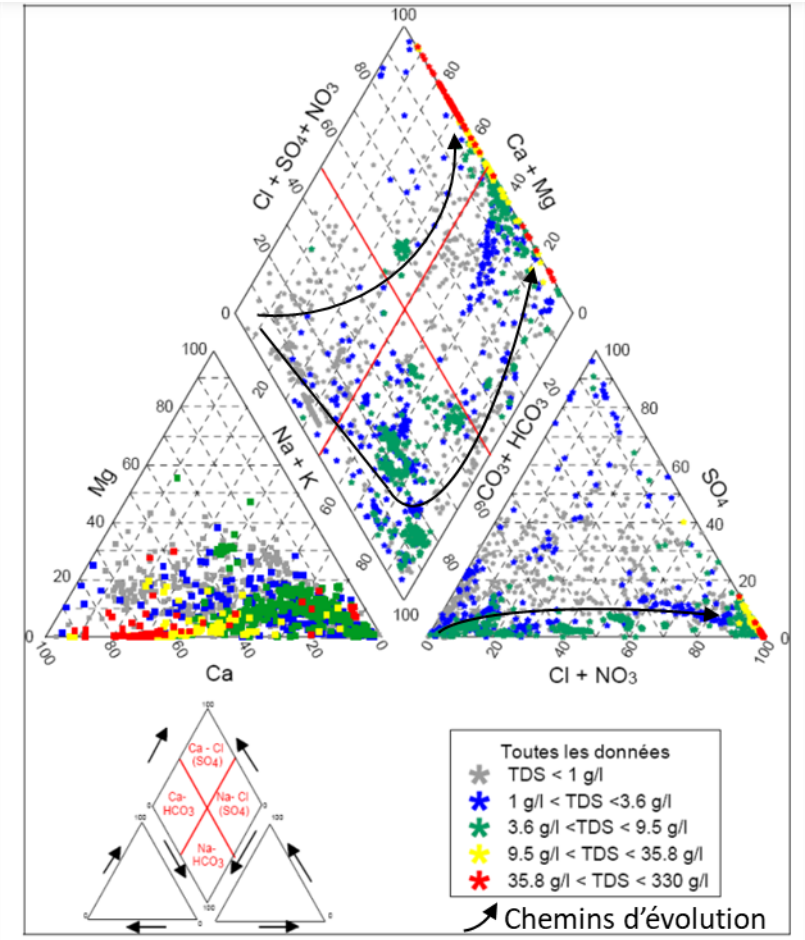

Figure 1-1: Classification de 1800 échantillons d'eau souterraine au sein d'un diagramme de Piper en fonction de leur TSD. Ces eaux proviennent de différents endroits à travers le monde (boucliers Canadien, Fennoscandien, Ukrainien, les socles cristallins de l'Europe). La figure a été modifiée à partir de l'étude de Casanova et al. (2004). Les chemins d'évolution sont tirés de l'étude de Walter et al. (2019).

1.2.2. Évolution des eaux souterraines

Dans ce projet de doctorat, l'évolution de l'eau souterraine est définie comme un processus de vieillissement de l'eau jeune (eau météorique) après son infiltration. Cette évolution se traduit généralement par la salinisation de l'eau souterraine (Tóth, 1999). La sous-section 1.2.2.1 présente les progrès scientifiques concernant la compréhension générale de l'évolution des eaux souterraines et ces concepts de base. Les sous-sections suivantes présentent en détails l'état des connaissances des modèles d'évolution de l'eau souterraine dans des milieux sédimentaires (sous-section 1.2.2.2) et cristallins (sous-section 1.2.2.3).

1.2.2.1. Modèle d'évolution global des eaux souterraines

À l'aide des analyses théoriques des écoulements de l'eau souterraine dans un petit bassin versant, l'étude de Tóth (1963) a permis de mettre en évidence des modèles d'écoulement hiérarchiques, liant ainsi, la dynamique de l'eau souterraine à son évolution chimique. Dans la suite de ses travaux initiaux, Tóth (1999) propose dans un bassin idéalisé un model associant l'évolution de la chimie des eaux (évolution typique des anions majeurs), leur régime hydraulique, ainsi que la taille de la cellule d'écoulement (Figure 1-2). Une cellule d'écoulement définit le temps de résidence de l'eau souterraine. Par conséquent, les cellules d'écoulement peuvent être locales (jours-semaines) de type bicarbonaté, intermédiaires (10^2 - 10^4 années) évoluant vers un pôle sulfaté, et régionales (> 10^5 années) évoluant vers un pôle chloruré. Chaque système d'écoulement, quelle que soit sa disposition (cellule d'écoulement), possède une zone de recharge et une zone de résurgence. D'après ce modèle, l'évolution hydrogéochimique se déroule en même temps à toutes échelles d'espace et de temps. Les travaux de Tóth (1999) suggère également l'existence d'eaux fossiles restées piégées, ne participant donc pas directement au cycle de l'eau mais pouvant constituer des sources de mélanges à l'origine de la dégradation de la qualité des eaux souterraines des cellules d'écoulement d'échelle locale (Figure 1-2).

De nos jours, plusieurs projets de recherche ont étudié l'influence des propriétés hydrogéologiques des formations rocheuses et des structures géologiques et leur impact sur la circulation des fluides souterrains (Achtziger-Zupančič et al., 2017; Janos et al., 2018; Snowdon et al., 2021; Ferguson et al., 2023). Par exemple, McIntosh et Ferguson (2021) ont cartographié les profondeurs de circulation d'eau météorique. Les auteurs ont démontré que l'eau météorique pénètre en profondeur principalement lorsque le rapport entre le dénivelé topographique (différence d'altitude entre le point de recharge et le point de décharge) et la profondeur excède une valeur critique d'environ 0.2. Ce seuil de 0.2 est la valeur théorique requise pour qu'une saumure de densité élevée (environ 1,200 kg/m^3) puisse être lessivée par l'eau météorique, surmontant ainsi le piégeage dû à la flottabilité négative. Snowdon et al. (2021) a montré les différences de perméabilité entre les zones de fractures (< 500 m) et la matrice rocheuse non-fracturé (caractéristique des environnements

profonds). Ces différences exercent une influence directe sur le temps de résidence des eaux souterraines et leur circulation. Ces études présentées ici mettent en évidence que l'évolution de l'eau souterraine n'est pas homogène, mais plutôt un système dynamique, dépendant du substrat rocheux, de sa structuration, et de la topographie du milieu.

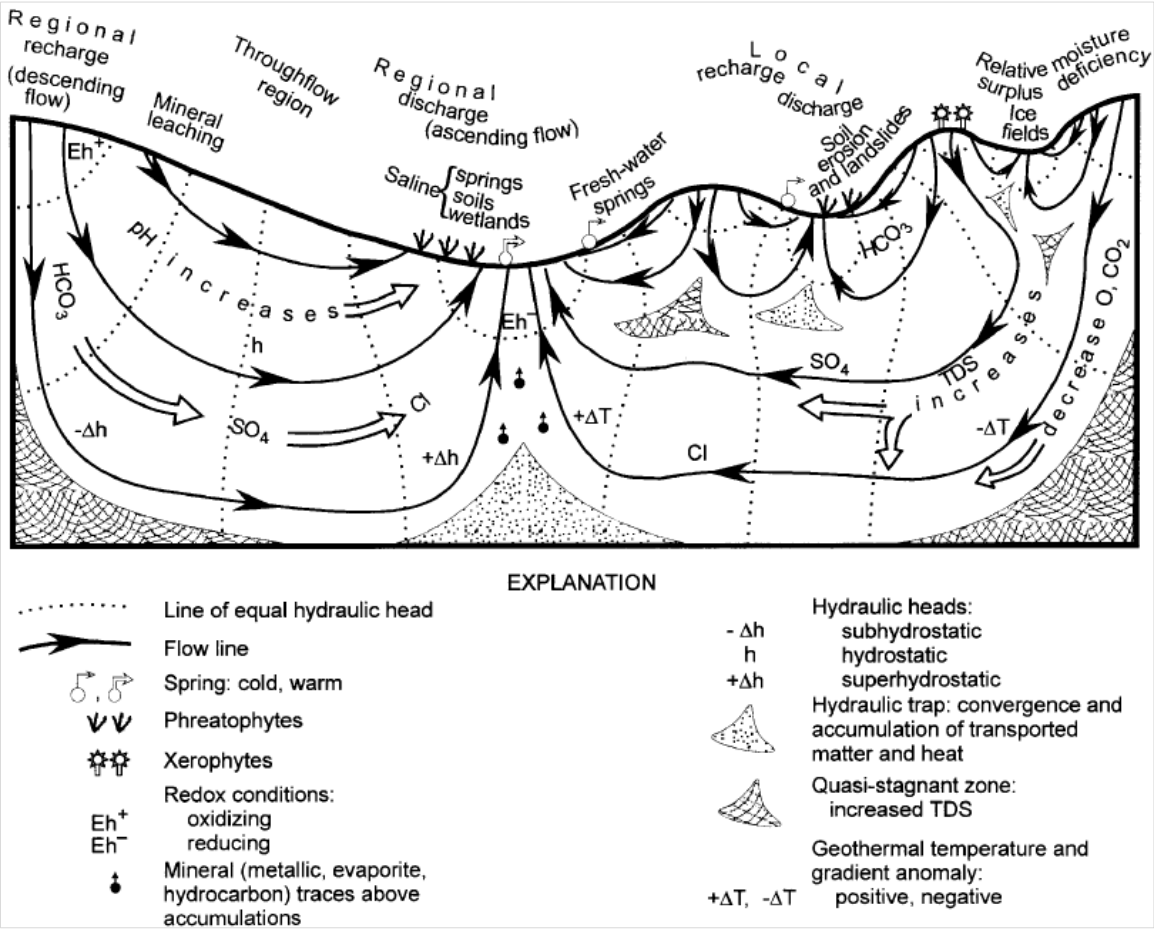

Figure 1-2: Effets et manifestations de l'écoulement conduit par la topographie dans un bassin hydrographique régional non confiné (Tóth, 1999). Reproduit avec la permission de Springer Nature.

1.2.2.2. Évolution de l'eau souterraine en contexte sédimentaire

En raison de leur porosité élevée, les bassins sédimentaires fournissent les plus grands réservoirs de fluides accessibles dans la croûte supérieure (Yardley et Bodnar, 2014). Ils sont également les mieux étudiés, du moins lorsqu'ils sont associés aux hydrocarbures et aux métaux de base. D'après Domenico (1972) les bassins sédimentaires peuvent être subdivisés en trois principales zones : supérieure, intermédiaire et inférieure. Ces zones définissent les principaux

stades d'évolution de la chimie de l'eau souterraine (qui sont fonction du TSD) et sont généralement observées selon la profondeur :

a. La zone supérieure représente généralement les premiers 100-200 m de profondeur. L'eau souterraine a généralement un TSD faible avec l'anion dominant HCO_3^-. Les concentrations en HCO_3^- de l'eau qui s'infiltre viennent généralement du CO_2 du sol (provenant de l'activité microbienne, de la décomposition des matières organiques et de la respiration des plantes), et de la dissolution de la matière organique des sédiments, de la dolomite et de la calcite (Freeze et Cherry, 1979).
b. La zone intermédiaire – le TSD est plus élevé que dans la zone supérieure, cette augmentation est due à un temps de résidence plus long. Dans cette zone, l'anion dominant est généralement l'ion sulfate (SO_4^{2-}). En effet, les eaux souterraines peuvent devenir sulfatées en présence de minéraux sulfurés (tels que le gypse $CaSO_4\ 2H_2O$ et l'anhydrite $CaSO_4$).
c. La zone inférieure – Les écoulements dans cette zone sont lents et l'eau souterraine tend à évoluer vers des saumures riches en Cl^-. Le contact prolongé de l'eau souterraine et des minéraux chlorurés très solubles comme la halite (NaCl) et la sylvite (KCl) en est la cause (Chebotarev, 1955). Ces minéraux sont généralement rencontrés dans des bassins sédimentaires profonds, qui ont été déposés au moment de l'évaporation de bassins marins fermés.

En conséquence de cette évolution en contexte sédimentaire, certaines saumures qui sont dominées par le NaCl résultent de la dissolution de minéraux évaporitiques, principalement contrôlés par la halite (Land et Macpherson, 1992; Hanor, 1994). Par ailleurs, d'après Yardley et Bodnar (2014), les saumures issues de la précipitation de la halite sont riches en calcium (Ca^{2+}) et en brome (Br^-). En effet, en précipitant la halite à partir d'une solution riche en Na^+ et Cl^-, telle qu'une eau de mer ou une saumure de type NaCl, la solution s'appauvrit en Na^+ et Cl^-, entrainant un enrichissement en Ca^{2+} ou Br^- dans le fluide résiduel.

La Figure 1-3 montre comment différents fluides peuvent évoluer en fonction de la source de l'eau et des minéraux avec lesquels ils peuvent interagir. Cet organigramme montre aussi que les processus hydrogéochimiques (évaporation, dolomitisation, dissolution, interaction avec les silicates) peuvent se superposer. Les eaux météoriques peuvent être modifiées par réaction avec des minéraux (carbonates et silicates) mais restent des eaux à faible teneur en Cl^-. Dans le contexte sédimentaire, l'évolution des eaux carbonatées ou silicatées vers des pôles salins est principalement due à un mélange avec une composante marine. Tandis que les fluides hautement salins (eau de mer) peuvent évoluer dans différentes directions, dépendamment des interactions avec les roches encaissantes, e.g. dissolution, dolomitisation, albitisation (Figure 1-3). Dans la littérature, plusieurs termes descriptifs ont été utilisés pour désigner les fluides aqueux profonds dans les bassins sédimentaires : saumures sédimentaires, eaux de formation, saumures de champ pétrolifère, saumures de bassin et eaux de bassin (Kharaka et Hanor, 2003). Ces termes décrivent généralement le contexte dans lequel les saumures ont été identifiées et, ont été utilisés dans ce projet doctoral pour décrire ce type de saumures continentales.

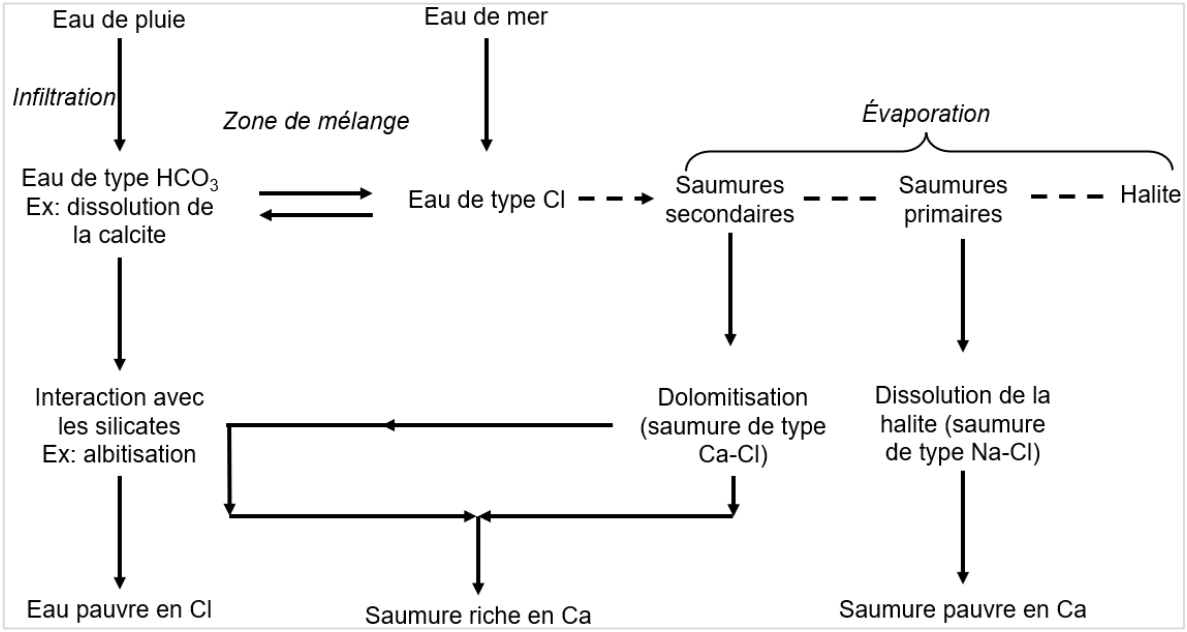

Figure 1-3: Diagramme de flux pour montrer les facteurs possibles déterminant l'évolution de la chimie de la saumure pendant la diagenèse. Saumures primaires désignent les saumures issues de la dissolution des évaporites, saumures secondaires désignent les saumures issues de la précipitation des évaporites. L'évaporation contrôle l'évolution des saumures primaires et secondaires jusqu'à la formation de halite. La figure est inspirée des études de Yardley et Bodnar (2014) et de Freeze et Cherry (1979).

1.2.2.3. Évolution de l'eau souterraine en contexte cristallin

Selon le modèle représentatif de l'évolution chimique des eaux souterraines (Figure 1-4), appliqué aux roches plutoniques du Bouclier Canadien, les eaux souterraines douces sont généralement identifiées à des profondeurs où les écoulements par advection prédominent sur la diffusion (Gascoyne et Kamineni, 1994). Ces eaux présentent également une faible acidité et une signature de type calcique-bicarbonaté ($Ca\text{-}HCO_3$). Par la suite, ces eaux souterraines peuvent s'enrichir en sulfates, surtout en présence de minéraux sulfurés. À plus grandes profondeurs, les temps de résidence augmentent (> 1 Ma), les processus de diffusion dominent sur l'advection et permettent ainsi la dissolution des sels dans la matrice poreuse de la roche. Cette évolution est observée en fonction de la profondeur, quel que soit le type de roche (granite, gabbro et gneiss). Gascoyne et Kamineni (1994) ont observé que les eaux souterraines des roches cristallines à des profondeurs supérieures à 1 000 m sont majoritairement des saumures (TSD > 35 g/L). Sur la base de ces observations, Gascoyne et Kamineni (1994) ont proposé un modèle d'évolution des faciès chimiques de l'eau souterraine en fonction de la profondeur jusqu'à des pôles salins (Figure 1-4). Tout le long de ce projet doctoral, les saumures des boucliers continentaux cristallins ont été décrit comme des saumures cristallines, saumures Précambriennes ou encore saumures crustales.

Gascoyne et Kamineni (1994) indiquent que la variabilité et l'évolution de la composition chimique de l'eau souterraine observées s'expliquent à partir d'un certain nombre de réactions chimiques ayant cours dans le milieu cristallin (Tableau 1-2). D'après les auteurs, l'hydrolyse du feldspath est le processus chimique dominant sans différencier les types de roches cristallines étudiés (granites, granodiorites…). La dissolution et la dissociation du dioxyde de carbone (CO_2) dans les eaux souterraines (Équation 1.1) permettent d'expliquer l'augmentation du pH conduisant à l'altération du feldspath (Équations 1.2 et 1.3). La précipitation de la calcite et l'échange d'ions avec les minéraux argileux nouvellement formés peut expliquer la diminution du calcium dissous (Équations 1.4 et 1.5). L'altération de la biotite et du feldspath potassique peut expliquer la prédominance des minéraux argileux (kaolinite et illite) dans les granites (Équations 1.6 et 1.7). Bien que ces réactions d'altération produisent du potassium (K^+) et du magnésium dissous (Mg^{2+}),

Gascoyne et Kamineni (1994) observent que, dans les eaux souterraines diluées de tous types de roches plutoniques, les concentrations de K^+ et de Mg^{2+} restent faibles (< 10 mg/L). Les auteurs expliquent ces faibles concentrations par l'échange d'ions avec les minéraux argileux et la faible solubilité des espèces hydroxy (biotite, hornblende) et des carbonates à pH élevé.

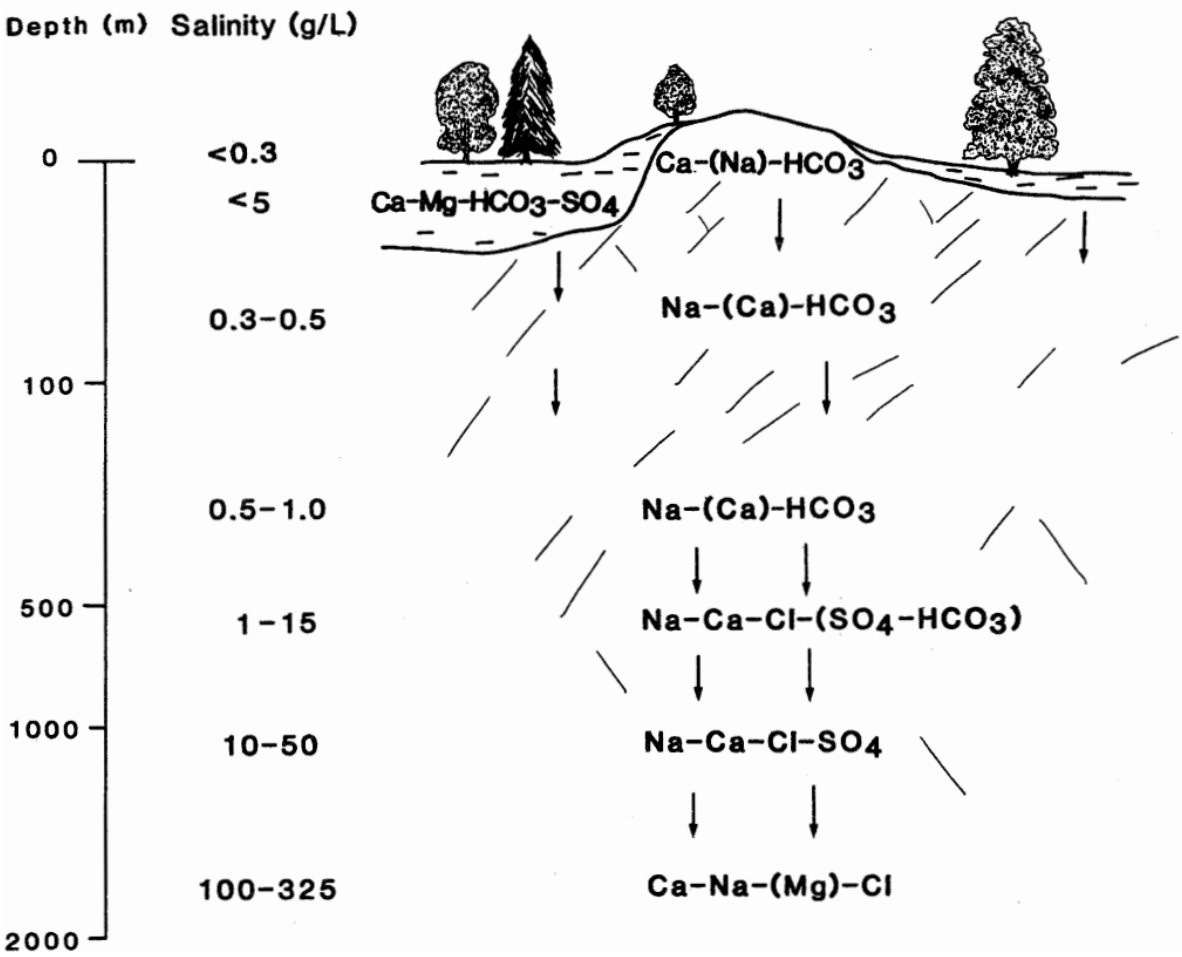

Figure 1-4: Représentation schématique de l'évolution géochimique de l'eau souterraine dans les roches plutoniques en fonction de la profondeur (Gascoyne et Kamineni, 1994). Reproduit avec la permission de Springer Nature.

Tableau 1-2: Réactions chimiques expliquant la composition chimique des eaux souterraines dans les roches plutoniques (Gascoyne et Kamineni, 1994).

N°	Équations de réaction
1.1	$H_2O + CO_2 \leftrightarrow H_2CO_3 \leftrightarrow H^+ + HCO_3$
1.2	$2NaAlSi_3O_8 + 2H^+ + H_2O \rightarrow 2Na^+ + Al_2Si_2O_5(OH)_4 + 4SiO_2$ (albite) (kaolinite)
1.3	$CaAl_2Si_2O_8 + 2H^+ + H_2O \rightarrow Ca^{2+} + Al_2Si_2O_5(OH)_4$ (anorthite) (kaolinite)
1.4	$Ca^{2+} + 2HCO_3^- \rightarrow CaCO_3 + H_2O + CO_2$ (calcite)
1.5	$Ca^{2+} + 2M\text{-}R \rightarrow 2M^+ + Ca\text{-}R_2$ Où M est H^+ ou Na^+ et R est un substrat minéral argileux
1.6	$2KMg_3AlSi_3O_{10}(OH)_2 + 14H^+ \rightarrow 2K^+ + 6Mg^{2+} + 7H_2O + 4SiO_2 + Al_2Si_2O_5(OH)_4$ (biotite) (kaolinite)
1.7	$3KAlSi_3O_8 + 2H^+ \rightarrow 2K^+ + 6SiO_2 + KAl_3Si_3O_{10}(OH)_2$ (microcline) (illite)

En somme, les modèles d'évolution des faciès chimiques de l'eau souterraine présentés dans cette section expliquent qualitativement la variabilité géochimique de l'eau souterraine et l'évolution naturelle de la salinité de ces eaux vers des saumures continentales. Ces modèles d'évolution et les équations de réactions qui les composent sont basés sur la compréhension des éléments majeurs, lesquels tirent leur origine de multiples sources. Il est aussi important de mettre en évidence que les processus au cours du temps se superposent les uns aux autres, comme illustré dans l'organigramme (Figure 1-3).

Une école de pensée suggère que les interactions entre la roche et l'encaissant au cours des temps géologiques tendent à effacer les caractéristiques chimiques de l'eau initiale comme par exemple l'eau météorique ou l'eau de mer (Savoye, 1998). Ceci rend ardue la détermination de l'origine de la salinité des saumures continentales et la compréhension de leur évolution à travers le temps. Dans ce sens, plusieurs hypothèses quant aux processus naturels de salinisation des saumures continentales ont été formulées dans la littérature (Guha et Kanwar, 1987; Bottomley et

al., 1994; Bucher et Stober, 2010). Ces processus naturels peuvent être subdivisés en deux grandes catégories : processus allochtones et processus autochtones (Nordstrom et al., 1989).

1.2.3. Hypothèses des processus de salinisation des saumures continentales

1.2.3.1. Processus allochtones

Un processus naturel de salinisation des eaux souterraines est dit allochtone lorsque l'origine des chlorures est externe à la roche, et qu'ils sont donc importés dans le système géochimique (Nordstrom et al., 1989). Le système géochimique est ici pris comme un espace clos, contenant des composantes chimiques en interaction. Ci-dessous, la liste de quelques processus de salinisation allochtones :

a) L'intrusion marine est due à la diminution du niveau de la nappe d'eau souterraine côtière ou l'élévation du niveau de l'eau de mer entrainant une infiltration d'eau de mer dans la nappe (Kloppmann et al., 2011).
b) L'intrusion d'une paléo eau de mer est une transgression d'une paléo-mer laissant une saumure résiduelle après évaporation qui s'est infiltrée dans les roches anciennes (Bottomley et al., 1994).
c) L'évaporation de l'eau de mer est à l'origine de la formation de saumures dites « primaires », qui peuvent conduire à la formation de roches évaporitiques. Ces dernières, lorsqu'elles entrent en contact avec des eaux souterraines ou de surface peuvent se dissoudre (processus de dissolution), ce qui donne naissance à des saumures dites « secondaires » (Kloppmann et al., 2011).
d) La cryo-concentration est aussi un processus de salinisation des saumures proposé dans la littérature (Herut et al., 1990). Pour qu'un tel processus se mette en place, des conditions spécifiques sont nécessaires : un climat polaire et une eau de mer cryo-concentrée durant cet épisode de glaciation (Bein et Arad, 1992). La saumure viendrait donc du mélange entre une eau météorique et une eau de mer cryo-concentrée.

e) L'infiltration des aérosols marins est un processus ayant lieu dans des climats arides/semi-arides près de la côte et dans la bande côtière. Les aérosols de sel marin sont absorbés par les pluies et incorporés dans les eaux de recharge, contribuant à la salinité des eaux souterraines (Li et al., 2020).

1.2.3.2. Processus autochtones

Un processus autochtone comprend les réactions et processus géochimiques entre les eaux souterraines et la roche dans laquelle elles résident. L'origine des chlorures vient de l'interaction avec la roche et inclut :

a) L'eau connée qui désigne de l'eau souterraine piégée dans les interstices de la roche (sédimentaire ou cristalline) au moment de sa mise en place (Bjørlykke, 2015). L'eau connée peut être plus dense et salée comparée à l'eau de mer.

b) L'ultrafiltration, aussi appelée hyperfiltration ou osmose inverse naturelle, qui est proposée comme processus de salinisation des saumures continentales, dans des bassins sédimentaires pauvres en évaporites. Les milieux géologiques riches en argiles peuvent servir de membranes semi-perméables qui retardent le transport des ions par rapport à l'eau, ce qui accumule les sels du côté amont ou à l'intérieur de l'unité-membrane, selon le régime de transport (Neuzil et Person, 2017). Kharaka et Berry (1973) définissent une séquence de retardement des anions à une température de 70 °C : $HCO_3^- < I^- < B(OH)_3 < SO_4^{2-} < Cl^- < Br^-$.

c) L'interaction avec les roches favorisée par des températures et pressions élevées (fluides hydrothermaux) à l'occasion d'activités géothermiques (Edmunds et al., 2003). En effet, l'augmentation de la température favorise la dissolution des ions de la roche à l'eau.

d) L'hydrolyse des minéraux silicatés : en effet, les minéraux hydroxysilicates (biotite, apatite, tourmaline, topaze, hornblende et muscovite) peuvent contenir de fortes quantités de chlorures, lesquelles pourraient être relarguées dans l'eau durant les

processus d'altération (Frape et Fritz, 1987). Warr et al. (2021) propose que ce processus se déroule à des températures relativement basses (< 100 °C).

e) La lixiviation des inclusions fluides est proposée comme hypothèse de salinisation des saumures continentales. En effet, Nordstrom et al. (1989) propose que des fluides microscopiques surconcentrés en sels et piégés dans la structure cristalline d'un minéral contribuent fortement à la salinisation des saumures continentales.

f) La radiolyse, proposée comme processus de salinisation, consiste à décomposer des molécules d'eau (H_2O) sous l'effet de radiations issues de radionucléides (e.g. ^{238}U), en produisant des gaz (H_2, O_2) et des oxydants (H_2O_2). Si ces produits radiolytiques ne parviennent pas à se recombiner en quantités suffisantes pour reformer l'eau, cela entraîne une perte nette d'eau dans le système, et donc une concentration progressive des sels dissous jusqu'à formation d'une saumure hypersaline (Vovk, 1981; Nisson et al., 2023).

1.3. Problématique générale

Des progrès significatifs ont été réalisés dans la compréhension des processus naturels de salinisation des saumures continentales et de leur évolution. En effet, Tóth (1999) fournit un cadre général pour comprendre l'évolution hydrogéochimique à travers l'espace et le temps (Figure 1-2). Selon ce modèle classique, les eaux souterraines tendent à évoluer naturellement vers des pôles salins dont l'état saumuré est défini comme le stade final d'évolution des processus de salinisation continentale. Cette évolution naturelle des eaux souterraines s'intègre dans la notion générale du cycle de l'eau, laquelle est relativement bien comprise et largement étudiée en subsurface (< 100 m) (Rouleau et al., 2013; Abascal et al., 2022; Boumaiza et al., 2022a). La présence d'eau météorique à de grandes profondeurs a également été documenté (McIntosh et Ferguson, 2021; Boumaiza et al., 2024).Toutefois, les connaissances actuelles sur la participation de ces fluides profonds au cycle de l'eau demeurent limitées, principalement dues à la difficulté d'accès et des échelles de temps relativement longues des eaux souterraines dans ces environnements. Par exemple, l'application de modèles d'évolution classiques dans des milieux géologiques complexes, comme les boucliers

anciens ou les grands bassins sédimentaires, présente certaines limites. Ces limites s'expliquent par l'influence marquée des structures géologiques locales (failles, fractures, zones de cisaillement), des activités tectoniques (surpressions, circulations verticales), de la lithologie (composition chimique), ainsi que par les interactions entre les fluides profonds et de surface, qui contribuent à l'évolution chimique des eaux souterraines. Aussi, la participation au cycle de l'eau des fluides provenant de la base de la croûte ou directement du manteau lithosphérique sub-continental, n'est pas considérée dans des modèles d'évolution classique. De plus, l'évolution des eaux souterraines vers des saumures continentales se déroule sur des échelles de temps géologiques pouvant atteindre le milliard d'années dans certains boucliers continentaux (Sherwood-Lollar et al., 2021; Warr et al., 2022). À ces échelles, les processus hydrogéochimiques se superposent et dépendent de paramètres multiples (cf. Section 1.2.1) liés aux contextes géologiques et à l'héritage paléohydrogéologique, ce qui rend leur identification complexe. Tel qu'illustré dans la Section 1.2.2, les éléments chimiques majeurs (provenant de sources multiples et variées) sont couramment utilisés pour décrire l'évolution des saumures continentales (évaporation, dissolution d'évaporites, interactions eau-roche). Toutefois, les éléments traces et mineurs, bien que documentés dans certains contextes spécifiques, e.g. Li^{+}, B^{3+}, Sr^{2+} (Pauwels et al., 1993; Bottomley et al., 1999), demeurent moins intégrés dans des modèles évolutifs régionaux. Ainsi, ces complexités et limites, tant géochimiques qu'hydrauliques, influençant directement l'évolution des eaux souterraines et les processus naturels de salinisation continentale, requièrent la nécessité de travaux scientifiques de fond. Ce projet doctoral vise donc à étendre les modèles d'évolution aux contextes géologiques complexes, à évaluer le rôle des fluides profonds dans le cycle de l'eau et à intégrer l'étude des éléments mineurs et traces pour affiner la compréhension des processus de salinisation continentale.

1.4. Région d'étude

Des études dans la région du Saguenay-Lac-Saint-Jean (SLSJ) ont montré qu'il y avait une évolution naturelle des eaux souterraines vers des pôles salins (Walter, 2010). En effet, la variété géochimique du type de roche (contextes cristallin et sédimentaire), et la particularité de la topographie régionale, pouvant permettre une infiltration profonde des eaux souterraines font du

SLSJ un laboratoire naturel de premier choix pour répondre à la problématique de recherche (Section 1.3). Dans cette section, le travail a consisté à présenter en premier lieu le contexte hydrogéologique régional (Section 1.4.1) et ensuite les travaux déjà réalisés dans la région d'étude (Section 1.4.2 et 1.4.3).

1.4.1. Contexte hydrogéologique au Saguenay-Lac-Saint-Jean

La géologie de la région du SLSJ est en grande partie Précambrienne (Figure 1-5), et dominée par des roches plutoniques, dont la composition varie de felsique à intermédiaire, ainsi que par un complexe d'orthogneiss et de paragneiss appartenant à la Province du Grenville (Rivers et al., 1989; Hébert et Lacoste, 1998). Entre 1.5 et 1 Ga, la région du SLSJ a subi plusieurs phases d'intrusions anorthositiques Mésoprotérozoïque, à l'origine de la suite anorthositique du Lac-Saint-Jean (SALSJ); (Hébert et Van Breemen, 2004). La SALSJ couvre une superficie de 20 000 km^2, soit 25% du territoire d'étude. Au-dessus du socle grenvillien se superposent des roches sédimentaires datant du Paléozoïque, composées de roches telles que des calcaires et des shales argileux de l'Ordovicien moyen (d'environ 450 Ma). À cela s'ajoutent des sédiments fluvioglaciaires du Pléistocène (Wisconsinien tardif), des argiles post-glaciaires de la mer de Laflamme et les sédiments deltaïques et littoraux datant du Pléistocène et du début de l'Holocène (Rouleau et al., 2013).

Le graben du Saguenay (orienté ONO-ESE) est le principal élément qui contrôle la topographie de la région d'étude (Roy et al., 2011). Les failles bordant le graben du Saguenay séparent les hautes-terres des basses-terres. Ces failles se sont formées initialement à partir de la division du supercontinent Rodinia au Cambrien (environ 600 Ma) durant la phase précoce d'océanisation Iapétus. Vers l'Ordovicien moyen, une collision entre un arc insulaire et l'Amérique du Nord (l'orogénie Taconienne) a induit un régime de compression (Trudel et Malo, 1993), expliquant la présence du relèvement topographique du seuil de Kenogami de la région (Figure 1-5). La dernière phase de réactivation des failles du graben s'est produite au début de l'ouverture de l'océan Atlantique il y a environ 180 Ma (Lamontagne et Brouillette, 2022). Walter et al. (2017) suggèrent que la topographie en graben de la région prolonge le temps de résidence du système d'écoulement régional, qui se déverse ensuite dans les basses terres autour du lac Saint-Jean (Figure 1-6). Cette

hypothèse concorde avec le modèle de Tóth (1999), selon lequel la salinité des eaux souterraines augmente avec l'échelle des cellules d'écoulement (Figure 1-2).

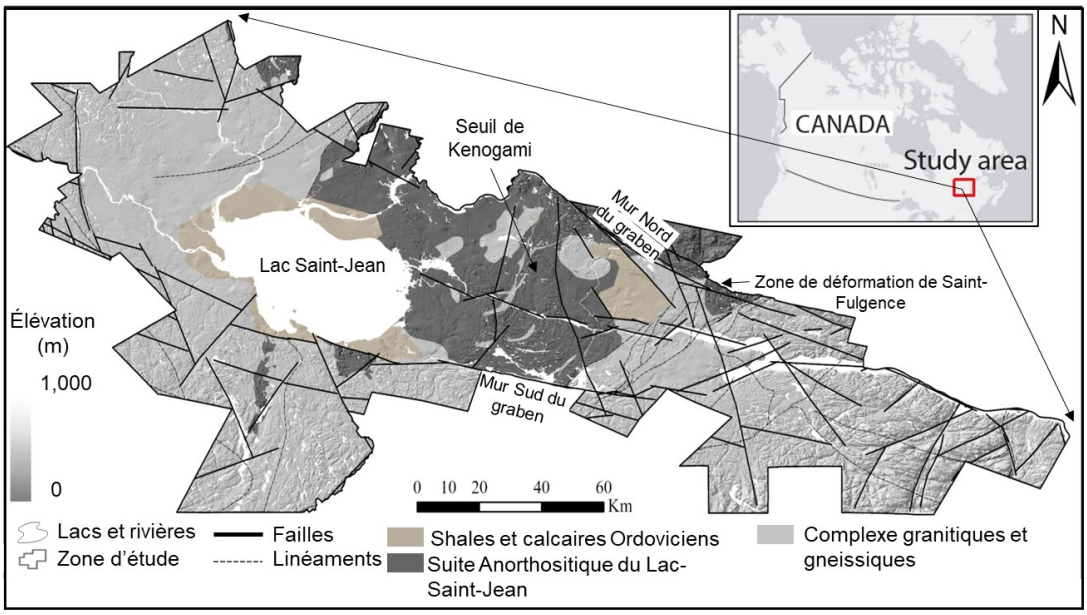

Figure 1-5: Géologie simplifiée du roc fracturé et de la physiographie régionale du SLSJ. Couches géologiques et structurales tirées de SIGEOM 2025. © Othniel Glodie Dominique Ngombe, 2025.

1.4.2. Évolution de la chimie des eaux souterraines au SLSJ

Les eaux souterraines constituent une ressource importante dans la région (Rouleau et al., 2013). Les études d'envergure menées au SLSJ, concluent généralement à une chimie de l'eau souterraine légèrement minéralisée et de bonne qualité (Dessureault, 1975; Rouleau et al., 2013). Néanmoins, la présence d'eaux saumâtres de différentes origines a mis en évidence une variabilité spatiale et temporelle importante dans la chimie des eaux souterraines (Roy et al., 2011).

Des travaux de recherche menés plus récemment, ont permis d'identifier des eaux souterraines saumâtres en subsurface (< 100 m) dans des puits domestiques forés dans la roche fracturée et dans les aquifères granulaires du Pléistocène (Walter et al., 2017; Walter et al., 2019). Ces investigations ont conduit à une première caractérisation des pôles hydrogéochimiques régionaux, révélant trois grands groupes distincts : (1) des eaux salées issues du Bouclier Précambrien, (2) des eaux salées associées aux argiles de la mer de Laflamme et (3) des eaux douces. La Mer de Laflamme, qui a recouvert une partie importante de la région après la déglaciation,

a laissé d'épais dépôts d'argile contenant de l'eau interstitielle salée (LaSalle et Tremblay, 1978). Le lessivage de cette eau de mer fossile, d'origine allochtone piégé dans la couche argileuse marine régionale, permet d'expliquer la présence d'eaux saumâtres dans certains aquifères confinés, notamment granulaires (Roy et al., 2011; Walter et al., 2017). Concernant les eaux souterraines prélevées dans le roc fracturé (cristallin et sédimentaire) au SLSJ, les auteurs ont suggéré une évolution naturelle vers des pôles salins (Walter et al., 2006; Walter et al., 2017), telle qu'observée dans le socle Précambrien fracturé ailleurs au Canada (Section 1.2.2.3). En effet, cette similarité chimique entre certains échantillons d'eau souterraine de la région avec des saumures du Bouclier Précambrien suggère la présence d'eau très ancienne et profonde, d'origine de salinité autochtone (Walter et al., 2019). Par conséquent, les interactions entre l'eau et les roches cristallines, y compris la dissolution de minéraux comme les silicates (ex: plagioclases tel que l'albite) ou l'altération de l'anorthite plagioclase, et l'échange cationique entre Ca^{2+} et Na^{+}, ont été proposées pour expliquer l'évolution de la salinité de ces eaux (Walter et al., 2023). En l'état actuel des connaissances, l'origine autochtone de la salinité pour les eaux salées issues du Bouclier Précambrien demeure à l'étape d'hypothèse.

1.4.3. Identification des marqueurs de l'origine de la salinité au SLSJ

Dans le but de mieux comprendre la dynamique de mélange et la contribution des pôles hydrogéochimiques régionaux, une nouvelle approche basée sur le concept d'Indice de Maturation de l'Eau (IME) a été développée (cf. Walter et al. (2023) pour les détails méthodologiques). Cette approche permet de standardiser les concentrations et de décrire l'enrichissement ou l'appauvrissement en différents éléments chimiques au fur et à mesure de l'évolution, incluant les éléments majeurs, mineurs et traces (Walter et al., 2023). Ainsi, les auteurs ont identifié des éléments chimiques caractéristiques des origines de salinité des eaux souterraines de la région. Les eaux ayant une origine de salinité allochtone présentent des IME élevés pour des éléments tels que le Mg^{2+}, HCO_3^{-}, Na^{+}, K^{+}, tandis que les eaux ayant une origine de salinité autochtone présentent des IME élevés pour des éléments tels que le Li^{+}, Br^{-}, Ca^{2+}, Sr^{2+} (Figure 1-6). Par conséquent, il serait

intéressant d'approfondir la connaissance de ces éléments discriminant en tant que traceurs d'origine.

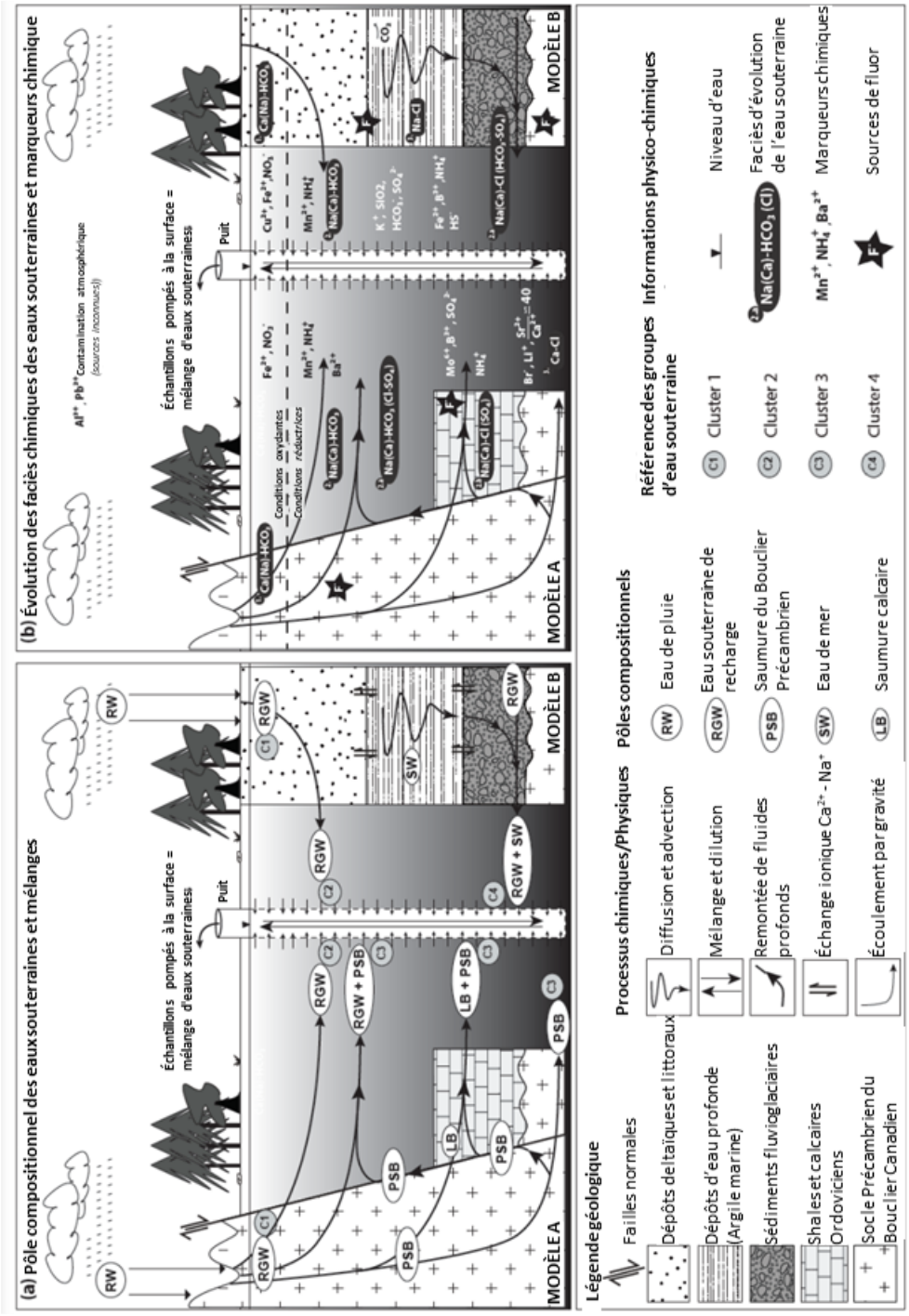

Figure 1-6: Modèle conceptuel d'écoulement contrôlé par la topographie de la région du SLSJ. Deux coupes transversales conceptuelles des unités chronostratigraphiques sont présentées dans la figure 1.6. Le modèle (A) représente les formations rocheuses régionales simplifiées en trois unités principales : les roches

Précambriennes du Bouclier Canadien et les calcaires et schistes ordoviciens. Une faille verticale schématique marque le contact discordant entre les roches calcaires ordoviciennes et les roches cristallines Précambriennes et représente les limites entre les hautes terres et les basses terres (Fossé du Saguenay). Le modèle (B) représente les unités pléistocènes régionales simplifiées en trois unités principales : Les sédiments fluvioglaciaires du Pléistocène, les dépôts profonds d'argile post-glaciaire d'eau de mer du Pléistocène (mer de Laflamme) et les dépôts deltaïques et littoraux du Pléistocène. La figure est modifiée à partir de l'étude de Walter et al. (2023). Reproduit avec la permission de Elsevier.

1.5. Problématique spécifique et objectif général de l'étude

Bien que des avancées majeures aient été faites dans la compréhension de l'évolution des eaux souterraines au SLSJ, plusieurs questions subsistent à ce jour. La présence, dans les eaux saumâtres, de signatures chimiques similaires à celles des saumures Précambriennes profondes en subsurface soulève des questions sur leur migration, les conditions hydrodynamiques ayant permis leur mise en place et l'interconnectivité entre les aquifères de subsurface et les environnements profonds. Dans la région d'étude, les eaux saumâtres dans le roc fracturé ont été identifiées dans le socle cristallin Précambrien et dans les roches sédimentaires, lesquels sont les deux plus grands réservoirs de saumures continentales au monde (Sections 1.2.2.2 et 1.2.2.3). Dans leur étude, Walter et al. (2023) observent un amalgame des signatures chimiques caractéristiques des deux environnements géologiques dans ces eaux collectées dans les aquifères fracturés. Cette observation met en lumière la nécessité de comprendre l'influence du contexte géologique dans l'évolution des saumures continentales et l'importance de déterminer des éléments chimiques discriminatoires entre les saumures cristallines et sédimentaires. Plusieurs études au SLSJ mettent en évidence la diversité et l'évolution de la composition chimique des eaux souterraines à l'échelle régionale, en identifiant différents types d'eau et les processus géochimiques qui les contrôlent, ainsi que leur répartition spatiale. Cependant, l'origine autochtone de la salinité des eaux saumâtres provenant du roc fracturé demeure à l'étape d'hypothèse, soulignant la nécessité d'approfondir la compréhension des processus géochimiques impliqués et du rôle de l'histoire hydrogéologique de la région.

Les travaux de recherche et les observations démontrent la nécessité d'un travail scientifique de fond portant sur la connaissance de l'évolution géochimique des saumures et de leur mobilité au SLSJ, en considérant l'influence des contextes géologiques et du temps de résidence sur la chimie

des eaux souterraines. Ce projet doctoral vise à préciser l'origine et les processus géochimiques des saumures continentales en fonction du contexte géologique, à reconstituer les trajections des écoulements des eaux souterraines profondes en contexte de graben, en clarifiant le rôle des structures géologiques dans leur mobilité, et à estimer l'influence relative des fluides anciens sur les systèmes hydrogéologiques locaux. Ce faisant, le projet doctoral a pour objectif général de compléter le modèle conceptuel hydrogéologique régional proposé par Walter et al. (2023), en y apportant, un aspect hydraulique testé quantitativement, et une meilleure compréhension du rôle des fluides anciens et des processus hydrogéochimiques impliqués.

1.6. Hypothèses de recherche et objectifs spécifiques de l'étude

Sur la base de la revue de littérature (Section 1.2) et des questions de recherche issues des études antérieures dans la région d'étude (Section 1.4), ce projet de recherche repose sur trois hypothèses de base. Celles-ci structurent les trois objectifs majeurs de ce projet doctoral.

1.6.1. Remontée des fluides profonds via les structures géologiques du graben

La distribution des eaux saumâtres provenant du Bouclier Précambrien près des systèmes de failles dans les basses terres du SLSJ suggère que la topographie et les failles du graben pourraient jouer un rôle important dans la remontée des fluides profonds vers la surface (Walter et al., 2017). Le mouvement ascendant des eaux souterraines profondes vers les zones de résurgence a été attribué à des pressions hydrodynamiques élevées en profondeur, combinées à l'existence de de connexion hydraulique avec la surface (Warner et al., 2012). Le graben du Saguenay crée une grande différence d'élévation entre les hautes terres et les basses terres de la région, pouvant permettre aux eaux souterraines de s'infiltrer profondément et de remonter au point de décharge régional. Par conséquent, un système d'écoulement régional selon ce modèle gravitaire (Figure 1-2) appliqué au graben du SLSJ pourrait expliquer le mélange entre les saumures profondes et les eaux douces de subsurface dans les basses terres de la région étudiée. L'hypothèse d'une remontée de fluides profonds le long des failles a été suggérée par Walter et al. (2017) pour expliquer la présence à de faibles profondeurs de saumures Précambriennes généralement retrouvées à plus de 1 000 m de profondeur (Gascoyne et Kamineni, 1994). Cependant, ni l'hypothèse d'un écoulement induit par

la gravité, ni le rôle des failles n'ont fait l'objet d'études quantitatives visant à expliquer la remontée des eaux souterraines salines profondes dans ces zones de décharge.

1.6.2. Caractéristiques chimiques uniques des saumures en fonction du contexte géologique

Dans la région du SLSJ, la présence probable de saumures Paléozoïques d'origine sédimentaire a déjà été suggérée mais jamais caractérisée (Walter, 2010). Dans leur étude, Walter et al. (2017) n'ont pas pu distinguer statistiquement la chimie des eaux salées venant des environnements sédimentaires des eaux salées provenant du Bouclier Précambrien. Toutefois, l'observation des IME élevés en B^{3+}, NH_4^+, Mo^{6+} caractéristique d'environnements sédimentaires pour le groupe d'échantillons ayant une signature de saumures Précambriennes suggère un amalgame entre ces deux origines (Walter et al., 2023). La Section 1.2.2, a mis en évidence des similitudes chimiques dans l'évolution des eaux souterraines des bassins sédimentaires et des boucliers cristallins sur la base des éléments chimiques majeurs. Cependant, si la salinisation continentale dépend en partie des interactions eau-roche, alors les différences géologiques entre milieux cristallins et sédimentaires impliquent que leurs saumures sont distinctes. Caractériser ces différences permettrait de clairement identifier les différentes origines de la salinité des eaux souterraines dans la région d'étude.

1.6.3. Héritage paléohydrogéologique dans le système hydrogéochimique actuel

La région du SLSJ située dans le Bouclier Canadien a connu une histoire hydrogéologique complexe, marquée notamment par des épisodes de transgression marine et des épisodes glaciaires-interglaciaires. À cela s'ajoute la contribution des fluides profonds aux cycles de l'eau tel que suggéré dans les études précédentes (Walter et al., 2017; Walter et al., 2019; Walter et al., 2023). La région a conservé des vestiges de son histoire hydrogéologique, tels que les dépôts d'argiles marins postglaciaires (mer Laflamme), les dépôts fluvio-glaciaires ou sédiments glaciolacustres et la présence de roches sédimentaires (e.g. calcaires, grès, shales), vestiges de la mer tropicale durant l'Ordovicien. Les études hydrogéochimiques réalisées dans la région d'étude ont suggéré que les signatures hydrogéochimiques de subsurface reflètent le mélange entre des

fluides profonds et des fluides marins postglaciaires avec l'eau météorique récente. En revanche, la contribution d'autres pôles compositionnels hydrogéochimiques (groupes d'échantillons d'eau de même origine) reflétant la paléohydrogéologie complexe de la région tels que l'eau sous-glaciaire datant du dernier épisode glaciaire ou des traces d'eau d'origine marine très ancienne (eau de mer ordovicienne), demeure au stade d'hypothèses (Walter, 2010; Roy et al., 2011; Walter et al., 2023). Malgré la superposition des processus hydrogéologiques à l'échelle de temps géologique considérée dans la présente étude (Section 1.3), le système hydrogéochimique actuel au SLSJ conserverait des caractéristiques de son passé hydrogéologique.

1.6.4. Objectifs spécifiques

Les sous-sections précédentes ont mis en évidence plusieurs hypothèses pour expliquer l'origine des eaux saumâtres prélevées dans le roc fracturé au SLSJ, lesquelles ont été traduites en objectifs pour ce projet doctoral :

- Expliquer la présence des eaux salées et anciennes à de faibles profondeurs au SLSJ. Cet objectif a pour but d'expliquer et discuter des mécanismes hydrodynamiques profonds contrôlant la mobilité des saumures Précambriennes et d'évaluer l'influence des structures géologiques sur l'évolution des eaux souterraines.
- Décrire l'évolution des saumures continentales et identifier les marqueurs géochimiques caractéristiques du contexte géologique. Cet objectif a pour but de déterminer si les saumures sédimentaires et les saumures cristallines ont bien des signatures chimiques distinctes, et d'évaluer l'influence directe du contexte géologique dans l'évolution naturelle des eaux souterraines vers des pôles salins ;
- Identifier les processus à l'origine des signatures géochimiques et isotopiques caractéristiques du passé hydrogéologique au SLSJ. Cet objectif vise à estimer l'influence relative des fluides anciens sur les systèmes hydrogéologiques de subsurface, et à évaluer l'interconnectivité entre divers réservoirs géologiques en contexte de graben.

1.7. Méthodologie de recherche

La méthodologie de recherche appliquée à ce projet doctoral se subdivise en trois étapes complémentaires, visant à mieux comprendre l'évolution des eaux souterraines à travers le temps. L'évolution de l'eau souterraine étant considérée comme le processus de vieillissement de l'eau, l'âge de l'eau est donc le point central et le dénominateur commun de toutes les études qui découlent de ce projet de recherche. Tout d'abord, l'approche combinée de la modélisation numérique de l'écoulement et de l'âge de l'eau avec les analyses isotopiques a été essentielle pour confirmer la présence d'eaux très anciennes et pour valider théoriquement les hypothèses relatives à la migration des fluides profonds vers la surface au SLSJ. Par la suite, à l'aide d'une base de données sur les saumures provenant des bassins sédimentaires et des boucliers cristallins (tirées de la littérature), l'influence des contextes géologiques sur l'évolution des fluides anciens a été évaluée et caractérisée. Enfin, une analyse multi-traceurs des échantillons des eaux souterraines provenant du roc fracturé régional a permis de compléter le portrait hydrogéochimique régional et l'identification des pôles compositionnels hydrogéochimiques, en mettant en évidence la connectivité hydraulique entre les aquifères de subsurfaces et les environnements profonds.

Les sous-sections suivantes permettent de lier les méthodes et les objectifs de ce projet de recherche, d'expliquer les raisons qui ont mené aux choix méthodologiques, et de définir les concepts de base des méthodes choisies.

1.7.1. Approche combinée entre la modélisation numérique et les analyses isotopiques

La présence d'eau saumâtre ayant des signatures chimiques similaires aux saumures profondes du Bouclier Canadien a mis en évidence la nécessité d'analyser l'interconnectivité entre les environnements profonds et ceux de subsurface. Pour ce faire, l'étude a visé d'abord à confirmer la présence d'eaux anciennes en subsurface à l'aide des analyses isotopiques et ensuite, à explorer les conditions hydrodynamiques de leur mise en place via la modélisation numérique. En premier lieu, les analyses isotopiques de l'eau ($\delta^{2}H$ et $\delta^{18}O$) et du strontium ($^{87}Sr/^{86}Sr$), qui renseignent indirectement sur l'âge de l'eau, ont été utilisées pour confirmer la présence d'eau ancienne au SLSJ. En effet, ces méthodes révèlent des informations sur les processus hydrogéochimiques qui modifient

la chimie de l'eau, tels que les mélanges entre les eaux de compositions et d'âges différents, ou encore les échelles de temps de certains processus d'interactions eau-roche (McNutt et al., 1984; Warr et al., 2021). Ensuite, la modélisation numérique, qui permet de représenter un phénomène naturel, incluant des processus physiques et chimiques, à l'aide d'équations mathématiques, a été appliquée pour explorer les conditions hydrodynamiques pouvant permettre la remontée d'eau ancienne et profonde vers la surface. En conséquence, un modèle bidimensionnel d'écoulement souterrain a été construit, établi sur le cadre théorique de l'écoulement gravitaire de Tóth (1999), afin d'évaluer comment les gradients verticaux générés par la configuration régionale (graben) peuvent permettre la remontée de l'eau souterraine profonde. Il est possible que les conditions hydrauliques aient variées au fil du temps, alors que les profils d'âge des eaux souterraines demeurent généralement stables, ce qui témoigne des conditions hydrauliques antérieures, notamment dans les milieux profonds où le mélange et le renouvellement des eaux souterraines sont limités (McCallum et al., 2020). Dans le cadre de cette étude, les simulations numériques du transport advectif-dispersif de l'âge de l'eau ont été réalisées à l'aide du code FLONET/TR2 (Molson et Frind, 2023). La combinaison de ces deux approches a permis d'analyser la distribution des eaux souterraines profondes et leur interconnectivité avec la subsurface, et a apporté des informations supplémentaires sur les échelles de temps et les profils d'âge des eaux souterraines profondes et peu profondes au SLSJ.

1.7.2. **Analyses statistiques multivariées de la composition chimique des saumures continentales**

Le roc fracturé de la région d'étude est constitué de roche cristalline et de lambeaux de plateformes sédimentaires (Section 1.4.1). Des questions subsistent concernant l'influence de ces contextes géologiques sur l'évolution hydrogéochimique. Ces deux contextes sont aussi reconnus pour être les deux plus importants réservoirs de saumures anciennes dans le monde (Shouakar-Stash et al., 2007; Boumaiza et al., 2024). Par conséquent, l'intérêt dans cette partie du projet doctoral, a été de définir les chemins d'évolution d'eau souterraine très ancienne en fonction des contextes géologiques, à partir d'une base de données mondiale de 308 échantillons de saumures

continentales (sédimentaires et cristallines) tirés de la littérature existante et préparée dans le cadre de ce projet. L'analyse hiérarchique en grappes, l'analyse en composantes principales et les tests statistiques non-paramétriques (Wilcoxon/Kruskal-Wallis et Kendall τ) ont été appliqués à la base de données afin d'identifier les éléments chimiques caractéristiques de l'évolution des saumures sédimentaires et cristallines. Les modèles ont été développés en se basant principalement sur les éléments majeurs, mineurs et traces. Lorsque des données isotopiques étaient disponibles, elles ont généralement confirmé l'interprétation basée sur la chimie ionique de l'eau. Tout d'abord, l'analyse hiérarchique en grappe, une méthode de classification statistique, a permis de regrouper les échantillons en fonction de leur similitude chimique. Ensuite, l'analyse en composantes principales a permis d'identifier les marqueurs géochimiques des saumures cristallines et des saumures sédimentaires. Enfin, les tests statistiques non-paramétriques de Wilcoxon/Kruskal-Wallis et Kendall τ ont permis de définir avec plus d'objectivité d'autres marqueurs géochimiques discriminants entre les deux contextes géologiques. Le test de Kendall τ a permis d'évaluer les corrélations entre les éléments, tandis que le test de Wilcoxon/Kruskal-Wallis a déterminé si un élément était discriminant pour distinguer les groupes de saumures (significatif si $p < 0.05$). Par ailleurs, les analyses géochimiques (indice de saturation, de facteur d'enrichissement et de graphique binaire) ont permis d'évaluer les processus de salinisation et de présenter les séquences d'évolution hydrogéochimique des saumures provenant des contextes cristallins et sédimentaires.

1.7.3. Analyses multi-traceurs des eaux saumâtres de la région du SLSJ

La paléohydrogéologie de la région du SLSJ s'étend sur de longues périodes de temps (Walter, 2010). Les études précédentes ont mis en évidence la grande variabilité chimique et temporelle des eaux souterraines au SLSJ (Section 1.4.2). Par conséquent, la compréhension de l'évolution de l'eau souterraine au SLSJ à travers le temps passe par la compréhension des interactions hydrogéochimiques entre les systèmes hydrogéologiques passés et présents. Les origines de la présence des éléments majeurs, mineurs et traces dans l'eau souterraine peuvent être nombreuses et variées, tandis que les fractionnements isotopiques sont spécifiques à certains processus géochimiques (Clark et Fritz, 1997). Ainsi, une approche multi-traceurs a été appliquée à

un ensemble d'échantillons prélevés dans le roc fracturé de la région d'étude. La première étape a été de mener une campagne d'échantillonnage des eaux salées provenant du roc fracturé de la région, notamment à l'aide de sondages dans les médias sociaux « crowdsourcing ». Ici, la méthodologie a consisté à faire appel au grand public via les réseaux sociaux, dans le but de cibler parmi les utilisateurs ceux qui ont des puits domestiques d'eau salée dans des zones dominées par les roches sédimentaires et cristallines. La valeur seuil de salinité a été considérée en fonction de la classification de Kharaka et Hanor (2003), i.e. > 1 g/L. La seconde étape a été d'analyser les échantillons d'eaux salées pour les éléments chimiques majeurs, mineurs et traces, des isotopes et des gaz rares. Le projet doctoral s'est intéressé à l'étude de traceurs isotopiques spécifiques, entre autres, le strontium ($^{87}Sr/^{86}Sr$), lithium ($\delta^{7}Li$), le bore ($\delta^{11}B$), le brome ($\delta^{81}Br$), le chlore ($\delta^{37}Cl$), le carbone-14 (^{14}C), et les gaz rares pour atteindre le troisième objectif du projet de recherche. Toutes les analyses chimiques et isotopiques ont été réalisées dans des laboratoires certifiés et un laboratoire de recherche a permis de réaliser les analyses des gaz rares.

Les isotopes du strontium ont été utilisés pour comprendre les processus d'interaction eau-roche, car le ratio isotopique dans l'eau reflète celui de la roche et n'est modifié que par mélange (Négrel et al., 2007); les isotopes de bore ont été utilisés car ils permettent de distinguer les contributions de différentes sources (marines, continentales, anthropiques) aux eaux souterraines et d'étudier les conditions hydrologiques passées (Barth, 1993; Négrel et al., 2007). Les isotopes stables du lithium fournissent des informations supplémentaires sur l'altération des silicates, car les minéraux silicatés ont été identifiés comme la source prédominante de Li^{+} dans les eaux, même dans les environnements dominés par les carbonates (McDonough et al., 2021). Les isotopes stables du chlore et du brome sont des outils précieux pour étudier l'origine des sels et des fluides contenant ces éléments, ainsi que pour identifier les processus qui causent le fractionnement isotopique dans les milieux naturels (Eggenkamp et Coleman, 2009; Bagheri et al., 2014). Le ^{14}C et les gaz rares ont été utilisés car ils fournissent des informations sur le temps de résidence des eaux souterraines (Warr et al., 2022; Gimeno et al., 2023).

1.7.4. Format de thèse

Le présent projet doctoral en Sciences de la Terre et de l'Atmosphère adopte le format d'une thèse par articles, qui se compose de trois manuscrits d'articles scientifiques rédigés en anglais. Conformément aux exigences du programme, les articles scientifiques inclus dans ce mémoire de thèse sont, au moment de sa soumission, soumis et/ou publiés dans des revues à comités de lecture. Par conséquent, le présent document est composé de huit chapitres, incluant le présent chapitre introductif, les trois chapitres d'articles scientifiques, un chapitre de discussion qui met en évidence les principales contributions du projet doctoral et qui permet d'ouvrir la voie à des travaux futurs, un chapitre de conclusion générale de l'étude qui rappelle le squelette de l'étude, i.e. la problématique et les objectifs et méthodes, réponse à la question de recherche, retombées et poursuite de la recherche, retombées pour la société. Le Chapitre 7 regroupe toutes les références bibliographiques de cette thèse doctorale et le Chapitre 8 les annexes.

Le présent chapitre a établi le cadre conceptuel de l'étude, en présentant l'état des connaissances sur l'évolution des eaux souterraines, les principaux courants de pensée associés, ainsi que les hypothèses dominantes concernant les processus de salinisation. À partir de cette revue de la littérature, la problématique de recherche a été formulée. Appliquée à la région du SLSJ, cette problématique a conduit à l'énonciation de trois hypothèses de recherche, à partir desquelles ont été définis les trois objectifs principaux de cette thèse. Pour chacun de ces objectifs, une méthodologie appropriée a été mise en œuvre. Chacun de ces objectifs a par ailleurs donné lieu à un article scientifique.

Le second chapitre de ce projet de recherche a permis d'atteindre le premier objectif de cette thèse. Le manuscrit (Ngombe et al., 2025), a été publié dans la revue *Hydrogeology Journal, Special Issue "SI-07 Interplay of Groundwater, Geology and Geological Processes"* en mai 2025 avec comme titre « **Numerical modelling and isotopic evidence of upwelling and mixing of deep, old groundwater with shallow fresh groundwater within the Grenville Province of the Canadian Shield** ». Cet article fournit un aperçu des processus de mélange entre les eaux souterraines profondes et anciennes et les eaux souterraines peu profondes et fraîches à l'aide d'une approche

combinée d'analyse isotopique et de modélisation numérique. L'étude met également en évidence l'influence de la topographie et des structures géologiques sur les régimes d'écoulement, qui ont un impact sur l'évolution chimique des eaux souterraines, et fournit des informations sur les échelles de temps et les profils d'âge des eaux souterraines profondes dans la région du SLSJ.

Le troisième chapitre répond principalement au deuxième objectif de ce projet de recherche. Le manuscrit (Ngombe et al., 2024), a été publié dans la revue *Applied Geochemistry* en mai 2024 et a pour titre « **Application of hierarchical cluster analysis and principal component analysis to identify compositional trends of brine in crystalline basements and sedimentary basins** ». Cette étude explore le contrôle géochimique dans l'évolution des eaux souterraines très anciennes. En effet, l'article a permis d'identifier des signatures géochimiques distinctes des saumures profondes provenant de socles cristallins et de bassins sédimentaires à l'aide d'une base de données mondiale tirée de la littérature. Sur la base de ces différences, un modèle hydrogéochimique conceptuel a été développé, décrivant l'évolution des saumures cristallines et sédimentaires dans leurs milieux respectifs. Les marqueurs géochimiques des saumures identifiés à partir d'outils statistiques dans ce manuscrit ont été utilisés dans la région d'étude afin de compléter l'identification de pôles compositionnels régionaux.

Le quatrième chapitre répond au troisième objectif de thèse. Le manuscrit (Ngombe et al., en cours de publication) a été soumis dans la revue *Journal of Hydrology* en septembre 2025 et a pour titre « **Geochemistry of ancient brines and glacial meltwaters reveals a hydraulic connection between the deep Canadian Precambrian Shield and shallow aquifers** ». Cette étude vise à comprendre comment les systèmes hydrogéologiques anciens et actuels se mélangent et évoluent au fil du temps dans les aquifères fracturés peu profonds de la région étudiée. En effet, à l'aide de l'approche multi-traceurs, l'étude a fourni un aperçu du portrait hydrogéochimique régional en identifiant plusieurs pôles compositionnels régionaux, pour certains hérités de contextes paléohydrogéologiques, complétant ainsi le modèle conceptuel régional proposé par Walter et al. (2023), et mettant en évidence la connectivité hydraulique entre les aquifères de subsurface et les environnements profonds.

1.8. Références

Abascal, E., Gómez-Coma, L., Ortiz, I., et Ortiz, A. 2022. Global diagnosis of nitrate pollution in groundwater and review of removal technologies. Science of the Total Environment **810**: 152233.

Achtziger-Zupančič, P., Loew, S., et Mariethoz, G. 2017. A new global database to improve predictions of permeability distribution in crystalline rocks at site scale. Journal of Geophysical Research: Solid Earth **122**(5): 3513–3539.

Bagheri, R., Nadri, A., Raeisi, E., Eggenkamp, H., Kazemi, G., et Montaseri, A. 2014. Hydrochemical and isotopic (δ18O, δ2H, 87Sr/86Sr, δ37Cl and δ81Br) evidence for the origin of saline formation water in a gas reservoir. Chemical Geology **384**: 62–75.

Barth, S. 1993. Boron isotope variations in nature: a synthesis. Geologische Rundschau **82**: 640–651.

Bein, A., et Arad, A. 1992. Formation of saline groundwaters in the Baltic region through freezing of seawater during glacial periods. Journal of Hydrology **140**(1-4): 75–87.

Bjørlykke, K. 2015. Subsurface water and fluid flow in sedimentary basins. Springer. pp. 279–300.

Bottomley, D.J., Conrad Gregoire, D., et Raven, K.G. 1994. Saline ground waters and brines in the Canadian Shield: Geochemical and isotopic evidence for a residual evaporite brine component. Geochimica et Cosmochimica Acta **58**(5): 1483–1498. doi: 10.1016/0016-7037(94)90551-7.

Bottomley, D.J., Katz, A., Chan, L., Starinsky, A., Douglas, M., Clark, I., et Raven, K. 1999. The origin and evolution of Canadian Shield brines: evaporation or freezing of seawater? New lithium isotope and geochemical evidence from the Slave craton. Chemical Geology **155**(3-4): 295–320.

Boumaiza, L., Stotler, R., et Frape, S. 2024. A review of the major chemical and isotopic characteristics of groundwater in crystalline rocks of the Canadian Shield. Chemical Geology: 122366.

Boumaiza, L., Walter, J., Chesnaux, R., Lambert, M., Jha, M.K., Wanke, H., Brookfield, A., Batelaan, O., Galvão, P., et Laftouhi, N.E. 2022a. Groundwater recharge over the past 100 years: Regional spatiotemporal assessment and climate change impact over the Saguenay-Lac-Saint-Jean region, Canada. Hydrological Processes **36**(3): e14526.

Boumaiza, L., Walter, J., Chesnaux, R., Stotler, R.L., Wen, T., Johannesson, K.H., Brindha, K., et Huneau, F. 2022b. Chloride-salinity as indicator of the chemical composition of groundwater: empirical predictive model based on aquifers in Southern Quebec, Canada. Environmental Science and Pollution Research **29**(39): 59414–59432.

Bucher, K., et Stober, I. 2010. Fluids in the upper continental crust. Geofluids **10**(1-2): 241–253.

Casanova, J., Négrel, P., Petelet-giraud, E., Brach, M., Bourguignon, A., et Millot, R. 2004. Projet PALÉOHYD II Paléohydrologie et géoprospective: modèles conceptuels et processus d'acquisition de la chimie des eaux dans les massifs granitiques: BRGM. Rapport BRGM/RP-53469-FR. 124 p. 98 ill.

Chebotarev, I. 1955. Metamorphism of natural waters in the crust of weathering—1. Geochimica et Cosmochimica Acta **8**(1-2): 22–48.

Clark, I.D., et Fritz, P. 1997. Environmental isotopes in hydrogeology. CRC Press.

Dessureault, R. 1975. Hydrogeologie du Lac Saint-Jean. Partie Nord-Est. Ministère des Richesses Naturelles du Québec. Rapport hydrogéologique No. HG7. pp. 1–90.

Domenico, P.A. 1972. Concepts and models in groundwater hydrology. McGraw Hill.

Edmunds, W., Guendouz, A., Mamou, A., Moulla, A., Shand, P., et Zouari, K. 2003. Groundwater evolution in the Continental Intercalaire aquifer of southern Algeria and Tunisia: trace element and isotopic indicators. Applied Geochemistry **18**(6): 805–822.

Eggenkamp, H., et Coleman, M.L. 2009. The effect of aqueous diffusion on the fractionation of chlorine and bromine stable isotopes. Geochimica et Cosmochimica Acta **73**(12): 3539–3548.

Ferguson, G., McIntosh, J., Warr, O., et Sherwood Lollar, B. 2023. The low permeability of the Earth's Precambrian crust. Communications Earth & Environment **4**(1): 323.

Frape, S., et Fritz, P. 1987. Geochemical trends for groundwaters from the Canadian Shield. Geological Association of Canada-Special Paper **33**: 19–38.

Freeze, R.A., et Cherry, J.A. 1979. Groundwater Prentice-Hall Inc. Eaglewood Cliffs, NJ.

Gascoyne, M., et Kamineni, D. 1994. The hydrogeochemistry of fractured plutonic rocks in the Canadian Shield. Applied Hydrogeology **2**(2): 43–49.

Gimeno, M.J., Tullborg, E.-L., Nilsson, A.-C., Auqué, L.F., et Nilsson, L. 2023. Hydrogeochemical characterisation of the groundwater in the crystalline basement of Forsmark, the selected area for the geological nuclear repositories in Sweden. Journal of Hydrology **624**: 129818.

Guha, J., et Kanwar, R. 1987. Vug brines-fluid inclusions: a key to the understanding of secondary gold enrichment processes and the evolution of deep brines in the Canadian Shield. *Dans* Saline water and gases in crystalline rocks. Ottawa: Geological Association of Canada Special Paper. pp. 95–101.

Hanor, J.S. 1994. Origin of saline fluids in sedimentary basins. Geological Society, London, Special Publications **78**(1): 151–174.

Hébert, C., et Lacoste, P. 1998. Géologie de la région de Jonquière-Chicoutimi Ministère des Ressources naturelles du Québec. . RG 97-08. p. 32.

Hébert, C., et Van Breemen, O. 2004. Mesoproterozoic basement of the Lac St. Jean Anorthosite Suite and younger Grenvillian intrusions in the Saguenay region, Québec: structural relationships and U-Pb geochronology. *Dans* Proterozoic tectonic evolution of the Grenville orogen in North America. *Sous la direction de* L.C. R. P. Tollo, J. M. McLelland & M. J. Bartholomew (Eds.). Geological Society of America. pp. 65–80.

Herut, B., Starinsky, A., Katz, A., et Bein, A. 1990. The role of seawater freezing in the formation of subsurface brines. Geochimica et Cosmochimica Acta **54**(1): 13–21.

Janos, D., Molson, J., et Lefebvre, R. 2018. Regional groundwater flow dynamics and residence times in Chaudière-Appalaches, Québec, Canada: Insights from numerical simulations. Canadian Water Resources Journal/Revue Canadienne des Ressources Hydriques **43**(2): 214–239.

Kharaka, Y.K., et Berry, F.A. 1973. Simultaneous flow of water and solutes through geological membranes—I. Experimental investigation. Geochimica et Cosmochimica Acta **37**(12): 2577–2603. doi: https://doi.org/10.1016/0016-7037(73)90267-6.

Kharaka, Y.K., et Dorsey, N.S. 2005. Environmental issues of petroleum exploration and production: Introduction. Environmental Geosciences **12**(2): 61–63.

Kharaka, Y.K., et Hanor, J. 2003. Deep fluids in the continents: I. Sedimentary basins. Treatise on Geochemistry **5**: 605.

Kloppmann, W., Bourhane, A., et Asfirane, F. 2011. Méthodologie de diagnostic de l'origine de la salinité des masses d'eau. BRGM. p. 129.

Lamontagne, M., et Brouillette, P. 2022. Faults and lineaments of the Quebec City, Charlevoix and Saguenay–Lac-St-Jean regions, Québec. Geological Survey of Canada. Open File 8826. p. 38.

Land, L., et Macpherson, G. 1992. Geothermometry from brine analyses: lessons from the Gulf Coast, USA. Applied Geochemistry **7**(4): 333–340.

LaSalle, P., et Tremblay, G. 1978. Dépôts meubles Saguenay-Lac-Saint-Jean. Québec (Province), Direction générale de la recherche géologique et minérale. RG191. p. 61.

Li, C., Gao, X., Li, S., et Bundschuh, J. 2020. A review of the distribution, sources, genesis, and environmental concerns of salinity in groundwater. Environmental Science and Pollution Research: 1–18.

McCallum, J.L., Dogramaci, S., Bai, A., Cook, P.G., Engdahl, N.B., Simmons, C.T., Skrzypek, G., et Grierson, P.F. 2020. Assessing temporal changes in groundwater recharge using spatial variations in groundwater ages. Water Resources Research **56**(8): e2020WR027240.

McDonough, L.K., Meredith, K.T., Nikagolla, C., et Banati, R.B. 2021. The influence of water–rock interactions on household well water in an area of high prevalence chronic kidney disease of unknown aetiology (CKDu). NPJ Clean Water **4**(1): 2.

McIntosh, J.C., et Ferguson, G. 2021. Deep meteoric water circulation in Earth's crust. Geophysical Research Letters **48**(5): e2020GL090461.

McNutt, R.H., Frape, S.K., et Fritz, P. 1984. Strontium isotopic composition of some brines from the Precambrian Shield of Canada. Chemical Geology **46**(3): 205–215.

Molson, J., et Frind, E. 2023. FLONET/TR2, user guide version 6.0; a two-dimensional simulator for groundwater flownets, contaminant transport and residence time. *Dans* Université Laval and University of Waterloo.

Négrel, P., Lemiere, B., Machard de Grammont, H., Billaud, P., et Sengupta, B. 2007. Hydrogeochemical processes, mixing and isotope tracing in hard rock aquifers and surface waters from the Subarnarekha River Basin,(east Singhbhum District, Jharkhand State, India). Hydrogeology Journal **15**: 1535–1552.

Neuzil, C.E., et Person, M. 2017. Reexamining ultrafiltration and solute transport in groundwater. Water Resources Research **53**(6): 4922–4941.

Ngombe, O.G., Walter, J., Chesnaux, R., et Molson, J. 2024. Application of hierarchical cluster analysis and principal component analysis to identify compositional trends of brine in crystalline basements and sedimentary basins. Applied Geochemistry: 106030.

Ngombe, O.G.D., Walter, J., Molson, J., et Chesnaux, R. 2025. Numerical modeling and isotopic evidence of upwelling and mixing of deep, old groundwater with shallow fresh groundwater within the

Grenville Province of the Canadian Shield. Hydrogeology Journal. doi: 10.1007/s10040-025-02914-2.

Nisson, D., Kieft, T., Drake, H., Warr, O., Lollar, B.S., Ogasawara, H., Perl, S., Friefeld, B., Castillo, J., et Whitehouse, M.J. 2023. Hydrogeochemical and isotopic signatures elucidate deep subsurface hypersaline brine formation through radiolysis driven water-rock interaction. Geochimica et Cosmochimica Acta **340**: 65–84.

Nordstrom, D.K., Ball, J.W., Donahoe, R.J., et Whittemore, D. 1989. Groundwater chemistry and water-rock interactions at Stripa. Geochimica et Cosmochimica Acta **53**(8): 1727–1740.

Pauwels, H., Fouillac, C., et Fouillac, A.-M. 1993. Chemistry and isotopes of deep geothermal saline fluids in the Upper Rhine Graben: Origin of compounds and water-rock interactions. Geochimica et Cosmochimica Acta **57**(12): 2737–2749.

Rivers, T., Martignole, J., Gower, C., et Davidson, A. 1989. New tectonic divisions of the Grenville Province, southeast Canadian Shield. Tectonics **8**(1): 63–84.

Rouleau, A., Daigneault, R., Walter, J., Germaneau, D., Tremblay, M.L., et Lambert, M. 2013. Résultats du programme d'acquisition de connaissances sur les eaux souterraines de la région Saguenay-Lac-Saint-Jean (Results of the groundwater knowledge acquisition programme in the Saguenay-Lac-Saint-Jean region). Ministère du Développement durable, de l'Environnement et de la Lutte contre les changements climatiques (Ministry of Sustainable Development, Environment and the Fight Against Climate Change), MDDELCC p. 248.

Roy, D.W., Beaudoin, G., Leduc, É., Rouleau, A., Walter, J., Chesnaux, R., et Cousineau, P.A. 2011. Isostasie postglaciaire différentielle au Lac-Saint-Jean (Québec) et implications sur la qualité de l'eau souterraine. Geohydro 2011, Québec.

Savoye, S. 1998. Origine de la salinité des eaux souterraines en milieu granitique: identification et caractérisation des sources de chlorure. Thèse de doctorat, Terre, océan, espace, Paris 11, Paris, France.

Sherwood-Lollar, B., Heuer, V.B., McDermott, J., Tille, S., Warr, O., Moran, J., Telling, J., et Hinrichs, K.-U. 2021. A window into the abiotic carbon cycle–Acetate and formate in fracture waters in 2.7 billion year-old host rocks of the Canadian Shield. Geochimica et Cosmochimica Acta **294**: 295–314.

Shouakar-Stash, O., Alexeev, S., Frape, S., Alexeeva, L., et Drimmie, R. 2007. Geochemistry and stable isotopic signatures, including chlorine and bromine isotopes, of the deep groundwaters of the Siberian Platform, Russia. Applied Geochemistry **22**(3): 589–605.

Snowdon, A.P., Normani, S.D., et Sykes, J.F. 2021. Analysis of crystalline rock permeability versus depth in a Canadian Precambrian rock setting. Journal of Geophysical Research: Solid Earth **126**(5): e2020JB020998.

Tóth, J. 1963. A theoretical analysis of groundwater flow in small drainage basins. Journal of Geophysical Research **68**(16): 4795–4812.

Tóth, J. 1999. Groundwater as a geologic agent: an overview of the causes, processes, and manifestations. Hydrogeology Journal **7**(1): 1–14.

Trudel, C., et Malo, M. 1993. Analyses des contraintes par méthodes graphiques dans une zone de coulissage: exemple de la région de Matapédia, Gaspésie, Appalaches du Québec. Canadian Journal of Earth Sciences **30**(3): 591–602.

Vovk, I. 1981. Radiolytic model of formation of composition of brines in crystalline basement of the shields. Geokhimiya(4): 467–480.

Walter, J. 2010. Les eaux souterraines à salinité élevée autour du lac Saint-Jean, Québec: origines et incidences. Mémoire de maîtrise, Sciences de la Terre et de l'Atmosphèree, Université du Québec à Chicoutimi, Québec, Canada.

Walter, J., Chesnaux, R., Boumaiza, L., Brindha, K., et Regenspurg, S. 2023. Conceptual model for the chemical evolution of groundwater in a region of the Canadian Precambrian shield covered by soft Quaternary deposit of glacial and marine origin. Applied Geochemistry **150**: 105574.

Walter, J., Chesnaux, R., Cloutier, V., et Gaboury, D. 2017. The influence of water/rock− water/clay interactions and mixing in the salinization processes of groundwater. Journal of Hydrology: Regional Studies **13**: 168–188.

Walter, J., Chesnaux, R., Gaboury, D., et Cloutier, V. 2019. Subsampling of regional-scale database for improving multivariate analysis interpretation of groundwater chemical evolution and ion sources. Geosciences **9**(3): 139.

Walter, J., Rouleau, A., Clark, I.D., et Guha, J. 2006. A first investigation of groundwater geochemistry in the crystalline bedrock around lake Saint-Jean, Québec. 59th Canadian Geotechnical Conference and 7th Joint CGS/IAH-CNC Groundwater Specialty Conference - Sea to Sky Geotechnique 2006, Fairmont Hotel, Vancouver, British Columbia, Canada, October 1–4, 2006, X-CD Technologies Incorporated, pp. 1553–1560.

Warner, N.R., Jackson, R.B., Darrah, T.H., Osborn, S.G., Down, A., Zhao, K., White, A., et Vengosh, A. 2012. Geochemical evidence for possible natural migration of Marcellus Formation brine to shallow aquifers in Pennsylvania. Proceedings of the National Academy of Sciences **109**(30): 11961–11966.

Warr, O., Ballentine, C., Onstott, T., Nisson, D., Kieft, T., Hillegonds, D., et Sherwood Lollar, B. 2022. 86Kr excess and other noble gases identify a billion-year-old radiogenically-enriched groundwater system. Nature Communications **13**(1): 3768.

Warr, O., Giunta, T., Onstott, T.C., Kieft, T.L., Harris, R.L., Nisson, D.M., et B, S.L. 2021. The role of low-temperature 18O exchange in the isotopic evolution of deep subsurface fluids. Chemical Geology **561**: 120027.

Yardley, B.W., et Bodnar, R.J. 2014. Fluids in the continental crust. Geochemical Perspectives **3**(1): 1–2.

Chapitre 2 : NUMERICAL MODELLING AND ISOTOPIC EVIDENCE OF UPWELLING AND MIXING OF DEEP, OLD GROUNDWATER WITH SHALLOW FRESH GROUNDWATER WITHIN THE GRENVILLE PROVINCE OF THE CANADIAN SHIELD

Othniel G.D. Ngombe[1,3]*, Julien Walter[1,3], John Molson[2], Romain Chesnaux[1,3]

[1] Département des Sciences appliquées, Université du Québec à Chicoutimi, Saguenay, Québec, G7H 2B1, Canada

[2] Département de géologie et de génie géologique, Université Laval, Québec, Québec, G1V 0A6, Canada

[3] Centre d'études sur les ressources minérales, Groupe de recherche Risque Ressource Eau, Université du Québec à Chicoutimi, Saguenay, Québec, G7H 2B1, Canada

HYDROGEOLOGY JOURNAL

Special Issue "SI-07 Interplay of Groundwater, Geology and Geological Processes"

2025

2.1. Mise en contexte

Ce chapitre sert l'objectif 1 en testant l'hypothèse de remontée de fluides profonds le long des failles du graben et de leur mélange avec des eaux météoriques peu profondes. Pour ce faire, une approche intégrée combine les analyses isotopiques ($\delta^{2}H$-$\delta^{18}O$, $^{87}Sr/^{86}Sr$) et une modélisation 2D de l'écoulement et du transport advectif-dispersif de l'âge pour explorer les conditions hydrodynamiques profondes. Les évidences isotopiques indiquent que certains échantillons d'eau saumâtre collectés en subsurface ont subi d'intense interaction avec la roche durant des centaines de millions d'années. La simulation de l'âge montre également des âges > 100 Ma. Les simulations montrent que le fort gradient topographique régional entre les hautes terres et les basses terres peut induire des flux ascendants amenant des eaux très anciennes à faibles profondeurs. Les failles du Graben du Saguenay agissent comme voies préférentielles. Ainsi, le Chapitre 2 établit le cadre hydrodynamique qui valide l'objectif 1 et précise les paramètres (profils d'âges des eaux souterraines et interconnectivité entre divers réservoirs géologiques) à considérer pour la suite de la thèse.

2.2. Author contribution

Othniel G.D. Ngombe: Investigation, Methodology, FLONET/TR2 input file editing, Visualization, Writing – original draft, Writing – review & editing.

Julien Walter: Project administration, Methodology, Supervision, Writing – review & editing.

John Molson: Supervision, Methodology, FLONET/TR2 code revisions, Visualization, Writing – review & editing.

Romain Chesnaux: Supervision, Methodology, Writing – review & editing.

2.3. Abstract

Shallow brackish groundwater is a significant issue affecting water supplies in the Saguenay-Lac-Saint-Jean region of the Grenville Province, Canada. A sample taken from a 45 m deep well in 2023 returned a total dissolved solids value of around 30 g/L, which represents the most saline groundwater found in the region. To explain this anomaly, two-dimensional numerical simulations of groundwater flow and advective-dispersive age transport were conducted, along with isotopic analyses. The role of Saguenay Graben faults on deep brine migration to the surface was also investigated. Stable water isotopes and strontium isotope ratios suggest that brackish groundwater from fractured bedrock in the region represents a mixture between meteoric water and deep brines within the Precambrian Shield, which has experienced extensive water-rock interaction over geological time scales. Numerical models demonstrated that deep, old groundwater could upwell towards the surface within a regional hydraulic system. The results highlight that, under the imposed boundary conditions, vertical hydraulic gradients can sustain this deep upward flow. However, regional flow is less significant in comparison to local flow systems which dilute the upwelling brine. The simulated deep groundwater ages, on the order of hundreds of millions of years, are similar to some ages of deep Precambrian Shield brines identified elsewhere in the Canadian Shield. Parametric tests suggest that graben faults facilitate groundwater upwelling and act as preferential pathways for deep and ancient groundwater. These findings help explain the presence of shallow brackish groundwater through the mixing of shallow freshwater and old groundwater.

Keywords: regional flow, numerical modelling, fault-conduit flow, groundwater age, Canada.

2.4. Introduction

Saline groundwaters are frequently found in deep crystalline basements around the world at depths of several kilometers (Bottomley et al., 1999; Hebig et al., 2012; Gimeno et al., 2023). In the Canadian Shield, brines have been identified both in the context of deep nuclear waste disposal sites and mining sites (Frape et Fritz, 1982; Frape et Fritz, 1987). These brines have been the subject of several scientific studies, and important advances have been made concerning their chemical origin.

Groundwater salinity generally increases with depth and residence time as water-rock interactions progress (Tóth, 1999). In the Canadian Shield, freshwater is generally found at depths of less than 200 m, saline water is found between 200 and 500 m, while brines, which have reacted with silicate minerals over time periods of hundreds of millions of years, are generally found at depths greater than 1,000 m (Gascoyne et Kamineni, 1994; Boumaiza et al., 2024). According to the gravity-driven flow system of the Tóth (1999) model, which introduced a hydraulic dimension to groundwater evolution, a direct link exists between the chemical evolution of groundwater, the hydraulic regime, residence time, and the scale of the flow system (local, intermediate and regional). Fossil groundwaters, trapped in less permeable geological units, can also reach geologic timescales in age (Warr et al., 2022) until mobilized by tectonic or anthropogenic processes which create or reactivate fractures and faults (Warr et al., 2018).

The salinization of shallow groundwater from deep brines has been described in several studies. For instance, the upward movement of deep groundwater to discharge areas has been attributed to high hydrodynamic pressures at depth, combined with the existence of high-permeability fracture zones, which provide pathways to the surface (Warner et al., 2012). Based on hydrogeochemical evidence in the east-central Permian basin, Stueber et al. (1998) showed evidence of migration and mixing of deep brine into shallow aquifers.

Faults can act as preferential flow pathways for deep groundwater. For example, based on geophysical and geochemical datasets, Llewellyn (2014) showed that deep Appalachian Basin brine

had migrated upward into shallow aquifers through inferred faults and topographic lineaments. In the crystalline basement of the Black Forest region, Germany, Stober et Bucher (1999) observed distinct upwelling of deep groundwater in response to topography-driven flow. Furthermore, during construction of the Gotthard rail base tunnel in Switzerland, Bucher et Stober (2010) observed significant fluid fluxes at depths of 2,500 m, carrying deep saline groundwaters toward discharge areas. More recently, using flow and advective-dispersive age transport modelling, Janos et al. (2018) suggested that the Jacques Cartier River fault in southern Quebec, Canada, can act as a major pathway for upward migration of deep saline fluids, driven by regional flow towards discharge zones.

Recent research in the Saguenay-Lac-Saint-Jean (SLSJ) region in Quebec, Canada, through the PACES program (Quebec Groundwater Knowledge Acquisition Program) has provided important information on regional aquifers and groundwater quality (Walter et al., 2018). Some of these studies identified saline groundwater from shallow residential wells with total dissolved solids (TDS) > 1 g/L, making it an important regional issue. These groundwaters have been found in granular aquifers from the Pleistocene period and in fractured aquifers from Ordovician sedimentary rocks and from the Grenville Province of the Canadian Shield. Based on multivariate statistical analyses, Walter et al. (2017) describe two evolutionary salinity pathways in this area. The first pathway involves interactions between shallow groundwater and clays from the Laflamme Sea, which flooded the lowland areas of the SLSJ region approximately 10,000 to 12,000 yrs ago. The second pathway involves groundwater from water-rock interactions, which is assumed to be a diluted member of deep Precambrian Shield brines (PSB), which are known to be ancient, i.e., > 1 Ma (Holland et al., 2013). Walter et al. (2023) proposed a conceptual model for hydrogeochemical evolution of groundwater in the SLSJ region, which invokes upwelling of deep, old PSB to explain the presence of brackish groundwater from fractured bedrock in shallow residential wells.

In the SLSJ region, upwelling of deep groundwater can be facilitated by geological structures such as the Saguenay Graben faults. The distribution of brackish groundwater from fractured bedrock along such fault systems in the study area suggests that faults may indeed play an important role in upwelling of deep fluids towards the surface (Walter et al., 2017). A regional flow model of Tóth

(1999), applied to the Saguenay Graben and its fault system, could explain the presence of brackish groundwater from shallow fractured rock in regional discharge zones (Walter et al., 2017; Walter et al., 2023). However, neither the gravity-driven flow hypothesis nor the role of faults has been quantitatively studied to explain the upwelling of deep saline groundwater in these discharge zones. A fundamental need therefore exists to analyze the spatial distribution of deep groundwater flow paths in order to explain the presence of these assumed ancient groundwaters in the shallow fractured aquifers of the SLSJ region. The present study aims to test existing hypotheses, including hydraulic aspects of the SLSJ conceptual hydrogeochemical evolution model proposed by Walter et al. (2023).

To identify and confirm the presence of diluted-PSB in the study area, we incorporate isotopic evidence, including water isotopes ($\delta^{18}O$ and $\delta^{2}H$) and strontium isotope ratios ($^{87}Sr/^{86}Sr$). A two-dimensional numerical gravity flow and age model was developed from existing data. Numerical modelling without faults was first used to investigate whether a gravity flow model alone could explain deep PSB upwelling in a 56.3 km long and 5.4 km deep cross-section (Figure 2-1). Finally, a parametric study on the role of graben faults was carried out to assess their role as preferential pathways for deep groundwater to migrate toward the surface.

The present paper provides a detailed view of the mixing processes between deep, old groundwater and shallow, fresh groundwater using a combined approach of isotopic analysis and numerical modelling. The study also highlights how topography and geological structure influence flow regimes, which affect the chemical evolution of groundwater, and offers insights into the time scales and age patterns of deep groundwater in the Grenville province of the Canadian Shield. This knowledge can support regional decision-makers responsible for water policy and management, to protect drinking water resources in shallow aquifers.

2.5. Study area

The SLSJ region covers an area of 98,710 km^2, and has a population of about 271,500 which is concentrated mainly around Lac Saint-Jean (a large freshwater lake) and the Saguenay River (Walter et al., 2018). Figure 2-1 shows the municipal boundaries of the SLSJ region, which represent

approximately 15% of the administrative region. Geologically, the 180-million-year-old Saguenay Graben controls the region's topography. The graben is bound by west-northwest (WNW) trending faults (Du Berger et al., 1991; Walter et al., 2017), separating the highlands, which rise up to 1,000 m above sea level (asl), from the lowlands, which are between 0 and 200 m asl. The present study focuses on a specific area, encompassing both of these main geomorphological structures, i.e., highlands and lowlands (Figure 2-1).

The geology of the SLSJ region is dominated by plutonic rocks from the Canadian Precambrian Shield, specifically relating to the Grenville Province (Hébert et Lacoste, 1998), approximately 25% of which is characterized by anorthosite intrusions (Hébert et al., 2005). This part of the Grenville Province is partially overlain by Paleozoic sedimentary formations from the Middle Ordovician, dated around 450 Ma. Sedimentary rocks include siliciclastic strata, micritic limestones, and alternating layers of limestone and shale which are sometimes very fossil-rich. Above these fractured rocks, late Wisconsinian fluvioglacial deposits, postglacial clays from the Laflamme Sea, and deltaic and littoral sediments which accumulated in the Late Pleistocene and Early Holocene, complete the regional stratigraphy (Walter et al., 2018).

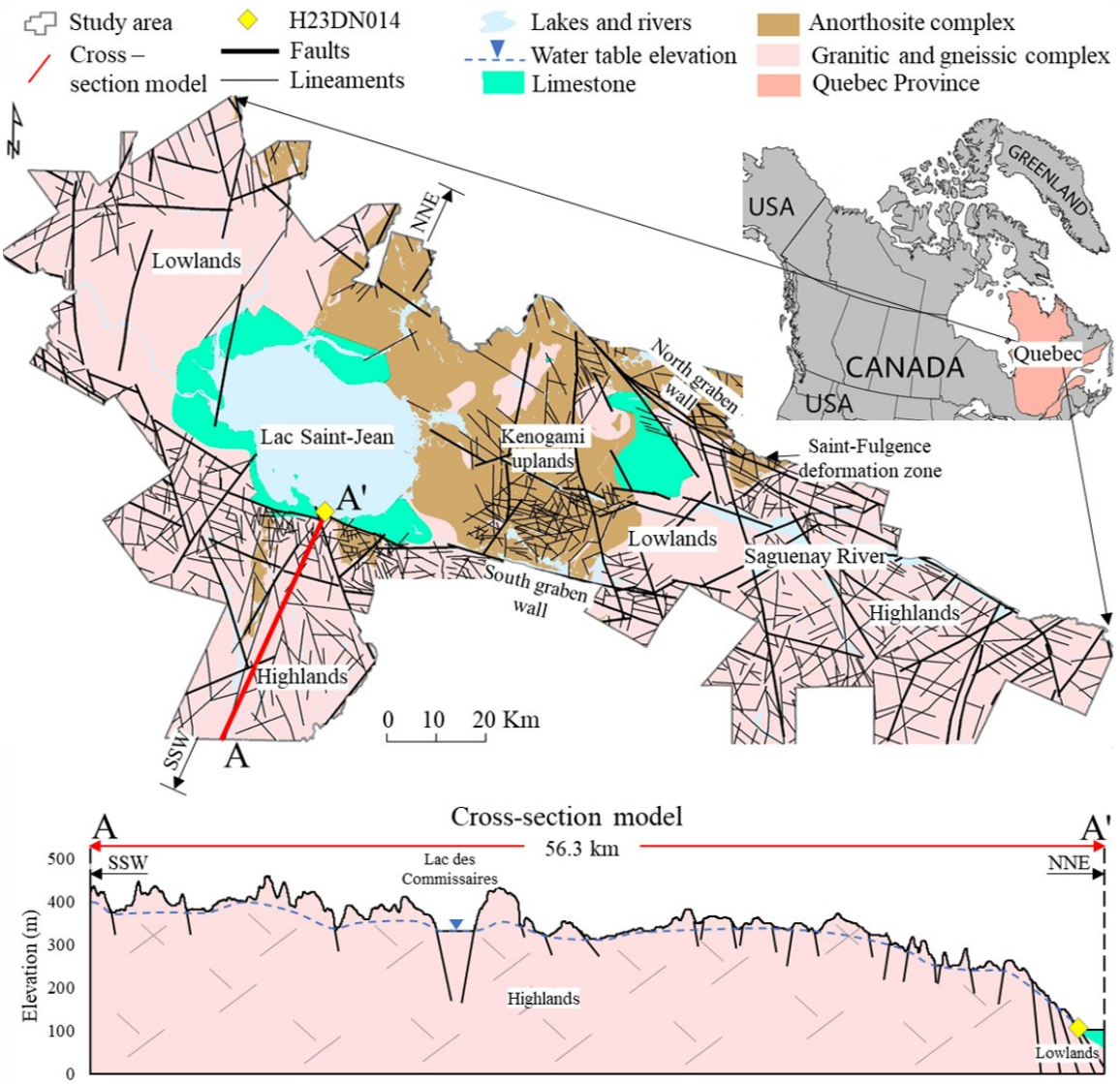

Figure 2-1: Location of the SLSJ study area, showing simplified geological features, and location of the hydro-stratigraphic cross-section (A-A') used in the two-dimensional model. Faults and lineaments are from the PACES-SLSJ study (Rouleau et al. 2013). Vertical exaggeration is 20×. Geological and structural layers taken from SIGEOM 2025.

2.6. Methodology

Isotopic data was used to identify and confirm the presence of deep PSB in shallow aquifers of the study area. Numerical simulations of groundwater flow and age transport were also performed in order to investigate whether a gravity flow model could explain the deep PSB upwelling.

2.6.1. **Isotopic data collection**

Isotopic data ($\delta^{18}O$ and $\delta^{2}H$ and $^{87}Sr/^{86}Sr$) from brackish groundwater samples were all obtained from domestic wells from the outlet of an outside tap. A total of 14 samples were selected based on their geological locations (crystalline rocks) and their TDS content, i.e. where TDS > 1 g/L. To date, sample H23DN014 (TDS = 29.6 g/L), identified along cross-section AA', represents the most saline groundwater found in the region. This sample was collected from a 45-m-deep domestic well, with a water level of 5.8 m below the ground surface and located 60 m upgradient from Lac Saint-Jean. The well, screened to limestone above crystalline bedrock, intersects a thin layer of Laflamme Sea clay (< 1 m) at the ground surface.

A 20 L flow cell was used during sampling to minimize external contamination. A garden hose Y-adapter was used to connect the flow cell to the house outlet. Another Y-shaped adapter at the outlet of the flow cell was used to collect strontium isotope samples in 250 mL HDPE bottles. Strontium was analyzed for the ratio $^{87}Sr/^{86}Sr$ using a thermal ionization mass spectrometer (TIMS) at the Environmental Isotope Laboratory (University of Waterloo, Canada). Water stable isotope samples were collected directly from the flow cell into 30 mL glass containers. The containers were sealed with septum caps to prevent any exchange with air. Samples were then analyzed for $\delta^{18}O$ and $\delta^{2}H$ at the Geotop-UQAM laboratories (Université du Québec à Montréal, Canada) using an isotope ratio mass spectrometer (IRMS) after preparation with the AquaPrep^{TM} system. The 14 brackish water samples were analyzed for major, minor and trace elements, which were collected in appropriate containers and preserved with suitable agents supplied by the ALS Laboratory Group Ltd. in Waterloo, ON, Canada. In this study, the results for dissolved strontium content are also presented.

2.6.2. **Theoretical framework**

In the context of understanding deep flow systems, groundwater age, defined as the time elapsed since water entered the subsurface (Xie et al., 2022b; Starn et al., 2023), is a central theme, as old groundwaters in cratons are generally associated with higher salinity and greater depths (Gascoyne et Kamineni, 1994). Although hydraulic conditions may evolve, groundwater age patterns may remain unchanged, reflecting past hydraulic conditions, particularly in deep environments where

mixing and groundwater renewal are limited (McCallum et al., 2020). Consequently, to explain the presence of assumed deep ancient groundwater at shallow depths, groundwater flow simulations were coupled to an advective-dispersive age transport model. This coupling explored the hydrodynamic conditions under which deep groundwater upwelling could occur and added further insight into time scales and deep and shallow groundwater age patterns in the study region.

In the present study, ancient groundwater was defined as any groundwater older than 1 Ma. Bedrock was subdivided into shallow fractured aquifers (0 – 100 m), where local flow occurs, less fractured bedrock (100 – 500 m), where intermediate flow occurs, and unfractured bedrock (> 500 m), where regional flow occurs (Figure 2-2). Local flow was defined as being dominated by young groundwater and regional flow as dominated by ancient groundwater. Intermediate flow is found in transition zones between young and ancient groundwater.

2.5.3. Numerical modelling approach

2.5.3.1. Groundwater flow

In this article, a two-dimensional numerical model was developed to simulate regional-scale groundwater flow as described in the theoretical approach of Tóth (1999), using potentiometric data from the PACES-SLSJ database (Rouleau et al., 2013; Walter et al., 2018), and for simulating mean groundwater age using an advective-dispersive equation (Goode, 1996). Various fault configurations were included to evaluate their effect on groundwater ages in the regional discharge zone.

The FLONET/TR2 code was used for all simulations of groundwater flow and mean age transport (Molson et Frind, 2023). The two-dimensional steady-state groundwater flow system is represented by solving the following equations for hydraulic heads (Eq. 1) and stream functions (Eq. 2):

$$\frac{\partial}{\partial x}\left(K_{xx}\frac{\partial \varphi}{\partial x}\right)+\frac{\partial}{\partial z}\left(K_{zz}\frac{\partial \varphi}{\partial z}\right)=0 \quad (2.1)$$

$$\frac{\partial}{\partial x}\left(\frac{1}{K_{zz}}\frac{\partial \psi}{\partial x}\right)+\frac{\partial}{\partial z}\left(\frac{1}{K_{xx}}\frac{\partial \psi}{\partial z}\right)=0 \quad (2.2)$$

where x and z are the horizontal and vertical coordinate directions, respectively (L), K_{xx} and K_{zz} are the principal components of the hydraulic conductivity tensor (L/T), φ is the hydraulic head (L) and ψ is the stream function (L^2/T). The approach assumes steady-state saturated flow with a uniform temperature and salinity.

2.5.3.2. Groundwater age

Following execution of the flow model, the steady-state flow field was used to simulate mean steady-state groundwater age using Equation (3):

$$\frac{\partial}{\partial x_i}\left(D_{i,j}\frac{\partial A}{\partial x_j}\right) - v_i\frac{\partial A}{\partial x_i} + 1 = 0 \qquad (2.3)$$

where A is the mean groundwater age (T), x_i are the spatial coordinates, D_{ij} is the hydrodynamic dispersion tensor (L^2/T), v_i is the flow velocity vector (L/T), and the +1 term indicates water aging by 1 day/day.

For the transport model, we assume a four-component dispersion formulation (Lichtner et al., 2002), with two horizontal components α_L^H = 20 m, α_L^V = 10 m, and two transverse components α_T^H and α_T^V which were both set at 0.05 m. Similar to a conservative tracer, a molecular diffusion coefficient of 5×10^{-10} m^2/s was applied in the model (Molson et Frind, 2012). See Molson et Frind (2023) for further details on the method.

2.5.4. Domain description

The numerical model domain corresponds to a two-dimensional geologic cross-section, which is 56.3 km long with a maximum depth of 5.4 km (Figure 2-1 shows the first 400 meters) and oriented north-northeast (NNE), extending from the boundary of the Lac Saint-Jean watershed to Lac Saint-Jean, which acts as the regional groundwater discharge zone (Walter et al., 2018).

2.5.5. Material properties

In this study, shallow Quaternary sediments, mainly consisting of till, were neglected since they are generally thin (< 1 m) and discontinuous in the highlands. Although greater thicknesses, of the order of several tens of meters, are sometimes found in valleys and in the transition zone between

the highlands and lowlands, the contrast in hydraulic properties leads to rapid shallow flow systems over short distances. Including these deposits would unnecessarily complexify the model. Thus, the study area was subdivided vertically into three bedrock layers: a shallow regional aquifer (fractured bedrock), an intermediate layer of less fractured bedrock, and deep unfractured bedrock (Figure 2-2).

2.5.5.1. Shallow aquifer

Hydraulic properties in the region are only documented for the first 100 m (within the shallow fractured rock aquifer), and are summarized by Richard et al. (2016) who provided an overview of the bedrock hydraulic properties in the SLSJ region using historical records of specific yield data. The average transmissivity (T) of the fractured rock aquifer was estimated at 4.25×10^{-5} m^2/s. Chesnaux (2013) determined regional recharge into the rock aquifer through an analytical interpretation of the hydraulic head profiles within the Kenogami Uplands aquifer (Figure 2-1) of the SLSJ area. His results show an average hydraulic conductivity of the aquifer of 4.3×10^{-7} m/s and a recharge equivalent to approximately 3.5 mm/yr.

Hydraulic conductivity values (K) for shallow crystalline aquifers vary significantly across different rock types (Richard et al., 2011). For example, anorthosite, which is generally less fractured, shows both the highest and lowest K values in the regional crystalline fractured rocks of the SLSJ area. However, for the sake of consistency with previous research in the region, a horizontal hydraulic conductivity (K_x) of 4.3×10^{-7} m/s (representing the average K value of Kenogami Uplands) and a porosity according to Montcoudiol et al. (2017) (see Tableau 2-1 for details) were applied in the shallow aquifer. The model also includes an anisotropy ratio of $K_x/K_z = 5$, which is consistent with the groundwater flow simulation study of Montcoudiol et al. (2017) in a part of the Canadian Shield also featuring Grenville Province crystalline rocks, as is the case in the study area.

2.5.5.2. Intermediate and deep layers

Several studies have shown exponential decreases in hydraulic conductivity with depth in continental shield environments (Normani et Sykes, 2012; Ferguson et al., 2023). Using a global database of in situ permeability measurements in crystalline rocks, Achtziger-Zupančič et al. (2017)

derived a linear log-log relationship where permeability decreases by more than three orders of magnitude to a depth of 2,000 m below the ground surface (from 10^{-12} m^2 at shallow depths to 10^{-15} m^2). Stevenson et al. (1996) showed that at depths > 500 m, hydraulic conductivity in unaltered and unfractured crystalline rock systems is commonly lower than in the near-surface zone, varying from 10^{-9} to 10^{-13} m/s. In the Canadian Shield, Snowdon et al. (2021) developed an exponential relationship between permeability and depth. Their research showed differences between fracture zones, whose permeability reaches 10^{-14} m^2 at 500 m, and the unfractured rock matrix, which has an average permeability of 10^{-16} m^2. Using noble gas residence times, Ferguson et al. (2023) estimated permeability values at greater depths (> 1,000 m) in shield environments, which showed no significant correlation with depth. These estimated values are at least an order of magnitude lower than previous studies, reaching, for example, 10^{-18} m^2 at 3,000 m (Ferguson et al., 2023). To maintain consistency with the literature, i.e. decreasing hydraulic properties with depth, and to address the lack of hydraulic conductivity data at greater depths in the SLSJ study area, the numerical model developed here subdivides the less fractured bedrock into two sub-layers based on their hydraulic properties (Tableau 2-1). A deep hydraulic conductivity of 4.3×10^{-11} m/s was applied in the current model. All hydraulic parameters applied in the model are presented in Tableau 2-1.

Tableau 2-1: Hydraulic conductivities and porosities of the protolith layers applied in the numerical model. An anisotropy factor of K_{Px}/K_{Pz} =5 is applied to all layers. At corresponding depths, fault porosities were assumed the same as in the adjoining bedrock layers.

Bedrock layers	Depth (m)	K_{Px}[1] (m/s)	Porosity[2]	References[3]
Fractured bedrock	0 - 100	4.3×10^{-7}	0.03	Chesnaux (2013), Caine (2006), Welch et Allen (2014)
Less fractured bedrock	100 - 300	4.3×10^{-8}	0.02	Montcoudiol et al. (2017), Desbarats (2002)
	300 - 500	4.3×10^{-9}	0.01	Kuchling et al. (2000), Stober et Bucher (2007)
Unfractured bedrock	> 500	4.3×10^{-11}	0.01	Janos et al. (2018), Farvolden et al. (1988)

[1] K_{Px}: Principal hydraulic conductivity of the protolith (in the horizontal x direction)
[2] Porosity was applied according to Montcoudiol et al. (2017)
[3] References which support the chosen values.

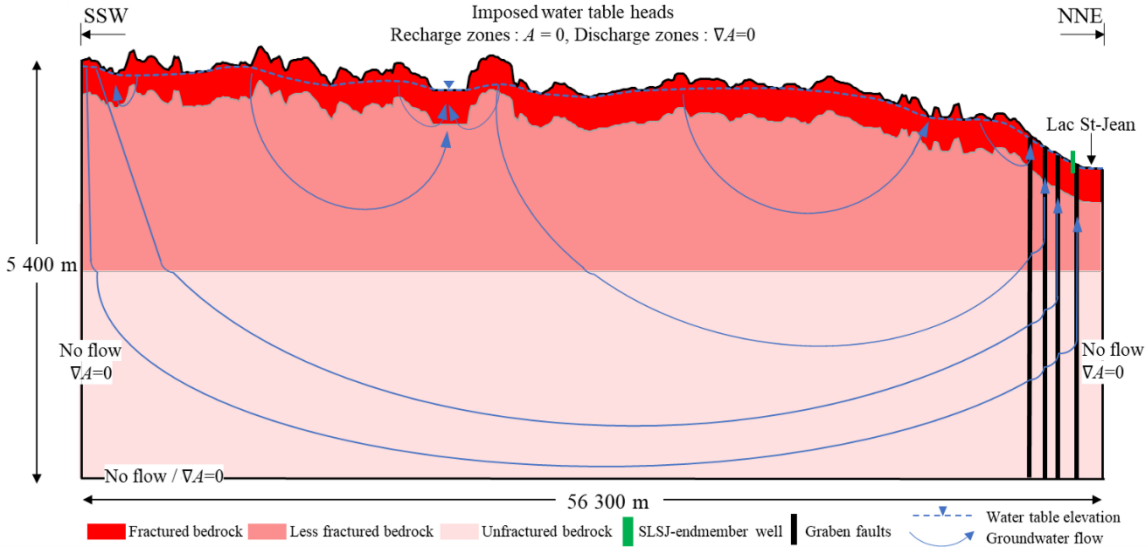

Figure 2-2: Conceptual model showing bedrock structure and fault locations, as well as the assumed boundary conditions used in the flow and age transport simulations. Vertical exaggeration is 10×.

2.5.6. Fault configurations

Faults can act as either flow conduits or barriers, in either case facilitating groundwater upwelling (Janos et al., 2018). In the SLSJ region, visible fault displacements (areas where one part of the bedrock has moved relative to another) have not been directly observed. However, the presence of geomorphological structures such as the Saguenay Graben or Kenogami Uplands (Figure 2-1) provides a reasonable basis for their inclusion in the present model (Du Berger et al., 1991; Roy et al., 1993; Walter et al., 2018). Within the study area, graben faults are located where the main topographic lineaments shown in Figure 2-1 mark the boundary between the lowlands and the highlands of the graben, and which correspond to zones with an elevation difference of approximately 120 meters over 5 km (Figure 2-2 and Figure 2-3a). The present report assumes that fault zones, with their hydraulic conductivity altered by deformation, differ from the undeformed surrounding protolith (Tableau 2-2). Specifically, the surrounding damage zone, which is more fractured and more permeable, may serve as a conduit for upward fluid flow, while the fault core, which is frequently less permeable due to deformation, may act as a barrier (Bense et al., 2013). In this study, fault behavior (as a conduit or barrier) was interpreted according to the study of Janos et

al. (2018). The objective of the present approach is to assess the effect of hydraulic conductivity contrasts within these fault structures on upward movement of deep ancient pore fluids.

Tableau 2-2: Simulated fault hydraulic conductivity scenarios. See Figure 2-3 for fault geometry. All values represent principal components of the K tensor in the respective rock units, i.e. the horizontal component in the protolith (P) and vertical components in the fault zones (FC and DZ). In all cases, the orthogonal K component was 5× lower.

Fault hydraulic behavior[1]	Scenarios	Fault core (FC)	Damage zone (DZ)
Basic case	A	K_{FC}[2] = K_P[3]	K_{DZ} [4]= K_P
Barrier	B	$K_{FC} = K_P \times 0.1$	$K_{DZ} = K_P$
Barrier	C	$K_{FC} = K_P \times 0.01$	$K_{DZ} = K_P$
Conduit	D	$K_{FC} = K_P$	$K_{DZ} = K_P \times 10$
Conduit-barrier-conduit	E	$K_{FC} = K_P \times 0.1$	$K_{DZ} = K_P \times 10$
Conduit-barrier-conduit	F	$K_{FC} = K_P \times 0.01$	$K_{DZ} = K_P \times 10$
Conduit	G	$K_{FC} = K_P$	$K_{DZ} = K_P \times 100$
Conduit-barrier-conduit	H	$K_{FC} = K_P \times 0.1$	$K_{DZ} = K_P \times 100$
Conduit-barrier-conduit	I	$K_{FC} = K_P \times 0.01$	$K_{DZ} = K_P \times 100$

[1] Fault hydraulic behavior was interpreted according to the study of Janos et al. (2018).
[2] K_{FC}: Principal hydraulic conductivity of the fault core (vertical direction).
[3] K_P: Principal hydraulic conductivity of the protolith (horizontal direction), (=K_{Px} in Tableau 2-1)
[4] K_{DZ}: Principal hydraulic conductivity of the damage zone (vertical direction).

The numerical cross-sectional model was developed to examine four fault configurations, which define the boundaries between the highlands and lowlands (Figure 2-1). In the SLSJ model, faults were placed at principal topographic slope ruptures (Figure 2-3a). The sampling site where the H23DN014 sample was collected is located at the NNE of the model in the lowest topographic elevation area. The possibility of faults acting as preferential pathways for deep groundwater upwelling was investigated by looking at how flow and age transport are modified by different hydraulic conductivity contrasts between the fault core and damage zones (Figure 2-3). In the current study, for the sake of simplicity, graben faults are assumed to be vertical and represented by an equivalent porous medium. Fault porosities were applied at corresponding depths according to Tableau 2-1. The fault introduces anisotropy into the medium, making permeability dependent on direction of the fault (Cartaud, 2004). Assuming the principal K in a fault is along the fault direction, and that groundwater flow is mainly vertical in the faults (Figure 2-3b), all faults were assigned an anisotropy of K_x/K_z = 1/5. Graben fault K values differ by up to two orders of magnitude from the surrounding protolith from one scenario to the next (Figure 2-3).

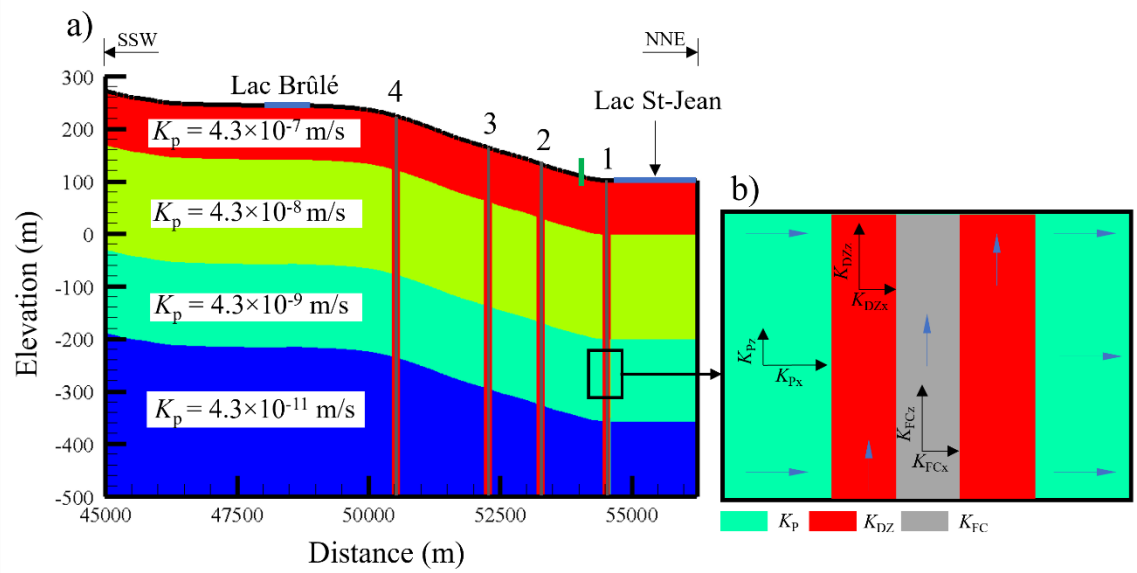

Figure 2-3: a) Conceptual representation of Saguenay Graben fault structures near Lac Saint-Jean, numbered 1 to 4. The green mark indicates the location of the well where sample H23DN014 was collected. K_P values are listed in Tableau 2-1. Vertical exaggeration is 10×; b) Detailed structure of a fault. Black arrows represent K anisotropy and blue arrows indicate the conceptual principal flow direction in different geological structures (protolith (green), fault core (grey) and damage zone (red)).

2.5.7. Boundary conditions

Vertical no-flow (symmetry) boundaries are located below Lac Saint-Jean on the right (NNE) side of the model and at the Lac Saint-Jean watershed boundary at the left (SSW) (Figure 2-2). Additionally, a no-flow boundary was assigned at a depth of 5,400 m where fracturing is assumed to be negligible. At the top boundary, a type-1 (Dirichlet) water table boundary condition was imposed using the interpolated and smoothed regional potentiometric data from the PACES-SLSJ database (Walter et al., 2018). In this case, the FLONET/TR2 code calculates the recharge automatically, which depends on the applied hydraulic properties and water table gradients. The calculated recharge was checked to be realistic with independently-estimated values of recharge into crystalline bedrock, which generally vary from 1 to 20 mm/yr (Bockgård, 2004; Raposo et al., 2012; Chesnaux, 2013).

Boundary conditions for age transport are also shown in Figure 2-2. Recharge zones at the watertable are defined by a Type 1 Dirichlet boundary with a mean age of A=0 yrs, while all other boundaries have a Neumann zero-gradient condition.

2.5.8. Model discretization

Spatial and temporal discretization of the model was governed by the grid Peclet and Courant criteria, respectively (Daus et al., 1985; Molson et Frind, 2023). The Peclet criterion was respected everywhere within the domain using a mesh composed of 2,250 elements in the horizontal direction and 170 elements in the vertical direction, for a total of 382,500 rectangular elements, each of which is divided into two triangles for the flow domain, with a uniform horizontal spacing of 25 m. The transport domain retains the rectangular elements. Element layers within each hydrostratigraphic unit range in thickness from 62.5 m at the bottom to 1 m at the top. Time steps in the age transport model started at 10^3 days, increasing to 10^9 days at later time. While the Courant criteria was somewhat exceeded in the shallow upstream zone of the model, the age solution nevertheless converged well with no oscillations. The age simulation was run to a maximum simulation time of 2.7 Ga, which was verified to represent steady-state conditions throughout the domain for all scenarios.

2.5.9. Assumptions and limitations

Several assumptions have been considered to simplify the numerical model. Crystalline bedrock was considered as an equivalent porous medium, with hydraulic properties representing a relatively uniform distribution of fractures. The cross-section is assumed to follow a principal flow direction, being perpendicular to the elevation contours and parallel to the regional piezometric gradients. According to Abhervé (2019), the influence of topography on flow directions and groundwater age is most significant in shallow aquifers, while deeper zones are much less affected by topographic variations. Topographic variations over geological time in the study area have been neglected. However, pre- and post-graben conditions were considered by including several scenarios with different fault permeabilities, in addition to a base case without faults.

Fluid density and viscosity are also assumed uniform, based primarily on the consideration that the effects of density and viscosity variations on hydraulic conductivity are less important compared to the significant decrease in the intrinsic hydraulic conductivity with depth (Ferguson et al., 2021; Xie et al., 2022a). In addition, based on MATLAB algorithms released in the Seawater Thermophysical Properties Library (Sharqawy et al., 2010), changes in viscosity with depth can be

limited since viscosity decreases with increasing temperature but increases with increasing salinity. For example, the viscosity of a fluid at 50 °C and 50 g/L (0.61 mPa·s) is about 1.7 times that of a fluid at 100 °C and 100 g/L (0.37 mPa·s), which is a negligible difference compared with the orders of magnitude decreases in permeability with depth.

The Canadian Shield is regarded as a cold crust (Morgan, 2018b), having average thermal gradients between 15 – 20 °C/km (Grasby et al., 2011). Based on an estimate of the Rayleigh number for normal conditions in the study area, which include very low intrinsic hydraulic conductivities at kilometer-scale depths, these temperature differences are not enough to allow thermal convection (Hiscock et Bense, 2014).

Sedimentary rocks covered the Canadian Shield from the middle Paleozoic to the late Mesozoic (Patchett et al., 2004). In the SLSJ region, the sedimentary cover was thinner than in the Saint Lawrence Lowlands further south. The study area is located in the Canadian Shield, at a high altitude, and has undergone intense glacial erosion. Present-day thickness for sedimentary rocks does not exceed 200 m (Walter et al., 2018). Although sedimentary rocks have influenced ancient groundwater dynamics in the study area through changes in bedrock topography or infiltration of ancient marine water, for example, the available data were insufficient to take this into account in the numerical model.

Finally, steady-state conditions are assumed. Glacial events, which have occurred every 50,000 to 100,000 yrs and produced 2 km thick ice sheets in the study area (Dyke et Prest, 1987), generate high-pressure pulses that should have an impact on the regional flow system, e.g. at depths of 10 km (Lemieux et al., 2008a). However, these events are rare and brief compared with the stable hydraulic conditions that dominated on geological timescales similar to those of the PSB, the groundwater age of which can reach up to 2 Ga (Holland et al., 2013; Sherwood-Lollar et al., 2021). Consequently, for practical reasons, temporal geological variations such as glaciation and erosion are also neglected.

Potentiometric data used here were obtained from the PACES-SLSJ database (Walter et al., 2018), which was interpolated from lake and river levels and from piezometric levels in the rock and surficial deposits. This approach assumed that hydrographic and piezometric level data belong to a regional single water body (Rouleau et al., 2013). As result, a good correlation was found between interpolated and observed data (r^2 = 0.92) (see Rouleau et al. (2013) for details).

2.6. Results

2.6.1. Isotopic data

Isotopic results of the brackish samples are presented in Tableau 2-3, which show a variation in TDS values between 1 and 29.6 g/L. Values of $\delta^{18}O$ vary from -17.73‰ to -13.14‰, while $\delta^{2}H$ values range from -127.28‰ to -92.76‰. In Figure 2-4, we compiled isotopic data of deep crystalline and sedimentary brines from the existing literature (see Ngombe et al. (2024) for details) and from SLSJ brackish groundwater samples. In Figure 2-4a, the results were similar to those for deep crystalline brines, with an enrichment in $\delta^{2}H$ relative to the local meteoric water line in Figure 2-4b. Strontium isotope ratios ($^{87}Sr/^{86}Sr$) range from 0.70709 to 0.71126, with a median value of 0.70805. Strontium ratios were observed to generally decrease as salinity and dissolved Sr^{2+} increase.

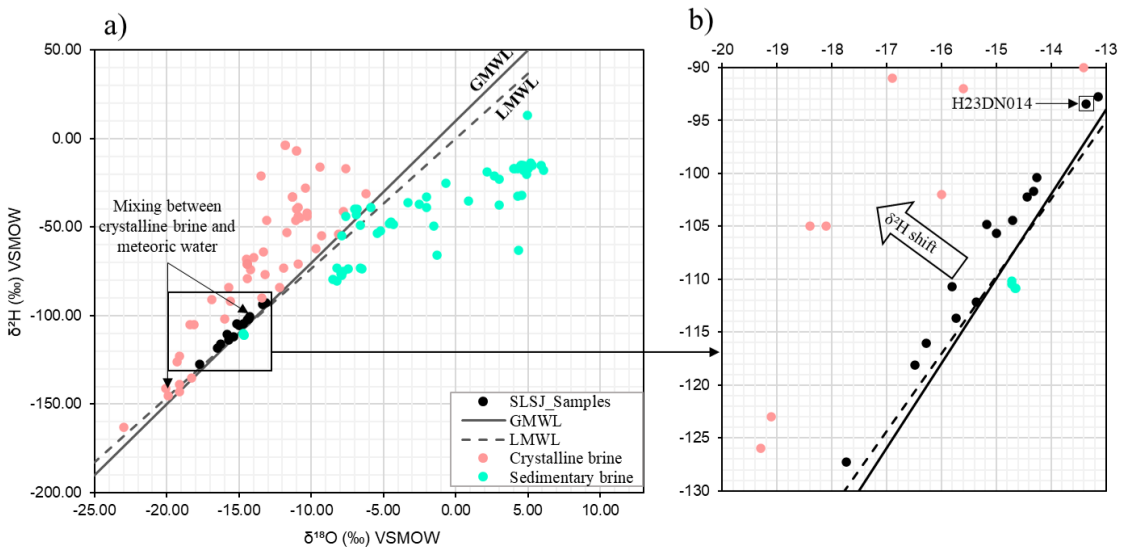

Figure 2-4: a) $\delta^{2}H$ and $\delta^{18}O$ plot for SLSJ brackish groundwater samples. The Global Meteoric Water Line (GMWL) follows the general equation of Craig (1961). The local meteoric water line (LMWL) was obtained from the PACES-SLSJ database (Rouleau et al., 2013). Figure modified from Ngombe et al. (2024) and mixing process interpretation is from Warr et al. (2021). b) Detail in SLSJ brackish samples showing $\delta^{2}H$ enrichment.

Tableau 2-3: Isotopic analysis of brackish groundwater in the SLSJ region. VSMOW: Vienna Standard Mean Ocean Water.

Sample ID	TDS (g/L)	$\delta^{18}O$ (‰) VSMOW (±0.2‰)	$\delta^{2}H$ (‰) VSMOW (±0.8‰)	$^{87}Sr/^{86}Sr$	Sr (mg/L)
H23DN001	2.67	-15.80	-110.66	0.70827	13.6
H23DN002	16.3	-17.73	-127.28	0.70709	127
H23DN003	1.65	-14.27	-100.36	0.70801	7.19
H23DN004	5.51	-16.48	-118.14	0.71126	0.0747
H23DN005	9.89	-15.37	-112.14	0.70712	36.4
H23DN006	3.99	-15.18	-104.79	0.70775	42.7
H23DN007	3.21	-14.70	-104.42	0.70779	21.2
H23DN008	1.00	-14.99	-105.65	0.70740	2.4
H23DN009	1.41	-13.14	-92.76	0.71015	0.608
H23DN010	11.6	-15.73	-113.71	0.70759	72.7
H23DN011	3.58	-14.44	-102.24	0.70863	0.704
H23DN012	1.73	-14.32	-101.71	0.70864	12.2
H23DN013	1.24	-16.28	-116.01	0.70809	5.29
H23DN014	29.6	-13.37	-93.44	0.70939	224

2.6.2. Steady-state flow

The gravity-driven model successfully demonstrated that topographic features play a significant role in controlling groundwater flow patterns, creating local, intermediate and regional flow systems (Figure 2-5a). Lac Saint-Jean, which represents the lowest topographic point of the region, is the regional groundwater discharge zone of the SLSJ aquifer system. Flow simulation results show that the influence of local topographic variations on groundwater flow decreases with depth (Figure 2-5a), consistent with the study of Zhang et al. (2022). At greater depths, flow is more closely controlled by regional hydraulic gradients rather than by local topographic variations. Also, the simulated regional flow system is less prominent than the local flow systems. For example, at a horizontal distance of 730 m in the highlands, horizontal Darcy fluxes reach 29.7 mm/yr near ground surface, decreasing to 0.75 mm/yr at 300 m depth, and to 8.9×10^{-5} mm/yr at the bottom; while at 54.4 km in the lowlands, fluxes reach 84 mm/yr near ground surface, decreasing to 2.4 mm/yr at 300 m depth, and to 0.003 mm/yr at the bottom.

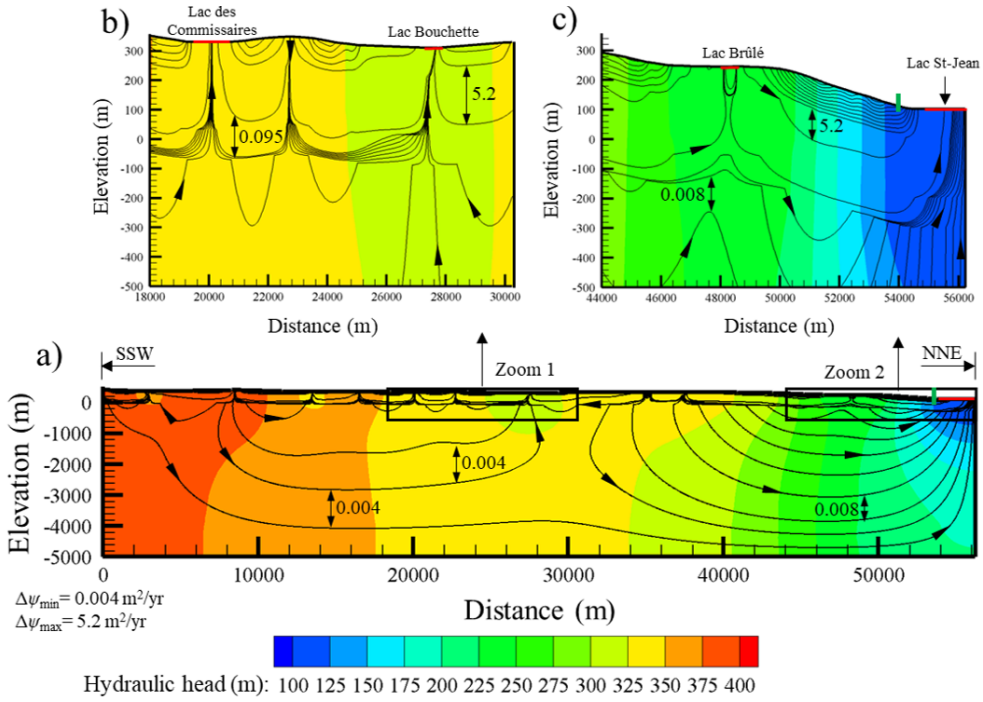

Figure 2-5: a) Steady-state base case flow simulation without faults showing hydraulic heads and streamlines. Vertical exaggeration is 2×. b) Zoom 1, magnified system in the highlands, and c) Zoom 2, magnified system in the lowlands; vertical exaggeration is 10× in both zoom plots. The vertical green mark near the top right is the location of the well where the H23DN014 sample was collected, and the red horizontal lines represent the lakes. For clarity, stream function intervals are not uniform (selected non-uniform intervals are labelled in m^2/yr).

The flow simulation shows that topographic peaks are preferential recharge zones, while rivers and lakes are discharge zones. For example, Lac des Commissaires, and the upgradient margin of Lac Brûlé in the highlands are discharge zones for local and intermediate flow systems (Figure 2-5b and c). Vertical profiles of hydraulic head in Figure 2-6 show increasing head with depth at 27 km (below Lac Bouchette) in the highlands (Figure 2-6a) and from 53.7 km to Lac Saint-Jean in the lowlands (Figure 2-6b). These trends indicate an upwelling of deep groundwater toward Lac Bouchette and in the region's lowlands, including Lac Saint-Jean, respectively the lowest elevation in the highlands, and the lowest elevations in the lowlands within the model domain (Figure 2-5b and c).

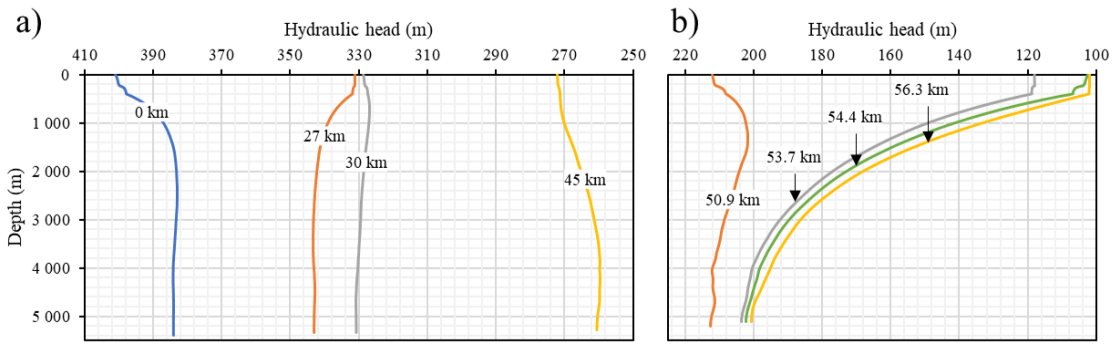

Figure 2-6: Vertical profiles of simulated hydraulic heads with depth at different distances along the model cross-section; distances are indicated in km. a) Hydraulic head profiles in highlands; b) Hydraulic head profiles in lowlands.

In areas of very steep topography such as at the boundaries of the highlands and lowlands, a high vertical hydraulic gradient may be expected. High hydraulic gradients favor high Darcy fluxes and, potentially, groundwater discharge. Fieldwork carried out as part of the PACES-SLSJ project has shown that steeply sloping areas in the region are associated with seepage phenomena (Walter et al., 2018). However, as shown in the flow simulation results (Figure 2-5c), at the main boundaries between the highlands and lowlands (specifically at shallow depth, i.e. < 100 m depth), topographic gradients favor a local flow system with a short residence time. Also, this change in water table slope separating the highlands from the lowlands (at about 50.9 km) generates a local recharge zone near the downgradient margin of Lac Brûlé (Figure 2-5c), while towards its upgradient margin, Lac Brûlé acts as an intermediate discharge zone. These topographic effects decrease with depth but can still be seen in the flowline below Lac Brûlé at an elevation of about -200 m, which marks the change from upward to downward flow directions (Figure 2-5c and Figure 2-6b). Consequently, this steady-state base case flow simulation without faults also indicates that areas of significant topographic depression can lead to local upwelling of deep fluids (Figure 2-5c).

2.6.3. Recharge verification

Since the interpolated piezometric surface was based on observed regional data (see Rouleau et al. (2013) for details) and applied as a fixed water table in the model, the near-surface heads within the fractured rock aquifer, including the water table, were considered to be accurate. However, the calculated fluxes crossing the water table, which depend on the local water table

gradient and hydraulic conductivity of the fractured rock, must be verified as being realistic. Indeed, the calculated mean recharge rate in the present study, of about 3 mm/yr (Figure 2-7), is consistent with published values in the Canadian Shield (Thorne, 2004; Chesnaux, 2013; Huet et al., 2016). Peak local recharge into the fractured rock reaches about 30 mm/yr while maximum discharge rates range between 20 and 30 mm/yr (Figure 2-7).

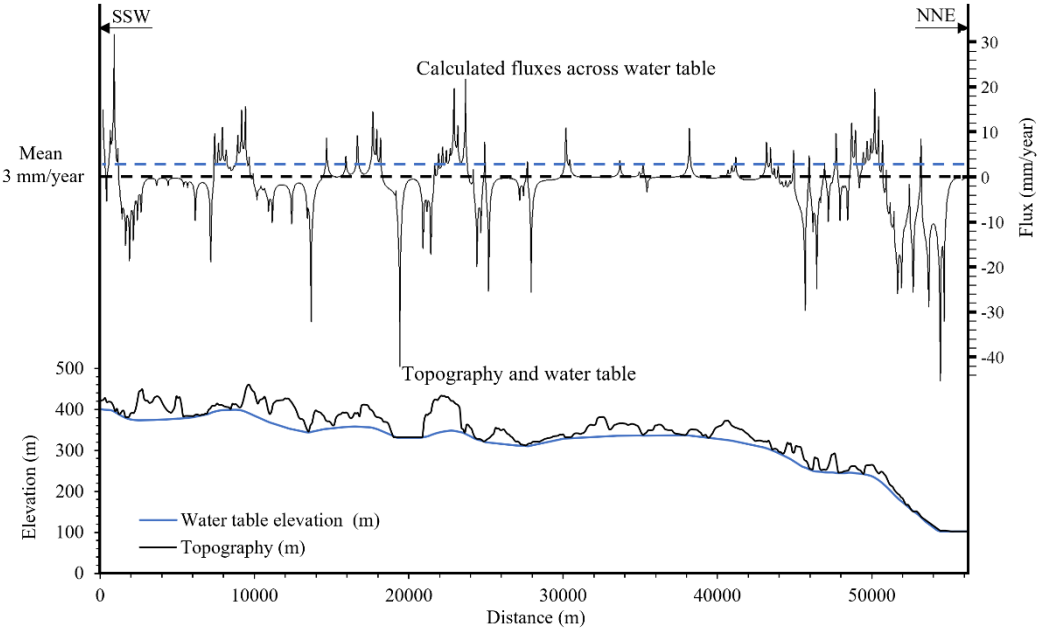

Figure 2-7: Model-derived fluxes across the water table within the fractured rock aquifer, imposed water table elevations (from interpolated piezometry) and topographic elevation along the model cross-section. Negative fluxes correspond to discharge and positive fluxes correspond to recharge. Mean recharge was calculated using only positive fluxes and is presented as a blue dashed line; the black dashed line represents 0 mm/yr. Vertical exaggeration is 20×.

A conventional model presented in the electronic supplementary material (ESM, ANNEXE I), applying fixed water table elevations at specific control points at streams, rivers and lakes, with imposed recharge elsewhere, and including surficial deposits and limestone, was also tested. A comparison of the results obtained with the two approaches showed similar results on a regional scale.

2.6.4. Steady-state mean groundwater ages

Following the flow simulation, advective-dispersive mean groundwater age was simulated using the steady-state velocity field. This base case age simulation reached a steady-state condition

by about 654 Ma, with maximum groundwater age reaching 338.4 Ma along the right-half of the model base, and along the NNE vertical boundary of the model domain. These maximum groundwater ages are consistent with groundwater age in similar contexts within the Precambrian Canadian Shield (Bottomley et al., 1999; Holland et al., 2013; Warr et al., 2018; Boumaiza et al., 2024).

The simulated mean groundwater age gradually increases with depth (Figure 2-8a). Shallow aquifers are characterized by young groundwater ranging in age from a few days up to 100 yrs (Figure 2-8b and c), in less fractured aquifers, groundwater ages increase rapidly, ranging from 100 yrs to 1 Ma, while in deep layers (1 000 – 3 000 m), ages are approximately 1 to 25 Ma. Maximum ages reach over 200 Ma along the lower right base and right boundaries. Also, the age transport simulation reveals the presence of ancient groundwater at an elevation of -200 m, where the rock is less fractured. At the ground surface, groundwater age is greatest in discharge zones, for example at Lac des Commissaires and Lac Bouchette, where groundwater age reaches about 10 000 yrs, while it reaches about 100 000 yrs at Lac Brûlé and 268.7 Ma at the NNE extent of the model at Lac Saint-Jean. Assuming a purely gravitational flow system with no faults, it appears that the regional topographic gradient in the study area allows upwelling of ancient groundwater, but only within the principal discharge zones (lakes, rivers and streams), and otherwise only to depths of between 400 and 500 m below the surface.

2.6.5. Parametric study on faults

Flow and age transport simulations from the parametric study on faults are illustrated in Figure 2-9 and arranged depending on the fault hydraulic behavior: base case, barrier fault, conduit fault and conduit-barrier fault scenarios.

2.6.5.1. Base case scenario

In Scenario A, although the fault core (K_{FC}) and the fault damage zone (K_{DZ}) have identical properties to the surrounding rock matrix, the 90-degree rotation of the anisotropic K tensor within the faults induces a significant contrast, resulting in preferential vertical flow along the faults. On the regional scale, faults lead to upwelling of deep, ancient fluid, increasing groundwater age at the NNE

boundary below Lac Saint-Jean from 268.7 Ma in the model without faults to 291.4 Ma in Scenario A.

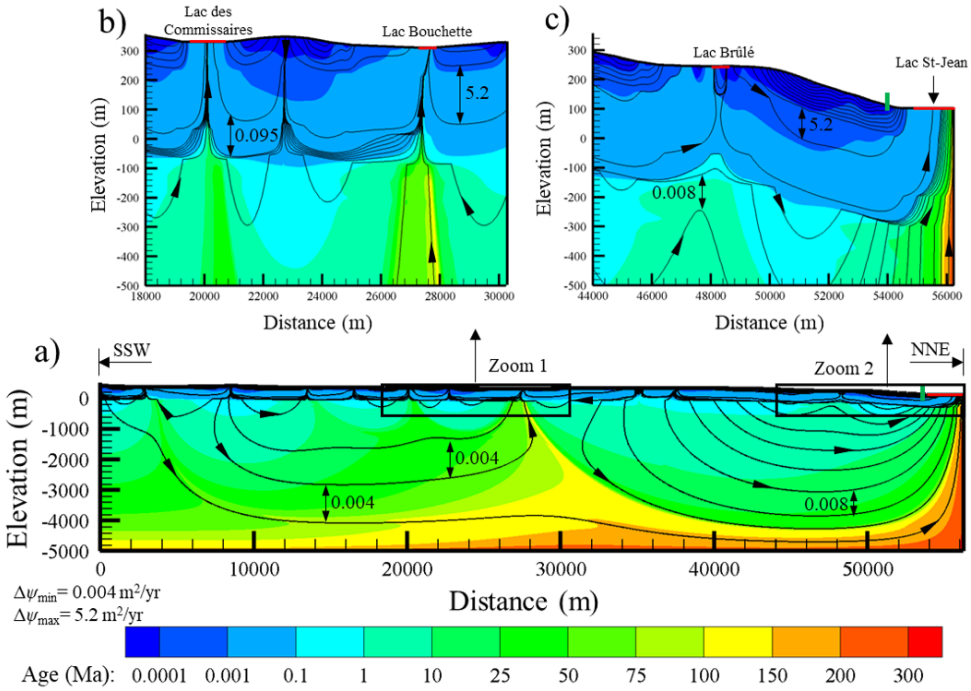

Figure 2-8: a) Simulated steady-state mean groundwater ages (Ma) (Base case, no faults) with superimposed streamlines from the flow model. Vertical exaggeration is 2×. b) Zoom 1, magnified system in the highlands. Vertical exaggeration is 10×. c) Zoom 2, magnified system in the lowlands. The vertical green mark indicates the location of the well where the H23DN014 sample was collected, and the red horizontal lines represent lakes. Vertical exaggeration is 10× in both zoom plots. For clarity, stream function intervals are not uniform (selected non-uniform intervals are labelled in m^2/yr).

2.6.5.2. Barrier fault scenarios

In Scenarios B and C, reducing K_{FC} to 10% and 1% of the surrounding matrix, respectively, results in greater upward flow deviation along the faults within the more permeable damage zone. Here, the effectively impermeable fault core acts as a barrier to groundwater flow. By blocking or restricting flow, barrier faults increase pressure and decrease horizontal flow, leading groundwater to seek alternative pathways, often resulting in upward movement along the fault plane or through adjacent fractures (Lapperre et al., 2019). In Scenario C, with a lower K_{FC} than in Scenario B, the upwelling effect of deep, ancient groundwater downgradient of the faults increases ages from 316.3 Ma in Scenario B to 428 Ma in Scenario C below Lac Saint-Jean.

2.6.5.3. Conduit fault scenarios

In Scenarios D and G, increasing K_{DZ} by a factor of 10 and 100 compared to the surrounding matrix, respectively, results in a significant increase in flow within the damage zone, reaching 299.8 Ma (Scenario D) and 368.3 Ma (Scenario G) below Lac Saint-Jean. In these scenarios, the fault zones act as conduits or preferential flow paths for deep groundwater and as a drain for the local flow system, which is consistent, for example, with studies conducted elsewhere in Quebec (Janos et al., 2018) and in siliciclastic sedimentary aquifers (Bense et Person, 2006). This dual effect can be explained by the contrast in hydraulic conductivity with the surrounding rocks, which are less permeable than the faults. Indeed, the high permeability of the conduit faults allows for a rapid dissipation of hydraulic pressure, leading to a local reduction in hydraulic head compared to the surrounding rock, which favours flow into the faults.

2.6.5.4. Conduit-barrier fault scenarios

In Scenarios E, F, H and I, where faults act as conduits and barriers (Figure 2-9), the age of groundwater below Lac Saint-Jean reaches 336.1 Ma, 504.9 Ma, 466 Ma and 1.23 Ga, respectively. The interaction between the low-permeability core and the high-permeability damage zone creates complex flow systems, characterized by major redirections of flow around the fault core as clearly shown in Scenario I. Scenario I shows the maximum potential for deep groundwater to move upward to the surface and exhibits a clear division of flow channels. In these scenarios, the fault core restricts fluid flow, while the damage zone allows greater flow, resulting in a distinctive distribution of flow with significant vertical movement along the damage zone and parallel to the fault plane. Upgradient of each fault, the damage zone channels the regional flow until it is blocked by the fault core, favoring upward migration of ancient groundwater, while downgradient of the faults, the damage zone acts as a drain for local flow. These downgradient high permeability fault zones allow young groundwater to penetrate deeper into the bedrock, creating a mixing zone.

The parametric study on faults clearly demonstrates the influence of fault hydraulic characteristics on groundwater flow. Regardless of the hydraulic configuration of the fault, faults enhance the upwelling effect of deep and ancient groundwater. Fault 1, located closest to Lac Saint-

Jean, has the most significant impact on regional flow by disrupting the regional flow system and enhancing upward movement. Nevertheless, regardless of the scenario, groundwater age at the point where the H23DN014 sample was collected remains young (see discussion below).

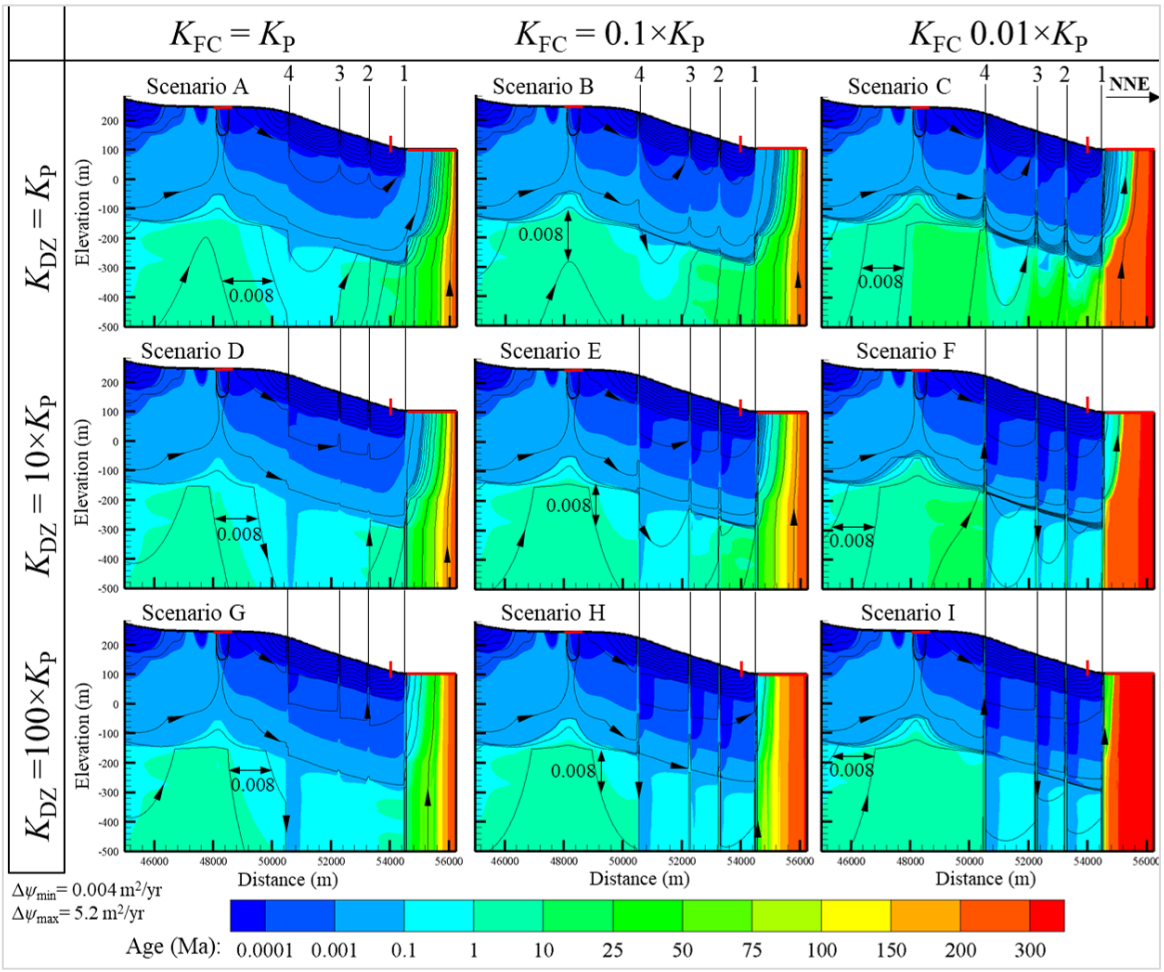

Figure 2-9: Steady-state mean groundwater ages with superimposed streamlines from the flow model for the various fault scenarios. See Tableau 2-2 for fault scenario definitions. Figures also show Saguenay Graben fault structures near Lac Saint-Jean, numbered 1 to 4. Black lines between scenarios show where faults are located. The vertical red line shows the location of the H23DN014 sample and the horizontal red lines represent Lac Brûlé and Lac Saint-Jean. Vertical exaggeration is 10×. For clarity, stream function intervals are not uniform (selected non-uniform intervals are labelled in m^2/yr).

2.7. Discussion

2.7.1. Deep brines in the subsurface

Recent hydrogeochemical studies in the SLSJ region have led to the hypothesis that a dilute member of deep brines, similar to those identified elsewhere in mines of the Canadian Shield, exists at shallow depths in the fractured rock. New isotopic data from this study, including stable water

isotope results, support this hypothesis. Firstly, SLSJ brackish groundwater samples are plotted along the meteoric line (Figure 2-4), which indicates a contribution of meteoric water to the chemistry of these samples. Secondly, the progressive $\delta^{18}O$ depletion and enrichment of $\delta^{2}H$ of SLSJ brackish samples indicate an influence of water-rock interactions on isotopic signatures over geological time scales (Warr et al., 2018; Boumaiza et al., 2024). Additionally, the distribution of stable isotope samples in Figure 2-4 also suggests that some SLSJ brackish groundwaters are a mix of crystalline brines and meteoric water.

The mixing of crystalline brine and meteoric water is also confirmed through the $^{87}Sr/^{86}Sr$ ratio which is a good tracer for mixing (Négrel et al., 2007). In the SLSJ brackish samples, the $^{87}Sr/^{86}Sr$ ratio in groundwater tends to decrease as the dissolved element content increases (Figure 2-10), suggesting mixing with deep brines (McNutt et al., 1984; Frost et Toner, 2004). Additionally, the wide distribution of $^{87}Sr/^{86}Sr$ ratios from 0.70709 to 0.71126 in SLSJ brackish samples suggests a mixture between a low radiogenic endmember (such as meteoric water) and a high radiogenic groundwater endmember (such as deep crystalline brine). Intense interaction between groundwater and old, radiogenic crustal rocks over geological time produces highly radiogenic brines, such as those observed in the Canadian Shield (Frape et al., 1984; Bottomley et al., 1999). The isotopic results therefore suggest that the sample taken at shallow depth in the area of lower regional topography (H23DN014) has a salinity equivalent to seawater and an isotopic signature ($\delta^{2}H$, $\delta^{18}O$, $^{87}Sr/^{86}Sr$) that suggests mixing between crustal water and meteoric water. The H23DN014 sample is therefore the regional mixing pole of the PSB (diluted-PSB) described in previous studies in the SLSJ region (Walter et al., 2017; Walter et al., 2019; Walter et al., 2023).

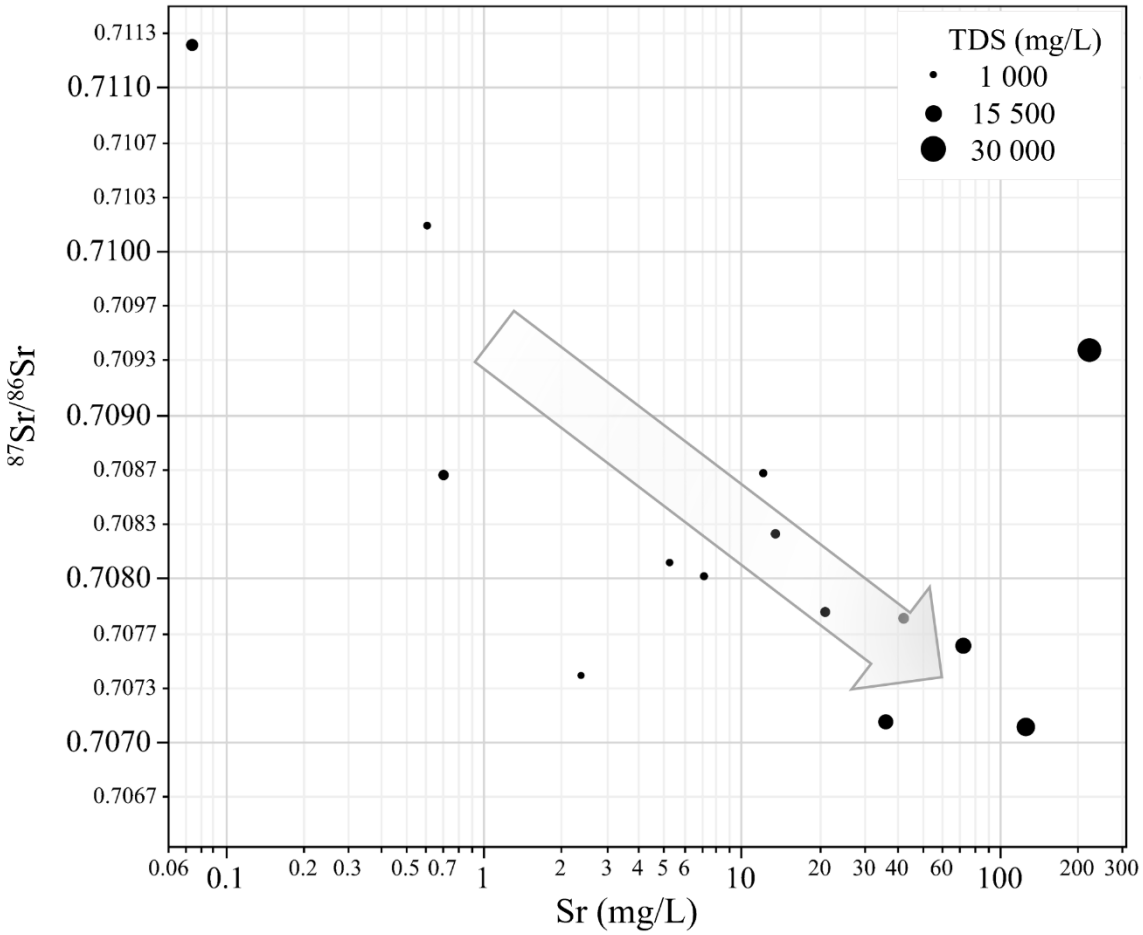

Figure 2-10: Sr^{2+} vs $^{87}Sr/^{86}Sr$ plot for SLSJ brackish groundwater samples. $^{87}Sr/^{86}Sr$ ratios tend to decrease as salinity increases (represented as Sr concentrations).

2.7.2. Conceptual model validation

According to the hypothesis proposed by Walter et al. (2017), the brackish groundwaters identified at shallow depth in the fractured rock would be the result of regional discharge along major geological structures (faults) associated with the Saguenay Graben. Under the assumed closed (symmetry) boundaries, and with no density effect (discussed below), the numerical flow model suggests that the graben configuration of the region generates a sufficient hydraulic gradient to sustain upwelling of deep groundwater. Age transport simulations have generated deep groundwater ages consistent with some ages of Precambrian crystalline brines identified elsewhere in the Canadian Shield (Holland et al., 2013; Sherwood-Lollar et al., 2021; Warr et al., 2022).

The simulated rapid increase of groundwater age with depth is consistent with the hydrogeochemical conceptual model proposed by Walter et al. (2023). In recharge areas, where rainwater infiltration occurs, recharged groundwater evolves to a Ca (Na)-HCO_3 water type (< 100 yrs), which further evolves to an intermediate-recharge groundwater of Na (Ca)-HCO_3 facies (from 100 yrs to 10 000 yrs). After long-term water-rock interaction, groundwater evolution tends to a Ca-Cl endmember (> 1 000 000 yrs). The age transport model applied to the study area reveals the presence of old groundwater at an elevation of -200 m, where the rock is less fractured. This observation suggests a complex flow system where older and younger groundwaters may interact. Simulated vertical age gradients within the local flow systems are consistent with the observed composition at comparable depths, which is confirmed by isotopic results obtained in this study.

The distribution of SLSJ brackish samples along such fault systems in the study area suggests that faults may play an important role in upwelling of deep fluids towards the surface (Walter et al., 2017). The parametric test on graben faults developed in this study gives results consistent with the hypothesis that faults play an important role in groundwater upwelling. Regardless of the chosen fault configuration scenario, the incorporation of faults into the numerical model systematically enhances groundwater migration towards the surface, focusing flow through preferential flow paths and thus increases the groundwater age gradient along the faults. Although regional flow in the SLSJ region is almost insignificant in comparison to the local flow systems, large-scale heterogeneities such as faults, which act as preferential pathways for deep flow, can enhance the detectability of regional flow signatures in near-surface groundwater samples (Janos et al., 2018). Nevertheless, the simulated ages (1 – 25 Ma) at depths between 1 000 and 3 000 m are 10 to 100 times younger than noble gas ages of PSBs estimated in the Canadian Shield at similar depths (Holland et al., 2013; Warr et al., 2018). Underestimated ages in the simulations could be attributed to factors such as (1) neglecting the impact of increased salinity at depth, which increases the density of groundwater. The density of deep brines is an important factor since negative buoyancy tends to oppose upward migration of deep groundwater which would significantly increase the age of groundwater (McIntosh et Ferguson, 2021; Neretnieks, 2024); (2) deep hydraulic conductivities in the numerical model of 4.7

× 10^{-11} m/s may have been overestimated by one or two orders of magnitude, thereby increasing deep groundwater flow rates and lowering simulated ages. Furthermore, it can be difficult to reproduce PSB groundwater ages derived from noble gases using a numerical simulation assuming an equivalent porous medium based on a well-developed fracture network (Hu et Walsh, 2022; Frampton, 2025).

Below 1 000 m, the low permeability favours the compartmentalization and isolation of different fracture systems, a characteristic commonly observed in crystalline shields, particularly in Canada (Ferguson et al., 2023). During resampling of fluids in the Kidd Creek mine of the Canadian Shield, for example, each borehole intersected several fracture networks containing fluids of different ages (Warr et al., 2018). Following these observations, Warr et al. (2018) proposed a conceptual model in which deep brines are located in hydrogeologically isolated and compartmentalized fracture networks with negligible exchange with regional flow systems. A similar effect could be reproduced if heterogeneity or a dual continuum approach were considered. In contrast to the hypothesis of Warr et al. (2018), this study assumes an equivalent porous medium approach that does not simulate discrete fractures, a commonly used simplification for regional-scale modelling, but which may contribute to the observed discrepancies.

In addition, subglacial recharge during the Wisconsinan period, which was not considered in the numerical model, could have disturbed the current flow regime. According to Lemieux et al. (2008a), the increase in pressure due to the weight of the ice and the infiltration of meltwater leads to an increase in the hydraulic head, reaching for example, more than 1 500 m (above hydrostatic) under the main ice dome at depths of up to 3 000 m, which could favour the upwelling of deep, old groundwater.

Although groundwater age in shallow discharge zones increased in all fault scenarios, age was still relatively young at the local sampling point of the diluted-PSB (from a 45 m deep well), likely due to limitations and assumptions of the numerical model, and since a regional scale model can never reproduce specific local-scale behavior. The two-dimensional model developed here also

neglects transverse (3D) flow, and effects of local pumping, discrete fractures and glacial events including isostatic rebound. Detail on the specific fault orientations and hydromechanical behavior is also lacking.

2.8. Conclusion

In the present study, isotopic signatures and two-dimensional numerical simulations of groundwater flow and age transport were used to explain the presence of brackish groundwater at shallow depths of the SLSJ fractured rock system and to validate a conceptual hydrogeochemical model proposed by Walter et al. (2023). Stable water isotopes and strontium isotope evidence suggests that some brackish groundwater samples, including the diluted-PSB (TDS = 29.6 g/L) sampled in fractured bedrock at a depth of 45 m, are a mix of meteoric water and deep Precambrian Shield brine, which has experienced long-term water-rock interaction over hundreds of millions of years. The numerical flow simulations indicate that, under the imposed boundary conditions, sufficiently high hydraulic heads are maintained at depth, generating vertical hydraulic gradients capable of sustaining the upwelling of deep and old groundwater. Parametric tests performed in this study suggest that graben faults facilitate groundwater upwelling and act as preferential pathways for deep and ancient groundwater. While the model does not independently confirm the natural geological process, it provides insights into the potential hydrodynamic behavior of the system. Therefore, the strong topographic contrasts (between the highlands and lowlands), associated with geological structures such as faults, favour emergence of deep, old groundwater in the near-surface.

Based on the steady-state flow systems, the groundwater age transport simulations generated deep groundwater ages consistent with some ages of Precambrian Shield brines identified elsewhere in the Canadian Shield. The study also reveals the presence of ancient groundwater 400 – 500 m below ground surface, suggesting a complex flow system where older and younger groundwaters may interact.

Although simulated ages in the local vicinity of the observed 45 m deep diluted-PSB member remained young, the results were still consistent with the conceptual model including upwelling of

deep old groundwater toward Lac Saint-Jean. Local fracture flow and other heterogeneities not included in the model could explain the local-scale discrepancy.

Despite this advance, further work is needed to obtain more details on the origin of Precambrian Shield brines in the SLSJ region and complete the regional conceptual hydrogeochemical model. While the numerical model captures key hydrodynamic mechanisms, further refinements are needed to assess their applicability to real geological systems, including for example, density variations, discrete fractures networks and the effects of the Wisconsinan Glaciation. In addition, complementary hydrogeochemical investigations, involving dating methods such as noble gases, and carbon-14, as well as isotopic analyses, and estimation of mixing proportions between recent meteoric waters and ancient groundwater, are required to further constrain the evolution of these brines. Understanding the hydraulic history of dilute Precambrian Shield brine is important to help regional decision-makers responsible for water policy and management, as it can provide valuable insights into the sustainability and potential risks associated with groundwater extraction in the region, and to better understand salinization processes involving mixing between shallow fresh water and deep brines. Excessive water pumping in certain areas favorable to the upwelling of ancient salt water (i.e. close to fault graben structures) poses a significant risk to the preservation of drinking water quality in the Saguenay-Lac-Saint-Jean region, Quebec, Canada, and in similar geological contexts.

2.9. References

Abhervé, R. 2019. Effet de la résolution topographique des modèles hydrogéologiques sur l'estimation des débits de base des rivières et des temps de résidence de l'eau souterraine (Effect of the topographic resolution of hydrogeological models on the estimation of base flows in rivers and groundwater residence times). Mémoire de maîtrise, Centre Eau Terre et Environnement, Université de Rennes 1, Rennes, France.

Achtziger-Zupančič, P., Loew, S., et Mariethoz, G. 2017. A new global database to improve predictions of permeability distribution in crystalline rocks at site scale. Journal of Geophysical Research: Solid Earth **122**(5): 3513–3539.

Bense, V., Gleeson, T., Loveless, S., Bour, O., et Scibek, J. 2013. Fault zone hydrogeology. Earth-Science Reviews **127**: 171–192.

Bense, V., et Person, M. 2006. Faults as conduit-barrier systems to fluid flow in siliciclastic sedimentary aquifers. Water Resources Research **42**(5).

Bockgård, N. 2004. Groundwater recharge in crystalline bedrock: processes, estimation, and modelling. Doctoral dissertation, Faculty of Science and Techmology, Acta Universitatis Upsaliensis, Uppsala, Swedish.

Bottomley, D.J., Katz, A., Chan, L., Starinsky, A., Douglas, M., Clark, I., et Raven, K. 1999. The origin and evolution of Canadian Shield brines: evaporation or freezing of seawater? New lithium isotope and geochemical evidence from the Slave craton. Chemical Geology **155**(3-4): 295–320.

Boumaiza, L., Stotler, R., et Frape, S. 2024. A review of the major chemical and isotopic characteristics of groundwater in crystalline rocks of the Canadian Shield. Chemical Geology: 122366.

Bucher, K., et Stober, I. 2010. Fluids in the upper continental crust. Geofluids **10**(1-2): 241–253.

Caine, J.S. 2006. Questa baseline and premining ground-water quality investigation 18. Characterization of brittle structures in the Questa Caldera and their potential influence on bedrock groundwater flow, Red River Valley, New Mexico. USGS Numbered Series. 2330-7102.

Cartaud, F. 2004. Modélisation des écoulements dans les interfaces des barrières d'étanchéité composites d'installation de stockage de déchets (Flow modelling in the interfaces of composite sealing barriers in waste storage facilities). Thèse de doctorat, Hydrologie et Hydrogéologie Quantitative, École Nationale Supérieure des Mines de Paris, Paris, France.

Chesnaux, R. 2013. Regional recharge assessment in the crystalline bedrock aquifer of the Kenogami Uplands, Canada. Hydrological Sciences Journal **58**(2): 421–436.

Craig, H. 1961. Isotopic variations in meteoric waters. Science **133**(3465): 1702–1703.

Daus, A., Frind, E., et Sudicky, E. 1985. Comparative error analysis in finite element formulations of the advection-dispersion equation. Advances in Water Resources **8**(2): 86–95.

Desbarats, A. 2002. A lumped-parameter model of groundwater influx to a mine adit in mountainous terrain. Water Resources Research **38**(11): 38–31–38–11.

Du Berger, R., Roy, D.W., Lamontagne, M., Woussen, G., North, R.G., et Wetmiller, R.J. 1991. The Saguenay (Quebec) earthquake of November 25, 1988: seismologic data and geologic setting. Tectonophysics **186**(1-2): 59–74.

Dyke, A.S., et Prest, V.K. 1987. Late Wisconsinan and Holocene history of the Laurentide ice sheet. Géographie Physique et Quaternaire **41**(2): 237–263.

Farvolden, R., Pfannkuch, O., Pearson, R., et Fritz, P. 1988. The Geology of North America, The Geological Society of America, 19th edition: Chapter 15 Region 12, Precambrian Shield. Hydrogeology **O-2**: 101–114.

Ferguson, G., McIntosh, J., Warr, O., et Sherwood Lollar, B. 2023. The low permeability of the Earth's Precambrian crust. Communications Earth & Environment **4**(1): 323.

Ferguson, G., McIntosh, J.C., Warr, O., Sherwood Lollar, B., Ballentine, C.J., Famiglietti, J.S., Kim, J.H., Michalski, J.R., Mustard, J.F., et Tarnas, J. 2021. Crustal groundwater volumes greater than previously thought. Geophysical Research Letters **48**(16): e2021GL093549.

Frampton, A. 2025. Flow channelling and variability in transit times and tortuosity in a fractured rock model with small scale heterogeneity. Advances in Geosciences **65**: 149–158.

Frape, S., et Fritz, P. 1982. The chemistry and isotopic composition of saline groundwaters from the Sudbury Basin, Ontario. Canadian Journal of Earth Sciences **19**(4): 645–661.

Frape, S., et Fritz, P. 1987. Geochemical trends for groundwaters from the Canadian Shield. Geological Association of Canada-Special Paper **33**: 19–38.

Frape, S., Fritz, P., et McNutt, R.t. 1984. Water-rock interaction and chemistry of groundwaters from the Canadian Shield. Geochimica et Cosmochimica Acta **48**(8): 1617–1627.

Frost, C.D., et Toner, R.N. 2004. Strontium isotopic identification of water-rock interaction and ground water mixing. Groundwater **42**(3): 418–432.

Gascoyne, M., et Kamineni, D. 1994. The hydrogeochemistry of fractured plutonic rocks in the Canadian Shield. Applied Hydrogeology **2**(2): 43–49.

Gimeno, M.J., Tullborg, E.-L., Nilsson, A.-C., Auqué, L.F., et Nilsson, L. 2023. Hydrogeochemical characterisation of the groundwater in the crystalline basement of Forsmark, the selected area for the geological nuclear repositories in Sweden. Journal of Hydrology **624**: 129818.

Goode, D.J. 1996. Direct simulation of groundwater age. Water Resources Research **32**(2): 289–296.

Grasby, S.E., Jessop, A., Kelman, M., Ko, M., Chen, Z., Allen, D., Bell, S., Ferguson, G., Majorowicz, J., et Moore, M. 2011. Geothermal energy resource potential of Canada. Geological Survey of Canada. 6914. p. 283.

Hébert, C., Cadieux, A.-M., et Breemen, O.v. 2005. Temporal evolution and nature of Ti Fe P mineralization in the anorthosite mangerite charnockite granite (AMCG) suites of the south-central Grenville Province, Saguenay Lac St. Jean area, Quebec, Canada. Canadian Journal of Earth Sciences **42**(10): 1865–1880.

Hébert, C., et Lacoste, P. 1998. Géologie de la région de Jonquière-Chicoutimi Ministère des Ressources naturelles du Québec. . RG 97-08. p. 32.

Hebig, K.H., Ito, N., Scheytt, T., et Marui, A. 2012. Deep groundwater research with focus on Germany. Hydrogeology Journal **20**(2): 227.

Hiscock, K.M., et Bense, V.F. 2014. Hydrogeology: principles and practice. John Wiley & Sons éd. Wiley-Blackwell, Chichester, United Kingdom.

Holland, G., Sherwood-Lollar, B., Li, L., Lacrampe-Couloume, G., Slater, G., et Ballentine, C. 2013. Deep fracture fluids isolated in the crust since the Precambrian era. Nature **497**(7449): 357–360.

Hu, R., et Walsh, S.D. 2022. The Role of Heterogeneity on Deformation and Flow in Fractured Coal Slopes. Minerals **12**(10): 1297.

Huet, M., Chesnaux, R., Boucher, M.-A., et Poirier, C. 2016. Comparing various approaches for assessing groundwater recharge at a regional scale in the Canadian Shield. Hydrological Sciences Journal **61**(12): 2267–2283.

Janos, D., Molson, J., et Lefebvre, R. 2018. Regional groundwater flow dynamics and residence times in Chaudière-Appalaches, Québec, Canada: Insights from numerical simulations. Canadian Water Resources Journal/Revue Canadienne des Ressources Hydriques **43**(2): 214–239.

Kuchling, K., Chorley, D., et Zawadzki, W. 2000. Hydrogeological modeling of mining operations at the Diavik Diamonds project. Proceedings of the Sixth International Symposium on Environmental Issues and Management of Waste in Energy and Mineral Production. Taylor and Francis, Calgary, Alberta, 30 May–2 June, pp. pp 1–8.

Lapperre, R.E., Kasse, C., Bense, V.F., Woolderink, H.A., et Van Balen, R.T. 2019. An overview of fault zone permeabilities and groundwater level steps in the Roer Valley Rift System. Netherlands Journal of Geosciences **98**: e5.

Lemieux, J.M., Sudicky, E., Peltier, W., et Tarasov, L. 2008a. Simulating the impact of glaciations on continental groundwater flow systems: 2. Model application to the Wisconsinian glaciation over the Canadian landscape. Journal of Geophysical Research: Earth Surface **113**(F3).

Lichtner, P.C., Kelkar, S., et Robinson, B. 2002. New form of dispersion tensor for axisymmetric porous media with implementation in particle tracking. Water Resources Research **38**(8): 21–21–21–16.

Llewellyn, G.T. 2014. Evidence and mechanisms for Appalachian Basin brine migration into shallow aquifers in NE Pennsylvania, USA. Hydrogeology Journal **22**(5): 1055.

McCallum, J.L., Dogramaci, S., Bai, A., Cook, P.G., Engdahl, N.B., Simmons, C.T., Skrzypek, G., et Grierson, P.F. 2020. Assessing temporal changes in groundwater recharge using spatial variations in groundwater ages. Water Resources Research **56**(8): e2020WR027240.

McIntosh, J.C., et Ferguson, G. 2021. Deep meteoric water circulation in Earth's crust. Geophysical Research Letters **48**(5): e2020GL090461.

McNutt, R.H., Frape, S.K., et Fritz, P. 1984. Strontium isotopic composition of some brines from the Precambrian Shield of Canada. Chemical Geology **46**(3): 205–215.

Molson, J., et Frind, E. 2012. On the use of mean groundwater age, life expectancy and capture probability for defining aquifer vulnerability and time-of-travel zones for source water protection. Journal of Contaminant Hydrology **127**(1-4): 76–87.

Molson, J., et Frind, E. 2023. FLONET/TR2, user guide version 6.0; a two-dimensional simulator for groundwater flownets, contaminant transport and residence time. *Dans* Université Laval and University of Waterloo.

Montcoudiol, N., Molson, J., et Lemieux, J.-M. 2017. Numerical modelling in support of a conceptual model for groundwater flow and geochemical evolution in the southern Outaouais Region, Quebec, Canada. Canadian Water Resources Journal/Revue Canadienne des Ressources Hydriques **43**(2): 240–261.

Morgan, A.L.F. 2018b. Low temperature geothermal resources in abandoned mines of the Canadian Shield: a case study in the Chapais and Chibougamau area, Québec, Canada. Master's Thesis, Department of Engineering, Reykjavík University, Reykjavik, Islande.

Négrel, P., Lemiere, B., Machard de Grammont, H., Billaud, P., et Sengupta, B. 2007. Hydrogeochemical processes, mixing and isotope tracing in hard rock aquifers and surface waters from the Subarnarekha River Basin,(east Singhbhum District, Jharkhand State, India). Hydrogeology Journal **15**: 1535–1552.

Neretnieks, I. 2024. Saline groundwaters counteract up-flow of contaminants-implications for radionuclide repositories? Journal of Contaminant Hydrology **262**: 104309.

Ngombe, O.G., Walter, J., Chesnaux, R., et Molson, J. 2024. Application of hierarchical cluster analysis and principal component analysis to identify compositional trends of brine in crystalline basements and sedimentary basins. Applied Geochemistry: 106030.

Normani, S., et Sykes, J. 2012. Paleohydrogeologic simulations of Laurentide ice-sheet history on groundwater at the eastern flank of the Michigan Basin. Geofluids **12**(1): 97–122.

Patchett, P., Embry, A., Ross, G., Beauchamp, B., Harrison, J., Mayr, U., Isachsen, C., Rosenberg, E., et Spence, G. 2004. Sedimentary cover of the Canadian Shield through Mesozoic time reflected by Nd isotopic and geochemical results for the Sverdrup Basin, Arctic Canada. The Journal of Geology **112**(1): 39–57.

Raposo, J., Molinero, J., et Dafonte, J. 2012. Parameterization and quantification of recharge in crystalline fractured bedrocks in Galicia-Costa (NW Spain). Hydrology and Earth System Sciences **16**(6): 1667–1683.

Richard, S., Chesnaux, R., et Rouleau, A. 2011. Estimating the hydraulic properties of aquifers from specific capacity data: Saguenay-Lac-Saint-Jean, Quebec. *Sous la direction de*. *Dans* Proceedings of GeoHydro 2011, Joint Meeting of the Canadian Quaternary Association and the Canadian Chapter of the International Association of Hydrogeologists, Canada, pp. 28–31.

Richard, S.K., Chesnaux, R., Rouleau, A., et Coupe, R.H. 2016. Estimating the reliability of aquifer transmissivity values obtained from specific capacity tests: examples from the Saguenay-Lac-Saint-Jean aquifers, Canada. Hydrological Sciences Journal **61**(1): 173–185.

Rouleau, A., Daigneault, R., Walter, J., Germaneau, D., Tremblay, M.L., et Lambert, M. 2013. Résultats du programme d'acquisition de connaissances sur les eaux souterraines de la région Saguenay-Lac-Saint-Jean (Results of the groundwater knowledge acquisition programme in the Saguenay-Lac-Saint-Jean region). Ministère du Développement durable, de l'Environnement et de la Lutte contre les changements climatiques (Ministry of Sustainable Development, Environment and the Fight Against Climate Change), MDDELCC p. 248.

Roy, D., Schmitt, L., Woussen, G., et DuBerger, R. 1993. Lineaments from airborne SAR images and the 1988 Saguenay earthquake, Quebec, Canada. Photogrammetric Engineering and Remote Sensing **59**(8): 1299–1305.

Sharqawy, M.H., Lienhard, J.H., et Zubair, S.M. 2010. Thermophysical properties of seawater: a review of existing correlations and data. Desalination and water treatment **16**(1-3): 354–380.

Sherwood-Lollar, B., Heuer, V.B., McDermott, J., Tille, S., Warr, O., Moran, J., Telling, J., et Hinrichs, K.-U. 2021. A window into the abiotic carbon cycle–Acetate and formate in fracture waters in 2.7 billion year-old host rocks of the Canadian Shield. Geochimica et Cosmochimica Acta **294**: 295–314.

Snowdon, A.P., Normani, S.D., et Sykes, J.F. 2021. Analysis of crystalline rock permeability versus depth in a Canadian Precambrian rock setting. Journal of Geophysical Research: Solid Earth **126**(5): e2020JB020998.

Starn, J.J., Kauffman, L.J., et Feinstein, D.T. 2023. Groundwater residence times in glacial aquifers—A new general simulation-model approach compared to conventional inset models. US Geological Survey. 2328-0328.

Stevenson, D., Kozak, E., Davison, C., Gascoyne, M., et Broadfoot, R. 1996. Hydrogeologic characteristics of domains of sparsely fractured rock in the granitic Lac du Bonnet Batholith, Southeastern Manitoba, Canada. Atomic Energy of Canada Limited Report.

Stober, I., et Bucher, K. 1999. Deep groundwater in the crystalline basement of the Black Forest region. Applied Geochemistry **14**(2): 237–254.

Stober, I., et Bucher, K. 2007. Hydraulic properties of the crystalline basement. Hydrogeology Journal **15**: 213–224.

Stueber, A.M., Saller, A.H., et Ishida, H. 1998. Origin, migration, and mixing of brines in the Permian basin: geochemical evidence from the eastern central basin platform, Texas. AAPG Bulletin **82**(9): 1652–1672.

Thorne, G. 2004. Hydrological processes in Precambrian Shield catchments of southeastern Manitoba. *Sous la direction de*. *Dans* AGU Spring Meeting Abstracts, pp. H53E–02.

Tóth, J. 1999. Groundwater as a geologic agent: an overview of the causes, processes, and manifestations. Hydrogeology Journal **7**(1): 1–14.

Walter, J., Chesnaux, R., Boumaiza, L., Brindha, K., et Regenspurg, S. 2023. Conceptual model for the chemical evolution of groundwater in a region of the Canadian Precambrian shield covered by soft Quaternary deposit of glacial and marine origin. Applied Geochemistry **150**: 105574.

Walter, J., Chesnaux, R., Cloutier, V., et Gaboury, D. 2017. The influence of water/rock− water/clay interactions and mixing in the salinization processes of groundwater. Journal of Hydrology: Regional Studies **13**: 168–188.

Walter, J., Chesnaux, R., Gaboury, D., et Cloutier, V. 2019. Subsampling of regional-scale database for improving multivariate analysis interpretation of groundwater chemical evolution and ion sources. Geosciences **9**(3): 139.

Walter, J., Rouleau, A., Chesnaux, R., Lambert, M., et Daigneault, R. 2018. Characterization of general and singular features of major aquifer systems in the Saguenay-Lac-Saint-Jean region. Canadian Water Resources Journal/Revue Canadienne des Ressources Hydriques **43**(2): 75–91.

Warner, N.R., Jackson, R.B., Darrah, T.H., Osborn, S.G., Down, A., Zhao, K., White, A., et Vengosh, A. 2012. Geochemical evidence for possible natural migration of Marcellus Formation brine to shallow aquifers in Pennsylvania. Proceedings of the National Academy of Sciences **109**(30): 11961–11966.

Warr, O., B, S.L., Fellowes, J., Sutcliffe, C.N., McDermott, J.M., Holland, G., Mabry, J.C., et Ballentine, C.J. 2018. Tracing ancient hydrogeological fracture network age and compartmentalisation using noble gases. Geochimica et Cosmochimica Acta **222**: 340–362.

Warr, O., Ballentine, C., Onstott, T., Nisson, D., Kieft, T., Hillegonds, D., et Sherwood Lollar, B. 2022. 86Kr excess and other noble gases identify a billion-year-old radiogenically-enriched groundwater system. Nature Communications **13**(1): 3768.

Warr, O., Giunta, T., Onstott, T.C., Kieft, T.L., Harris, R.L., Nisson, D.M., et B, S.L. 2021. The role of low-temperature 18O exchange in the isotopic evolution of deep subsurface fluids. Chemical Geology **561**: 120027.

Welch, L., et Allen, D. 2014. Hydraulic conductivity characteristics in mountains and implications for conceptualizing bedrock groundwater flow. Hydrogeology Journal **22**(5): 1003.

Xie, Y., Liu, G., Chen, Y., Yang, M., Xia, C., et Huang, X. 2022a. The effects of temperature, pressure and concentration on the hydraulic conductivity of deep groundwater-bearing layers. Hydrogeology Journal **30**(4): 1295–1313.

Xie, Y., Love, A.J., Simmons, C.T., Costar, A., et Wu, J. 2022b. Groundwater age persistence in topography-driven groundwater flow over paleohydrogeologic time scales. Geology **50**(6): 731–735.

Zhang, X., Jiao, J.J., et Guo, W. 2022. How Does Topography Control Topography-Driven Groundwater Flow? Geophysical Research Letters **49**(20): e2022GL101005.

Chapitre 3 : APPLICATION OF HIERARCHICAL CLUSTER ANALYSIS AND PRINCIPAL COMPONENT ANALYSIS TO IDENTIFY COMPOSITIONAL TRENDS OF BRINE IN CRYSTALLINE BASEMENTS AND SEDIMENTARY BASINS

Othniel G.D. Ngombe[1,3]*, Julien Walter[1,3], John Molson[2], Romain Chesnaux[1,3]

[1] Département des Sciences appliquées, Université du Québec à Chicoutimi, Saguenay, Québec, G7H 2B1, Canada

[2] Département de géologie et de génie géologique, Université Laval, Québec, Québec, G1V 0A6, Canada

[3] Centre d'études sur les ressources minérales, Groupe de recherche Risque Ressource Eau, Université du Québec à Chicoutimi, Saguenay, Québec, G7H 2B1, Canada

APPLIED GEOCHEMISTRY

2024

3.1. Mise en contexte

Ce chapitre a permis de répondre à l'objectif 2, lequel vise à distinguer les signatures chimiques des saumures continentales profondes selon leur contexte géologique et à proposer un modèle conceptuel de leur évolution. Pour cela, une base mondiale de 308 échantillons issus du socle cristallin et de bassins sédimentaires a été compilée dans le cadre de cette étude. L'approche repose sur plusieurs outils statistiques: l'analyse hiérarchique en grappes et l'analyse en composantes principales ont permis de mettre en évidence les différentes tendances compositionnelles, et des tests non paramétriques (Wilcoxon/Kruskal-Wallis et Kendall τ) ont permis d'identifier des marqueurs géochimiques objectivement. Des indices de saturation et des facteurs d'enrichissement ont ensuite permis de préciser et discuter des processus de salinisation continentale. Les résultats montrent que les saumures sédimentaires sont dominées par la dissolution/précipitation de la halite, tandis que celles du socle sont contrôlées par l'hydrolyse des silicates et la formation d'argiles. Enfin, des équations linéaires et un graphique discriminant (B/Br vs Li/Br) offrent un cadre quantitatif pour distinguer les deux trajectoires évolutives.

3.2. Author contribution

Othniel G.D. Ngombe: Investigation, Methodology, Visualization, Writing – original draft, Writing – review & editing.

Julien Walter: Project administration, Supervision, Methodology, Writing – review & editing.

Romain Chesnaux: Supervision, Methodology, Writing – review & editing.

John Molson: Supervision, Methodology, Writing – review & editing.

3.3. Abstract

The present study identifies distinct geochemical signatures of deep brines originating from crystalline basements and sedimentary basins. A corresponding conceptual hydrogeochemical model is developed outlining the evolution of crystalline and sedimentary brines. The combined application of Hierarchical Cluster Analysis and Principal Component Analysis allowed the identification of evolutionary trends of groundwater towards crystalline and sedimentary brines. Using 308 brine samples from the existing literature, eight chemical species were considered in the analysis: sodium, magnesium, potassium, calcium, strontium, chlorine, sulphate, and bromine, from which two salinity evolution pathways towards common Ca-Cl brines were derived: (1) the evolution of crystalline brines, which evolved from recharge water to brine through hydration of silicates, is described by the linear equation Ca = -1610 + 0.4*Cl; and (2) the evolution of sedimentary brines, which evolved from recharge water to brine through dissolution and precipitation of halite, is described by the linear equation Cl/Br = 103 + Na/Br. We also discuss differences in water isotopes, and in lithium and boron concentrations which directly reflect various temperature-dependent processes that control the evolution of sedimentary and crystalline brines. This leads to development of a discriminatory graphical tool using B/Br and Li/Br ratios, with crystalline brines having B/Br and Li/Br ratios below 0.01 and sedimentary brines above 0.01. Our results improve our understanding of deep crustal brine evolution through brine-rock interaction.

Keywords: hydrogeochemistry, brines, multivariate statistical analysis, hydrogeochemical evolution, trace elements.

3.3. Introduction

Brines are waters that are highly concentrated in dissolved elements, i.e. with total dissolved solids (TDS) > 35 g/L (Kharaka et Hanor, 2003). In recent years, interest in the formation and evolution of deep brines has been increasing. This is partly due to the growing scientific interest in new energy storage technologies, such as electrical energy storage in lithium-ion batteries which is largely based on the exploitation of Li-rich brines (Araoka et al., 2014; Yu et al., 2022). Deep brines also play a role in alternative energy sources such as natural hydrogen, which can be stored in brine reservoirs (Aslannezhad et al., 2023), and can affect geothermal energy development (Al Radi et al., 2022) and security of deep geological repositories for nuclear waste (Bottomley et al., 1999). Also, upwelling of deep brines can be a serious problem because it contributes to the salinization of subsurface groundwater (Janos et al., 2018), making it unsuitable for domestic, agricultural and industrial uses.

Research dealing with deep brines has been carried out in various contexts, including nuclear waste storage, geodynamics, mine waters, protection of drinking water resources, and the origin of life. In the vast majority of cases, brines have been characterized and interpreted on the basis of their geochemistry. When sampling is possible, direct measurement of the brine composition provides information on the physical and chemical processes to which these fluids have been exposed. Geochemical analysis is the best method to investigate these processes that can otherwise only be investigated indirectly, due to difficulties in accessing such deep underground environments. Thus, the study of deep brines allows us to better understand some fundamental processes in Earth Sciences.

Numerous brine reservoirs in deep environments have been identified around the world (Downing et al., 1987; Bucher et Stober, 2000; Shouakar-Stash et al., 2007), the most important of which have been found in (1) crystalline cratonic rocks e.g., the Miramar Con mine in the Canadian Shield (Bottomley et al., 1999), and the Forsmark and Laxemar sites in the Fennoscandian Shield (Gimeno et al., 2014); and (2) sedimentary basins hosting oil fields (Kharaka et Dorsey, 2005). These two geological environments are distinguished not only on the basis of their composition, such as mineralogy and fracture characteristics, but also on the basis of environmental factors such as

temperature. Crystalline cratonic rocks have an assemblage of silicate minerals, oxides, and crystallized carbonates, low primary porosity, and contain geological structures inherited mainly from tectonic history. Sedimentary basin rocks correspond to assemblages of detrital and orthochemical minerals that show low to high primary porosity and geological structures inherited from depositional mechanisms and tectonic history. Regarding temperature, crystalline rocks have relatively high thermal conductivities and thus show generally lower geothermal gradients than sedimentary rocks (Clauser et Huenges, 1995). These differences between crystalline and sedimentary geological settings result in a wide variety of brine formation processes including, for example, seawater intrusion (Qi et al., 2019), seawater evaporation (Carpenter et al., 1974), dissolution of evaporitic rocks (Kim et al., 2022), cryo-concentration of seawater (Herut et al., 1990), hydrolysis of silicate minerals (Frape et Fritz, 1987), and leaching of fluid inclusions (Nordstrom et al., 1989).

One school of thought suggests that intensive water-rock interaction tends to erase the chemical characteristics of the initial water, be it atmospheric water or seawater (Frape et Fritz, 1987; Savoye, 1998). Based on lithium isotope data, Bottomley et al. (1999) suggested that brines from the Miramar Con mine in Yellowknife have a marine origin and experienced intensive water-rock interaction. Several studies have also assessed the contribution of crystalline and sedimentary settings to groundwater chemistry. Frape et al. (2003) and Kharaka et Hanor (2003) who reviewed the geochemistry of deep waters in crystalline and sedimentary rocks; Walter et al. (2023) used calcium (Ca^{2+}), bromide (Br^{-}), lithium (Li^{+}), and strontium (Sr^{2+}) to investigate the influence of crystalline rock to chemistry of brackish groundwater in Saguenay–Lac–Saint–Jean region. Kaleem et al. (2021), who used barium (Ba^{2+}) and Sr^{2+} as hydrogeochemical tracers to distinguish weathered igneous rocks from sedimentary rocks in the South Mor Range of Balochistan; Yang et al. (2022), who observed through laboratory experiments that the difference of Sr^{2+} concentrations in groundwater between crystalline and sedimentary rocks in northern China was due to Sr-rich minerals such as celestite, gypsum, calcite, and strontianite which are more dominant in sedimentary rocks. Thus, the physical and chemical composition of rocks clearly plays a major role in the chemical composition of groundwater. Considering the significant differences between crystalline and

sedimentary geological settings mentioned above, the chemistry of crystalline and sedimentary brines is also expected to have distinct signatures.

Several studies have already distinguished crystalline and sedimentary brines, e.g. the Canadian Shield, the Central Massif in France, and the Siberian Platform. In most cases the authors used chemistry and isotopic parameters together to separate brine types. While isotopic signatures are very useful in water-rock studies (Clark et Fritz, 1997; Kharaka et Hanor, 2003), large databases collected on a regional scale generally do not include isotopic data (Montcoudiol et al., 2015; Boumaiza et al., 2022b; Walter et al., 2023). This paper aims to identify distinct geochemical signatures of brines originating from crystalline basements and brines from sedimentary basins based mainly on inorganic chemistry (major and minor elements), and discusses the implications with respect to brine genesis. When isotopic data are available, they generally confirm the interpretation based on inorganic chemistry. For this purpose, the specific objectives of the present study are: (1) to define distinct geochemical markers of crystalline brines from basements and from sedimentary basins; (2) to interpret geochemical markers based on physical and chemical differences between crystalline and sedimentary basin settings; and (3) to present different sequences of hydrogeochemical brine evolution through crystalline basements and sedimentary basins.

To achieve the objectives of this study, we compiled 308 analyses of brines from 20 studies in 9 countries which were collected at different depths in the two main host rock types: 133 in crystalline cratonic rocks and 175 in sedimentary basins. In addition to this compiled brine database, several hydrogeochemical poles (endmembers) were also compiled which designated fluids with specific chemical characteristics, such as marine surface water, atmospheric water, geothermal brine, and fluid inclusions. These endmembers were used to identify different contributions to the chemical signatures of brines and to infer hydrogeochemical and environmental characteristics of brines from crystalline basements and sedimentary basins. A multivariate statistical approach is applied to the compiled brine database. This approach has allowed for less subjectivity when grouping brines according to their geological setting, specifically between crystalline and sedimentary rock environments (Walter et al., 2017; Walter et al., 2019), and makes it possible to discuss differences in their geochemical composition.

The present study enhances our knowledge of chemical evolution pathfinders and the general understanding of brine evolution through brine-rock interaction, offering important information and insights to be applied in a variety of fields, including the exploration and development of energy resources and the protection of drinking water.

3.4. Data compilation and geological setting

3.4.1. Data compilation

A total of 20 hydrogeochemical studies were compiled as shown in Tableau 3-1, which included 16 major, minor, trace, and isotopic chemical parameters, and 5 physicochemical parameters as shown in Tableau 3-2 also presents descriptive statistics of the brine database, including the number of observations and the minimum, maximum, and median values of each parameter. Brine samples were selected according to the TDS classification of Kharaka et Hanor (2003). In this database, the TDS of brines ranges from 37 g/L to 512 g/L, and the brine is generally acidic, with 76% of the dataset samples having a pH of below 7 (Tableau 3-2). In addition to 308 brine samples, we compiled 8 samples of surface brines, 22 fluid inclusions, 5 samples of Salton Sea geothermal brines (Tableau 3-1), and 9 endmembers from the study of Laaksoharju et al. (1999) (brine, glacial water, seawater, altered marine and meteoric reference waters and Littorina sea water, sediment pore water, precipitation, and possible subglacial water). The present study also aims to develop hydrogeochemical model based mainly on inorganic chemistry. Nevertheless, in order to interpret these systems more thoroughly than based mainly on inorganic chemistry alone, this study also incorporates isotopic evidence, as water isotope ($\delta^{18}O$ and $\delta^{2}H$) and strontium isotope ($^{87}Sr/^{86}Sr$). The complete database including brine samples and endmembers, which contains data on each sample from the existing literature including their geological contexts, physicochemical parameters, major, minor, trace, and isotopic chemical parameters, is presented in the supplementary material (ANNEXE II).

Most brine samples in this database are located in geological settings that are dominated by one of two rock types: crystalline or sedimentary (Tableau 3-1). These include groundwater in formations of large sedimentary basins, e.g., samples from Carpenter et al. (1974); deep fluids in crystalline rocks, e.g., samples from Bucher et Stober (2010); brines encountered in the context of

deep nuclear waste disposal sites in crystalline rocks, e.g., samples from Blomqvist (1999), and brines encountered during mining exploitation, e.g., samples from Frape et Fritz (1982).

The compiled source data and their geological source locations are presented in Tableau 3-1. Brines compiled for this study were collected at great depths as listed in Tableau 3-2, with 83% of the dataset samples having been collected deeper than 500 m. At these depths, the increase in lithostatic pressure decreases the permeability of the geological medium (Jiang et al., 2009), and favor dispersion over advection (Gascoyne et Kamineni, 1994). In these cases, geological environments with very low permeability can be considered as closed systems (Zuddas, 2010) which subsequently leads to an increase in the residence time of groundwater. This topic was confirmed by several studies such as Gerber et al. (2017), who, based on ^{81}Kr and noble gases, suggest that deep sedimentary brines in the Baltic Artesian Basin are very old, ranging from 300 Ka to 1.3 Ma. Deep crystalline brines can also be geologically old (Frape et al., 2003), as illustrated by Warr et al. (2022) who used ^{86}Kr excess and noble gases to derive residence times on billion-year geologic timescales. Such extended residence times amplify the degree of maturity of water-rock interactions. In such cases, it is reasonable to accept the hypothesis that, over the associated long-time scales, the brines have been imprinted with the chemical signature of the host geological medium. Thus, in this study, rock types were defined according to the geological setting of each referenced study compiled in the database, as shown in Tableau 3-1.

Tableau 3-1: Data sources used to create the brine database.

Data source	Geology/Location	Country	Crystalline basement	Fluid inclusion	Geothermal brine	Sedimentary basin	Surface water
Blomqvist (1999)	Fennoscandian Shield	Finland	2	-	-	-	-
Bottomley et al. (1999)	Canadian Shield	Canada	16	-	-	-	-
Bucher et Stober (2010)	Bohemian Massif	Germany	1	-	-	-	-
	Canadian Shield	Canada	3	-	-	-	-
	Fennoscandian Shield	Sweden	1	-	-	-	-
	Hercynian Crystalline Massif	France	3	-	-	-	-
	Ukrainian Shield	Ukraine	1	-	-	-	-
Carpenter et al. (1974)	Central Mississippi Salt Dome Basin	USA	-	-	-	80	-
Cortecci et al. (2001)	Aeolian Archipelago	Italy	-	-	-	-	2
Edmunds et al. (1984)	Cornubian Batholith	United Kingdom	11	-	-	-	-

Frape et Fritz (1987)	Canadian Shield	Canada	18	-	-	-	-
Frape et al. (1984)	Canadian Shield	Canada	11	-	-	-	-
Frape et al. (2003)	Canadian Shield	Canada	16	-	-	-	-
	Fennoscandian Shield	Finland	10	-	-	-	-
		Sweden	2	-	-	-	-
	Siberian Platform	Russia	6	-	-	-	-
Frape et Fritz (1982)	Alberta Basin	Canada	-	-	-	3	-
	Canadian Shield	Canada	5	-	-	-	-
	Illinois Basin	USA	-	-	-	1	-
	Israel	Israel	-	-	-	-	1
	Michigan (Centennial mine)	USA	1	-	-	-	-
	Michigan Basin	USA	-	-	-	2	-
	Nevada (Comstock mine)	USA	1	-	-	-	-
	New Mexico (Salado)	USA	-	-	-	1	-
	New York	USA	1	-	-	-	-
	Salton Sea - Geothermal brines	USA	-	-	1	-	-
	Siberian Platform	Russia	1	-	-	-	-
	Utah Great Salt Lake	USA	-	-	-	-	1
Gascoyne et Kamineni (1994)	Canadian Shield	Canada	2	-	-	-	-
Kim et al. (2022)	Paradox Basin	USA	-	-	-	28	2
Kelly et al. (1986)	Fennoscandian Shield	Sweden	1	-	-	-	-
Lucas et al. (2010)	Hercynian Crystalline Massif	France	1	-	-	-	-
Nordström et al. (1985)	Fennoscandian Shield	Sweden	1	-	-	-	-
Nurmi et al. (1988)	Fennoscandian Shield	Sweden	2	-	-	-	-
Pauwels et al. (1993)	Hercynian Crystalline Massif	France	11	-	-	-	-
Steuber (1999)	Permian Basin	USA	-	-	-	31	1
Tellam (1995)	Mersey Basin	United Kingdom	-	-	-	14	-
Unpublished data	Canadian Shield	Canada	5	-	-	-	-
Yardley (2013)	Alberta Basin	Canada	-	-	-	4	-
	Au-Quartz Fluids - Brusson	Italy	-	3	-	-	-
	Black Smoker Fluids	N/A	-	1	-	-	-
	Central Mississippi Salt Dome Basin	United Kingdom	-	-	-	2	-
	Columbian Emerald deposits - metamorphic fluid	Colombia	-	2	-	-	-
	Cornubian Batholith	United Kingdom	-	4	-	-	-

	Kakkonda - magmatic fluids	Japan	-	1	-	-	-
	Michigan Basin	USA	-	-	-	3	-
	Modum Complex, Norway	Norway	-	3	-	-	-
	Mole granite - magmatic fluids	Australia	-	3	-	-	-
	North Sea - oil field formation waters	United Kingdom	-	-	-	3	-
	Offshore Louisiana	USA	-	-	-	3	-
	Pyrenees metamorphic fluids	France	-	5	-	-	-
	Salton Sea - Geothermal brines	USA	-	-	4	-	-
	Seawater	-	-	-	-	-	1
Total			133	22	5	175	8

3.4.2. Geological settings

3.4.2.1. Crystalline basements

Crystalline basement brines compiled in this study come from diverse geological environments, with host rock ages varying from Precambrian to Late Paleozoic. Precambrian shields generally outcrop at the surface but are locally covered by Quaternary sediments. Because Precambrian shields had not recently experienced any major tectonic events such as volcanism, they are considered geologically inactive anorogenic continental crusts (Dewey et al., 2021; Bungum et Eldholm, 2022). While younger rocks are generally covered by thick sequences of sedimentary rock, i.e. > 1 km (Pauwels et al., 1993; Bucher et Stober, 2010), these geological areas have compressed tectonic regimes. This is the case of the Variscan and Alpine orogens, which affected a large part of Europe, helping to form mountain ranges. Numerous glaciation-deglaciation events over geological time have led to the creation or reactivation of fractures in the crystalline rocks (Frape et al., 2003) which form favourable groundwater pathways.

Despite their differences, these crystalline basements have some common characteristics in terms of their lithologies and mineralogy (ANNEXE III). In permanent contact with groundwater, the assemblage of rock-forming minerals is one of the main factors affecting groundwater chemistry through water-rock interaction (André et al., 2006; Morales-Arredondo et al., 2022). Then, this study did not consider the age differences between crystalline rocks. Crystalline basements contain a wide

variety of igneous rocks, and metamorphic rocks such as granites, granodiorites, basalt, gabbro, gneiss, amphibolite, migmatites, schist, or greenstone rocks (Blomqvist, 1999; Bottomley et al., 1999; Bucher et Stober, 2000). Silicate minerals such as anorthite ($CaAlSi_3O_8$), K-feldspar ($KAlSi_3O_8$), albite ($NaAlSi_3O_8$), quartz (SiO_2), biotite ($KMg_3AlSi_3O_{10}(OH)_2$) and other accessory minerals are present in significant quantities in these formations (Perri, 2020), while alteration minerals such as mineralogical clays, zeolites, carbonates, and sulfates are often present in fractures (Stalder et al., 1980). Detailed lithologies by geological area are provided in ANNEXE III.

3.4.2.2. Sedimentary basins

All sedimentary brines compiled in this paper were collected from sedimentary basin oil fields, except for the study by Tellam (1995), and ranged in age from the Paleozoic to the Recent. As documented in the studies listed in the brine compilation Tableau 3-1, oilfield sedimentary basins are generally composed of clastic rocks such as shales, conglomerates or sandstones, sequences of evaporitic rocks, e.g., gypsum ($CaSO_4 \cdot 2H_2O$), halite (NaCl), sylvite (KCl), carnallite ($KMgCl_3 \cdot 6H_2O$), and carbonate rocks (physicochemical and micritic) such as limestone and dolomite. Silicate minerals are also present in sedimentary basins, and are encountered in sandstone, shale or conglomerate, for example (Mizutani, 1970).

3.4.3. Field sampling methods

Numerous sampling techniques were used to obtain brine samples from crystalline rocks in the referenced studies, ranging from hydrostatic or lithostatic drainage of boreholes to highly sophisticated pumps and pressurized samplers (Frape et al., 2003). Data from the sedimentary brines were mostly collected from oilfield sedimentary basins. During oil and gas development, brines are generally collected directly from the wellhead or from an oil-brine separator tank. Brines from sedimentary rocks were generally collected according to procedures given by Kharaka et al. (1987) and McIntosh et Walter (2005). Despite the various sampling methods used in the compiled brine database, good consistency was obtained for major and minor elements as shown in Section 3.6. This indicates that variations observed in the geochemical data are likely to be due to natural variations in the samples themselves, rather than artifacts of the applied sampling methods (Frape et

al., 2003; Kharaka et Hanor, 2003). We therefore assumed an absence of bias associated with the sampling methods.

Tableau 3-2: Descriptive statistics for the physicochemical parameters of the assembled brine database

Parameter	Crystalline basement				Sedimentary basin			
	N	Min	Med	Max	N	Min	Med	Max
TDS* (g/L)	133	37	108	512	175	37.2	209	441
Depth (m)	81	25	1372	5000	37	14	1522	2702
Alkalinity* (mg/L $CaCO_3$)	98	1.6	23	3311	51	4.9	127	2024
T (°C)	34	4	21.5	115	32	14.2	30.1	135
pH	55	5	6.6	9.1	42	5.18	6.5	8.2
Na (g/L)	133	0.5	14	64	175	9.82	53.9	122
Mg (g/L)	121	0	0.3	35.5	174	0.1	2.03	38.3
K (g/L)	131	0	0.2	28.9	173	0.01	0.86	22.6
Ca (g/L)	133	1.16	22.6	202	175	0.10	16.8	124
HCO_3 (mg/L)	98	2	28	4040	51	6	155	2470
Cl (g/L)	133	0.12	65.9	252	175	16.8	124	263
SO_4 (g/L)	118	0	0.21	78.6	118	0	0.42	222
Ba (mg/L)	32	0.09	2.55	17.1	142	0.04	20	780
B (mg/L)	41	0.03	3.4	40.3	50	0.01	18	142
Fe (mg/L)	34	0.20	8.33	400	159	0.01	47	490
Li (mg/L)	56	0.03	0.89	210	83	0.5	14	85
Sr (mg/L)	109	13	558	2279	160	2.3	799	6030
Mn (mg/L)	23	0.51	3.04	25.1	125	0.01	3	344
Br (mg/L)	113	137	726	14382	165	9	868	3109
$\delta^{18}O$ (‰)	53	-23	-11.9	12.1	55	-14.7	-1.3	6.1
$\delta^{2}H$ (‰)	53	-163	-64	81	55	-110	-37	12.9

*Estimated chemical parameters:
TDS = ∑ (chemical element, mg/L);
Alkalinity = [HCO3]/1.22 (mg/L $CaCO_3$)

3.5. Methodology

The statistical analysis approach that was used in this study is based on a combination of hierarchical cluster analysis (HCA), principal component analysis (PCA) (Güler et al., 2002), as well as Wilcoxon/Kruskal-Wallis and Kendall τ statistical tests (McKight et Najab, 2010; Pohlert, 2016). Enrichment factors (EFs), saturation indices (SI) and interpretation of biplot graphs were also used to discuss the origin of dissolved elements. The data treatment methods used to determine the geochemical characteristics of samples and the evolution of groundwater are presented in the following sections.

3.5.1. Statistical analysis

3.5.1.1. Selection of samples and chemical elements for multivariate statistical analysis

Chemical parameters missing from more than 25% of the samples were not used for the multivariate statistical analysis (Farnham et al., 2002). As a result, 8 chemical parameters were selected for the multivariate statistical analysis: sodium (Na^+), potassium (K^+), magnesium (Mg^{2+}), calcium (Ca^{2+}), strontium (Sr^{2+}), chlorine (Cl^-), sulfate (SO_4^{2-}) and bromine (Br^-). For these 8 chemical parameters, data below the detection limit (DL) were substituted by DL/2 (Farnham et al., 2002). Also, 2 samples with a charge balance exceeding the acceptability threshold of ±10% were excluded from the database (Kloppmann et al., 2011). Despite their importance, but due to limited data and to provide better focus, the multivariate statistical analysis applied here did not include parameters such as the geologic age and the lithology of the host rock, temperature, and fluid pressure.

3.5.1.2. Multivariate statistical analysis

While the approach assumes that the statistical distribution of input variables is normal (Brown et al., 1998), the distribution of geochemistry data is generally skewed and indeed, in this study, Na^+, Ca^{2+}, K^+, Mg^{2+}, Sr^{2+}, Br^-, Cl^-, and SO_4^{2-} concentrations did not follow a normal distribution based on the Shapiro-Wilk statistical test (Reimann et Filzmoser, 2000; Moussaoui et al., 2023). A base-10 log transformation was therefore applied to convert the data from asymmetric to normal distributions. To ensure equal weighting, each selected element was then standardized (Cloutier et al., 2008) using Eq. 3.1 (Davis, 2002) :

$$Z_i = \frac{(X_i - \overline{X})}{\sigma} \qquad (\text{Eq. } 3.1)$$

where Z_i is the standard score of sample i, X_i is the concentration of sample i, $\overline{X}$ is the mean concentration, and σ is the standard deviation. JMP version 16 software was used to perform the statistical analysis on all datasets (Sall et al., 2017).

3.5.1.2.1. Hierarchical cluster analysis

In this paper, HCA was used as a classification statistical method to objectively group the brines according to their rock type (crystalline or sedimentary). In the face of ambiguity concerning

the geological origin of brines, the application of HCA has been decisive, revealing the existence of unique chemical characteristics specific to crystalline and sedimentary brines. Also, HCA made it possible to verify if any brine samples would be grouped within the geothermal brine pole. For this reason, 5 samples from the Salton Sea geothermal brine were added to 308 brine samples. Güler et al. (2002) showed that Euclidean distance and Ward's method created the most distinct groundwater chemical analysis clusters; thus, this was the chosen approach for the present study.

3.5.1.2.2. Principal component analysis

PCA was used to define those geochemical markers able to distinguish crystalline from sedimentary brines. In this paper, the number of components retained was based on the Kaiser criterion (Kaiser, 1960; Yeomans et Golder, 1982).

3.5.2. Wilcoxon/Kruskal-Wallis and Kendall's τ tests

The objectivity of defining geochemical markers of brines was improved using Wilcoxon/Kruskal-Wallis and Kendall τ statistical tests, which are non-parametric tests and therefore do not require the assumption of normal distribution. The Kendall τ test was used to assess the correlation between two chemical elements (Pohlert, 2020; Boumaiza et al., 2022b). As the Kendall τ value approaches 1, the correlation between chemical elements increases. The Wilcoxon/Kruskal-Wallis test is a test of dependence (McKight et Najab, 2010), which was used here to compare quantitative values of chemical elements on HCA-generated clusters, i.e., to determine if a chemical element can be used to distinguish one cluster from others. The corresponding p-value was used to evaluate the level of significance of the statistical test, with a significance threshold of 0.05. The Wilcoxon/Kruskal-Wallis test is significant if $p < 0.05$, in which case the chemical element is considered discriminant for clusters. The test is not significant if $p > 0.05$, in which case the chemical element is not discriminant for clusters. This test has proved reliable for rigorously identifying the discriminating chemical parameters between crystalline and sedimentary brines.

3.5.3. Saturation indices and enrichment factors

To interpret geochemical markers of brines, SIs were calculated using PHREEQC (Appelo et Postma, 2005) in all samples with respect to halite, sylvite, carnallite, dolomite, calcite, anhydrite,

gypsum, and celestite. It is essential to note a limitation in calculating SIs for silicate minerals, which is mainly due to problems with degree of crystallinity, compositional variations, and lack of data on dissolved aluminum in the compiled brine database. To solve silicate-equilibria problems, several studies have used silicate stability diagrams (Helgeson, 1978; White et al., 2001; Gimeno et al., 2014; Houyun et al., 2022), which assume that all Al^{3+} is preserved in the weathering product. Unfortunately, the lack of data on silicic acid (H_4SiO_4) does not allow this method to be applied in our study. However, the interpretations made on the basis of the methods proposed herein are corroborated by a large body of scientific literature, and are thus considered robust in the context of meeting the study's objectives. Due to the high ionic strength of the highly concentrated brines in this study, the Pitzer thermodynamic database was applied (Plummer, 1988).

Enrichment factors (EF) were used to compare brine chemical compositions to seawater chlorine abundance. The aim of this comparison is to provide an analytical framework, without assuming the direct involvement of seawater in all cases. The observed deviations from seawater composition help us to explore other potential sources and processes affecting the salinity of the brines studied here. EFs for each component i are defined by Bottomley et al. (1999) as :

$$\mathrm{EF} = \frac{\left(\frac{\mathrm{X_i}}{\mathrm{Cl}}\right)_{\mathrm{Brine}}}{\left(\frac{\mathrm{X_i}}{\mathrm{Cl}}\right)_{\mathrm{seawater}}} \qquad (\mathrm{Eq.\ 3.2})$$

where X_i denotes the concentration of solute component i. The Atlantic Ocean sample from Goldberg et al. (1971) was used in this study as the standard seawater reference.

Standard Error was also used to assess the representativeness of mean values based on the dispersion of the variable around the mean. A standard error of about 5% suggests that there is a 95% probability that the mean value (chemical concentrations, EFs) is exact and statistically reliable (Di Leo et Sardanelli, 2020). Higher errors may be due to different mineral solubility constants, to different reaction kinetics, or to mixing between groundwaters of different chemical compositions.

3.6. Results

3.6.1. Hierarchical cluster analysis

HCA results are presented in a dendrogram (Figure 3-1) which shows that the degree of similarity between clusters increases from the bottom to the top of the graph. The number of clusters generated by HCA depends on the position of the Phenon line that cuts the dendrogram. Here, 205 brine samples from the dataset were grouped into five clusters, which were able to give the most satisfactory results, thus fulfilling the main objective of distinguishing crystalline basement brines from sedimentary basin brines. Tableau 3-3 presents a geographical and geological distribution of the clusters and Tableau 3-4 lists the descriptive statistics (minimum, maximum, and median) of all physicochemical and hydrogeochemical parameters of the HCA-generated clusters. All geochemical data comprising the HCA-generated clusters are presented in the supplementary material (ANNEXE IV).

Tableau 3-3: Geographical and geological distribution of clusters

Clusters	Geology/Location	Country	*N	Total
Cluster 1	Bohemian Massif	Germany	1	44
	Canadian Shield	Canada	31	
	Fennoscandian Shield	Finland	8	
		Sweden	4	
Cluster 2	Alberta Basin	Canada	3	41
	Hercynian Crystalline Massif	France	1	
	Mersey Basin	United Kingdom	8	
	Offshore Louisiana	USA	2	
	Paradox Basin	USA	13	
	Permian Basin	USA	13	
	Salton Sea - Geothermal brines	USA	1	
Cluster 3	Central Mississippi Salt Dome Basin	USA	5	50
	Fennoscandian Shield	Finland	2	
	Hercynian Crystalline Massif	France	9	
	Offshore Louisiana	USA	1	
	Paradox Basin	USA	10	
	Permian Basin	USA	18	
	Salton Sea - Geothermal brines	USA	4	
	Siberian Platform	Russia	1	
Cluster 4	Canadian Shield	Canada	36	37
	Siberian Platform	Russia	1	

Cluster 5	Alberta Basin	Canada	3	33
	Canadian Shield	Canada	4	
	Central Mississippi Salt Dome Basin	USA	22	
	Paradox Basin	USA	1	
	Siberian Platform	Russia	3	
Total				205

*N – number of samples in each cluster

Based on concentrations given in meq/L, major cations and anions were combined to define water type; see Cloutier et al. (2004) for details. Clusters C1 and C4 are predominantly Ca-Cl type, i.e., 88% and 97% of samples, respectively, while clusters C2 and C3 are both Na-Cl type, and cluster C5 is mainly Ca-Na-Cl type, i.e., for 81% of the samples (Figure 3-1b).

Cluster C1 and C4 samples were mainly collected in the crystalline basement (97% of cluster C1 samples and 100% of cluster C4 samples). Samples of clusters C2, C3, and C5 were collected mainly from sedimentary basins (95%, 68%, and 78%, respectively) (Figure 3-1c). Salton Sea geothermal brine samples and all samples collected in young crystalline rocks (specifically in the geological areas with significant sedimentary rock thickness) are also grouped in clusters C2, C3, and C5. We can also observe that 2 samples from the Fennoscandian Shield are grouped with cluster C3 and 4 samples from Canadian Shield are grouped with Cluster C5.

The median TDS values of clusters C1 and C2 are 74 g/L and 64 g/L, respectively, while clusters C3, C4 and C5 have higher median values of 182 g/L, 241 g/L and 280 g/L, respectively.

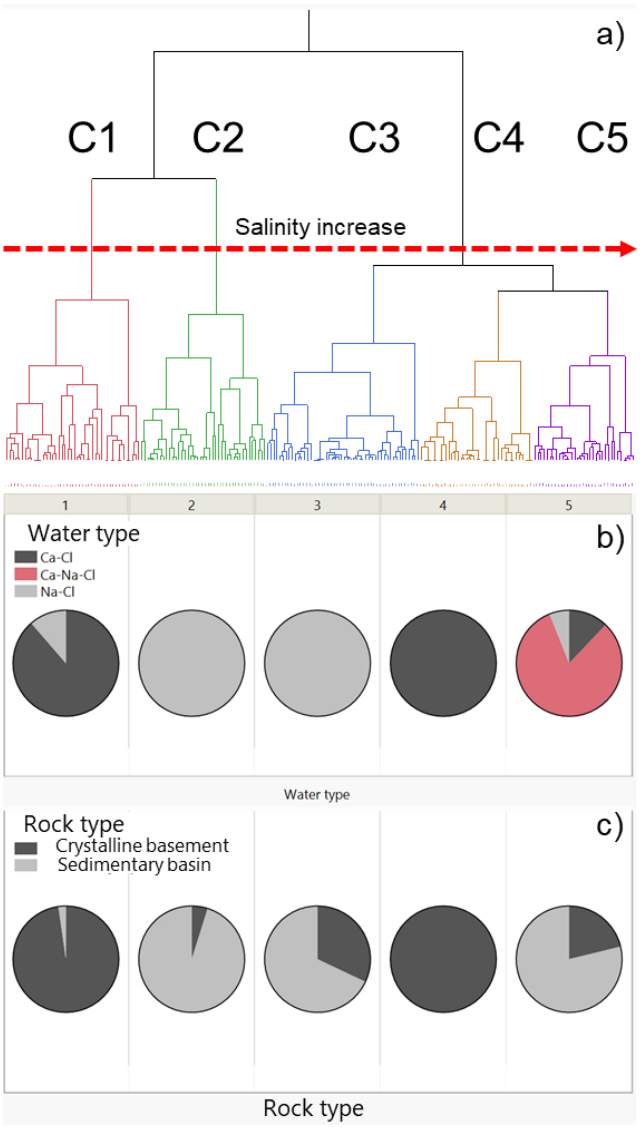

Figure 3-1: a) Graphical presentation of a dendrogram produced from HCA. Position of the Phenon line which divided samples into five groups. Colors on the dendrogram represent different HCA-generated clusters. b) Distribution of water type by HCA-generated clusters. c) Distribution of rock type by HCA-generated clusters.

3.6.2. Principal component analysis

Principal components were extracted from the symmetric correlation matrix (ANNEXE V), which was calculated from the dataset. The PCA analysis results are represented in a correspondence circle, with the horizontal axis of the circle corresponding to PC1 (49% of the total variance of the dataset) and the vertical axis of the circle corresponding to PC2 (24.8% of the total variance of the dataset). PC1 and PC2 explain 73.8% of the total variance of the dataset (Figure 3-2).

Samples of clusters C1 and C2 are located on the left side of PC1 in Figure 3-2a, while samples of clusters C3, C4, and C5 are located on the right side of PC1. From left to right of PC1, TDS increases, ranging from 37 g/L to 352 g/L. On the PC2 axe, samples from clusters C2, C3 and C5 have an almost positive load, reflecting their positive contribution to this axe, i.e. 93% of these samples are distributed in the positive part of PC2. Inversely samples from clusters C1 and C4 all have negative loads except one sample, i.e., 99% of these samples are distributed in the negative part of PC2.

PC2 separates chemical elements in two parts in the loading matrix (ANNEXE V): positive coefficients (Na^+, K^+, Mg^{2+}, SO_4^{2-}) and negative coefficients (Ca^{2+}, Sr^{2+}, Br^-) (Figure 3-2b). The variance of brine samples from sedimentary basin (C2, C3, and C5) is highly correlated with Na^+, K^+, Mg^{2+}, and SO_4^{2-}, while the variance of samples from crystalline basement (C1 and C4) is highly correlated with Ca^{2+}, Sr^{2+}, Br^-. Samples from cluster C2 are mainly characterized by a higher correlation with SO_4^{2-} and are anti-correlated with Br^-, Sr^{2+}, and Ca^{2+}, in comparison to clusters C3 and C5 (Figure 3-2). Cluster C5 is distinguished from cluster C3 by higher control of Br^- and Sr^{2+} on the sample variance. Samples from clusters C1 and C4 can be distinguished by their K^+ and Na^+ concentrations. Cluster C1 represents Na-K-poor brine and cluster C4 represents Na-K-rich brine.

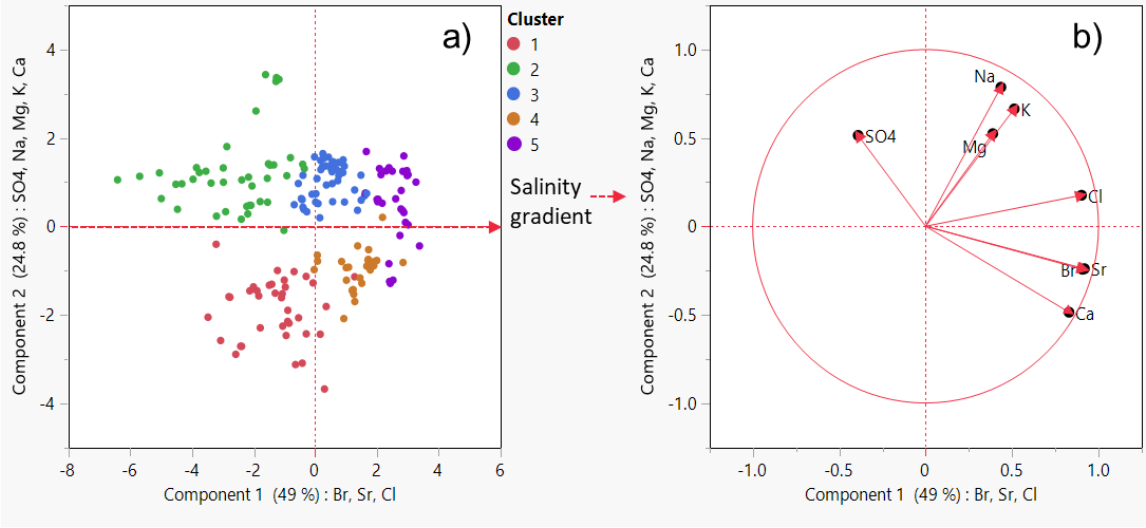

Figure 3-2: Graphical representations of two components derived from the principal component analysis (PCA). Component 1 (Br^-, Sr^{2+}, and Cl^-) explained 49% of the total variance of the data set while Component 2 (Na^+, K^+, Mg^{2+}, and Ca^{2+}) explained 24.8%. a) PCA diagram of samples classified by cluster. b) PCA showing the chemical element loadings.

In summary, HCA has allowed to distinguish 5 chemically distinct clusters. Clusters C2, C3, and C5 represent brines from sedimentary basins, while clusters C1 and C4 represent brines from crystalline basements. As the PC1 revealed, clusters are mainly distinguished by their TDS, from lower concentration brines (C1 and C2) to higher concentrations (C3, C4, and C5). This progressive increase of TDS from one cluster to another as shown in Figure 3-2a follows a salinization process from lower-concentration to higher-concentration brines, as a continuum (water-rock interactions and long residence time) or human-induced mixing between fresh water and brines (Frape et al., 2003).

PC2 represents the geological setting of the brines, which shows that brines from sedimentary basins have positive coefficients in the loading matrix, while those from crystalline basements have negative coefficients. In the following discussion, brines from sedimentary basins (C2, C3, and C5), characterized by the covariance of parameters Na^+, K^+, Mg^{2+}, and SO_4^{2-}, are designated as “sedbrine clusters”, with cluster C2 sedbrine 1, C3 sedbrine 2, and C5 sedbrine 3, while brines from crystalline basements (C1 and C4), characterized by the covariance of parameters Br^-, Sr^{2+}, and Ca^{2+}, are designated as “shieldbrine clusters”, with cluster C1 shieldbrine 1 and C4 shieldbrine 2.

Tableau 3-4: Statistical summary of clusters generated by HCA.

Parameter	Shieldbrine samples									
	Shieldbrine 1					Shieldbrine 2				
	N	Min	Med	Max	Std err. %	N	Min	Med	Max	Std err. %
TDS* (g/L)	44	37	74	225	6.91	37	109	241	324	3.98
Depth (m)	33	470	1300	4000	12	24	1220	1600	3600	6.19
Alkalinity* (mg/L $CaCO_3$)	43	5.7	21	82	11.2	28	1.6	14.3	83	19.3
T (°C)	13	4	20	23	7.85	16	9.5	21	22.5	3.88
pH	21	5	6.6	8.3	2.31	20	5	6.6	6.9	2.07
Na (g/L)	44	1.68	8.51	16	3.69	37	10.4	21.7	45	3.69
Mg (g/L)	44	0	0.27	5.26	9.83	37	0.01	0.29	5.1	9.83
K (g/L)	44	0	0.06	0.34	26.3	37	0.11	0.25	1.2	26.3
Ca (g/L)	44	4.2	16.1	65	8.31	37	22.8	63.8	109	8.31
HCO_3 (mg/L)	43	7	26	100	11.2	28	2	17.5	101	19.6
Cl (g/L)	44	19.2	45	156	11	37	65.9	156	207	11
SO_4 (g/L)	44	0	0.16	4.4	12.7	37	0.01	0.18	0.49	12.7
Ba (mg/L)	11	0.09	1	2.54	25.4	9	2.56	9	17.1	15.9
B (mg/L)	16	0.71	1.57	5.88	17.7	11	1.99	3.71	6.2	9.79

Fe (mg/L)	14	0.2	1.84	47	51.7	4	2.07	3.54	18.6	56.9
Li (mg/L)	20	0.03	0.48	6.13	35	20	0.07	0.81	4.35	19.5
Sr (mg/L)	44	28.8	319.5	1390	10.3	37	530	1247	2279	5
Mn (mg/L)	14	0.51	1.62	8	21.7	3	1.3	4.57	4.57	31.3
Br (mg/L)	44	137	451	1134	7.39	37	633	1250	4725	7.76
$\delta^{18}O$ (‰)	25	-23	-12.2	-7.6	6.53	20	-19.3	-13.6	-6.2	5.7
$\delta^{2}H$ (‰)	25	-163	-71	-16	11.8	20	-126	-65.5	-31	10.1
$^{87}Sr/^{86}Sr$	9	0.7075	0.7141	0.7188	0.14	5	0.7142	0.7144	0.7147	0.02

*Estimated chemical parameters:
TDS = ∑ (chemical element, mg/L);
Alkalinity = [HCO3]/1.22 (mg/L $CaCO_3$)
N/A: Non-available.

Table 3-4 (continued)

Parameter	Sedbrine samples									
	Sedbrine 1					Sedbrine 2				
	N	Min	Med	Max	Std err. %	N	Min	Med	Max	Std err. %
TDS* (g/L)	41	37.2	64	321	10.9	50	88.8	182	278	3.71
Depth (m)	20	14	242	4444	25.7	14	946	1924	5000	14.2
Alkalinity* (mg/L $CaCO_3$)	25	4.9	226	628	14.3	17	60	123	706	21.6
T (°C)	12	14.2	21.5	230	34.5	15	14.9	25.4	330	33.6
pH	22	5.75	6.61	8.2	2.03	14	5.45	6.21	9.1	3.83
Na (g/L)	41	11.5	22.5	122	12.5	50	27.4	54	99.6	3.69
Mg (g/L)	41	0.05	0.93	1.99	9.87	50	0.03	1.73	4.42	9.83
K (g/L)	41	0.03	0.41	2.71	18.7	50	0.38	0.85	17.7	26.3
Ca (g/L)	41	0.16	2.18	7.1	11.2	50	4.81	9.88	36.4	8.31
HCO_3 (mg/L)	25	6	276	766	14.3	17	73.3	150	861	21.6
Cl (g/L)	41	19.5	36.8	192	11	50	50.9	109	170	11
SO_4 (g/L)	41	0.01	1.24	4.69	12.7	50	0.01	0.35	1.59	12.7
Ba (mg/L)	30	0.04	0.3	53	56.3	38	0.26	3.2	353	35.3
B (mg/L)	26	0.01	11	92	24.8	25	4	32	271	25.2
Fe (mg/L)	40	0	0.63	86	38.6	45	0.25	36	1710	31.8
Li (mg/L)	25	0.5	5.2	55	28.8	28	2	14.2	210	22.1
Sr (mg/L)	41	2.3	77	499	14.4	50	156	485	1750	7.07
Mn (mg/L)	38	0.01	0.29	60	57.7	35	0.25	0.74	1500	53.5
Br (mg/L)	41	9	113	460	12.4	50	78	502	1219	6.94
$\delta^{18}O$ (‰)	26	-14.7	-6.7	4.36	16.7	30	-11.8	4.41	6.1	66.9
$\delta^{2}H$ (‰)	26	-111	-52	-19	9.33	30	-74.9	-17	-4.2	12.5
$^{87}Sr/^{86}Sr$	25	0.7072	0.7086	0.7175	0.07	27	0.7084	0.7088	0.7128	0.03

Table 3-4 (continued)

Parameter	Sedbrine samples				
	Sedbrine 3				
	N	Min	Med	Max	Std err. %
TDS* (g/L)	33	167	280	352	2.66
Depth (m)	5	500	834	2239	28.9
Alkalinity* (mg/L $CaCO_3$)	6	1.6	1.6	474	65.3
T (^oC)	5	22.5	34.8	124	35.9
pH	3	5.18	5.55	6.7	7.88
Na (g/L)	33	4.03	58.3	79.1	3.69
Mg (g/L)	33	0.92	2.79	27.6	9.83
K (g/L)	33	0.5	2.72	17.7	26.3
Ca (g/L)	33	23.5	38.7	94.7	8.31
HCO_3 (mg/L)	6	2	2	578	65.3
Cl (g/L)	33	103	173	212	11
SO_4 (g/L)	33	0	0.08	0.52	12.7
Ba (mg/L)	24	1.92	77	109	10.9
B (mg/L)	2	9.19	75.6	142	87.8
Fe (mg/L)	24	3	269.5	420	13.2
Li (mg/L)	13	1.67	49	64	12.3
Sr (mg/L)	33	702	1640	2340	4.81
Mn (mg/L)	22	0.49	60	181	16.5
Br (mg/L)	33	930	1550	5637	9.17
$\delta^{18}O$ (‰)	6	-14.4	-6.7	5	46.9
$\delta^{2}H$ (‰)	6	-73	-61.5	12.9	27.7
$^{87}Sr/^{86}Sr$	1	0.7097	0.7097	0.7097	N/A

3.6.3. Saturation index and enrichment factor

Tableau 3-5 shows statistical results (minimum, median, maximum) by cluster. SIs for calcite and dolomite were calculated for those samples where HCO_3^- concentrations were available. The median SI value for halite reveals that sedbrine 1 samples are generally undersaturated, except for five samples (where $[Cl^-]$ > 3 mol/L), four of which are from the Paradox Basin, Colorado Plateau, USA. Again, with respect to halite, sedbrine 2 and 3 samples are generally near saturation and saturated, respectively, indicating a general equilibrium with halite. Sedbrine clusters are undersaturated for sylvite and carnallite but oversaturated for calcite and dolomite. With respect to gypsum, anhydrite, and celestite, sedbrine and shieldbrine cluster SI values are mainly negative,

implying they are undersaturated with respect to these minerals. SIs for each sample are presented in ANNEXE VI. Even though silicate minerals don't dissolve easily, several studies on the thermodynamic equilibria between water and silicate minerals show how they can affect the chemistry of groundwater (Helgeson, 1978; White et al., 2001; Gimeno et al., 2014). Based on previous studies, for example, Bucher et Stober (2010) conclude that Na-plagioclase and biotite, as well as other iron and magnesium silicates, are generally not in equilibrium with deep groundwaters, whereas these waters are generally saturated with respect to potassium feldspar and quartz.

EFs were calculated for 14 chemical parameters (Na^+, K^+, Mg^{2+}, Ca^{2+}, Sr^{2+}, Cl^-, SO_4^{2-}, Br^-, Li^+, HCO_3^-, B^{3+}, Mn^{2+}, Fe^{2+}, Ba^{2+}) and provided in Tableau 3-6 (with median and standard errors in percentage). EF_{Na} values from sedbrine 1 samples have a median of 1.10 with a standard error of about 1.77%. For sedbrine 2 samples, the EF_{Na} median value is 0.92 with a standard error of about 1.92% which indicates a depletion of the Na/Cl ratio in comparison with sedbrine 1 samples. For sedbrine 3 samples, the median EF_{Na} value is 0.59 with a standard error of about 6.28% which indicates a depletion of the Na/Cl ratio in comparison with sedbrine 1 and 2 samples. High standard errors of EF_K of about 16.1%, 20.7%, and 16.5% for sedbrine 1, 2, and 3 samples, respectively, indicate a variability around the mean which suggests several sources of K^+ in the sedbrine clusters. EF_{Mg} and EF_{Ca} median values indicate a depletion of Mg^{2+} and enrichment of Ca^{2+} compared to seawater. High standard errors of EF_{Mg}, and EF_{Ca} indicate dispersion around the mean value which suggests different sources of Ca^{2+} and Mg^{2+} for sedbrine. Standard error differences of Ca/Sr ratios (ANNEXE V) of about 12% for shieldbrine 1 samples and 3.04% for shieldbrine 2 samples, indicate that there are more Ca^{2+} and Sr^{2+} mineral sources in shieldbrine 1 samples than in shieldbrine 2 samples.

Tableau 3-5: Statistical summary of saturation indices for the shieldbrine and sedbrine samples

Mineral	Shieldbrine samples							
	Shieldbrine 1				Shieldbrine 2			
	N	Min	Med	Max	N	Min	Med	Max
SI (halite)	44	-2.72	-2.18	-1.32	37	-1.62	-0.68	0.34
SI (dolomite)	43	-2.81	0.16	3.36	19	0.81	2.9	4.73
SI (calcite)	43	-0.05	0.75	1.8	19	1.02	2.23	2.73

SI (sylvite)	44	-4.82	-3.90	-2.84	37	-3.42	-2.44	-1.39
SI (anhydrite)	41	-2.96	-0.95	0.13	37	-1.95	-0.61	0.04
SI (gypsum)	41	-2.63	-0.63	0.46	37	-1.77	-0.5	-0.01
SI (carnallite)	44	-13.23	-10.24	-6.93	37	-8.73	-6.96	-3.29
SI (celestite)	41	-3.05	-0.67	0.48	37	-1.62	-0.28	0.15
SI (barite)	6	-0.04	0.31	1.48	9	-0.58	-0.37	0.16

Table 3-5 (continued)

Mineral	Sedbrine samples											
	Sedbrine 1				Sedbrine 2				Sedbrine 3			
	N	Min	Med	Max	N	Min	Med	Max	N	Min	Med	Max
SI (halite)	41	-2.47	-1.89	0.46	50	-1.61	-0.72	0.1	33	-1.27	-0.09	0.5
SI (dolomite)	25	-2.62	2.05	3.58	17	0.77	2.67	4.12	2	5.66	5.78	5.91
SI (calcite)	25	-1.37	0.88	1.6	17	0.9	1.57	2.78	2	2.91	3.03	3.14
SI (sylvite)	41	-4.49	-3.34	-1.66	50	-2.84	-2.27	-0.64	33	-2.23	-1.39	-0.09
SI (anhydrite)	41	-2.93	-0.82	0.36	50	-2.08	-0.62	0.07	32	-2.81	-0.63	0
SI (gypsum)	41	-2.62	-0.64	0.35	50	-1.94	-0.38	0.27	32	-2.67	-0.63	0.06
SI (carnallite)	41	-11.7	-9.51	-5.67	50	-8.56	-6.41	-5.39	33	-5.95	-4.06	-0.99
SI (celestite)	41	-2.36	-0.26	0.72	50	-1.96	0.04	0.62	32	-2.42	-0.10	0.57
SI (barite)	7	-0.07	0.6	1.25	29	0.23	0.82	1.71	24	-0.9	0.47	1.82

Tableau 3-6: Statistical summary of enrichment factor results

Component	Shieldbrine samples					
	Shieldbrine 1			Shieldbrine 2		
	N	Med	% Std err	N	Med	% Std err
Na^{+}	44	0.36	5.94	37	0.32	5
Mg^{2+}	44	0.1	27.3	37	0.03	20.3
K^{+}	44	0.06	10.8	37	0.08	9.67
Ca^{2+}	44	17.8	3.09	37	18.5	1.97
HCO_3^{-}	43	0.09	15.9	28	0.01	23
SO_4^{2-}	44	0.02	41.1	37	0.01	13.1
Sr^{2+}	44	16.3	7.27	37	19.8	3.65
Br^{-}	44	2.74	3.86	37	2.52	5.16
Li^{+}	20	1.39	38.9	20	0.81	18
Fe^{2+}	14	297	68.8	4	153	58.3
SiO_2	24	0.43	32	19	0.10	27.8
Mn^{2+}	14	489	26.2	3	267	29
B^{3+}	16	0.15	13	11	0.09	7.48
Ba^{2+}	11	20.5	22.1	9	52.9	12.9

Table 3-6 (continued)

Component	Sedbrine samples								
	Sedbrine 1			Sedbrine 2			Sedbrine 3		
	N	Med	% Std err	N	Med	% Std err	N	Med	% Std err
Na^+	41	1.10	1.77	50	0.92	1.92	33	0.59	6.28
Mg^{2+}	41	0.22	9.37	50	0.22	10.5	33	0.21	20.7
K^+	41	0.44	16.1	50	0.38	20.7	33	0.75	16.5
Ca^{2+}	41	3.38	9.49	50	4.61	5.46	33	10.5	6.4
HCO_3^-	25	0.62	18.5	17	0.27	26.9	6	0	66.9
SO_4^{2-}	41	0.14	18.3	50	0.03	11.7	33	0	20.2
Sr^{2+}	41	4.75	14.1	50	10.7	8.28	33	23.9	4.48
Br^-	41	0.59	13.1	50	1.46	5.36	33	2.96	8.08
Li^+	25	14	32.4	28	13	25.5	13	27.6	12.1
Fe^{2+}	40	97.4	45.5	45	2158	26.2	24	9747	13
SiO_2	27	0.59	18	29	0.19	35.6	3	0.17	47.9
Mn^{2+}	38	70.5	62.5	35	60.8	49.9	22	2873	16
B^{3+}	26	1.29	27.6	25	1.27	19.6	2	2.22	87.7
Ba^{2+}	30	7.40	57.9	38	29	31.5	24	360	11.5

3.6.4. Wilcoxon/Kruskal-Wallis and Kendall's τ tests

The Wilcoxon/Kruskal-Wallis test using Na^+, Ca^{2+}, Li^+, B^{3+}, and $\delta^{18}O$ revealed a significant difference ($p < 0.0001$), showing that these elements can be used to distinguish shieldbrine and sedbrine clusters. The same test performed for Ca^{2+}, Na^+, K^+, Sr^{2+}, Br^- and Cl^- between shieldbrine 1 and 2 samples was also significant ($p < 0.0001$), showing that shieldbrine clusters can be distinguished based on these elements. However, the test performed for Mg^{2+} and SO_4^{2-} between shieldbrine 1 and 2 samples was not significant ($p > 0.05$), therefore these elements cannot be used to distinguish shieldbrine clusters. Similarly, the test performed for Mg^{2+}, Ca^{2+}, Na^+, K^+, Sr^{2+}, Br^-, Cl^-, Fe^{2+}, Mn^{2+}, and SO_4^{2-} showed that these elements can be used to distinguish sedbrine clusters.

Results from a Kendall's τ test, which show a significant correlation with $p < 0.0001$, are presented in Tableau 3-7 and Tableau 3-8. For the sedbrine dataset, Cl^- is significantly correlated with the elements Ca^{2+}, Na^+, Sr^{2+}, K^+, Br^-, and Mg^{2+}, which are thus important in the salinization processes of sedbrines (Rittenhouse, 1967; Carpenter et al., 1974; Collins, 1975). From the point of view of SI, SI_{halite}, $SI_{carnallite}$, and $SI_{sylvite}$ are significantly correlated with TDS, which shows that dissolution/precipitation of halite, carnallite, and sylvite are important in the salinization processes of

sedbrine. Fe^{2+} and Mn^{2+} are significantly correlated while SO_4^{2-} is anti-correlated with Cl^-. For the shieldbrine dataset, Cl^- is significantly correlated with Ca^{2+}, Na^+, Sr^{2+}, K^+, and Br^-, therefore these chemical elements are important in the salinization processes of shieldbrine clusters (Frape et al., 1984; Bucher et Stober, 2010; Walter et al., 2017). Cl^- is not significantly correlated with Mg^{2+} and is anti-correlated with SO_4^{2-}. Despite the significant correlation in sedbrine and shieldbrine clusters between Cl^- and Ca^{2+}, Na^+, Sr^{2+}, K^+, and Br^-, the PCA distribution of these samples (Figure 3-2a) shows that their correlation is different. Then, the X/Cl ratios differ according to brine type. In both cases (shieldbrine and sedbrine clusters), Br^- is significantly correlated with almost all chemical elements except B^{3+} and HCO_3^-.

Tableau 3-7: Results of a Kendall τ statistical test for element molar concentrations of shieldbrine samples

Component 1	By component 2	Kendall τ
K^+	Na^+	0.54
Ca^{2+}	Na^+	0.54
Ca^{2+}	K^+	0.51
Cl^-	Na^+	0.63
Cl^-	K^+	0.55
Cl^-	Ca^{2+}	0.88
Sr^{2+}	Na^+	0.51
Sr^{2+}	K^+	0.64
Sr^{2+}	Ca^{2+}	0.7
Sr^{2+}	Cl^-	0.72
Br^-	Na^+	0.57
Br^-	K^+	0.58
Br^-	Ca^{2+}	0.77
Br^-	Cl^-	0.83
Br^-	Sr^{2+}	0.72

Tableau 3-8: Results of a Kendall τ statistical test for element molar concentrations of sedbrine samples

Component 1	By component 2	Kendall τ
Sr	Cl^-	0.59
Cl^-	Na^+	0.61
Cl^-	Ca^{2+}	0.70
Br^-	Ca^{2+}	0.75
Br^-	Cl^-	0.68
Br^-	Sr^{2+}	0.72
Li^+	K^+	0.73
Fe^{2+}	SO_4^{2-}	-0.58
Mn^{2+}	SO_4^{2-}	-0.63
Mn^{2+}	Fe^{2+}	0.66
Ba^{2+}	SO_4^{2-}	-0.62
Ba^{2+}	Fe^{2+}	0.65
Ba^{2+}	Mn^{2+}	0.63

TDS	SI_{halite}	0.94
TDS	$SI_{sylvite}$	0.69
TDS	$SI_{carnallite}$	0.86

3.7. Discussion

As part of this study, we compiled various studies of brines from several crystalline basements and sedimentary basins around the world (Tableau 3-1 and Tableau 3-3) This geographical and geological diversity offers a global perspective on the chemical characteristics of crystalline and sedimentary brines. Although this compilation provides a global overview of brines from the two geological settings of interest, there are inherent limitations to the representativeness of the compiled data. This is mainly due to the overrepresentation of certain geological regions, such as the Canadian Shield, from which 76 of the 134 crystalline rock samples were obtained. Future investigations involving a much larger range of sites would help validate and extend our observations and interpretations.

3.7.1. Evaporation of residual brines

Evaporite sequences are known to contribute strongly to the salinization of brines in deep sedimentary basins (Hanor, 1994). In this study, the correlation between SI_{halite}, $SI_{carnallite}$, and $SI_{sylvite}$ vs. TDS (Tableau 3-8) demonstrates that halite (Figure 3-3a), carnallite, and sylvite (ANNEXE V) control sedbrine salinization. The standard error of EF_K suggests that different sources of K^+ can contribute randomly to dissolved K^+ content in sedbrine clusters, considering many parameters such as mineral solubility constants and reaction rates of evaporitic minerals like carnallite and sylvite, or through mixing processes induced by human activity. Several studies show this mixing effect between sedimentary brines and water of different salinities, such as fresh water or seawater (Stueber et al., 1998; Kim et al., 2022; Person et Sazeed, 2022; Molofsky, 2023). Furthermore, sedbrine 1 samples, have a Na/Cl molar ratio of about 1:1 (Figure 3-3b) which corresponds to the stoichiometry of halite dissolution/precipitation according to:

$$Na^+ + Cl^- \leftrightarrow NaCl \qquad \text{(Eq. 3.3)}$$

Moreover, SI_{halite} for sedbrine 1 samples shows undersaturation in all samples (Figure 3-3a), which indicates that these samples reflect a tendency for halite dissolution. The $^{87}Sr/^{86}Sr$ ratio in

seawater has varied between 0.7070 and 0.7092 since the Precambrian period (Kharaka et Hanor, 2003). Evaporites, derived from seawater from a specific geological era, have a similar isotopic composition to that of seawater, which is also the case for sedbrine samples (Tableau 3-4). The presence of halite in sedimentary basins, a Na/Cl molar ratio of about 1:1, and an undersaturated state with halite indicate that Na^+ and Cl^- in sedbrine 1 samples are mainly controlled by halite dissolution (Pauwels et al., 1993; Steuber, 1999; Kim et al., 2022). This interpretation suggests that dissolution of marine evaporitic rocks, mainly halite, controls salinization of sedbrine 1 samples

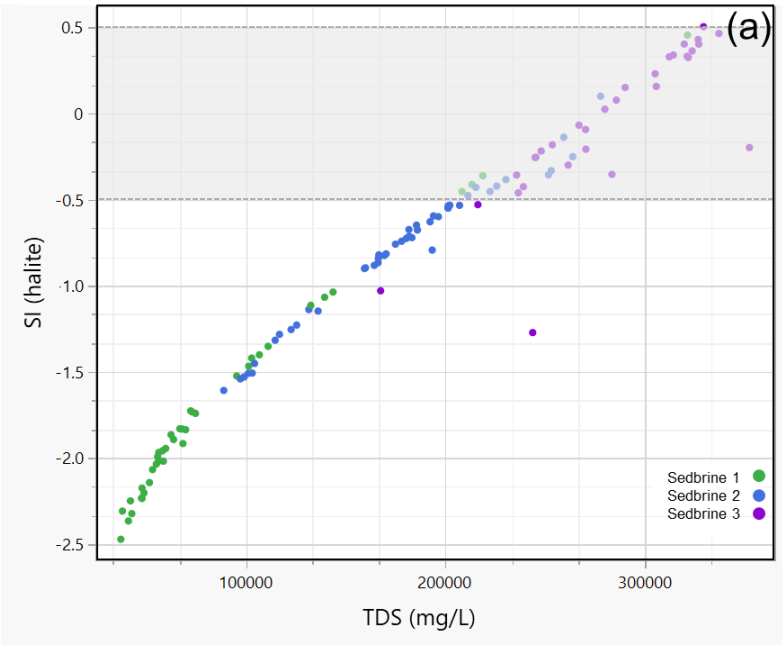

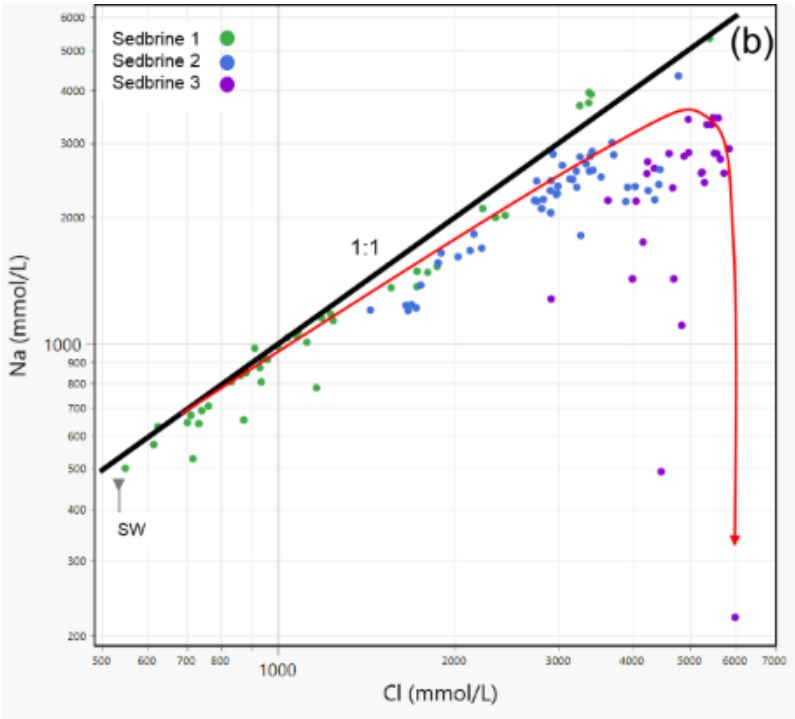

Figure 3-3: a) SI_{NaCl} vs TDS (mg/L). Saturation index was calculated at T = 25°C and pH = 7. Dashed area corresponds to the equilibrium state and the analytical errors. The overall uncertainty is ± 0.5 units. b) log-log plot of Na+ vs Cl- concentrations (in mmol/L). The black line represents a linear slope of 1:1, while the red line represents sedbrine evolution. SW = seawater.

Evaporation of groundwater leads to an increase in the concentration of dissolved ions in residual water (Rittenhouse, 1967; Carpenter et al., 1974), thus as conservative elements, Br^- and Cl^- concentrations for example, increase with evaporation (Hsissou et al., 1999; Yang et al., 2022). The strong correlation (r^2 = 0.94) between Cl^-, Br^- and Na^+ in the sedbrine samples (Figure 3-4) indicates that enrichment of Br^- and Cl^- and progressive depletion of Na^+ are strongly controlled by evaporation. The link between the equilibrium state with halite and Na^+ depletion of sedbrine 3 samples suggests that, after oversaturation with halite, sedbrine 3 samples precipitate halite to restore equilibrium according to Le Chatelier (1884). Dissolution-precipitation control of halite in the salinization of sedimentary brines has also been suggested by several authors (Collins, 1975; Clark et al., 2013; Yardley et Bodnar, 2014). Sedbrine 1 samples controlled by halite dissolution and characterized by Na-rich and Br-poor brines therefore represent the first stage of sedbrine evolution and are considered residual brines. Residual brines reflect the initial salinization conditions before other geochemical processes, such as evaporation or additional water-rock interactions, further modify their composition. Sedbrine 3 samples controlled by halite precipitation represent Br-rich and Na-poor

brines resulting from the evaporation of residual brine. Sedbrine 2 samples are considered to represent an intermediate stage between Na-rich and Br-poor brines and Br-rich and Na-poor brines. The strong correlation of Cl/Br vs. Na/Br ratios expressed by the equation Cl/Br = Na/Br + 103 characterizes the sedbrine clusters and can be used as a tool to determine if Cl^-, Br^-, and Na^+ originate from dissolution or precipitation of halite (Carpenter et al., 1974; Jones et Deocampo, 2003).

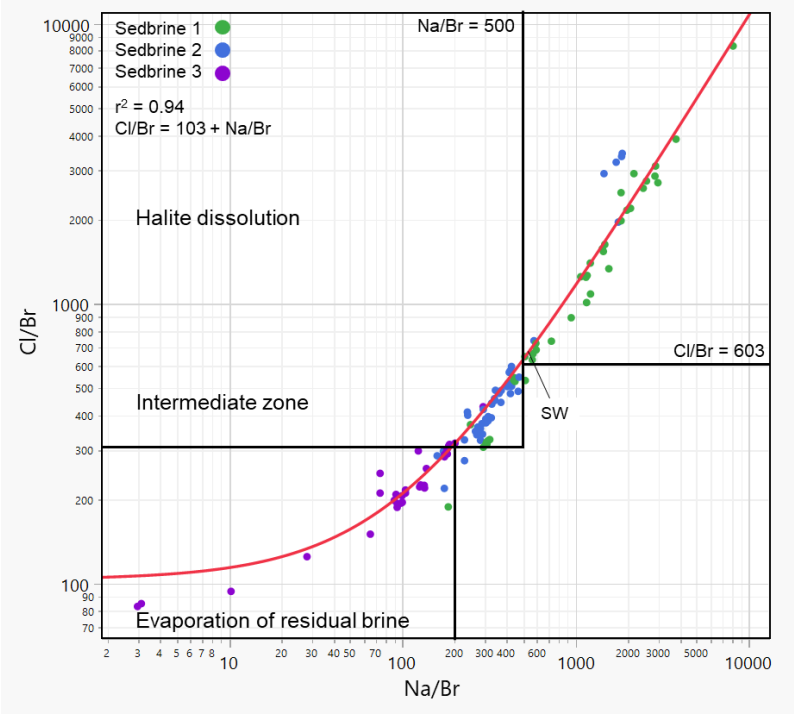

Figure 3-4: Cl/Br vs Na/Br ratios (from concentrations in mmol/L). The red line is a simple regression that represents the evolution of sedbrine, which can be characterized by the equation presented on the graph. SW = seawater.

According to Connolly et al. (1990), depletion of Mg^{2+} and K^+ and enrichment of Ca^{2+} relative to seawater indicate diagenetic alteration with carbonate and/or siliciclastic rocks. In this study, most sedbrine clusters are oversaturated with respect to calcite and dolomite (Figure 3-5), which indicates a tendency of these minerals to precipitate. Thus, Ca^{2+} enrichment and Mg^{2+} and K^+ depletion relative to seawater observed in these samples (Section 3.5.3) can be seen as indicative of diagenetic alteration processes such as formation of calcite and dolomite. Although the oversaturated state of the sedbrine clusters with respect to calcite and dolomite was determined at surface conditions (i.e., using a K_{sp} at 25°C, 1 bar, and pH = 7), at greater depths, the increase in temperature and pressure implies an increase in CO_2 fugacity (fCO_2) and leads brines to precipitate carbonate minerals such

as calcite (Hutcheon, 2000; Kharaka et Hanor, 2003; Bhattacherjee et al., 2023). Sedbrine clusters are thus also likely oversaturated with respect to these minerals under in-situ conditions.

Kinetic effects, i.e., retarded precipitation of calcite and dolomite, as suggested by Nordstrom et Ball (1989), can also help explain the oversaturation of calcite and dolomite in the sedbrine clusters. In anoxic conditions, anaerobic bacteria including iron-reducers, sulfate-reducers, and methanogens contribute to oversaturation and precipitation of carbonates (Bennett et al., 2000; Gimeno et al., 2009). Since manganese (Mn^{2+}) and iron (Fe^{2+}) are sensitive to microbiological processes (Grenthe et al., 1992; Gimeno et al., 2009), the good correlation between Mn^{2+} and Fe^{2+} (Tableau 3-8) indicates the importance of biological activity in the sedbrine clusters, and might also explain the calcite and dolomite oversaturation in sedbrines clusters.

Interactions between groundwater and sulfate minerals such as gypsum ($CaSO_4 \cdot 2H_2O$), anhydrite ($CaSO_4$), and celestite ($SrSO_4$) may have an important role in enrichment of Ca^{2+} and Sr^{2+} (Nordstrom et al., 1989; Yang et al., 2022). In this study, the primarily negative values for SI_{gypsum}, $SI_{anhydrite}$, and $SI_{celestite}$ for sedbrine clusters and shieldbrine clusters (Tableau 3-5) also indicate a tendency of gypsum, anhydrite, and celestite to dissolve. Therefore, if these minerals are present (as they should be – see Section 0), they will tend to dissolve, contributing to the increase of Ca^{2+} and Sr^{2+} in the sedbrine and shieldbrine clusters. Aforementioned microbiological processes such as sulfate-reduction can explain the decrease of SO_4^{2-} in the sedbrine clusters (ANNEXE V) (Boschetti, 2013; Bowles et al., 2014; Papizadeh et al., 2017; Li et al., 2022).

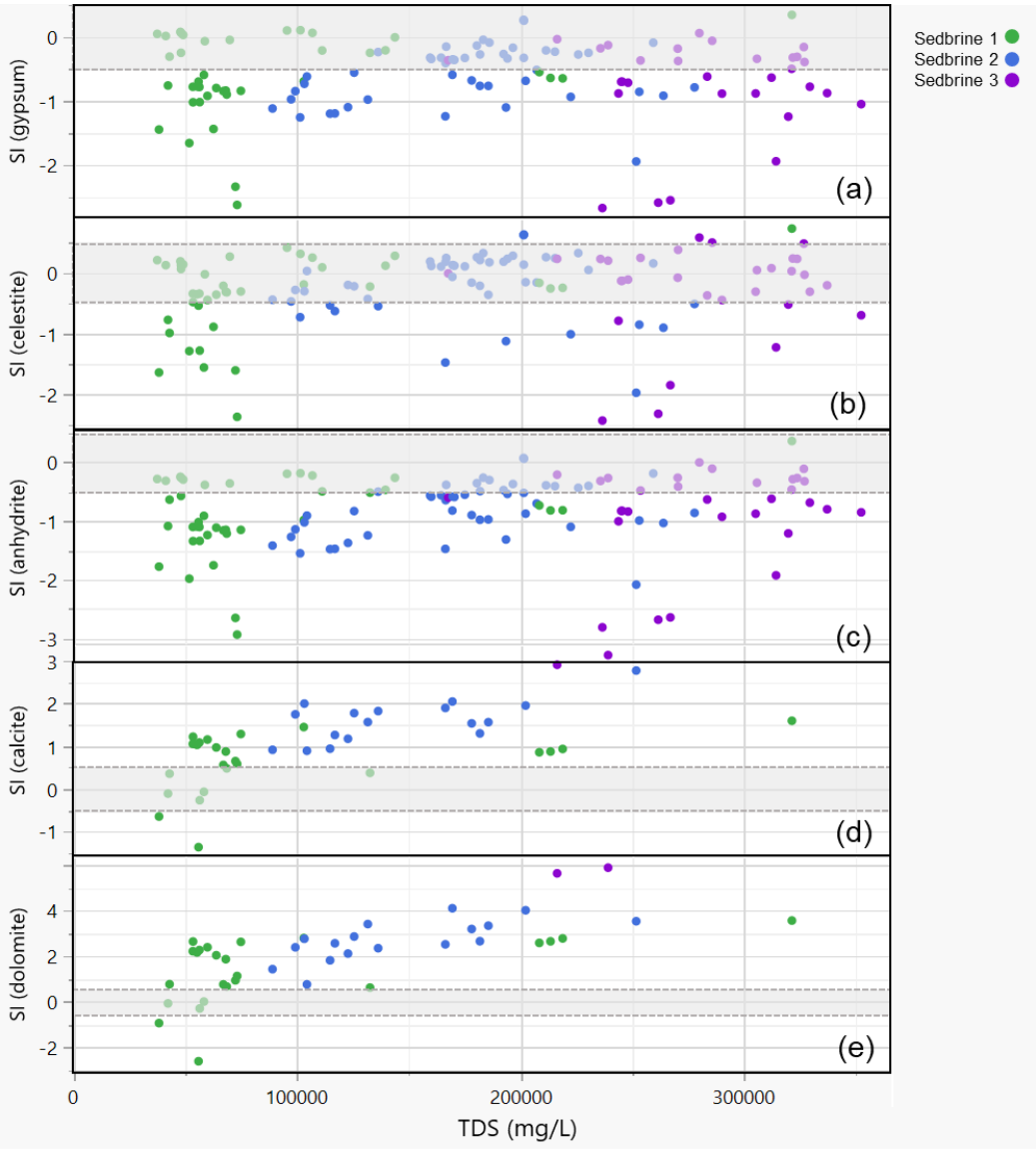

Figure 3-5: Saturation indices (K_{sp} at T = 25°C, pH = 7, 1 bar) of sedbrine clusters with respect to (a) gypsum (b) celestite (c) anhydrite, (d) calcite, and (e) dolomite. Dashed area corresponds to the equilibrium state and the analytical errors. The overall uncertainty is ± 0.5 units.

3.7.2. Control of water-rock interaction processes

In crystalline rocks, we can categorize chemical elements into two main groups for simplicity: (1) “stable elements” like Ca^{2+}, Na^{+} and Al^{3+}, whose concentrations are influenced by the solubility of minerals such as calcite and clays that form within the rock; and (2) “volatile elements” such as Cl^{-} and Br^{-}, which are more readily dissolved in water and are less likely to be incorporated into the rock structure (Zuddas, 2010). Therefore, a comparison of Cl/Br ratios in groundwater relative to those of the solid phase (rocks or minerals) is a clear indicator of water-rock interactions. Figure 3-6 shows that the Cl/Br ratio in samples from crystalline environments, which we refer to as shieldbrine,

averages around 100. This is similar to the ratio found in igneous rocks (Stober et Bucher, 1999), indicating that the chemistry of these groundwaters is influenced by interaction with such rocks. Specifically, igneous rocks contain a mix of mineral types, with felsic minerals (rich in lighter elements like silicon and oxygen) generally having lower Cl/Br ratios of about 40, and mafic minerals (richer in heavier elements like magnesium and iron) having higher ratios of about 700 (Teiber et al., 2014). The Cl/Br ratios of shieldbrine samples are closer to the felsic-rich mineral pole. This observation suggests that several minerals (e.g., biotite, apatite, amphibole) contribute to the release of Cl^- and Br^- in the shieldbrine samples. Constant Cl/Br ratios of shieldbrine 1 and 2 samples and the standard errors of about 3.4% and 5.2%, respectively, suggest that the respective mineral solubilities do not influence Cl/Br ratios.

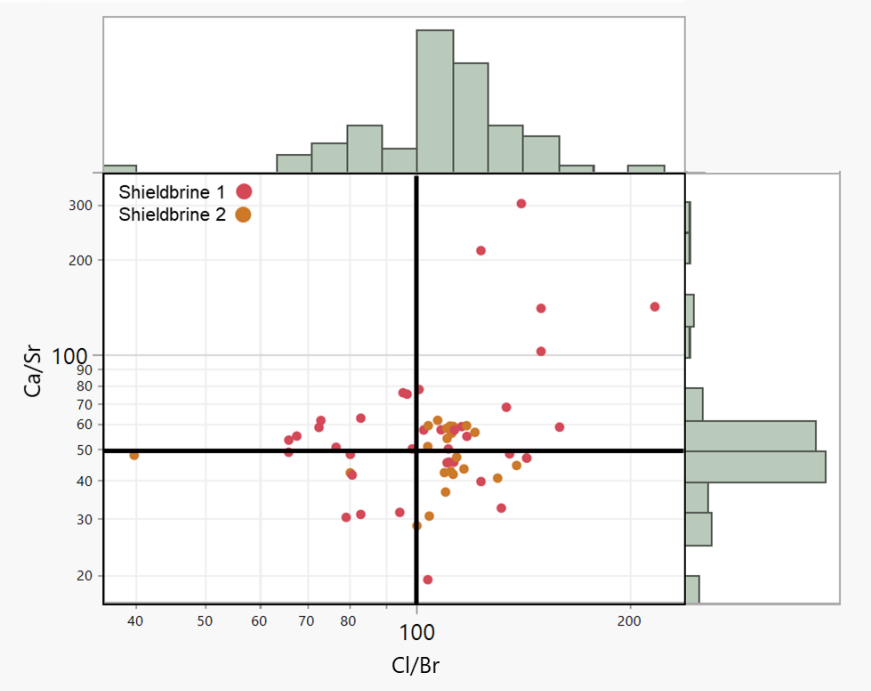

Figure 3-6: log-log Ca/Sr vs Cl/Br ratios for the shieldbrine samples (from concentrations in mg/L). Black lines represent rock ratios, $Ca/Sr_{(crustal\ rock)} = 50$, $Cl/Br_{(igneous\ rock)} = 100$.

Assuming that Cl^- and Br^- of the shieldbrine samples come mainly from water-rock interactions (Stober et Bucher, 1999), any good correlation in shieldbrine samples between Cl^- and Br^- chemical elements would suggest the same origin for the respective chemical element. The good correlation of Ca^{2+} and Sr^{2+} with Br^- and Cl^- (Tableau 3-7) suggests that Ca^{2+} and Sr^{2+} also come from water-rock interactions. Moreover, Ca/Sr ratios are widely used as a tracer of water-rock interactions

when Sr^{2+} is present. This ratio generally reflects the rock's chemistry (Banks et Frengstad, 2006). Among Ca/Sr ratios of known rocks, including basaltic-andesitic rocks (Ca/Sr ≈ 121), gypsum (≈ 112) (Peiffer et al., 2011), carbonates (≈ 1700) and shale (≈ 200) (Négrel et al., 2007), the shieldbrine samples (Figure 3-6) have approximately the same ratio as crustal rocks (≈ 50) (Bucher et Stober, 2000). This observation indicates that water–crustal rock interaction controls Ca^{2+} and Sr^{2+} concentrations in the shieldbrines. The variability of shieldbrine 1 samples is caused by 5 outliers (Figure 3-6), where 4/5 samples come from the Fennoscandian Shield. The variability in Ca/Sr ratios is due to the local mineralogical variability which depends on (1) different mineral solubilities, e.g., Ca-Sr-rich minerals like calcite, which is 2 or 3 times more soluble than apatite, which is more soluble than plagioclase (Le Roux et al., 2006), (2) different mineral Ca/Sr ratios, e.g., Ca/Sr ratios in apatite and calcite, which are higher than in plagioclase (Beaucaire et Michard, 1982).

Ca/Sr ratios can be influenced by local factors such as precipitation and/or dissolution of minerals, making them less conclusive for identifying specific sources or mechanisms. The $^{87}Sr/^{86}Sr$ ratio, is more specific for water-rock interaction studies, as this ratio in groundwater reflects that of Sr-bearing minerals (McNutt et al., 1984; Qian et al., 2023). This ratio therefore reflects geological history and long-term processes, including variations due to fluid mixing. Due to the decay of ^{87}Rb to ^{87}Sr over time, the $^{87}Sr/^{86}Sr$ ratio of old igneous rocks is mainly dependent on how much rubidium (Rb) is in the rock (Shand et al., 2009), such as those in the Canadian or Fennoscandian Shield. The median ratios of shieldbrine 1 and 2 samples are about 0.7141 and 0.7144, with standard errors of 0.14% and 0.02%, respectively. The uniform and high radiogenic ratios demonstrate that brines have reacted with silicate minerals (Négrel, 1999; McDonough et al., 2021; Nisson, 2023). Since shieldbrine samples are Sr-rich (Tableau 3-4), radiogenic Sr^{2+} from mixing with meteoritics or subsurface waters has less impact (Bottomley et al., 1999). Several studies grouped in shieldbrine 1 and 2 clusters confirm these observations on water-silicates rock interaction (Blomqvist, 1999; Bottomley et al., 1999; Frape et al., 2003).

Silicate mineral weathering acts as a pH buffer, and would lead to low pH brines (Blake et Walter, 1999; Appelo et Postma, 2005; Yardley et Bodnar, 2014), which is the case for the shieldbrine samples (Tableau 3-4). Silicate mineral weathering by water consumption, desiccation of pore space

and fractures, and formation of secondary minerals, as expressed by the following hydration reaction (Bucher et Stober, 2000): silicate mineral + H_2O-(low TDS) → secondary minerals + H_2O-(high TDS) (Eq.4) are in agreement with the results of the present study (Eq.3.4). The strong correlation of Ca/Cl ratios (r^2 = 0.93) expressed by the equation: Ca = -1610 + 0.4Cl, characterizes the shieldbrines. Thus, this equation can be used as a tool to determine if Ca^{2+} and Cl^- come from water-felsic rock interaction.

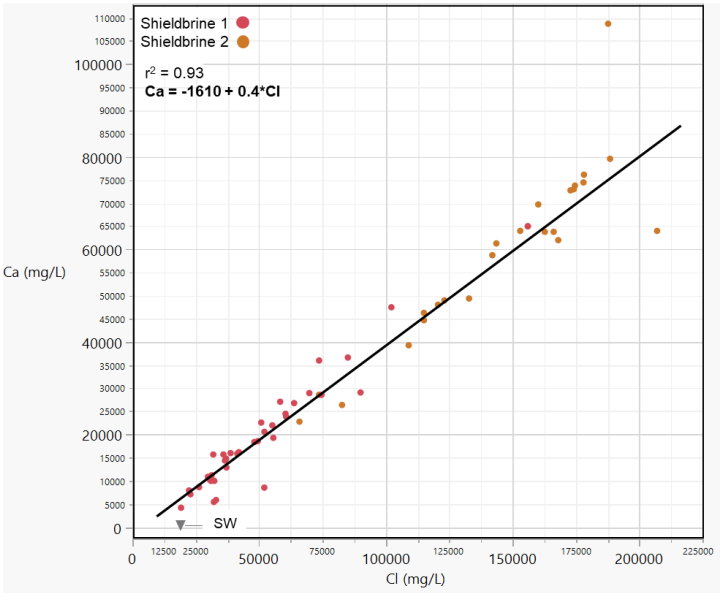

Figure 3-7 : Ca^{2+} vs Cl^- concentrations (in mg/L). The solid line represents a linear regression line.

3.7.3. Temperature factors of sedbrine and shieldbrine samples

Several studies have revealed that most concentrated crystalline and sedimentary brines have different $\delta^{18}O$ and $\delta^{2}H$ signatures (Frape et al., 2003; Warr et al., 2021). While crystalline brines plot above and left of the Global Meteoric Waterline (GMWL), sedimentary brines appear to the right side of the GMWL. The HCA-generated clusters in this study representing crystalline and sedimentary brines (Section 3.6.1 and 3.6.2) follow the same trend (Figure 3-8a). Recent studies have found that water-rock interaction occurring at low temperatures over long geologic timescales can drive progressive $\delta^{18}O$ depletion and enrichment of $\delta^{2}H$ in crystalline brine (Warr et al., 2021). This is a result of hydration of silicates and exchange of oxygen isotopes between the fluids and the host rocks, highlighting the long-term impact of water-rock interactions on isotopic signatures. Hydration and long-term water-rock exchange at low temperatures can lead to depleted $\delta^{18}O$ and enriched $\delta^{2}H$ in shieldbrines (Frape et Fritz, 1982; Warr et al., 2021). The sedbrine samples are distributed in the

zone dominated by evaporation and high-temperature water-rock exchange (Figure 3-8a), being well-known processes (Clark et Fritz, 1997; Birkle et al., 2009; Kim et al., 2022; Yan et al., 2023). The occurrence of high temperatures and evaporation in sedimentary geological settings explains the $\delta^{18}O$ and $\delta^{2}H$ enrichment in the sedbrine clusters relative to the shieldbrines.

Temperature is a discriminating factor between sedbrine and shieldbrine clusters. In this study, the application of PCA and the Wilcoxon/Kruskal-Wallis test to brine samples has enabled the rigorous identification of several shieldbrine and sedbrine geochemical markers (Sections 3.6.2 and 3.6.4), such as temperature-sensitive elements specific to each medium: Br^-, Li^+, and B^{3+} (McCaffrey et al., 1987; Williams et al., 2015). Thus, based on statistical tools, a discriminatory graph between the chemical signatures of sedimentary and crystalline environments has been developed in this study.

Li^+ and B^{3+} dissolved contents directly reflect various temperature-dependent processes that control the evolution of shieldbrine and sedbrine waters. Since silicate minerals are identified as the main source of Li^+, even in sedimentary geological settings (Kısakűrek et al., 2005; Dugamin et al., 2023), high Li concentrations observed in the sedbrine clusters (Tableau 3-4) are mainly due to higher temperatures (Millot et al., 2010). The good correlation between Li^+, Br^- and Cl^- shows that Li^+ in sedbrine samples behaves conservatively (Tableau 3-8). Several studies show that high temperature and water-rock interaction processes play a major role in Li^+ enrichment in oil field brines (Dugamin et al., 2023; Yan et al., 2023; Bishop et Robbins, 2024; Yu et al., 2024). Low-permeability oil and gas shales are known to be rich in B^{3+} (William 2015) and since shales are usually present in sedimentary basins (see Section 3.4.2.2), the leaching of these shales, combined with the higher temperatures, can control the B-sedbrine dissolved content.

The mechanisms controlling low-Li concentrations in crystalline brines can be influenced by various factors such as brine origin, interactions with host rocks, and mixing processes. Water-rock interaction at low-temperature as shown in the shieldbrine water isotopes cannot lead to enrichment of Li^+ as seen in the sedbrine samples. Bottomley et al. (1999) attributed low-Li contents in Canadian Shield brines to the mixing of a Li-poor meteoric water endmember with a Li-rich brine endmember. This mixing process results in the dilution of Li^+ in the brine, leading to lower concentrations in the

final solution. The interaction between Li and mineral phases within crystalline rocks often leads to Li^+ adsorption onto or incorporation into mineral, ion exchange or the precipitation of lithium-bearing minerals, reducing its aqueous concentration surfaces (Beaucaire et Michard, 1982; Hoyer et al., 2015). Tellam (1995) also proposed adsorption onto clay products to explain low-B^{3+} contents. Thus, low-temperature water-rock interaction and mixing provide mechanisms for controlling low Li^+ and B^{3+} shieldbrine concentrations.

In addition to Li^+, B^{3+} and Br^- sedbrine and shieldbrine chemical signatures, fluid inclusion samples were also incorporated into the database. In the present study, fluid inclusions are microscopic fluids trapped at the time of quartz crystallization (Yardley, 2013), which typically occurs from magma at temperatures between 450 - 800 °C (Wark et Watson, 2006). Since these fluid inclusions have reached very high temperatures, Li^+, B^{3+} and Br^- signatures of fluid inclusions compiled in this study could be used as temperature indicators.

B/Br vs Li/Br ratios show a clear difference between shieldbrine and sedbrine clusters (Figure 3-8b). In particular, Li/Br ratios of the shieldbrines are below 0.01 while those for the sedbrines are above 0.01. B/Br ratios of shieldbrines are below 0.01 and those for sedbrines are above 0.01. The covariance between fluid inclusion samples and sedbrine clusters in Figure 3-8 suggests that sedbrines have reached a higher temperature than shieldbrines; this can be explained by considering the characteristic temperature regimes for each basin type. Upper crustal shield rocks have relatively high geothermal gradients primarily due to radioactive decay, although they are generally not as high than active sedimentary basins (Norden et Fröster, 2006; Nagaraju et al., 2012). In fact, sedimentary rocks have a lower thermal conductivity than crystalline rocks, this difference can contribute to higher geothermal gradients in sedimentary basins (Vosteen et Schellschmidt, 2003). In contrast, crystalline shields are generally composed of older, denser, more thermally conductive rocks (Clauser et Huenges, 1995), which help dissipate heat and maintain lower temperatures than sedimentary rocks.

Figure 3-8 (a and b) are discriminant for crystalline and sedimentary brines. However, exceptions are noted where three sedbrine samples from the Fennoscandian Shield (Blomqvist, 1999) and one sedbrine sample from the Canadian Shield (Frape et Fritz, 1982) are grouped with the shieldbrines samples in Figures 8a and b, respectively. These samples were identified at sites

abundant in sodium-rich minerals, such as albite (Blomqvist, 1999). In a geological environment, sources of major elements are many and varied, as in the case of albite or halite, which are two of the most common sources of dissolved sodium in crystalline and sedimentary geological settings and can therefore lead to statistical bias, as observed in Section 3.6.1. Nevertheless, this study shows that minor elements offer more specific insight into different geological environments. This needs to be further investigated.

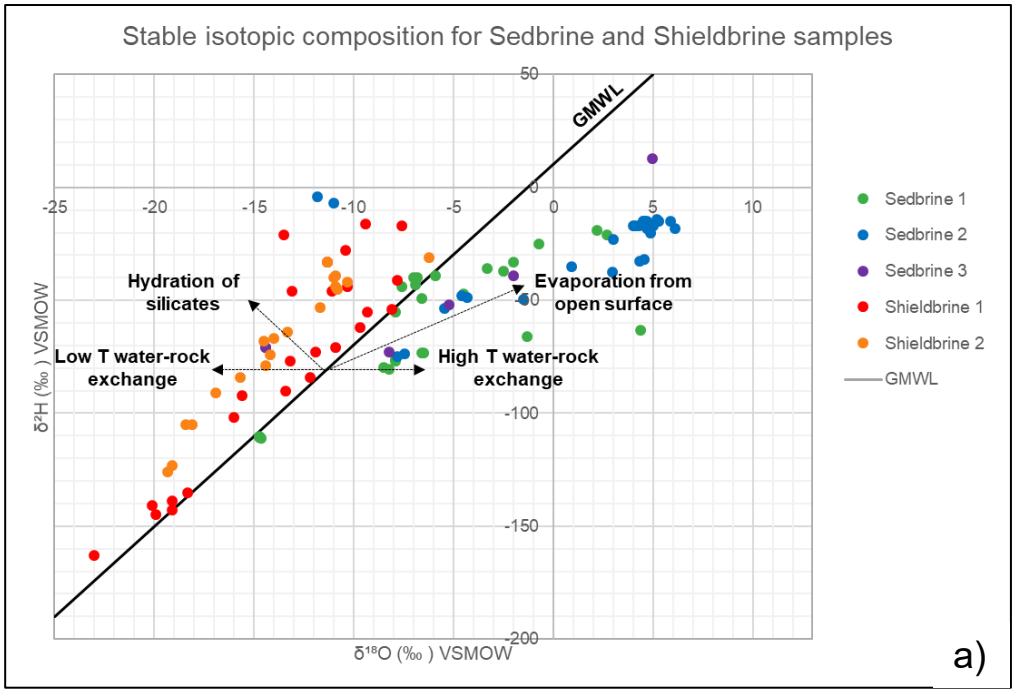

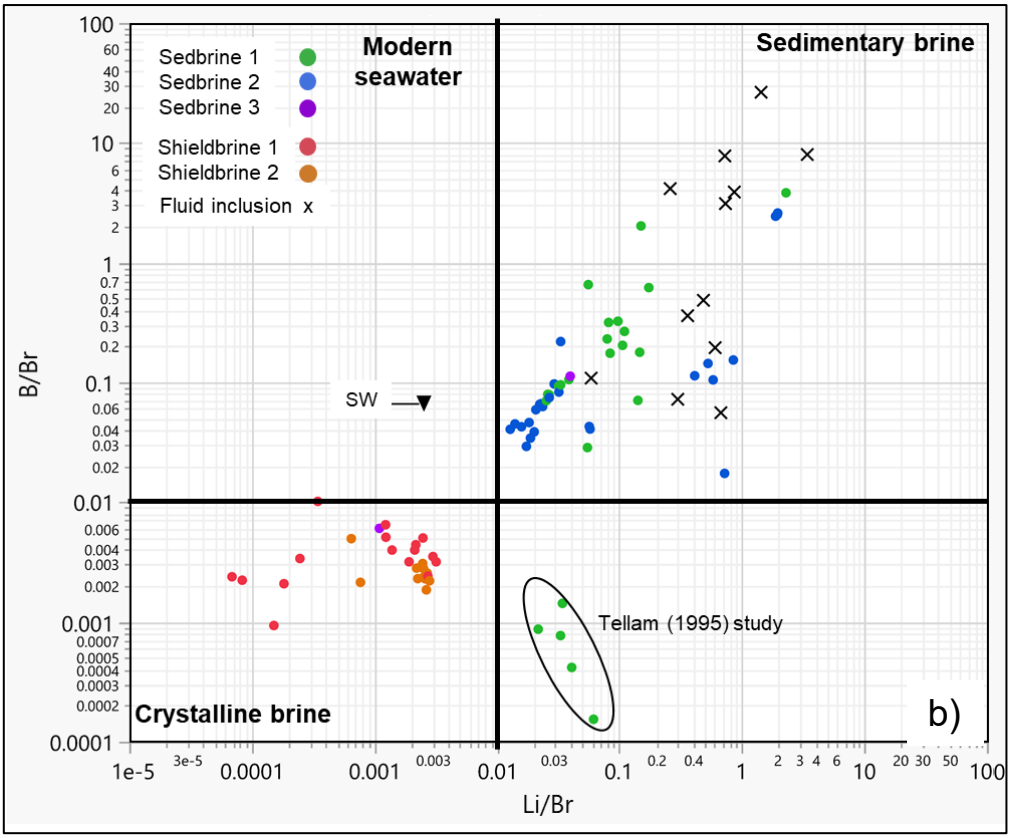

Figure 3-8: a) Subsurface processes that can affect the δ^2H and $\delta^{18}O$ isotopic signatures of sedbrine and shieldbrine clusters. Process interpretations from Clark et Fritz (1997). b) log-log plot of B/Br vs Li/Br ratios (from concentrations in mg/L) for all sedbrine and shieldbrine samples. Solid black lines are shown to distinguish shieldbrine and sedbrine sample ratios. SW = seawater.

3.7.4. Conceptual model of continental brine evolution

Figure 3-9a shows several endmembers, including marine endmembers (seawater, altered marine water, Littorina sea, and sediment pore water), atmospheric endmembers (meteoric water, glacial water, and precipitation), brine reference water, a possible subglacial endmember, and a temperature endmember (fluid inclusions and geothermal brines). These endmembers together with the sedbrine and shieldbrine samples are plotted in the PCA presented in Section 3.6.2. The result shows that atmospheric reference water and shieldbrines are plotted in negative load, while marine components, fluid inclusions, and sedbrines are distributed in positive load (Figure 3-9a). Interdependence of Na^+, K^+, Mg^{2+}, SO_4^{2-} and groundwater are therefore characteristics of marine environments, while fluid inclusions and geothermal brines show that temperature played an important role in the evolution of sedbrine waters. Interdependence of Br^-, Ca^{2+}, and Sr^{2+} and groundwater are characteristics of groundwater evolution, a phenomenon mainly controlled by water-

felsic rock interactions. Moreover, Figure 3-9a shows the covariances of shieldbrine 2 and sedbrine 3 samples, which indicate that although groundwater may have different origins and may have undergone different processes, they would all evolve towards a Ca-Cl endmember and to high Br^- and Sr^{2+} concentrations. In this case, the salinization is controlled by the chemistry of the fluids rather than by the rock chemical composition.

The PCA result allows summarizing the chemical evolution of groundwater through water-rock interactions within both crystalline and sedimentary rocks towards a Ca-Cl endmember (Figure 3-9). This has led to the development of a corresponding conceptual hydrogeochemical model outlining the evolution of crystalline and sedimentary brines (Figure 3-9b). The conceptual hydrogeochemical model developed here is based on the chemistry of brine samples compiled and discussed in Sections 4.1 and 4.2. This study also highlighted the importance of temperature on the chemical evolution of crystalline and sedimentary brines (Section 4.3). Geothermal gradients of the geological media considered here support this hypothesis, for example, comparing the geothermal gradients of about 6 – 7 °C/km of the Canadian and Fennoscandian Shields (Kukkonen et Peltonen, 1999; Morgan, 2018a) with those of the Alberta and Mersey Basin of about 25 – 45 °C/km (Bachu, 1999; Ruppel et al., 2005).

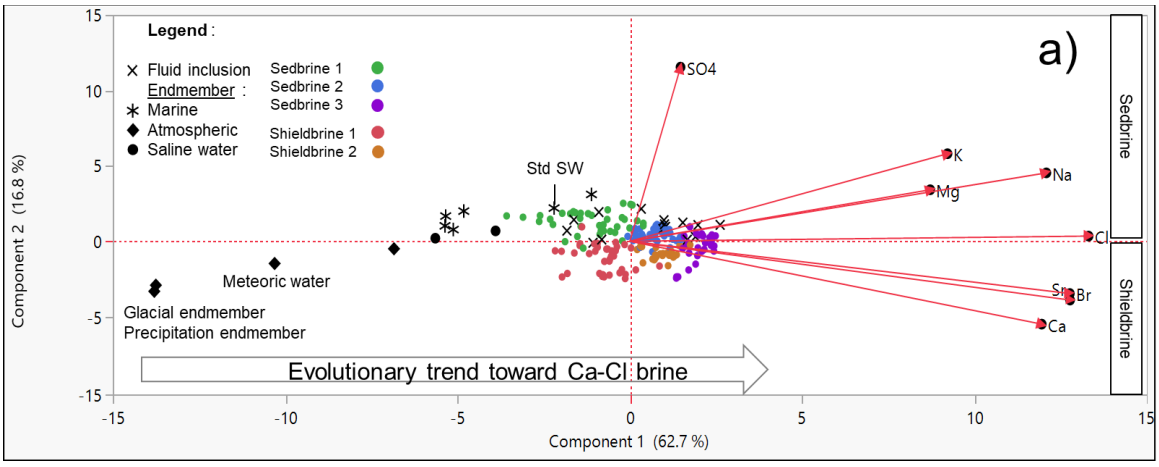

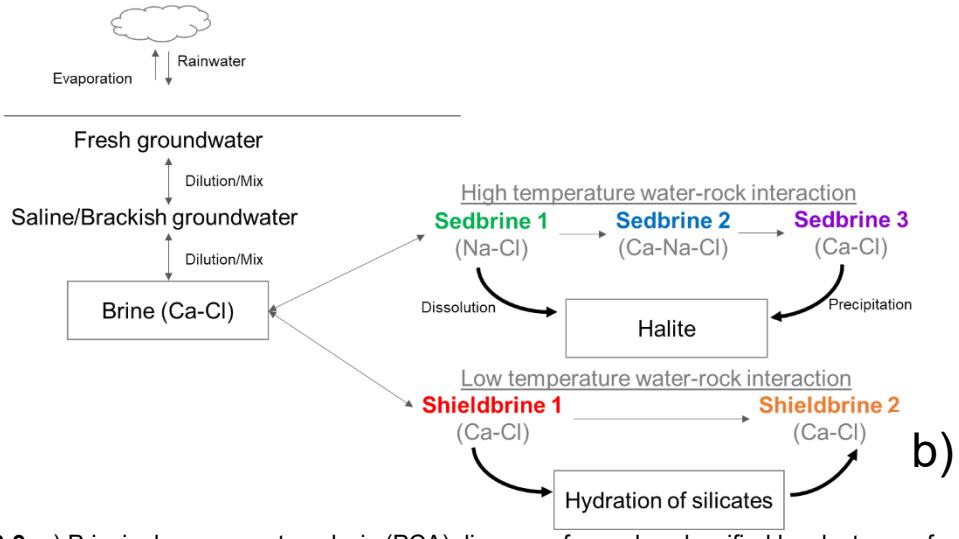

Figure 3-9: a) Principal component analysis (PCA) diagram of samples classified by clusters, reference waters, endmembers, and fluid inclusions, showing a graphical representation of two components derived from the PCA. Component 1 (Cl^-) explained 62.7% of the total variance of the data set while Component 2 (Na^+, K^+, Mg^{2+}, and Ca^{2+}) explained 16.8%. b) Conceptual hydrogeochemical model of crystalline and sedimentary brine evolution through water-rock interactions.

3.8. Conclusion

Groundwater evolution can be understood as a process of groundwater maturation, resulting in increasing salinity until formation of a brine. We have here defined markers for sedimentary and crystalline brines, and highlighted the hydrogeochemical singularities of brines issued from both geological settings.

Based on 8 chemical parameters (Na^+, Mg^{2+}, K^+, Ca^{2+}, Sr^{2+}, Cl^-, SO_4^{2-} and Br^-), two salinization paths towards brines were described: evolution of shieldbrine groundwater which is mainly controlled by water-felsic rock interaction, and evolution of sedbrine groundwater which is mainly controlled by evaporitic rock dissolution and water evaporation. Na^+, K^+, Mg^{2+}, and SO_4^{2-} have been defined as markers of sedbrines while Ca^{2+}, Sr^{2+}, and Br^- have been defined as markers of shieldbrines. Interdependence of Na^+, K^+, Mg^{2+}, and SO_4^{2-} characterises the main hydrogeochemical processes that control brines in sedimentary basins: dissolution-precipitation of evaporitic minerals such as halite, sylvite, carnallite, gypsum, anhydrite and celestite, formation of carbonates during diagenetic alteration, sulfate reduction through microbiological processes and mixing. Interdependence of Ca^{2+}, Sr^{2+}, Br^-, low-Li^+, and low-B^{3+} characterises the main hydrogeochemical processes that control brines in crystalline basements: intensive water-felsic rock interaction through

silicates hydration, formation of secondary minerals, adsorption and mixing processes. The evolution of the sedbrines can be described by Cl/Br vs Na/Br ratios which show a positive linear correlation of the general form Cl/Br = 103 + Na/Br, while shieldbrines can be described by the linear equation Ca = -1610 + 0.4*Cl. These equations can be used as tools to determine if Cl^-, Br^- and Na^+ come from dissolution-precipitation of halite, and if Ca^{2+} and Cl^- come from water-felsic rock interaction. As useful indicators of brine origins, $\delta^{18}O - \delta^{2}H$, Li^+, and B^{3+}concentrations, as well as B/Br and Li/Br ratios, can be used to distinguish crystalline brines from sedimentary brines. These latter ratios reflect various temperature-dependant processes that control the evolution of sedimentary and crystalline brines. Trace elements like Br^-, Li^+, and B^{3+} provide useful opportunities to investigate the influence of geology and temperature on groundwater evolution.

The present study provides data that are of significant interest to improve our understanding of brine-rock interactions. Geochemical markers defined in this study provide valuable information about the composition and characteristics of brines from crystalline basements and sedimentary basins.

3.9. References

Al Radi, M., Adil Al-Isawi, O., Abdelghafar, A.A., Fayez Abu Qiyas, A., AlMallahi, M., Khanafer, K., et Assad, M.E.H. 2022. Recent progress, economic potential, and environmental benefits of mineral recovery geothermal brine treatment systems. Arabian Journal of Geosciences **15**(9): 832.

André, L., Rabemanana, V., et Vuataz, F.-D. 2006. Influence of water–rock interactions on fracture permeability of the deep reservoir at Soultz-sous-Forêts, France. Geothermics **35**(5-6): 507–531.

Appelo, C., et Postma, D. 2005. Geochemistry. Groundwater and Pollution **536**.

Araoka, D., Kawahata, H., Takagi, T., Watanabe, Y., Nishimura, K., et Nishio, Y. 2014. Lithium and strontium isotopic systematics in playas in Nevada, USA: constraints on the origin of lithium. Mineralium Deposita **49**(3): 371–379.

Aslannezhad, M., Ali, M., Kalantariasl, A., Sayyafzadeh, M., You, Z., Iglauer, S., et Keshavarz, A. 2023. A review of hydrogen/rock/brine interaction: Implications for Hydrogen Geo-storage. Progress in Energy and Combustion Science **95**: 101066.

Bachu, S. 1999. Regional-scale geothermal and hydrodynamic regimes in the Alberta basin: A synthesis. *Dans* Geothermics in basin analysis. Springer. pp. 81–98.

Banks, D., et Frengstad, B. 2006. Evolution of groundwater chemical composition by plagioclase hydrolysis in Norwegian anorthosites. Geochimica et Cosmochimica Acta **70**(6): 1337–1355.

Beaucaire, C., et Michard, G. 1982. Origin of dissolved minor elements (Li, Rb, Sr, Ba) in superficial waters in a granitic area. Geochemical Journal **16**(5): 247–258.

Bennett, P.C., Hiebert, F.K., et Rogers, J.R. 2000. Microbial control of mineral–groundwater equilibria: Macroscale to microscale. Hydrogeology Journal **8**(1): 47–62.

Bhattacherjee, R., Botchway, K., Pashin, J.C., Chakraborty, G., et Bikkina, P. 2023. Machine learning-based prediction of CO2 fugacity coefficients: Application to estimation of CO2 solubility in aqueous brines as a function of pressure, temperature, and salinity. International Journal of Greenhouse Gas Control **128**: 103971.

Birkle, P., García, B.M., et Padrón, C.M.M. 2009. Origin and evolution of formation water at the Jujo–Tecominoacán oil reservoir, Gulf of Mexico. Part 1: chemical evolution and water–rock interaction. Applied Geochemistry **24**(4): 543–554.

Bishop, B.A., et Robbins, L.J. 2024. In-Situ Water-Rock Interactions as the Source of Brine-Hosted Lithium: Implications for Developing a Deposit Model. Geoconvention, Calgary, Canada, 17–19 June 2024, p. 4.

Blake, R., et Walter, L. 1999. Kinetics of feldspar and quartz dissolution at 70–80 C and near-neutral pH: effects of organic acids and NaCl. Geochimica et Cosmochimica Acta **63**(13-14): 2043–2059.

Blomqvist, R. 1999. Hydrogeochemistry of deep groundwaters in the central part of the Fennoscandian Shield. Geological Survey of Finland. GTK-YST-101.

Boschetti, T. 2013. Oxygen isotope equilibrium in sulfate–water systems: A revision of geothermometric applications in low-enthalpy systems. Journal of Geochemical Exploration **124**: 92–100.

Bottomley, D.J., Katz, A., Chan, L., Starinsky, A., Douglas, M., Clark, I., et Raven, K. 1999. The origin and evolution of Canadian Shield brines: evaporation or freezing of seawater? New lithium isotope and geochemical evidence from the Slave craton. Chemical Geology **155**(3-4): 295–320.

Boumaiza, L., Walter, J., Chesnaux, R., Stotler, R.L., Wen, T., Johannesson, K.H., Brindha, K., et Huneau, F. 2022b. Chloride-salinity as indicator of the chemical composition of groundwater: empirical predictive model based on aquifers in Southern Quebec, Canada. Environmental Science and Pollution Research **29**(39): 59414–59432.

Bowles, M.W., Mogollón, J.M., Kasten, S., Zabel, M., et Hinrichs, K.-U. 2014. Global rates of marine sulfate reduction and implications for sub–sea-floor metabolic activities. Science **344**(6186): 889–891.

Brown, P.J., Vannucci, M., et Fearn, T. 1998. Multivariate Bayesian variable selection and prediction. Journal of the Royal Statistical Society: Series B (Statistical Methodology) **60**(3): 627–641.

Bucher, K., et Stober, I. 2000. The composition of groundwater in the continental crystalline crust. *Dans* Hydrogeology of Crystalline Rocks. Springer. pp. 141–175.

Bucher, K., et Stober, I. 2010. Fluids in the upper continental crust. Geofluids **10**(1-2): 241–253.

Bungum, H., et Eldholm, O. 2022. The conundrums of the postglacial tectonic response of the Fennoscandian and Canadian Shields. Earth-Science Reviews: 104146.

Carpenter, A.B., Trout, M.L., et Pickett, E.E. 1974. Preliminary report on the origin and chemical evolution of lead-and zinc-rich oil field brines in central Mississippi. Economic Geology **69**(8): 1191–1206.

Clark, I.D., Al, T., Jensen, M., Kennell, L., Mazurek, M., Mohapatra, R., et Raven, K. 2013. Paleozoic-aged brine and authigenic helium preserved in an Ordovician shale aquiclude. Geology **41**(9): 951–954.

Clark, I.D., et Fritz, P. 1997. Environmental isotopes in hydrogeology. CRC Press.

Clauser, C., et Huenges, E. 1995. Thermal conductivity of rocks and minerals. Rock Physics and Phase Relations: A Handbook of Physical Constants **3**: 105–126.

Cloutier, V., Lefebvre, R., Savard, M., et Therrien, R. 2004. Groundwater origin and geochemical processes in the Basses-Laurentides sedimentary rock aquifer system, St. Lawrence Lowlands, Quebec, Canada. *Sous la direction de*. *Dans* Proceedings, 57th Canadian Geotechnical Conference and 5th Joint CGS/IAH Conference, pp. 18–25.

Cloutier, V., Lefebvre, R., Therrien, R., et Savard, M.M. 2008. Multivariate statistical analysis of geochemical data as indicative of the hydrogeochemical evolution of groundwater in a sedimentary rock aquifer system. Journal of Hydrology **353**(3-4): 294–313.

Collins, A. 1975. Geochemistry of oilfield waters. Elsevier Scientific Publishing Company, Amsterdam.

Connolly, C.A., Walter, L.M., Baadsgaard, H., et Longstaffe, F.J. 1990. Origin and evolution of formation waters, Alberta Basin, Western Canada Sedimentary Basin. II. Isotope systematics and water mixing. Applied Geochemistry **5**(4): 397–413.

Cortecci, G., Dinelli, E., Bolognesi, L., Boschetti, T., et Ferrara, G. 2001. Chemical and isotopic compositions of water and dissolved sulfate from shallow wells on Vulcano Island, Aeolian Archipelago, Italy. Geothermics **30**(1): 69–91.

Dewey, J., Kiseeva, E.S., Pearce, J., et Robb, L. 2021. Precambrian tectonic evolution of Earth: an outline. South African Journal of Geology 2021 **124**(1): 141–162.

Di Leo, G., et Sardanelli, F. 2020. Statistical significance: p value, 0.05 threshold, and applications to radiomics—reasons for a conservative approach. European Radiology Experimental **4**(1): 1–8.

Downing, R., Edmunds, W., et Gale, I. 1987. Regional groundwater flow in sedimentary basins in the UK. Geological Society, London, Special Publications **34**(1): 105–125.

Dugamin, E.J., Cathelineau, M., Boiron, M.-C., Richard, A., et Despinois, F. 2023. Lithium enrichment processes in sedimentary formation waters. Chemical Geology **635**: 121626.

Edmunds, W., Andrews, J., Burgess, W., Kay, R., et Lee, D. 1984. The evolution of saline and thermal groundwaters in the Carnmenellis granite. Mineralogical Magazine **48**(348): 407–424.

Farnham, I.M., Singh, A.K., Stetzenbach, K.J., et Johannesson, K.H. 2002. Treatment of nondetects in multivariate analysis of groundwater geochemistry data. Chemometrics and Intelligent Laboratory Systems **60**(1-2): 265–281.

Frape, S., Blyth, A., Blomqvist, R., McNutt, R., et Gascoyne, M. 2003. Deep fluids in the continents: II. Crystalline rocks. Treatise on Geochemistry **5**: 605.

Frape, S., et Fritz, P. 1982. The chemistry and isotopic composition of saline groundwaters from the Sudbury Basin, Ontario. Canadian Journal of Earth Sciences **19**(4): 645–661.

Frape, S., et Fritz, P. 1987. Geochemical trends for groundwaters from the Canadian Shield. Geological Association of Canada-Special Paper **33**: 19–38.

Frape, S., Fritz, P., et McNutt, R.t. 1984. Water-rock interaction and chemistry of groundwaters from the Canadian Shield. Geochimica et Cosmochimica Acta **48**(8): 1617–1627.

Gascoyne, M., et Kamineni, D. 1994. The hydrogeochemistry of fractured plutonic rocks in the Canadian Shield. Applied Hydrogeology **2**(2): 43–49.

Gerber, C., Vaikmäe, R., Aeschbach, W., Babre, A., Jiang, W., Leuenberger, M., Lu, Z.-T., Mokrik, R., Müller, P., et Raidla, V. 2017. Using 81Kr and noble gases to characterize and date groundwater and brines in the Baltic Artesian Basin on the one-million-year timescale. Geochimica et Cosmochimica Acta **205**: 187–210.

Gimeno, M.J., Auqué, L.F., Acero, P., et Gómez, J.B. 2014. Hydrogeochemical characterisation and modelling of groundwaters in a potential geological repository for spent nuclear fuel in crystalline rocks (Laxemar, Sweden). Applied Geochemistry **45**: 50–71.

Gimeno, M.J., Auque, L.F., Gomez, J.B., et Acero, P. 2009. Water-rock interaction modelling and uncertainties of mixing modelling. SDM-Site Laxemar. Swedish Nuclear Fuel and Waste Management Co. SKB R-08-110.

Goldberg, E., Broecker, W., Gross, M., et Turekian, K. 1971. Radioactivity in the marine environment. National Academy of Science, Washington, DC **137**.

Grenthe, I., Stumm, W., Laaksuharju, M., Nilsson, A., et Wikberg, P. 1992. Redox potentials and redox reactions in deep groundwater systems. Chemical Geology **98**(1-2): 131–150.

Güler, C., Thyne, G.D., McCray, J.E., et Turner, K.A. 2002. Evaluation of graphical and multivariate statistical methods for classification of water chemistry data. Hydrogeology Journal **10**(4): 455–474.

Hanor, J.S. 1994. Origin of saline fluids in sedimentary basins. Geological Society, London, Special Publications **78**(1): 151–174.

Helgeson, H.C. 1978. Summary and critique of the thermodynamic properties of rock-forming minerals. American Journal of Science, A **278**: 1–229.

Herut, B., Starinsky, A., Katz, A., et Bein, A. 1990. The role of seawater freezing in the formation of subsurface brines. Geochimica et Cosmochimica Acta **54**(1): 13–21.

Houyun, S., Xiaoming, S., Xiaofeng, W., Ziran, C., Wei, L., Xingkai, H., Xia, L., Zhiqiang, Y., et Wenbo, L. 2022. Formation mechanism of metasilicate mineral water in Chengde, Hebei Province: Evidence from rock weathering and water-rock interaction. Geology in China **49**(4): 1088–1113.

Hoyer, M., Kummer, N.-A., et Merkel, B. 2015. Sorption of lithium on bentonite, kaolin and zeolite. Geosciences **5**(2): 127–140.

Hsissou, Y., Mudry, J., Mania, J., Bouchaou, L., et Chauve, P. 1999. Utilisation du rapport Br/Cl pour déterminer l'origine de la salinité des eaux souterraines: exemple de la plaine du Souss (Maroc). Comptes Rendus de l'Académie des Sciences-Series IIA-Earth and Planetary Science **328**(6): 381–386.

Hutcheon, I. 2000. Principles of diagenesis and what drives mineral change. Fluids and Basin Evolution **28**: 93–114.

Janos, D., Molson, J., et Lefebvre, R. 2018. Regional groundwater flow dynamics and residence times in Chaudière-Appalaches, Québec, Canada: Insights from numerical simulations. Canadian Water Resources Journal/Revue Canadienne des Ressources Hydriques **43**(2): 214–239.

Jiang, X.W., Wan, L., Wang, X.S., Ge, S., et Liu, J. 2009. Effect of exponential decay in hydraulic conductivity with depth on regional groundwater flow. Geophysical Research Letters **36**(24).

Jones, B., et Deocampo, D. 2003. Geochemistry of saline lakes. Treatise on Geochemistry **5**: 605.

Kaiser, H.F. 1960. The application of electronic computers to factor analysis. Educational and Psychological Measurement **20**(1): 141–151.

Kaleem, M., Naseem, S., Bashir, E., Shahab, B., et Rafique, T. 2021. Discrete geochemical behavior of Sr and Ba in the groundwater of Southern Mor Range, Balochistan, a tracer for igneous and sedimentary rocks weathering and related environmental issues. Applied Geochemistry **130**: 104996.

Kelly, W.C., Rye, R.O., et Livnat, A. 1986. Saline minewaters of the Keweenaw Peninsula, northern Michigan; their nature, origin, and relation to similar deep waters in Precambrian crystalline rocks of the Canadian Shield. American Journal of Science **286**(4): 281–308.

Kharaka, Y., Maest, A., Carothers, W., Law, L., Lamothe, P., et Fries, T. 1987. Geochemistry of metal-rich brines from central Mississippi Salt Dome basin, USA. Applied Geochemistry **2**(5-6): 543–561.

Kharaka, Y.K., et Dorsey, N.S. 2005. Environmental issues of petroleum exploration and production: Introduction. Environmental Geosciences **12**(2): 61–63.

Kharaka, Y.K., et Hanor, J. 2003. Deep fluids in the continents: I. Sedimentary basins. Treatise on Geochemistry **5**: 605.

Kim, J.-H., Bailey, L., Noyes, C., Tyne, R.L., Ballentine, C.J., Person, M., Ma, L., Barton, M., Barton, I., et Reiners, P.W. 2022. Hydrogeochemical evolution of formation waters responsible for sandstone bleaching and ore mineralization in the Paradox Basin, Colorado Plateau, USA. Bulletin **134**(9-10): 2589–2610.

Kısakűrek, B., James, R.H., et Harris, N.B. 2005. Li and δ7Li in Himalayan rivers: proxies for silicate weathering? Earth and Planetary Science Letters **237**(3-4): 387–401.

Kloppmann, W., Bourhane, A., et Asfirane, F. 2011. Méthodologie de diagnostic de l'origine de la salinité des masses d'eau. BRGM. p. 129.

Kukkonen, I., et Peltonen, P. 1999. Xenolith-controlled geotherm for the central Fennoscandian Shield: implications for lithosphere–asthenosphere relations. Tectonophysics **304**(4): 301–315.

Laaksoharju, M., Tullborg, E.-L., Wikberg, P., Wallin, B., et Smellie, J. 1999. Hydrogeochemical conditions and evolution at the Äspö HRL, Sweden. Applied Geochemistry **14**(7): 835–859.

Le Chatelier, H.L. 1884. A general statement of the laws of chemical equilibrium. Comptes Rendus **99**: 786–789.

Le Roux, G.I., Laverret, E., et Shotyk, W. 2006. Fate of calcite, apatite and feldspars in an ombrotrophic peat bog, Black Forest, Germany. Journal of the Geological Society **163**(4): 641–646.

Li, K., Cai, C., Tan, X., Jiang, H., et Fan, J. 2022. Massive dolomitization driven by MgSO4-rich seawater and its effects on thermochemical sulfate reduction, Upper Permian Changxing Formation, northeastern Sichuan, China. Energy Exploration & Exploitation **40**(5): 1315–1343.

Lucas, Y., Schmitt, A., Chabaux, F., Clément, A., Fritz, B., Elsass, P., et Durand, S. 2010. Geochemical tracing and hydrogeochemical modelling of water–rock interactions during salinization of alluvial groundwater (Upper Rhine Valley, France). Applied Geochemistry **25**(11): 1644–1663.

McCaffrey, M., Lazar, B., et Holland, H. 1987. The evaporation path of seawater and the coprecipitation of Br (super-) and K (super+) with halite. Journal of Sedimentary Research **57**(5): 928–937.

McDonough, L.K., Meredith, K.T., Nikagolla, C., et Banati, R.B. 2021. The influence of water–rock interactions on household well water in an area of high prevalence chronic kidney disease of unknown aetiology (CKDu). NPJ Clean Water **4**(1): 2.

McIntosh, J., et Walter, L. 2005. Volumetrically significant recharge of Pleistocene glacial meltwaters into epicratonic basins: Constraints imposed by solute mass balances. Chemical Geology **222**(3-4): 292–309.

McKight, P.E., et Najab, J. 2010. Kruskal-wallis test. The Corsini Encyclopedia of Psychology: 1–1.

McNutt, R.H., Frape, S.K., et Fritz, P. 1984. Strontium isotopic composition of some brines from the Precambrian Shield of Canada. Chemical Geology **46**(3): 205–215.

Millot, R., Vigier, N., et Gaillardet, J. 2010. Behaviour of lithium and its isotopes during weathering in the Mackenzie Basin, Canada. Geochimica et Cosmochimica Acta **74**(14): 3897–3912.

Mizutani, S. 1970. Silica minerals in the early stage of diagenesis. Sedimentology **15**(3-4): 419–436.

Molofsky, L.J. 2023. Isotopic Insights into Water of Condensation, Cross-Formation Water Flow, and Natural Hydrocarbon Migration in Sedimentary Basins. Doctoral dissertation, Geological Sciences The University of Texas at El Paso, Texas, United States.

Montcoudiol, N., Molson, J., Lemieux, J.-M., et Cloutier, V. 2015. A conceptual model for groundwater flow and geochemical evolution in the southern Outaouais Region, Québec, Canada. Applied Geochemistry **58**: 62–77.

Morales-Arredondo, J., Hernández, M.A., Cuellar-Ramírez, E., Morton-Bermea, O., et Ortega-Gutiérrez, J. 2022. Hydrogeochemical behavior of Ba, B, Rb, and Sr in an urban aquifer located in central Mexico and its environmental implications. Journal of South American Earth Sciences **116**: 103870.

Morgan, A.L.F. 2018a. Low temperature geothermal resources in abandoned mines of the Canadian Shield: a case study in the Chapais and Chibougamau area, Québec, Canada.

Moussaoui, I., Rosa, E., Cloutier, V., Neculita, C.M., et Dassi, L. 2023. Chemical and isotopic evaluation of groundwater salinization processes in the Djebeniana coastal aquifer, Tunisia. Applied Geochemistry **149**: 105555.

Nagaraju, P., Ray, L., Ravi, G., Akkiraju, V.V., et Roy, S. 2012. Geothermal investigations in the Upper Vindhyan sedimentary rocks of Shivpuri area, central India. Journal of the Geological Society of India **80**: 39–47.

Négrel, P. 1999. Geochemical study of a granitic area–the Margeride Mountains, France: chemical element behavior and 87Sr/86Sr constraints. Aquatic Geochemistry **5**: 125–165.

Négrel, P., Lemiere, B., Machard de Grammont, H., Billaud, P., et Sengupta, B. 2007. Hydrogeochemical processes, mixing and isotope tracing in hard rock aquifers and surface waters from the Subarnarekha River Basin,(east Singhbhum District, Jharkhand State, India). Hydrogeology Journal **15**: 1535–1552.

Nisson, D.M. 2023. Hydrogeochemical Support for Microbial Habitability in an Ancient, Hypersaline, Thermal, and Radiogenic Subsurface Brine in South Africa. Doctoral dissertation, Department of Geosciences, Princeton University, New Jersey, United States.

Norden, B., et Fröster, A. 2006. Thermal conductivity and radiogenic heat production of sedimentary and magmatic rocks in the Northeast German Basin. AAPG Bulletin **90**(6): 939–962.

Nordström, D., Andrews, J., Carlsson, L., Fontes, J.-C., Frits, P., Moser, H., et Olsson, T. 1985. Hydrogeological and hydrogeochemical investigations in boreholes-final report of the phase I geochemical investigations of the Stripa groundwaters. Swedish Nuclear Fuel and Waste Management Co.

Nordstrom, D., et Ball, J.W. 1989. Mineral saturation states in natural waters and their sensitivity to thermodynamic and analytic errors. Etat de saturation des minéraux dans les eaux naturelles et sensibilité des tests aux données thermodynamiques et aux erreurs analytiques. Sciences Géologiques, Bulletins et Mémoires **42**(4): 269–280.

Nordstrom, D.K., Ball, J.W., Donahoe, R.J., et Whittemore, D. 1989. Groundwater chemistry and water-rock interactions at Stripa. Geochimica et Cosmochimica Acta **53**(8): 1727–1740.

Nurmi, P.A., Kukkonen, I.T., et Lahermo, P.W. 1988. Geochemistry and origin of saline groundwaters in the Fennoscandian Shield. Applied Geochemistry **3**(2): 185–203.

Papizadeh, M., Roayaei Ardakani, M., Fakour, H., Ghaderi, G., et Firouzei, Y. 2017. Microbio-ecology and hydro-geochemistry of saline sulfur springs of Ghale-Madreseh, Khuzestan, Iran. Pollution **3**(4): 623–637.

Pauwels, H., Fouillac, C., et Fouillac, A.-M. 1993. Chemistry and isotopes of deep geothermal saline fluids in the Upper Rhine Graben: Origin of compounds and water-rock interactions. Geochimica et Cosmochimica Acta **57**(12): 2737–2749.

Peiffer, L., Taran, Y., Lounejeva, E., Solís-Pichardo, G., Rouwet, D., et Bernard-Romero, R. 2011. Tracing thermal aquifers of El Chichón volcano–hydrothermal system (México) with 87Sr/86Sr, Ca/Sr and REE. Journal of Volcanology and Geothermal Research **205**(3-4): 55–66.

Perri, F. 2020. Chemical weathering of crystalline rocks in contrasting climatic conditions using geochemical proxies: an overview. Palaeogeography, Palaeoclimatology, Palaeoecology **556**: 109873.

Person, M.A., et Sazeed, N. 2022. Continental Brackish Groundwater Resources. *Dans* Unconventional Water Resources. Springer. pp. 111–128.

Plummer, L.N. 1988. A computer program incorporating Pitzer's equations for calculation of geochemical reactions in brines. Department of the Interior, US Geological Survey.

Pohlert, T. 2016. Non-parametric trend tests and change-point detection. CC BY-ND **4**.

Pohlert, T. 2020. Non-Parametric Trend Tests and Change-Point Detection. 1.1.6. R Foundation for Statistical Computing, Vienna, Austria. https://CRAN.R-project.org/package=trend.

Qi, H., Ma, C., He, Z., Hu, X., et Gao, L. 2019. Lithium and its isotopes as tracers of groundwater salinization: a study in the southern coastal plain of Laizhou Bay, China. Science of The Total Environment **650**: 878–890.

Qian, K., Sun, H., Li, J., et Xie, X. 2023. Strontium isotopes as tracers for water-rocks interactions of groundwater to delineate iodine enrichment in aquifer of Datong Basin, northern China. Applied Geochemistry **158**: 105783.

Reimann, C., et Filzmoser, P. 2000. Normal and lognormal data distribution in geochemistry: Death of a myth. Consequences for the statistical treatment of geochemical and environmental data. Environmental Geology **39**(9).

Rittenhouse, G. 1967. Bromine in oil-field waters and its use in determining possibilities of origin of these waters. AAPG Bulletin **51**(12): 2430–2440.

Ruppel, S.C., Jones, R.H., Breton, C.L., et Kane, J.A. 2005. Preparation of maps depicting geothermal gradient and Precambrian structure in the Permian basin. USGS Order(04CRSA0834).

Sall, J., Stephens, M.L., Lehman, A., et Loring, S. 2017. JMP start statistics: a guide to statistics and data analysis using JMP. 6 éd. SAS Institute Inc., Cary, North Carolina, United States.

Savoye, S. 1998. Origine de la salinité des eaux souterraines en milieu granitique: identification et caractérisation des sources de chlorure. Thèse de doctorat, Terre, océan, espace, Paris 11, Paris, France.

Shand, P., Darbyshire, D.F., Love, A.J., et Edmunds, W.M. 2009. Sr isotopes in natural waters: Applications to source characterisation and water–rock interaction in contrasting landscapes. Applied Geochemistry **24**(4): 574–586.

Shouakar-Stash, O., Alexeev, S., Frape, S., Alexeeva, L., et Drimmie, R. 2007. Geochemistry and stable isotopic signatures, including chlorine and bromine isotopes, of the deep groundwaters of the Siberian Platform, Russia. Applied Geochemistry **22**(3): 589–605.

Stalder, H.A., Sicher, V., et Lussmann, L. 1980. Die Mineralien des Gotthardbahntunnels und des Gotthardstrassentunnels. Verlag nicht ermittelbar.

Steuber, T. 1999. Isotopic and chemical intra-shell variations in low-Mg calcite of rudist bivalves (Mollusca-Hippuritacea): disequilibrium fractionations and late Cretaceous seasonality. International Journal of Earth Sciences **88**: 551–570.

Stober, I., et Bucher, K. 1999. Deep groundwater in the crystalline basement of the Black Forest region. Applied Geochemistry **14**(2): 237–254.

Stueber, A.M., Saller, A.H., et Ishida, H. 1998. Origin, migration, and mixing of brines in the Permian basin: geochemical evidence from the eastern central basin platform, Texas. AAPG Bulletin **82**(9): 1652–1672.

Teiber, H., Marks, M.A., Wenzel, T., Siebel, W., Altherr, R., et Markl, G. 2014. The distribution of halogens (F, Cl, Br) in granitoid rocks. Chemical Geology **374**: 92–109.

Tellam, J.H. 1995. Hydrochemistry of the saline groundwaters of the lower Mersey Basin Permo-Triassic sandstone aquifer, UK. Journal of Hydrology **165**(1-4): 45–84.

Vosteen, H.-D., et Schellschmidt, R. 2003. Influence of temperature on thermal conductivity, thermal capacity and thermal diffusivity for different types of rock. Physics and Chemistry of the Earth, Parts a/b/c **28**(9-11): 499–509.

Walter, J., Chesnaux, R., Boumaiza, L., Brindha, K., et Regenspurg, S. 2023. Conceptual model for the chemical evolution of groundwater in a region of the Canadian Precambrian shield covered by soft Quaternary deposit of glacial and marine origin. Applied Geochemistry **150**: 105574.

Walter, J., Chesnaux, R., Cloutier, V., et Gaboury, D. 2017. The influence of water/rock− water/clay interactions and mixing in the salinization processes of groundwater. Journal of Hydrology: Regional Studies **13**: 168–188.

Walter, J., Chesnaux, R., Gaboury, D., et Cloutier, V. 2019. Subsampling of regional-scale database for improving multivariate analysis interpretation of groundwater chemical evolution and ion sources. Geosciences **9**(3): 139.

Wark, D.A., et Watson, E.B. 2006. TitaniQ: a titanium-in-quartz geothermometer. Contributions to Mineralogy and Petrology **152**(6): 743–754.

Warr, O., Ballentine, C., Onstott, T., Nisson, D., Kieft, T., Hillegonds, D., et Sherwood Lollar, B. 2022. 86Kr excess and other noble gases identify a billion-year-old radiogenically-enriched groundwater system. Nature Communications **13**(1): 3768.

Warr, O., Giunta, T., Onstott, T.C., Kieft, T.L., Harris, R.L., Nisson, D.M., et B, S.L. 2021. The role of low-temperature 18O exchange in the isotopic evolution of deep subsurface fluids. Chemical Geology **561**: 120027.

White, A.F., Bullen, T.D., Schulz, M.S., Blum, A.E., Huntington, T.G., et Peters, N.E. 2001. Differential rates of feldspar weathering in granitic regoliths. Geochimica et Cosmochimica Acta **65**(6): 847–869.

Williams, L.B., Elliott, W.C., et Hervig, R.L. 2015. Tracing hydrocarbons in gas shale using lithium and boron isotopes: Denver Basin USA, Wattenberg Gas Field. Chemical Geology **417**: 404–413.

Yan, K., Wang, C., Chen, R., Liu, C., Wang, J., Yu, X., Shen, L., Li, R., Zhou, Y., et Zhou, Q. 2023. Origin and evolution of deep lithium-rich brines in the southwest Jianghan Basin, central China: Evidence from hydrochemistry and stable isotopes. Journal of Hydrology **626**: 130163.

Yang, N., Su, C., Liu, W., et Zhao, L. 2022. Occurrences and mechanisms of strontium-rich groundwater in Xinglong County, northern China: insight from hydrogeological and hydrogeochemical evidence. Hydrogeology Journal **30**(7): 2043–2057.

Yardley, B.W. 2013. The chemical composition of metasomatic fluids in the crust. *Dans* Metasomatism and the chemical transformation of rock. Springer. pp. 17–51.

Yardley, B.W., et Bodnar, R.J. 2014. Fluids in the continental crust. Geochemical Perspectives **3**(1): 1–2.

Yeomans, K.A., et Golder, P.A. 1982. The Guttman-Kaiser criterion as a predictor of the number of common factors. The Statistician: 221–229.

Yu, X., Liu, C., Wang, C., Wang, J., Li, Q., et Meng, L. 2022. Origin of Li brine-type deposits in the Cretaceous gypsum-bearing formation of the Jitai Basin, South China: Constraints from geochemistry and H, O, Li, B, and Sr isotopes. Applied Geochemistry **139**: 105257.

Yu, X., Wang, C., Huang, H., et Yan, K. 2024. Origin of lithium in oilfield brines in continental petroliferous basin: Insights from Li and Sr isotopes in the Jianghan Basin, central China. Marine and Petroleum Geology **160**: 106576.

Zuddas, P. 2010. Water–rock interaction processes seen through thermodynamics. Elements **6**(5): 305–308.

Chapitre 4 : GEOCHEMISTRY OF ANCIENT BRINES AND GLACIAL MELTWATERS REVEALS A HYDRAULIC CONNECTION BETWEEN THE DEEP CANADIAN PRECAMBRIAN SHIELD AND SHALLOW AQUIFERS

Othniel G.D. Ngombe[1,4]*, Julien Walter[1,4], Romain Chesnaux[1,4], John Molson[2], D. L. Pinti[3]

[1] Département des Sciences appliquées, Université du Québec à Chicoutimi, Saguenay, Québec, G7H 2B1, Canada

[2] Département de géologie et de génie géologique, Université Laval, Québec, Québec, G1V 0A6, Canada

[3] GEOTOP & Département des sciences de la Terre et de l'atmosphère, Université du Québec à Montréal, Montréal, Québec, H3C 3P8, Canada

[4] Centre d'études sur les ressources minérales, Groupe de recherche Risque Ressource Eau, Université du Québec à Chicoutimi, Saguenay, Québec, G7H 2B1, Canada

JOURNAL OF HYDROLOGY

2025

4.1. Mise en contexte

Ce chapitre a permis de répondre à l'objectif 3, qui visait à évaluer la contribution relative des eaux anciennes (âges et compositions différentes) au système hydrogéologique actuel et la participation des fluides profonds aux cycles de l'eau en contexte de graben. Pour ce faire, une approche multi-traceurs a été utilisée sur des eaux saumâtres échantillonnées dans le roc fracturé au SLSJ. La méthodologie combine analyses des éléments majeurs, mineurs et traces, isotopes stables et radiogéniques ($\delta^{11}B$, $\delta^{7}Li$, $\delta^{37}Cl$, $\delta^{81}Br$, $^{87}Sr/^{86}Sr$, ^{14}C) et gaz rares (He, Ar, Ne). Cette combinaison d'outils permet d'identifier les principales sources de salinité (marine holocène, Paléozoïque, Précambrienne) et de reconstruire les trajectoires de mélange régionales. Le chapitre 4 met ainsi en évidence la superposition temporelle et l'importante diversité des processus hydrogéochimiques impliqués. La présence d'une grande quantité d'hélium radiogénique, y compris des traces d'hélium mantellique, confirme clairement l'existence d'une connectivité entre les environnements profonds du socle cristallin et les aquifères de surface. Cette connectivité hydraulique est probablement contrôlée par des failles crustales profondément enracinées qui bordent le graben du Saguenay, principale caractéristique structurale de la zone étudiée.

4.2. Author contribution

Othniel G.D. Ngombe: Investigation, Sampling Campaign, Methodology, Visualization, Writing – original draft, Writing – review & editing.

Julien Walter: Project administration, Supervision, Methodology, Writing – review & editing.

Romain Chesnaux: Supervision, Methodology, Writing – review & editing.

John Molson: Supervision, Methodology, Writing – review & editing.

Daniele L. Pinti: Supervision, Methodology, Visualization, Writing – review & editing

4.3. Abstract

The Saguenay-Lac-Saint-Jean (SLSJ) region of the Canadian Precambrian Shield is used as a natural laboratory to investigate the imprint of paleo flow systems and hydrogeochemical processes on shallow groundwater by applying a multi-tracer approach combining ion chemistry, groundwater isotopes ($^{87}Sr/^{86}Sr$, ^{14}C, $\delta^{11}B$, $\delta^{7}Li$, $\delta^{37}Cl$, $\delta^{81}Br$), and noble gases (He, Ne and Ar). Results reveal three distinct sources of salinity at shallow depth: (1) Holocene marine water associated with the Laflamme Sea and partly modified by interactions with marine clays, (2) Paleozoic marine brine resulting from evaporation of local Ordovician sea water, and (3) Precambrian Shield brine hundreds of millions of years old associated with Canadian Shield rocks, and containing 1-5% of mantle helium. One highly radiogenic $^{87}Sr/^{86}Sr$ sample, containing some mantle helium and radiogenic $^{40}Ar^{*}$, confirms the presence of deep Precambrian Shield brines (7.5 to 12.5 km deep) in the SLSJ region, migrating upwards through Saguenay Graben faults. The study also confirms, for the first time in this region, that traces of Wisconsinian glacial waters (~8,225 to 25,500 yrs BP) are indeed preserved below ground. High values of $\delta^{81}Br$, $\delta^{11}B$, and $\delta^{7}Li$ observed in the Paleozoic marine and Precambrian Shield brines indicate significant modifications of their chemical evolution through cryo-concentration processes during the last glaciation, extending previous works. Beyond the SLSJ area, this research highlights how shallow aquifers and Precambrian shields can be hydraulically connected, and clarifies the multiple origins of groundwaters, being fundamental knowledge for effective water management in complex flow systems.

Keywords: Saguenay Graben, mantle helium, Precambrian Shield brine, Wisconsinian glaciation, Paleo-marine waters, Quaternary-Paleozoic-Precambrian mixing system.

4.4. Introduction

In the face of growing impacts of climate change and increasing water demand pressure, a more rigorous approach to groundwater resource management is needed (Galloway, 2010; Adombi et al., 2024). One of the main challenges is to understand the processes of mixing between ancient and recent groundwater (Meyzonnat et al., 2023), and related groundwater chemical evolution over geological time (Saby et al., 2016), which influence the long-term renewal, quality, and availability of groundwater (Laaksoharju et al., 1995). Water chemistry evolution can be further complicated by aquifer connectivity, where different aquifers containing water masses recharged in different periods interact with different lithologies and, then mix water flow, during tectonically induced, e.g. Campbell et al. (2025), or topographically induced, e.g. Tóth (1978). Understanding aquifer connectivity in complex aquifer systems is vital for water management. Indeed, it can affect how groundwater flows and how quickly contaminants can spread through the subsurface, affecting regional water resources. It enables a more accurate prediction of how changes in recharge or extraction from one part of a connected system may affect other parts. Finally, it helps water managers understand potential changes in groundwater levels and inflows/outflows, which is crucial for sustainable management.

Precambrian shields are part of complex hydrogeological systems due to the heterogeneous compartmentalization of the aquifers and their long hydrogeological histories (Abi et al., 2022; Gimeno et al., 2023). The presence of fracture zones with variable hydraulic conductivity and connectivity results in a heterogeneous distribution of groundwater (Chandra et al., 2019; Allen et Nott, 2021). In addition to this structural heterogeneity, shield groundwater is also chemically diverse, evolving from a classical dilute Ca-HCO_3/Na-HCO_3 type water toward Ca-Cl brines (Frape et al., 1984; Boumaiza et al., 2024). Precambrian Shield brines (PSB) have been found in numerous localities of the Canadian Precambrian Shield (Frape et Fritz, 1987) and Fennoscandian Shield (Blomqvist, 1999), mainly intercepted in deep mines (> 500 m) such as Yellowknife Con, Kidd Creek, and Kotalahti mines. Their chemical evolution reflects the progressive long-term water-rock interaction, and strongly marked by the complex hydrogeological history of these regions (Clark et al., 2000; Douglas

et al., 2000). For example, Bottomley et Clark (2004) suggested that the PSBs in the Yellowknife Con Mine had a component of recent water and paleo-subglacial meltwater dating from the late Pleistocene. According to Warr et al. (2021), the significant depletion of $\delta^{18}O$ in comparison to meteoric water line, characteristic of PSB, is explained by the low-temperature isotopic exchange of oxygen between fluids and host rocks, occurring over long geological time scales. PSBs exhibit enrichment in radiogenic isotopes, such as ^{4}He, ^{21}Ne, among others (Bottomley et al., 1984; Holland et al., 2013), indicating that these brines have a residence time of hundreds of millions of years or even billions of years. These brines were believed to reside exclusively in the crystalline basement of these old cratons. However, Pinti et al. (2011) found similar brines in the Ordovician aquifers of the St. Lawrence Lowlands sedimentary platform, Québec. These brines have salinities of up to 10 times that of seawater, Na-Ca-Cl chemistry, and very high radiogenic $^{87}Sr/^{86}Sr$ ratios identical to those of PSB. Pinti et al. (2011) suggested a minimum Devonian age of these brines.

The hydrogeological history of the Canadian Shield is characterized by multiple events, including marine transgressions, glacial-interglacial cycles, postglacial isostatic adjustments, paleo-hydrothermal activities, and tectonic reactivations (Frape et al., 1984; Bottomley et al., 1999; Person et al., 2007). This history has led to the superposition of several distinct hydrogeochemical signatures over time, making it challenging to identify and understand ancient hydrogeochemical processes. Although significant progress has been made in understanding the mechanisms involved in the mixing of waters from different compositions and ages (Douglas et al., 2000; Montcoudiol et al., 2015; Boumaiza et al., 2024), these complex hydrogeochemical processes over geological time scales still give reason for debate, particularly in deep environments (e.g. Greene et al. (2008)). In this context, the Saguenay-Lac-Saint-Jean (SLSJ) region, located in the Grenville geological province of the Canadian Shield, englobe the large tectonic depression of the Saguenay graben, is an ideal field of study. Pioneering hydrogeochemical studies within the SLSJ region have revealed the presence of brackish waters at shallow depths around Lac Saint-Jean, which suggested that their origin may be related to the mixing of post-glacial infiltration of seawater (Laflamme Sea) and deep Precambrian Shield brines (Dessureault, 1975; Walter et al., 2006; Walter, 2010). The regional hydrochemical variability at shallow depth, combined with a complex hydrogeological history and the presence of

crustal-scale tectonic features bordering the Saguenay graben, provides a unique opportunity to study connectivity between aquifers and groundwater mixing dynamics.

This study hypothesised that the presence of old groundwater within shallow fractured aquifers in the SLSJ region indicates that the current hydrogeological system has preserved the imprint of its complex hydrogeological history. However, fundamental questions remain regarding the relative contributions of past hydrogeochemical signatures, which have been maintained despite multiple influences over geological time, to the current hydrogeological system of the region. The relative contributions of several events to the current hydrogeological system have never been assessed, including glacial episodes, marine transgressions older than the Laflamme Sea, or fluids from the base of the crust, or even from the sub-continental mantle, migrating through the Graben faults. Achieving this general objective requires (1) identifying and characterizing distinct hydrogeochemical signatures from shallow groundwater to deep brines in regional fractured aquifers and (2) identifying salinization processes of fluids with different compositions and ages.

The present study uses a multi-tracer approach, including radiogenic isotopes ($^{87}Sr/^{86}Sr$), stable isotopes ($\delta^{11}B$, $\delta^{7}Li$, $\delta^{37}Cl$, $\delta^{81}Br$), age tracers (^{14}C), and noble gases (He, Ne, and Ar isotopes) to discriminate the respective contributions inherited from the past on the current hydrogeological system. Each tracer provides precise and complementary information on the evolution of groundwater. The multi-tracer approach provides a more comprehensive understanding of groundwater evolution, aquifer connectivity and groundwater mixing dynamics, while also capturing the multiple contributions resulting from the region's complex hydrogeological history. This knowledge can support decision-makers in identifying areas at risk of salinization and anticipate potential impacts on groundwater use.

4.5. Geological context and hydrogeological background of the region

The SLSJ region is in the central part of southern Quebec, north of the St. Lawrence River. The region covers an area of 13,210 km^2, where the territory extends around Lac Saint-Jean to the west (approximately 40 km long) and along the Saguenay River, which drains Lac Saint-Jean into the St. Lawrence River (Walter et al., 2018).

The bedrock of the region is composed of Precambrian crystalline rocks and Paleozoic sedimentary rocks, overlain by unconsolidated Quaternary deposits (Figure 4-1). The Precambrian rocks of the Grenville Province are characterized by various plutonic rocks with compositions ranging from felsic to intermediate, as well as a complex of orthogneiss and paragneiss (Laurin et Sharma, 1975). The investigated region has undergone several phases of Mesoproterozoic anorthositic intrusions (~1,500 and 1,000 Ma), which have led to the formation of the anorthosite-mangerite-charnockite-granite (AMCG) suite (Hébert et Van Breemen, 2004). The Lac-Saint-Jean anorthositic suite (LSJAS) is one of the largest intrusive masses in the Grenville Province, which constitutes a significant part of the study area (Figure 4-1). The fractured bedrock of the region also includes eroded limestones and shales (Figure 4-1). These rocks, found in the lowlands of the region, are described as the remains of a tropical sea from the Ordovician period, which covered some regions of the Canadian Shield from 450 to 200 million years ago (Desbiens et Lespérance, 1989). The regional fractured bedrocks are covered by unconsolidated deposits from the Quaternary period, which are mainly composed of late Wisconsinian fluvioglacial deposits, postglacial clays from the Laflamme Sea (forming a regional aquitard), and deltaic and littoral sediments from the Late Pleistocene and early Holocene (Tremblay, 1971). The lowlands are characterized by significant local accumulations of Pleistocene deposits, up to 180 m thick (Rouleau et al., 2013). Moreover, the region is marked by the presence of the Saguenay Graben, a topographical depression oriented from northwest to southeast and delineated by west-northwest fault systems that mark the boundaries between the highlands and the lowlands (Walter et al., 2018). This geological structure played a major role in the formation of the main unconsolidated deposits in the lowlands and protected some units of Paleozoic sedimentary rock from erosion.

The SLSJ region offers favourable conditions for the development of regional and local hydraulic connections (Chesnaux et al., 2012). The regional bedrock is covered by the fractured Precambrian Shield, Ordovician limestones and shales, and by generally more permeable unconsolidated deposits, which include fluvio-glacial sediments, till (glacial drifts), marine clays, and deltaic and shore deposits (Figure 4-2).

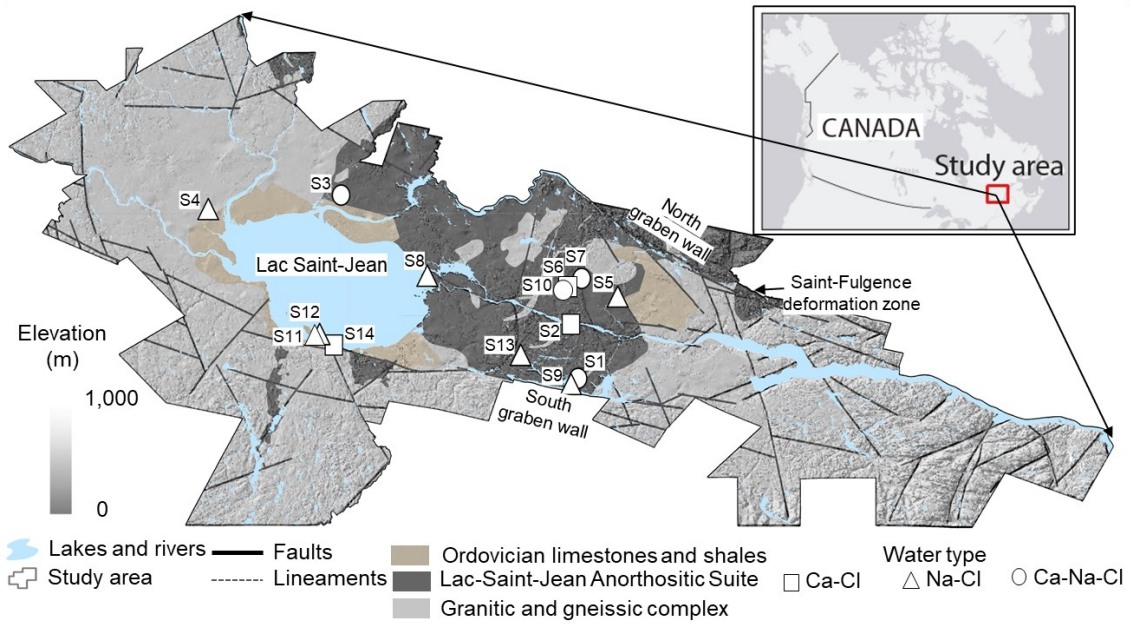

Figure 4-1: Simplified geology of the SLSJ region illustrating the main fractured rocks, faults and lineaments, rivers and lakes, and graben topography. Locations of 14 brackish groundwater samples and their water type are also shown. Geological and structural layers obtained from SIGEOM 2025.

Previous studies in the SLSJ region have also indicated that paleo-hydrogeological controls, acting through connected flow paths between the fractured bedrock and the overlying unconsolidated deposits, govern groundwater salinity and its long-term evolution. Roy et al. (2011) highlighted the impact of the post-glacial context (marine incursion and differential isostatic rebound) on groundwater quality, suggesting that pockets of saline water could be trapped in the clays left by the Laflamme Sea. The regional hydrogeochemical characterization carried out through the PACES program (Quebec Groundwater Knowledge Acquisition Program) from 2009 to 2013 has also improved the knowledge of groundwater quality in the SLSJ region (Rouleau et al., 2013). The published results of multivariate statistical analyses conducted on an extensive hydrogeochemical database from residential wells highlighted two mechanisms that mainly control the salinity of groundwater and its evolution: (1) water–rock interactions, and (2) water–marine clay interactions (Walter et al., 2017; Walter et al., 2019). More recently, a conceptual model was proposed integrating these two processes, suggesting that the observed salinity results from interaction between freshwater and marine clays from the Laflamme Sea, and from intensive interaction (long term) between freshwater and Canadian Shield rocks and/or Ordovician limestones (Walter et al. (2023). Using isotopic evidence ($\delta^{18}O$, $\delta^{2}H$, and $^{87}Sr/^{86}Sr$) and numerical modelling, Ngombe et al. (2025) suggested that

some brackish groundwater from regional fractured aquifers has experienced intensive interaction over hundreds of millions of years. Based on a numerical modelling approach, it has also been shown that the Saguenay Graben faults are preferential pathways for hydraulically connecting deep structures (> 5,000 m) to the surface (Ngombe et al., 2025).

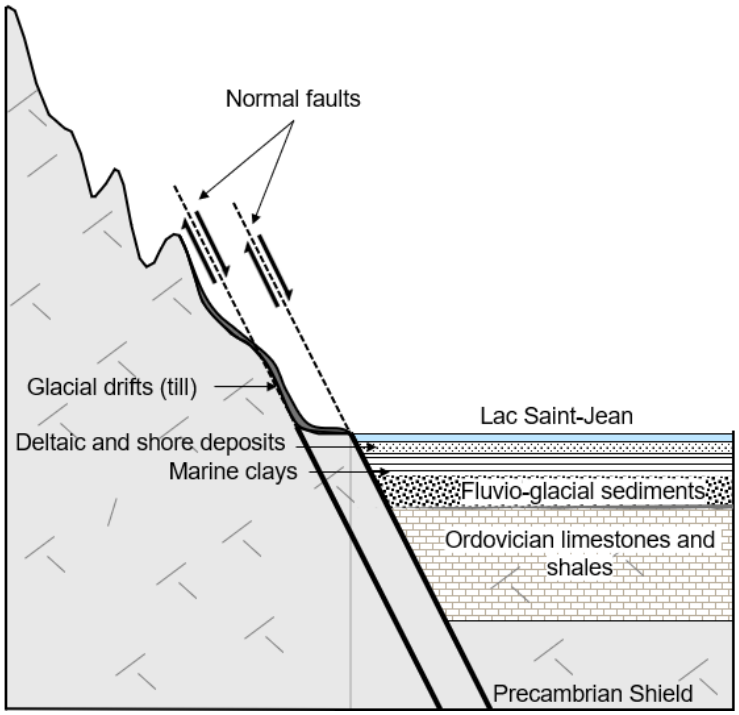

Figure 4-2: Conceptual cross-section of principal hydrogeological contexts encountered in the study area.

4.6. Methodology

4.6.1. Sampling methods

A sampling campaign of brackish water in the area was carried out in 2023. The sampling sites were selected based on their salinity (> 1 g/L) according to the classification of Kharaka et Hanor (2003), and the geology of the aquifer (Precambrian Shield and Ordovician limestones). A total of 14 brackish groundwater samples were taken from wells. Of these samples, 13 were taken from residential wells (< 100 m deep) and one, named S4 (Figure 4-1), from a well drilled as part of the PACES-SLSJ project (105 m deep) (Rouleau et al., 2013). ^{14}C activity was measured on the five saltiest samples collected as part of this study. Through this selection, we assumed that the oldest waters are the highest in salinity, according to the literature (Warr et al., 2022; Boumaiza et al., 2024).

Otherwise, samples of water analyzed for noble gases were collected in 2021 (9 samples) and 2023 (3 samples).

Prior to sample collection, we purged each well until the in situ parameters of temperature, pH, conductivity, and dissolved oxygen stabilized, according to the PACES protocol (Tremblay et al., 2021). In this study, two sampling methods were employed for all chemical parameters, depending on the accessibility of the well or the presence of a pump in the well. If no direct access to a residential well was possible, a garden hose Y-adapter was used to connect the flow cell to the house outlet. Another Y-shaped adapter was placed at the outlet of the pump to facilitate the distribution of water into the flow cell for in-situ measurements of physico-chemical parameters and into sample containers. Sampling was conducted directly at the wellhead using the low-flow sampling method to minimize disturbance to the aquifer and ensure an accurate representation of in-situ water chemistry.

Noble gases were collected in 14 cm^3 refrigeration-type annealed K-type copper tubes of 3/8" diameter, sealed at both ends with stainless steel clamps. The copper tubes were connected directly to the nearest faucet at the wellhead using reinforced high-pressure clear PVC tubing. To prevent air contamination, the other end of the PVC tubing was submerged in a water-filled bucket. Water was allowed to flow through the system for several minutes to purge the line before the clamps were closed, sealing the sample inside the copper tube. Where direct access to the well was possible, we used our own passive sampling pump. This bailer-type sampler (Solinst, Model 429 Point-Source Bailer) enables discrete water sampling at selected depths. In this case, the sampling depth depended on the depth of water where salinity was highest in the well. During the 2023 campaign, 2/3 of the noble gas isotope samples were collected using this passive sampling pump, following the same procedure as described above, with water flowing through the copper tube before sealing with stainless-steel clamps.

4.6.2. Analytical methods

Ion chemistry of water, groundwater isotopes and noble gas analyses were carried out in several laboratories, following different sampling and analysis protocols.

Major, minor and trace chemical analyses were carried out by the ALS Laboratory Group Ltd. in Waterloo, ON, Canada, sampled in HDPE bottles. For total metal analyses, samples were filtered in the field using a 0.45 µm filter before collection in 60 mL HDPE bottles pre-acidified with 1% v/v nitric acid (HNO_3) provided by the same laboratory.

$^{87}Sr/^{86}Sr$, $\delta^{37}Cl$, $\delta^{81}Br$, and ^{14}C were analyzed at the Environmental Isotope Laboratory (University of Waterloo). $\delta^{11}B$ and $\delta^{7}Li$ were analyzed at ALS-Scandinavia AB, Luleå, Sweden while noble gas isotopes were analyzed at the Rare Gas Laboratory in Montreal (GRAM) of the Geotop Centre, Université du Québec à Montréal (UQAM).

Samples for $^{87}Sr/^{86}Sr$ analysis were collected in 250 mL HDPE bottles and analyzed using a Thermo-Finnegan Triton thermal ionization mass spectrometer (TIMS). The reference material NIST-SRM-987 was used to calibrate the strontium isotopic results, for standard normalization and to correct for Rb interference with an average of $^{87}Sr/^{86}Sr$ = 0.710245 ± 0.000014 ($2\sigma\bar{x}$, n = 14). For $\delta^{37}Cl$ and $\delta^{81}Br$ analyses, samples were collected in 1 L HDPE bottles and analyzed using gas chromatography coupled with a continuous-flow isotope ratio mass spectrometer (GC-CF-IRMS). A sample precision of ± 0.1 % for $\delta^{37}Cl$ and $\delta^{81}Br$ aqueous analyses was calculated using the standard deviation (n = 14). For ^{14}C aqueous analysis, samples were filtered at 45 µm and collected in 1 L HDPE bottles. Samples were refrigerated after sampling to avoid contamination and microbial activity. The ^{14}C activity and ages were renormalized to -25 ‰ using the provided $\delta^{13}C$-DIC values. ^{14}C was analyzed using accelerator mass spectrometry (AMS). $\delta^{11}B$ and $\delta^{7}Li$ were analyzed using an ICP-SFMS (MC-ICP-SFMS) Neptune Plus multi-collector with samples collected in 1 L HDPE bottles. Boron measurements were calibrated using the NIST-SRM 951 reference standard, with a standard deviation of ± 0.64 ‰ (n = 14) to ensure accuracy of the results. $\delta^{7}Li$ was calibrated using the LSVEC NIST 8545 RM reference standard, with a standard deviation of ± 0.64 ‰ calculated from two independent consecutive measurements of ± 0.85 %.

For measuring abundances and isotopic ratios of noble gases He, Ne, and Ar, the copper tubes were flushed under a vacuum in a headspace, and the extracted gas was trapped in a stainless steel 12.5 cc finger closed with a Swagelok below valve. The finger was transferred on a stainless-

steel automatic purification line where the reactive gases were removed using two pure Ti getters (15 min at 600˚C and 10 min at ambient temperature) and a V-Fe nonevaporable getter ST-707 from SAES® (15 min at 125˚C and 10 min at ambient temperature). After the removal of all reactive gases, the gas mixture was trapped into an Advanced Research System (ARS®) cryogenic head DE-204 containing activated charcoal at 12K. Helium and neon were sequentially released at 40K (He), 90K (Ne) and 220K (Ar), analyzed on a Noble Gas Mass Spectrometer (NGMS) multicollection Helix-MC Plus system from Thermo®. All noble gas isotopes were measured on an axial Faraday cup except for ^{3}He, which was measured on an axial CDD (compact discrete dynode) copper-beryllium ion-counting electron multiplier. Samples were analyzed against an air standard with average errors on concentrations (calculated on a 2-month variation of the standard) of 2% for ^{4}He and 4% for ^{20}Ne and ^{36}Ar.

4.7. Results

4.7.1. Physico-chemical parameters and water types

The dataset comprises 14 samples (designated S1 to S14) collected within the study area from fractured rock aquifers (Figure 4-1). Samples S1, S2, S3, S5, S6, S7, S8, S9, S10, and S13 were collected in crystalline basement rocks, and samples S4, S11, S12 and S14 were collected in an Ordovician limestone-dominated geological context. Sample S14 is located near Lac-Saint-Jean and a few hundred meters from the contact between the Precambrian Shield (granitic and gneissic complex) and Ordovician limestones (Figure 4-1).

All physico-chemical parameters are presented in the Appendix (Tableau 8-4). Water temperatures during sampling varied from 7.3 to 14.4°C and the oxidation-reduction potential was between 130 and 321 mV, generally indicating weakly oxidizing conditions. The pH, generally neutral to alkaline, ranges between 6.6 (S3) and 9.6 (S4), with most samples between 7.0 and 8.5.

Total dissolved solids (TDS) show a significant variability, varying from 0.99 g/L (S8) to 29.6 g/L (S14). Water type was determined according to the meq/L concentrations for major cations and anions (Ca^{2+}, Na^{+}, K^{+}, Mg^{2+}, Cl^{-}, HCO_3^{-}, SO_4^{2-}) (Cloutier et al., 2004). The chemical facies of the samples were categorized into three main groups: Ca-Cl, Na-Cl and Ca-Na-Cl (Figure 4-1). For

samples collected in the LSJAS, the Ca-Cl and Ca-Na-Cl types predominate (e.g. S1, S2, S3, S6, S7, S10), and the Ordovician limestone samples mainly showed Na-Cl type waters (S4, S11, S12) except for S14 (Ca-Cl type).

4.7.2. Major, minor and trace elements

The complete dataset (physicochemical parameters, major, minor and trace elements, isotopes and noble gases) is provided in the supplementary material (Tableau 8-4). In this subsection of results, data are presented as a ratio of major, minor and/or trace ions in solution in the sampled groundwater. All ratios of chemical elements are presented in Tableau 8-5.

The combination of Ca/Sr, Ca/Mg, B/Br, Li/Br and Rb/Sr ratios characteristic of water-rock interaction (Connolly et al., 1990; Banks et Frengstad, 2006; Ngombe et al., 2024) highlights four distinct signatures among the samples collected in this study (Figure 4-3). Samples S11 and S12 (collected in Ordovician limestones) are characterized by a low Ca/Sr ratio with a median of 9.15, a moderate Ca/Mg ratio of about 1.58, and high Li/Br and B/Br ratios (> 0.01). Samples collected in the LSJAS and sample S14 are characterized by a moderate Ca/Sr ratio (between 16 and 38) and a high Ca/Mg ratio (> 3.5). Also, all LSJAS samples and S14 have low B/Br (< 0.1), Li/Br (< 0.01) and Rb/Sr (< 0.001) ratios. S4 is characterized by low Ca/Mg (0.04) and high Ca/Sr (70.68) and Rb/Sr (0.16) ratios. Li/Br (Figure 4-3) and B/Cl ratios of S4 are similar to those of seawater (Table S2). S9 is characterized by high Ca/Sr (250), Ca/Mg (10.9), Li/Br (0.02) and Rb/Sr (0.008) ratios and low Sr^{2+} (0.6 mg/L), and Br^{-} (0.5 mg/L) concentrations.

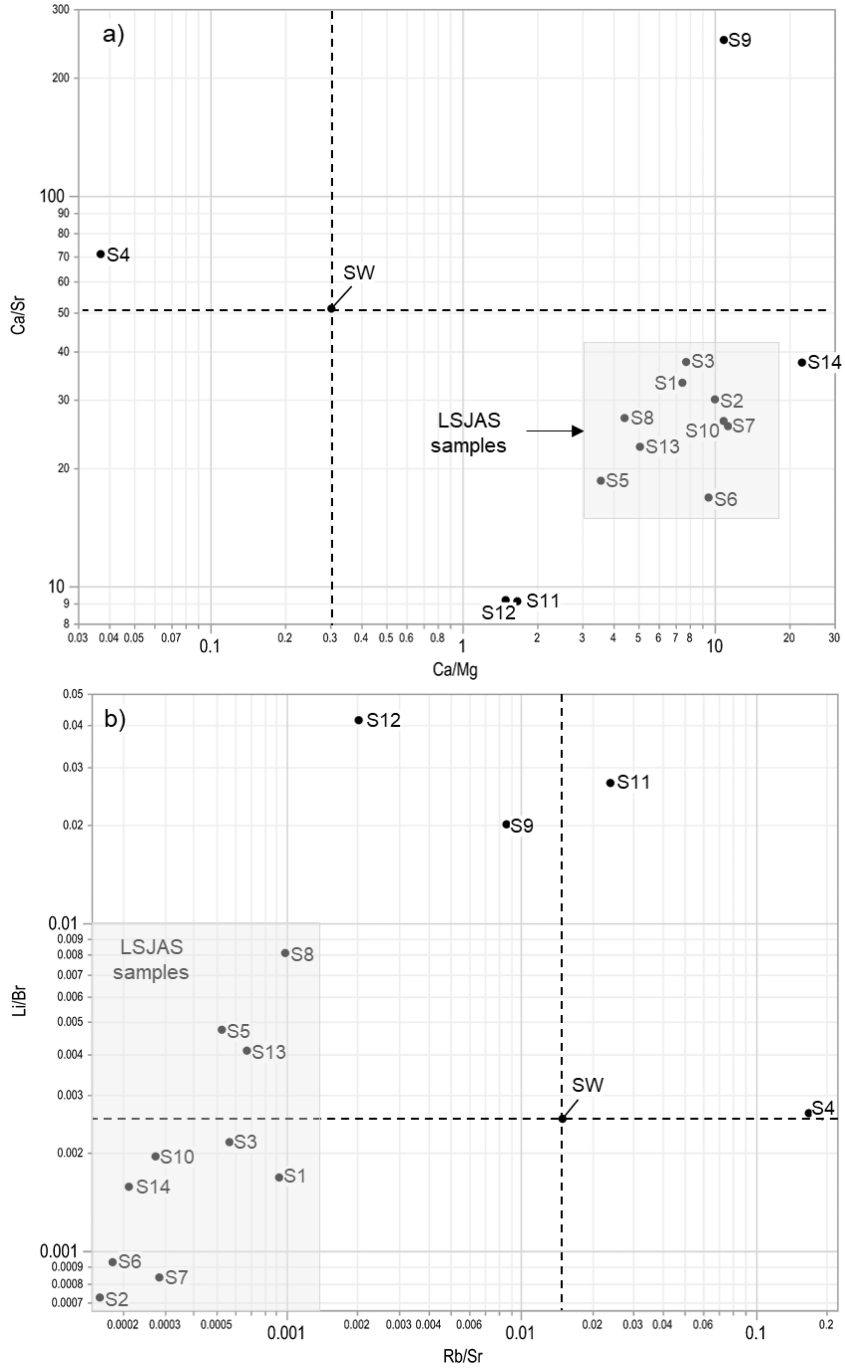

Figure 4-3: a) log-log plot of Ca/Sr vs. Ca/Mg ratios (from concentrations in mg/L) for all samples. b) log-log plot of Li/Br vs. Rb/Sr ratios (from concentrations in mg/L) for all samples. SW and the dotted black lines represent seawater (Goldberg et al., 1971).

4.7.3. Isotopic composition

4.7.3.1. Strontium isotopic composition

$^{87}Sr/^{86}Sr$ ratios vary from 0.70709 (S2) to 0.71126 (S4). Samples collected in Ordovician limestones (S4, S11, S12, S14) show values generally higher (median of 0.70902) than samples from

the LSJAS (median of 0.70777). In Figure 4-4, a positive correlation is seen between the isotopic ratio $^{87}Sr/^{86}Sr$ and ionic ratio Rb/Sr, except for sample S14, which does not show the same trend. While S4 presents the highest $^{87}Sr/^{86}Sr$ and Rb/Sr ratios, sample S2 has the lowest. Although S9 and S14 have similar $^{87}Sr/^{86}Sr$ ratios to Cambrian-Ordovician brines from Ontario and Michigan (Figure 4-4), the Rb/Sr ratio in S9 is 40 times higher than in S14. The samples with the highest $^{87}Sr/^{86}Sr$ ratio (S4 and S9) also have the lowest Sr^{2+} concentrations relative to Ca^{2+}. S11 and S12 collected in Ordovician limestone rocks have the same $^{87}Sr/^{86}Sr$ ratios, similar to typical values for the local Ordovician sea (Gao et Land, 1991; Qing et al., 1998).

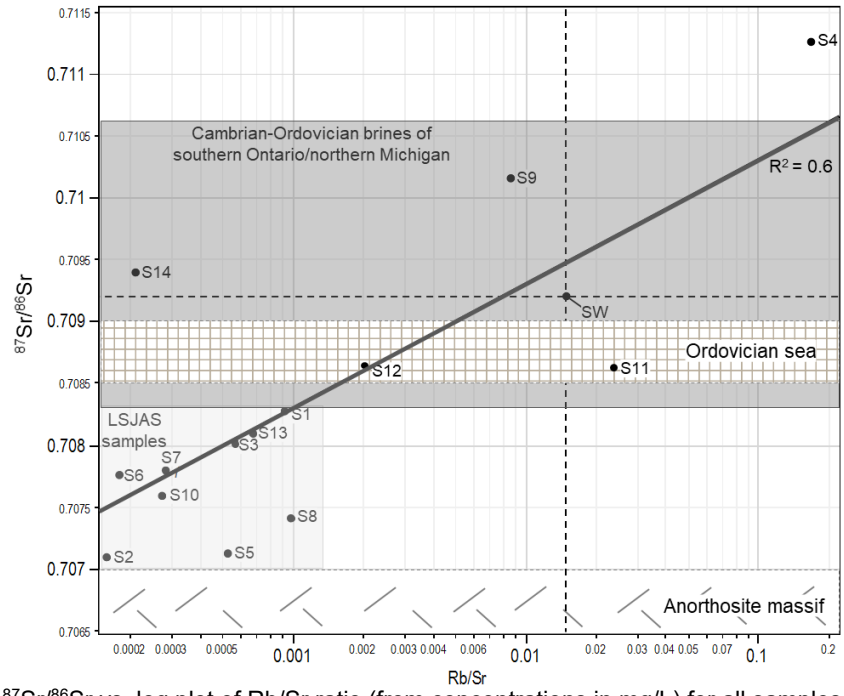

Figure 4-4: $^{87}Sr/^{86}Sr$ vs. log plot of Rb/Sr ratio (from concentrations in mg/L) for all samples. SW and the dotted black lines represent seawater (Goldberg et al., 1971). The solid black line represents the linear regression highlighting the positive correlation calculated with all samples. The dashed area represents the typical range of the Ordovician sea $^{87}Sr/^{86}Sr$ ratios (Gao et Land, 1991; Qing et al., 1998). Typical strontium isotope ratios of the anorthosite massif range from 0.7025 to 0.7070 (Taylor et al., 1984). Strontium isotope ratios of southern Ontario/northern Michigan brines range from 0.7083 to 0.7106 (Hobbs et al., 2011).

4.7.3.2. Boron and lithium isotopic composition

$\delta^{11}B$ showed values ranging from 1.96‰ (S9) to 42.03‰ (S12). All LSJAS samples have the same range as deep PSB samples, except for S9 (Figure 4-5a). S9 is similar to the composition of dilute surface water from Yellowknife Bay (Bottomley et Clark, 2004), indicating the presence of recently infiltrated groundwater. Samples S11 and S12, which have the highest $\delta^{11}B$ values, also

show the lowest Br/B ratios due to their B^{3+} enrichment compared to the other samples (Table S1). S14 presents the highest $\delta^{11}B$ value but is depleted in B^{3+} (Figure 4-5a).

The $\delta^{7}Li$ variations range from 23.51‰ (S9) to 47.9‰ (S8). Figure 4-5b highlights a positive linear regression of samples from the LSJAS comparing $\delta^{7}Li$ and Li/Br ratios (except S7 and S9), indicating a control of Li^{+} input on $\delta^{7}Li$ and Br^{-} variations. According to the geological context, S11 and S12 samples follow the same trend (samples with high-Li-$\delta^{7}Li$ and low-Br, and samples with low-Li-$\delta^{7}Li$ and high-Br).

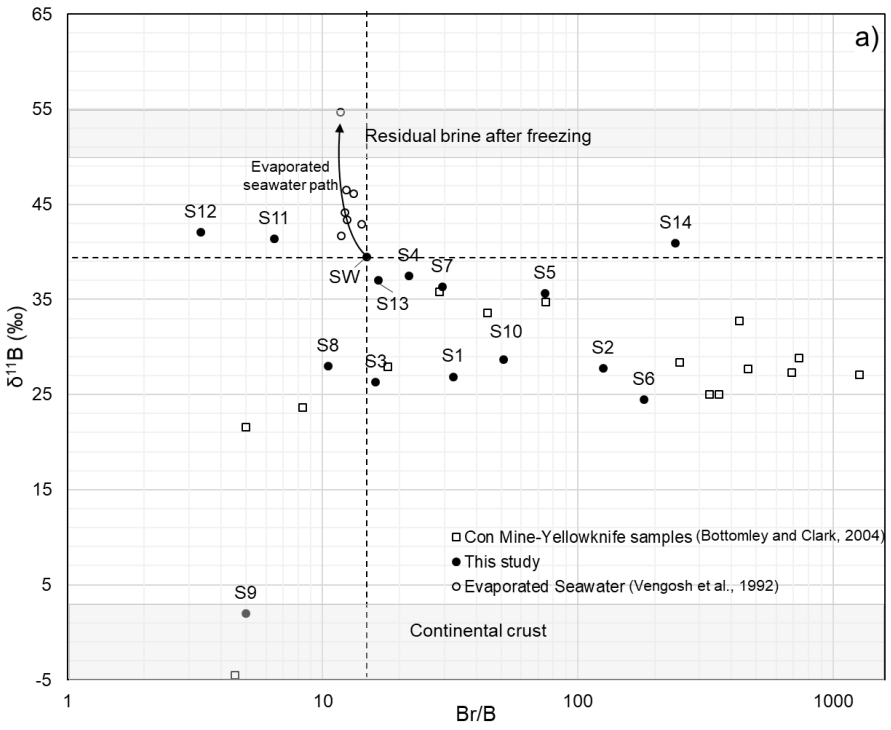

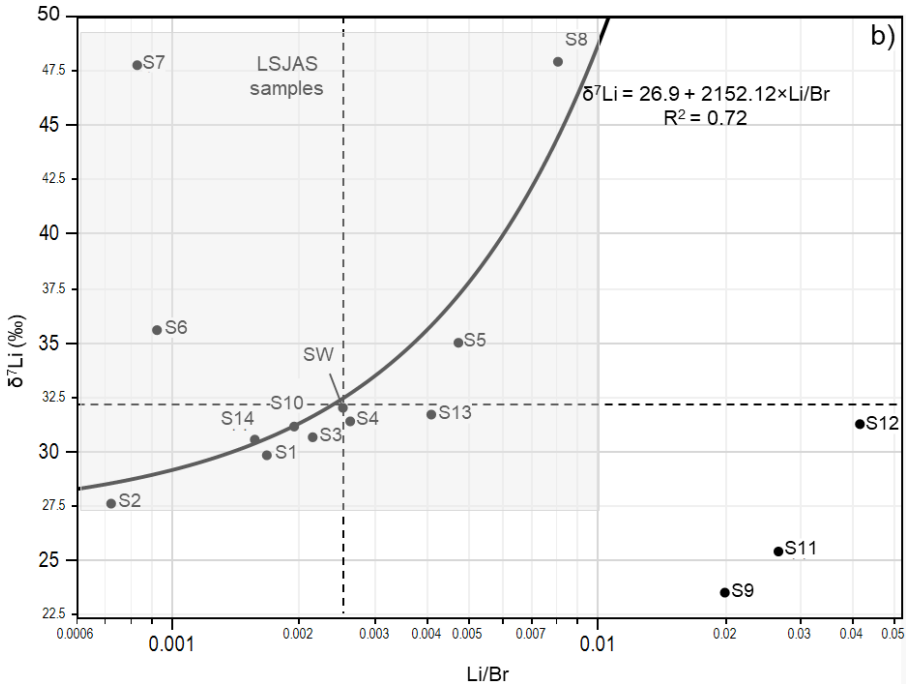

Figure 4-5: a) $\delta^{11}B$ vs. log (Br/B) ratios (from concentrations in mg/L) for all samples. Con Mine Yellowknife samples are described as deep Precambrian Shield Brine, the lowest value is described as surface water from Yellowknife Bay (Bottomley et Clark, 2004). Evaporated seawater data come from the study of Vengosh et al. (1992). Mean $\delta^{11}B$ of the continental crust is -3 ± 5‰ (Spivack et Edmond, 1987). The range for residual brine after freezing was obtained from the study of Casanova et al. (2005). b) $\delta^{7}Li$ vs. log (Li/Br) ratios (from concentrations in mg/L) for all samples. SW and the dotted black lines represent seawater (Goldberg et al., 1971). The solid black line represents the linear regression, highlighting the positive correlation of samples from the Lac Saint-Jean anorthositic suite (except S7 and S9).

4.7.3.3. Halogen isotopic composition

The isotopic variations of $\delta^{37}Cl$ and $\delta^{81}Br$ range from -0.42‰ (S14) to 0.41‰ (S12) and 0.59‰ (S5) to 1.80‰ (S12), respectively. Figure 4-6a compiles the chlorine and bromine isotope data from this study, with PSB identified elsewhere in Canada (Stotler et al., 2010). $\delta^{37}Cl$ data from this study show a similar range to that of deep PSB. In contrast, $\delta^{81}Br$ values are generally higher than deep PSB. While $\delta^{37}Cl$ does not show a clear trend with B/Br ratios, $\delta^{81}Br$ shows a positive correlation with the increase in $\delta^{81}Br$ and B/Br ratios. Samples S11 and S12 have both the highest $\delta^{81}Br$ values and the highest B/Br ratio (Figure 4-6b). LSJAS samples and S14 show an increase in $\delta^{81}Br$, an increase in the B/Br ratio, and a decrease in TDS (Figure 4-6b). In sample S9, $\delta^{81}Br$ was not measured due to its low Br^- concentration (Table S1), while its $\delta^{37}Cl$ value is typical of most shallow groundwaters reported in the literature (Frape et al., 2003; Shouakar-Stash et al., 2007).

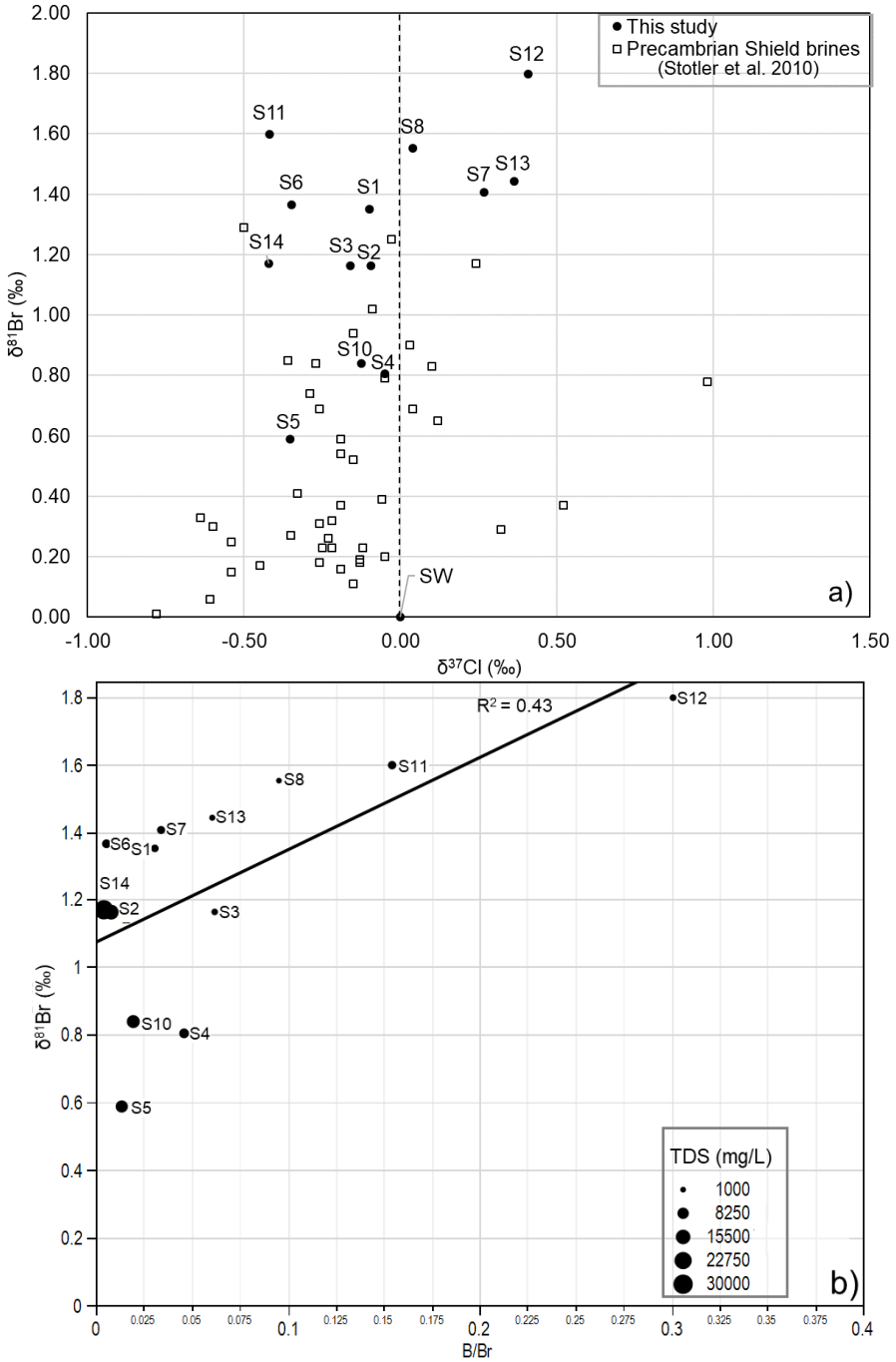

Figure 4-6: a) $\delta^{37}Cl$ (Standard Mean Ocean Chloride) vs. $\delta^{81}Br$ (Standard Mean Ocean Bromide). Precambrian Shield brine data reported for comparison come from the study of Stotler et al. (2010). SW represents seawater (Goldberg et al., 1971). The dotted black lines represent seawater. b) $\delta^{81}Br$ (Standard Mean Ocean Bromide) vs. B/Br ratios (from concentrations in mg/L) for all samples. The solid black line represents the linear regression highlighting the positive correlation of samples.

4.7.3.4. ^{14}C analyses

^{14}C dating is complicated by the multitude of processes affecting dissolved carbon in groundwater, particularly the dissolution of carbonates. Figure 4-7a shows a progressive decrease in

^{14}C as $\delta^{13}C$-DIC increases, which is consistent with the concept that the dissolution of 'dead' carbonates dilutes radiocarbon. However, S5, slightly above the carbonate dissolution line, indicates that its ^{14}C activity is higher than expected for a simple soil/carbonate mixture, which suggests that it has probably received an additional input of modern carbon (recent recharge water). ^{14}C analyses reveal uncorrected activities ranging from 4.2 pmC (S5) to 70.64 pmC (S14), which gives uncorrected ages ranging from about 2,800 BP (S5) to 25,500 BP (S14). Although the oldest sample is the most concentrated, we note that there is no direct correlation between salinity and the age of the groundwater samples. The saltiest samples, S2, S10, and S14, have low ^{14}C and HCO_3 concentrations, while S5 has the highest ^{14}C value and low HCO_3, and S4 has an intermediate ^{14}C value and is rich in HCO_3 (Table S3).

4.7.4. Noble gases

Results for noble gases are presented in the Appendix (Tableau 8-7). The indices "a and b" associated with the samples represent the samples that have been duplicated, with 'a indicating the first result and 'b' indicating its duplicate sample. The ^4He content, which generally increases with the residence time of groundwater, varies significantly within the study area (1.09×10^{-7} cm^3STP/g_{H2O} for S9 to 1.70×10^{-1} cm^3STP/g_{H2O} for S14-a). The first value is closer to that expected for groundwater in recharge zones (Air-Saturated Water (ASW) composition with ^4He = 4-5 $\times 10^{-8}$ cm^3STP/g_{H2O}). The latter concentration, among the highest ever recorded in Quebec aquifers and similar to those found in the Bécancour area by Pinti et al. (2011), suggests that some water may have remained at significant depths for hundreds of millions of years, accumulating substantial amounts of radiogenic crustal ^4He. Figure 4-7b illustrates a positive correlation between increasing ^4He concentrations and TDS, except for samples S8 and S13, which deviate from the overall trend. The $^3He/^4He$ ratios (R), normalized to that of the atmosphere ($R_a = 1.384 \times 10^{-6}$; Clarke et al. (1976)) or R/R_a, range from nearly an atmospheric value of 0.981 for sample S9 to 0.115 for sample S4. Samples with the larger amounts of radiogenic ^4He do not show typical crustal R/Ra values of 0.02-0.05, as expected by nucleogenic production of ^3He from ^6Li and radiogenic production of ^4He from U and Th decay (Ballentine et Burnard, 2002). The groundwater is slightly enriched in ^3He, indicating the presence of terrigenic helium, likely magmatic helium as observed in other regions of the province (Méjean et al.,

2020). The $^{20}Ne/^{22}Ne$ and $^{21}Ne/^{22}Ne$ ratios range from values close to the atmosphere (9.80 and 0.0290, respectively) or are slightly mass-fractionated to values of 11.12 and 0.0309 for sample S4, clearly indicating excesses of nucleogenic neon produced in the crust (Ballentine et Burnard, 2002). The $^{40}Ar/^{36}Ar$ and $^{38}Ar/^{36}Ar$ ratios also range from atmospheric values (295.5 and 0.1880, respectively) or are slightly mass fractionated to high $^{40}Ar/^{36}Ar$ ratios for sample S14 of 341.7 to 356.1, clearly indicating the presence of radiogenic $^{40}Ar^*$ produced in the crust from electron capture of ^{40}K.

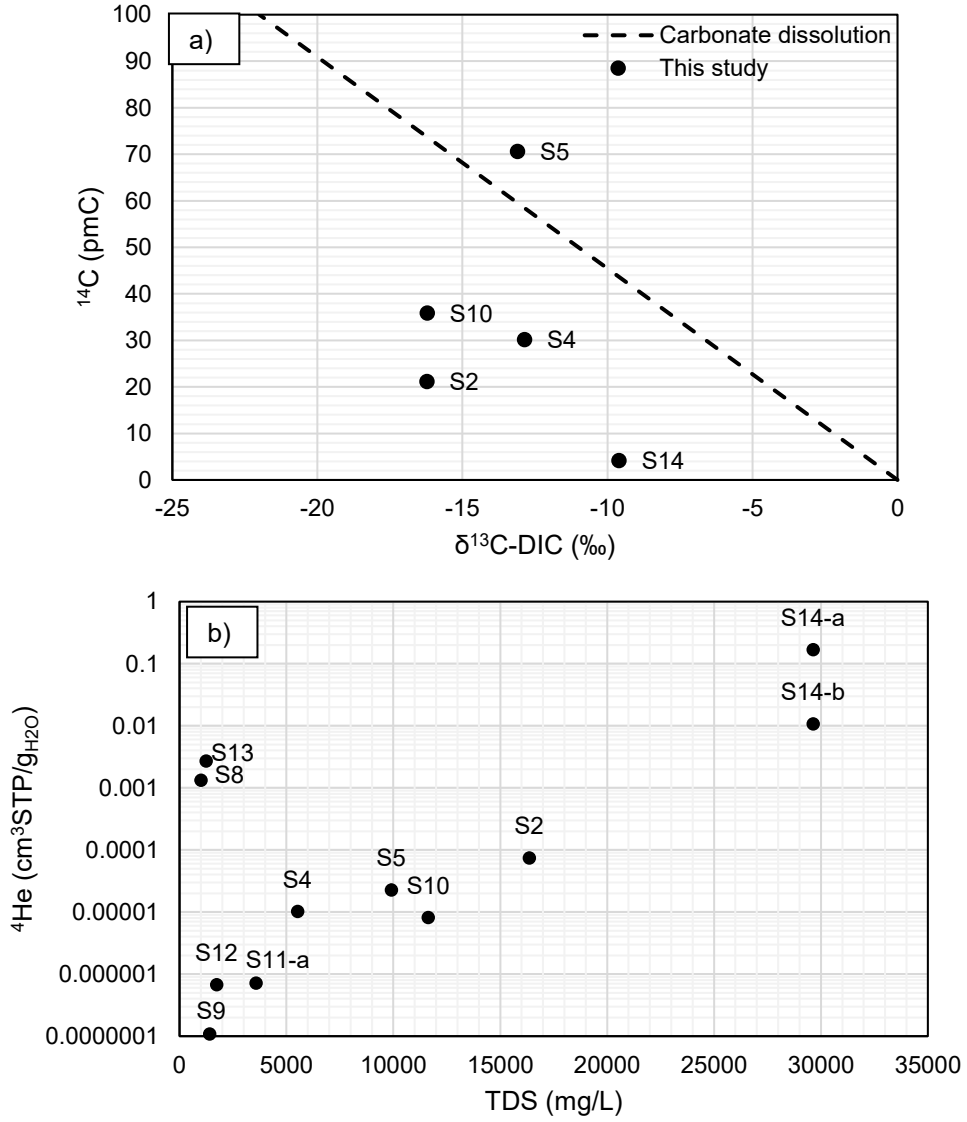

Figure 4-7: a) ^{14}C vs. $\delta^{13}C$-DIC. Dashed line represents carbonate dissolution, typical values for recharge water (^{14}C= 100 pmC, $\delta^{13}C$ = -23‰) and mineral values (^{14}C =0 pmC, $\delta^{13}C$=0‰) (Lefebvre et al., 2015). b) log-log plot of ^4He vs. TDS (Total Dissolved Solids). S14-a and S14-b are duplicate samples.

The results provide a solid basis for discussing the geochemical imprint of different spatio-temporal processes (intrusion of Paleozoic and Holocene seawater, infiltration of Wisconsinian glacial meltwater, and brine upwelling from the Precambrian Shield) within a complex geological environment (graben, multiple crystalline fractured rock formations, sedimentary and unconsolidated deposits, with a regional aquitard).

4.8. Discussion

4.8.1. Holocene marine water

4.8.1.1. Geochemical indicators of marine origin

Salinity proxies such as B/Cl and Li/Br ratios similar to seawater (B/Cl ≈ 0.24 × 10^{-3}, Li/Br ≈ 2.54 × 10^{-3}), suggest a marine origin. The Mg^{2+} enrichment compared to Ca^{2+} (Figure 4-3a) typical of marine environments (Folk et Land, 1975), supports this hypothesis. The $\delta^{37}Cl$, $\delta^{11}B$, and $\delta^{7}Li$ signatures similar to the marine standard ($\delta^{37}Cl$ ≈ 0‰, $\delta^{11}B$ ≈ 39.5 ‰, $\delta^{7}Li$ ≈ 31.2 ‰), clearly indicate that the Cl^- comes mainly from seawater and has not undergone significant fractionation.

4.8.1.2. Water clay interaction

Interaction between groundwater and marine clays has been proposed to explain the presence of brackish groundwater with chemical signatures similar to seawater in the study region (Walter et al., 2017). A radiocarbon age of 9,613 yrs BP corresponds to the post-glacial marine event of the Laflamme Sea during the Holocene, which left behind saltwater-saturated clays (Roy et al., 2011). $\delta^{81}Br$ and Br/Cl values higher than in seawater indicate a post-infiltration Br^- enrichment (Bagheri et al., 2014). In some areas of the SLSJ region, mineralogical analyses performed on deep marine deposits showed that microcline and illite, known to have high $^{87}Sr/^{86}Sr$ and Rb/Sr ratios (Vengosh et al., 2002), represent 41% and 21% of the argillaceous fraction of clay, respectively (Bouchard et al., 1983). At alkaline pH, B^{3+} predominantly exists as $B(OH)_4^-$, which adsorbs strongly onto neutral clay sites (Ring et al., 2025), favoring a B^{3+} depletion in groundwater.

Of all the samples in the study, S4 is the only one to present characteristics of marine water from the Holocene period, partly modified by interactions with the marine clays in the area, and similar to Champlain Sea water identified in other regions of Canada (e.g., Montcoudiol et al. (2015)). S4

was sampled in Ordovician limestone located in the lowlands of the study area (Figure 4-1), where ~32 m-thick Laflamme Sea marine clays overlie the bedrock (Rouleau et al., 2013), highlighting a clay-bedrock hydraulic connection.

4.8.2. Paleozoic marine brine

4.8.2.1. Geochemical indicators of Ordovician marine origin

The strontium isotope values of samples in contact with Ordovician limestones are typical of the Ordovician sea (Figure 4-4). Carbonates, such as those found in SLSJ limestones, also precipitate from seawater, and their $^{87}Sr/^{86}Sr$ ratio corresponds to that of strontium present in the water at the time of mineral precipitation (Veizer, 1989). In a closed or partially closed diagenetic system, where the fluid/rock ratio is low, the pore water remains close to the initial equilibrium with the carbonates (Dellinger et al., 2020). A δ^7Li value close to carbonates supports water-carbonate exchange processes (Jiang et al., 2022).

During the Ordovician, the seas were mainly “calcite seas” because calcite was the main carbonate mineral precipitated (Edwards et al., 2015), reflected by the low Ca/Sr ratio for some samples (Figure 4-3a). Dolomite ($CaMg(CO_3)_2$) is formed during the advanced stages of diagenesis, in water environments rich in Mg^{2+} (Stanienda-Pilecki, 2023). The Ca/Mg molar ratio of about 1:1, along with favourable diagenesis conditions in the Ordovician limestones, supports the hypothesis of dolomite formation and is clearly associated with the formation of sedimentary rocks, where calcite and dolomite dominate.

4.8.2.2. Evaporation of paleo-seawater

Some high $\delta^{11}B$, $\delta^{81}Br$, $\delta^{37}Cl$, Br/Cl, Li/Br values and low Br/B ratios are similar to those found in brines resulting from evaporation of paleo-seawater (Carpenter et al., 1974; Vengosh, 2003; Shouakar-Stash et al., 2007; Ngombe et al., 2024). When seawater is evaporated, particularly beyond halite saturation, the ionic and isotopic ratios of boron increase gradually with increasing degree of evaporation (Vengosh et al., 1992; Xiao et al., 2013). The enrichment of B^{3+} and $\delta^{11}B$ with respect to seawater (Figure 4-5a), suggests that B^{3+} and $\delta^{11}B$ have been modified by evaporation, consistent with the tropical climate condition during the Ordovician. Rayleigh evaporation of Cambrian-

Ordovician seas left residual brine depleted in ^{37}Cl and enriched in ^{81}Br (Kaufmann et al., 1993; Eggenkamp et al., 2019), supporting the evaporation hypothesis.

The chemical and isotopic evidence presented in this section indicates that the salinity of samples S11 and S12 originates from Paleozoic marine brines (Ordovician seawater) modified by evaporation and trapped in the limestones of the region over a long period of time, consistent with several studies of brines from large sedimentary basins (Rittenhouse, 1967; Hanor, 1994; Kharaka et Hanor, 2003). However, the higher value observed for $\delta^{7}Li$ and $\delta^{37}Cl$ in sample S12 in comparison to S11 suggests a contribution from another local source.

4.8.3. Precambrian Shield brines (PSBs)

4.8.3.1. Geochemical indicators of non-marine brine

$\delta^{37}Cl$ values from LSJAS samples all show modified marine signatures, which suggests that the origin of these brines is not directly related to recent seawater intrusion (Stotler et al., 2010). The similarity of $\delta^{37}Cl$ ranges between LSJAS samples and PSBs (Figure 4-6a) suggests a common source of salinity. $\delta^{81}Br$ is fractionated by diffusion, then the high values of LSJAS samples relative to seawater indicate enrichment of ^{81}Br by diffusion over long periods in low-permeability deep environments (Eggenkamp et Coleman, 2009). $\delta^{81}Br$ values in this study are mainly higher than those observed in PSBs (Figure 4-6a), suggesting an additional contribution from a heavy isotope-rich source or modification from a post-depositional process. In general, $^{87}Sr/^{86}Sr$ ratios of anorthosite massifs are relatively low (Taylor et al., 1984). In the SLSJ region, the Lac-Saint-Jean leuconorite had strontium isotope ratios ranging from 0.7029 to 0.7033 (Emslie et al., 1993), while ratios in the Lac-à-Paul rock massif in the northern part of the LSJAS ranged from 0.7046 to 0.7062 (Wavrant et al., 2017). The low $^{87}Sr/^{86}Sr$ and Rb/Sr ratios of LSJAS samples thus indicate a prolonged interaction with mantle rocks, such as anorthosites (which cover ~25% of the study region), and support an older non-marine origin. Moreover, the low Li/Br ratio (< 0.01), comparable to that of PSBs (Ngombe et al., 2024), together with a high Ca/Mg ratio, suggests a limited marine influence (Gimeno et al., 2023) and indicates that interactions with Precambrian Shield rocks primarily control salinity in the LSJAS

samples. This geochemical fingerprint of groundwater (low Rb/Sr, low Li/Br, and high Ca/Mg ratios) constitutes a useful proxy for long-term interactions with Proterozoic shield rocks.

Figure 4-8 shows a typical “Craig’s diagram” where the R/R_a values are plotted against the $^4He/^{20}Ne$ ratio (Torgersen et Jenkins, 1982). This plot enables the identification of the sources of helium and, indirectly, those of the fluids carrying helium in solution (e.g., Pinti et al. (2022)). The data clearly show that the fluids are a result of mixing between relatively recent meteoric water, represented by sample S9 which has a near-atmospheric R/R_a of 0.981 and ASW with a ^4He content of 1.09×10^{-7} $ccSTP/g_{H2O}$, and samples enriched in crustal radiogenic ^4He, representing PSBs. For comparison, we reported the PSB identified in the Bécancour gas field in the St. Lawrence Lowlands by Pinti et al. (2011), which shows a substantial enrichment in crustal ^4He. The dashed hyperbolas in Figure 4-8 represent the mixing lines. It is worth noting that the PSB endmembers contain between 1 and 5% of mantle-derived helium. These enrichments of mantle helium were also observed in Bécancour by Pinti et al. (2011) and other areas in southern Quebec by Méjean et al. (2020) and along the eastern margin of the North American plate (Torgersen et al., 1995).

The presence of mantle helium should not be surprising in sampled groundwater, being located in the SLSJ region which is bordered by deeply rooted normal faults, formed by the opening of the North Atlantic during the Mesozoic Era and recently reactivated by post-glacial isostatic rebound, leaving it seismogenetically active (e.g., Lamontagne et Brouillette (2022)). The presence of mantle helium on the eastern passive margin of the plate has been debated (e.g., Torgersen et al. (1995)) but its source may have been resolved. Indeed, Tyne et al. (2025) have recently shown the presence of mantle helium with little radiogenic argon in groundwater from the central plains of the US, and interpreted it as resulting from a crustal helium flux integrating orphan helium degassing from the sub-continental lithospheric mantle (SCLM). Deeper sources of helium in continents may not result exclusively from production within the continental crust but can also originate from helium released from the SCLM, which actively participates in Earth's degassing (Pinti, 2025). The passive ^4He degassing from the SCLM through continental crust well explains the high ^4He value with low TDS observed in samples S8 and S13 (Figure 4-7b).

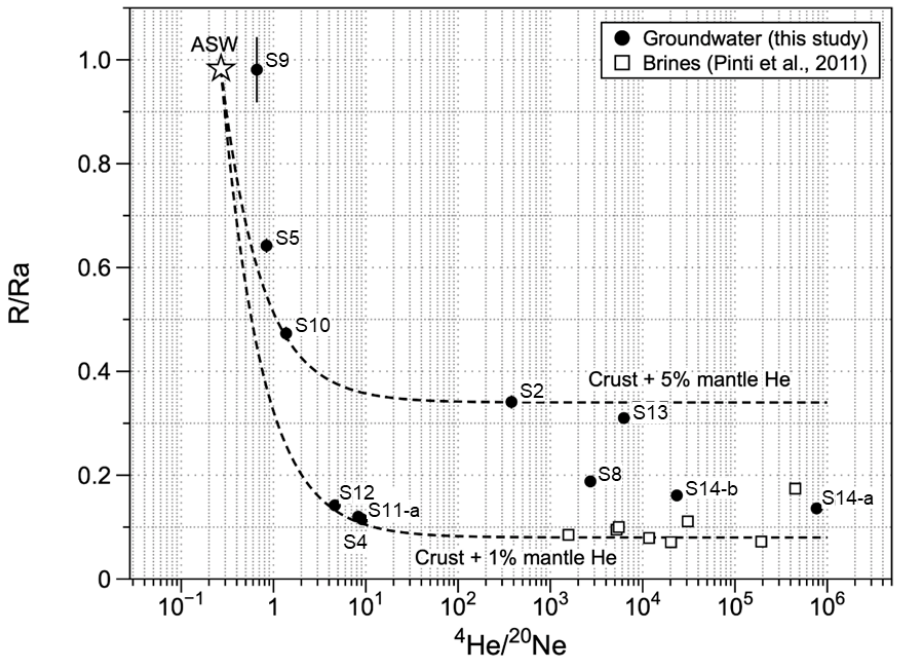

Figure 4-8: The $^3He/^4He$ ratio expressed as R/Ra vs. the $^4He/^{20}Ne$ ratio of SLSJ sampled groundwater. ASW : Air Saturated Water. The two dashed lines represent mixing between an endmember representing modern meteoric water and a fossil groundwater containing a mixture of 1-5% of mantle helium and 95-99% of crustal helium. Brines with similar chemistry and those of SLSJ and found in Bécancour, southern Quebec, are also reported for comparison (data from Pinti et al. (2011)).

The presence of deep PSB is also confirmed by the radiogenic values of $^{87}Sr/^{86}Sr$ ratios, which are higher than the Ordovician seawater but similar to those measured in Bécancour brines (Pinti et al., 2011) and in PSBs from Ontario/Michigan (Hobbs et al., 2011). Furthermore, deep PSB is identified by the very low Rb/Sr ratios similar to radiogenic PSB (McNutt et al., 1990), and by the presence of radiogenic $^{40}Ar^*$ in the helium-richest sample S14. Indeed, shallow groundwater does not contain radiogenic $^{40}Ar^*$ because this latter is retained in K-bearing minerals such as mica or feldspars (e.g., Ballentine et al. (1994)). The minimum closure temperatures for Ar range from 230˚C (for feldspars) to 300˚C for biotite (Snee, 2002). Its presence in the sampled waters indicates that fluids circulate sufficiently deep in the SLSJ to accumulate radiogenic argon leaking from K-bearing minerals. Assuming a geothermal gradient in the area between 24 and 31˚C/km (e.g., Liu et al. (2018); Oviedo et al. (2025)) the presence of radiogenic $^{40}Ar^*$ would suggest that these brines circulated or interacted with fluids located 7.5 to 12.5 km below the surface.

Based on the similarities of the sampled brines in the SLSJ region with the chemistry, isotopic signatures (R/R_a, $^{87}Sr/^{86}Sr$) and significantly high amounts of radiogenic crustal ^4He of brines found

in deep mines of western Canada (e.g., Bottomley et al. (1984); Holland et al. (2013); Warr et al. (2018)) and in Bécancour (Pinti et al., 2011), we suggest that the PSB circulating deep in the SLSJ region has an age of several hundred million years, possibly older than Ordovician. This interpretation supports the study of Ngombe et al. (2025), which was based on isotopic data and numerical modeling. The concept of ancient and deep shield brine upwelling can also be applied to other hydrogeological contexts with characteristics similar to those of the study area (including graben, fault, and shield rock flow systems).

4.8.3.2. Silicate hydrolysis and formation of hydrated clays

Reaction path calculations at low temperature (< 150°C) for silicate hydrolysis acting as a pH buffer demonstrated that the formation of hydrated clays (e.g., zeolite and chlorite) in low-permeability environments leads to a passive salinity increase in the residual fluids (Brady et al., 2019). At low-temperature, the presence of clay favors the preferential adsorption of light isotopes (^{6}Li, ^{10}B), leading to a decrease in Li^{+} and B^{3+} concentrations and an increase in $\delta^{7}Li$ and $\delta^{11}B$ in the residual fluids (Chan et al., 2002; Xiao et al., 2013). Consequently, the high values of $\delta^{7}Li$ and $\delta^{11}B$, the low Li^{+} and B^{3+} values and relatively neutral pH of the LSJAS samples suggest a predominant role of silicate hydrolysis and adsorption onto newly formed clay. Considering Br^{-} as an indicator of residence time and salinity (Bottomley et al., 1999), the low Li/Br and B/Br ratios for the saltiest samples support the hypothesis of passive salinization by silicate hydrolysis and formation of hydrated clays. This notably applies to samples S2, S10 and S14.

In contrast, the positive relationship between $\delta^{7}Li$ and Li/Br (Figure 4-5b) and $\delta^{81}Br$ and B/Br (Figure 4-6b) suggests the influence of more recent water, relatively depleted in Br^{-} but enriched in heavy isotopes. Although adsorption on clays explains $\delta^{11}B$ enrichment, the $\delta^{11}B$ values observed in LSJAS samples generally exceed those typically measured in water interacting with silicate rocks, which are generally -3 ± 5‰ (Spivack et Edmond, 1987), suggesting a contribution from an additional process. Bottomley et Clark (2004) state that Con Mine Yellowknife samples from the Canadian Shield are a mixture between recent meteoric water, deep PSB, and Laurentide glacial meltwater. The boron ionic and isotopic similarities between LSJAS samples and Con Mine Yellowknife samples

(Figure 4-5a) indicate that Laurentide glacial meltwater should be considered to explain the boron ionic and isotopic variability in this study.

4.8.4. Wisconsinian glacial meltwater

4.8.4.1. Geochemical indicators of Wisconsinian glacial water

Since radiocarbon has a half-life of 5,730 years, it has been used to date groundwater to at least 50,000 years ago (Suckow, 2014), covering the last glaciation period. As a result, chemical and isotopic signatures characteristic of PSBs (age > 100 Ma), ^{14}C apparent ages (about 8,225, 12,450 and 25,500 yrs BP) and low HCO_3^- concentrations, indicate a significant contribution from Wisconsinian glacial meltwater in the SLSJ region (Lemieux et al., 2008b; Roy et al., 2011; Warr et al., 2018; Boumaiza et al., 2024). On the contrary, unexpected high ^{14}C contents and very low HCO_3^- suggest contamination due to atmospheric CO_2 during sampling or analysis, as even minimal exposure in ancient groundwater can introduce modern radiocarbon, making these data unreliable for age determination (Aggarwal et al., 2014; Gimeno et al., 2023). This particularly applies to sample S5, as shown in Figure 4-7a.

Moreover, considering Br^- as an indicator of residence time and δ^7Li of weathering intensity (Millot et al., 2010; McDonough et al., 2021), Figure 4-5b shows a mixing trend in LSJAS samples linking high δ^7Li and low Br^- concentrations to more intense weathering, and conversely, low δ^7Li with high Br^- to longer residence times. During the Wisconsinian period, intense erosion at the base of the ice sheet generated fine sediments, enhancing water–rock interaction and silicate hydrolysis, as reflected in the clay-rich tills of the region (Roy et al., 2011; Rouleau et al., 2013). The δ^7Li values, particularly elevated in samples S7 and S8, are consistent with high weathering under cold subglacial conditions (Millot et al., 2010). This hypothesis explains the observed differences between samples with high-Li-δ^7Li and low-Br, and samples with low-Li-δ^7Li and high-Br (Figure 4-5b).

Observations reported in this section highlight the impact of the last glaciation on groundwater chemistry in hydrogeological systems, extending previous work (e.g. McIntosh et al. (2012), Person et al. (2007)) and confirmed with new data that illustrate these dynamics in the context studied. The identification of Wisconsinian glacial meltwater, which is slightly saline, i.e. ≈ 4 g/L of Cl^- (Douglas et

al., 2000), nuances the simplistic idea that salinity necessarily increases with the age of groundwater, and highlights the diversity of processes governing groundwater evolution.

4.8.4.2. Evidence of cryo-concentration

Figure 4-6b illustrates a positive correlation between $\delta^{81}Br$-enriched diluted waters and $\delta^{81}Br$-depleted concentrated brines, along with selective B^{3+} depletion across the salinity gradient. Since $\delta^{81}Br$ is fractionated by diffusion, the absence of a negative trend rules out simple mixing with meteoric water and implies an additional enriched source. During cryo-concentration, exclusion of ions from ice leads to their accumulation in residual fluids, with heavier isotopes such as ^{81}Br preferentially retained in the residual fluid. Combined with ^{14}C ages indicating Wisconsinian meltwater input, these patterns strongly support cryo-concentration during the last glaciation as the main process of $\delta^{81}Br$ enrichment in diluted samples in comparison to the most concentrated. Shouakar-Stash et al. (2007) proposed that a complex evolution involving water-rock interaction and permafrost formation explains the high observed values of the halogen signatures (reaching $\delta^{81}Br$ = 3.35‰) in some samples of Siberian platform brines.

Strong positive $\delta^{11}B$, different from the values expected for water salinity controlled by continental crust, i.e. < 3 ‰ (Spivack et Edmond, 1987), indicates post-origin isotopic modification. Boulton et al. (2001) demonstrated that deep permafrost can penetrate conductive crystalline rocks (> 480 m), a scenario applicable to the study area during the last glaciation. Under such conditions, freezing favors boron fractionation, enriching ^{11}B in residual water as ^{10}B is preferentially incorporated into ice, exceeding +50‰ in a periglacial climate (Casanova et al., 2005). Considering ^{14}C ages indicating Wisconsinian meltwater input, $\delta^{81}Br$ evidence of cryo-concentration, input of cryo-concentrated residual brine, and significantly modified $\delta^{11}B$ composition of LSJAS and S14 waters, explains the high $\delta^{11}B$ and low B^{3+} values of these samples (Figure 4-5a). Interestingly, sample S14, which dates from the last glacial maximum, exhibits the highest $\delta^{11}B$-value among the old non-marine samples.

4.8.5. Quaternary-Paleozoic-Precambrian mixing system

Figure 4-9 summarises the observations made in this study and schematically illustrates the spatial distribution of groundwater flow, showing infiltration and circulation pathways, as well as the hydrogeochemical signatures associated with different fluid types in the form of a conceptual stratigraphic section. The evolution of groundwater in the SLSJ region is the result of several paleo-hydrogeological episodes, which have contributed to the spatial and temporal heterogeneity of the regional aquifer. Brackish samples analyzed here reveal signature contributions of 1) Holocene marine water (Laflamme Sea) partly modified by interactions with marine clays; 2) Paleozoic marine brine (from Ordovician seawater), trapped in Ordovician limestone of the region over a long period of time; 3) Precambrian Shield brine driven by graben-controlled topography, which is responsible for the long residence time of the regional-scale flow system, migrating through the Graben faults toward the surface and containing 1-5% of mantle helium; 5) Wisconsinian glacial meltwater, which infiltrated the ground surface, creating new flow channels and modifying the chemical composition of Paleozoic marine brines and PSBs.

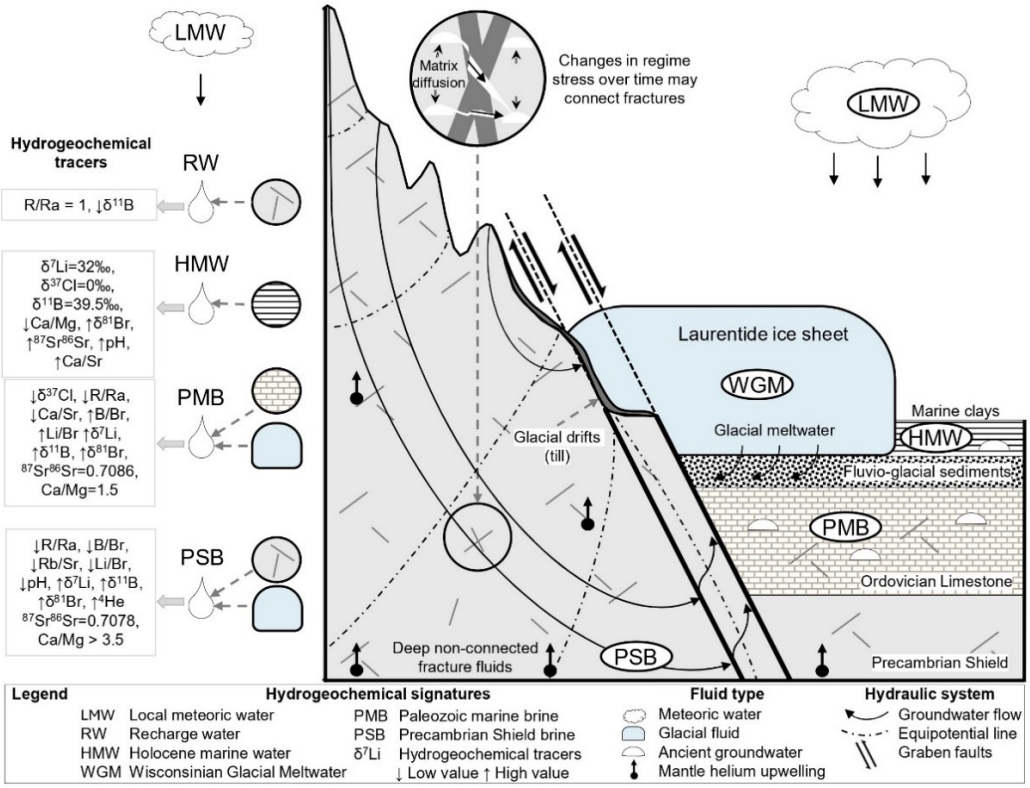

Figure 4-9: Conceptual hydrogeological model of Quaternary-Paleozoic-Precambrian mixing systems and the influence of regional geology and paleohydrogeological events during the salinization process. The surface morphology of the Precambrian Shield represents half of the graben of the SLSJ region.

4.9. Conclusion

This research hypothesised that past hydrogeological and hydrogeochemical processes shaped the chemistry and isotopic signatures of brackish groundwater collected from fractured rock in the SLSJ region. Preserved imprints of several paleo-hydrological episodes were identified, including: 1) Holocene marine water (Laflamme Sea) partly modified by interactions with marine clays, and characterized by B/Cl, Li/Br, $\delta^{11}B$, $\delta^{7}Li$, $\delta^{37}Cl$ values similar to recent seawater, low Ca/Mg ratios, high Ca/Sr, Rb/Sr ratios and high $^{87}Sr/^{86}Sr$ and pH with a corresponding age of 9,613 yrs BP; 2) Paleozoic marine brine (from Ordovician seawater) modified by evaporation and trapped in the regional limestones, and characterized by $^{87}Sr/^{86}Sr$ ratios typical of the Ordovician seawater, a molar Ca/Mg ratio of about 1:1, low Ca/Sr, low $\delta^{37}Cl$, high B/Br and Li/Br ratios, with $\delta^{11}B$ and $\delta^{81}Br$, and $\delta^{7}Li$ similar to carbonates; 3) Precambrian Shield brine hundreds of millions of years old and containing 1-5% of mantle helium, characterized by $^{87}Sr/^{86}Sr$ ratios similar to a Precambrian Shield rock mass, low $\delta^{11}B$ and $\delta^{7}Li$ isotopes, low B/Br, Li/Br, Rb/Sr and $^{40}Ar/^{36}Ar$ ratios, high Ca/Mg and $\delta^{81}Br$ isotope signatures, non-marine $\delta^{37}Cl$ and moderate Ca/Sr ratios (varying between 15 and 40) ; 5) Wisconsinian water dating from 8,225 to 25,504 BP, characterized by enrichment of $\delta^{81}Br$, $\delta^{11}B$, and $\delta^{7}Li$ observed in the Paleozoic marine and PSB signatures. The study confirms that some Precambrian Shield brines have circulated deep in the SLSJ region (7.5 to 12.5 km below the surface) and are flowing upwards through the deeply rooted normal faults bordering the graben.

The presence of a large amount of radiogenic ^{4}He, including a slight flavor of mantle helium, clearly supports the existence of connectivity between deep environments in the crystalline basement and surface aquifers, likely controlled by deeply rooted crustal faults that border the Saguenay graben, the main structural feature of the studied area. We reveal the existence of inter-aquifer hydraulic connections (through clay-bedrock) and highlight the major impact of the last glaciation on the chemistry of ancient groundwater, extending previous work, and providing new data. The latter nuances the notion that ancient water is necessarily the saltiest, helping to distinguish the composite nature of shallow brackish groundwater. These conclusions also place our work in a broader perspective, as an increasing number of studies in Quebec report evidence of paleo-glacial recharge waters (Boucher et al., 2015; Meyzonnat et al., 2023) and of the upward migration of very old and

deep fluids into surface aquifers, as documented here, or into sedimentary aquifers (Pinti et al., 2011). The study contributes fundamental insights into the paleo-hydrogeology of fractured continental shields, particularly the interactions between deep hydrogeochemical processes, past glacial climates, ancient marine intrusions, and groundwater dynamics in complex hydrogeological systems on a global scale. Moreover, this research enables regional decision-makers to refine salinization-risk mapping by integrating the hydrogeochemical signatures from this study with lithological, structural, and local water-use information.

The limited number of sites (14) relative to the large area of the territory and the limited depth of wells to the first ~100 m, leaving deeper flow systems poorly characterized, are the main limitations of this regional study. However, this study lays a solid foundation for understanding groundwater evolution and mixing, despite a long and complex hydrogeological history. Thus, the answers provided for understanding the current hydrogeological system pave the way for new questions such as the relative impact of the last glaciation (depth of permafrost, infiltration of meltwater), quantifying the relative contribution of diffusion and advection in the vertical distribution of isotopic proxies, assessing the kinetics of water-rock reactions controlling the mobility of halogens or the role of the continental crust in the transport of mantle gases.

4.10. References

Abi, A., Walter, J., Saeidi, A., et Chesnaux, R. 2022. A cluster-based multiparametric similarity test for the compartmentalization of crystalline rocks into structural domains. Quarterly Journal of Engineering Geology and Hydrogeology **55**(3): qjegh2021–2136.

Adombi, A.V.D.P., Chesnaux, R., Boucher, M.-A., Braun, M., et Lavoie, J. 2024. A causal physics-informed deep learning formulation for groundwater flow modeling and climate change effect analysis. Journal of Hydrology **637**: 131370.

Aggarwal, P.K., Araguas-Araguas, L., Choudhry, M., van Duren, M., et Froehlich, K. 2014. Lower groundwater 14C age by atmospheric CO2 uptake during sampling and analysis. Ground Water **52**(1): 20–24. doi: https://doi.org/10.1111/gwat.12110.

Allen, D.M., et Nott, A.H. 2021. How important are those fracture zones? Scale dependent characteristics revealed through field studies and an integrated hydrological model of a mountain headwater catchment. Frontiers in Water **3**: 767399.

Bagheri, R., Nadri, A., Raeisi, E., Eggenkamp, H., Kazemi, G., et Montaseri, A. 2014. Hydrochemical and isotopic (δ18O, δ2H, 87Sr/86Sr, δ37Cl and δ81Br) evidence for the origin of saline formation water in a gas reservoir. Chemical Geology **384**: 62–75.

Ballentine, C., Mazurek, M., et Gautschi, A. 1994. Thermal constraints on crustal rare gas release and migration: Evidence from Alpine fluid inclusions. Geochimica et Cosmochimica Acta **58**(20): 4333–4348.

Ballentine, C.J., et Burnard, P.G. 2002. Production, release and transport of noble gases in the continental crust. Reviews in Mineralogy and Geochemistry **47**(1): 481–538.

Banks, D., et Frengstad, B. 2006. Evolution of groundwater chemical composition by plagioclase hydrolysis in Norwegian anorthosites. Geochimica et Cosmochimica Acta **70**(6): 1337–1355.

Blomqvist, R. 1999. Hydrogeochemistry of deep groundwaters in the central part of the Fennoscandian Shield. Geological Survey of Finland. GTK-YST-101.

Bottomley, D., Ross, J., et Clarke, W. 1984. Helium and neon isotope geochemistry of some ground waters from the Canadian Precambrian Shield. Geochimica et Cosmochimica Acta **48**(10): 1973–1985.

Bottomley, D.J., et Clark, I.D. 2004. Potassium and boron co-depletion in Canadian Shield brines: evidence for diagenetic interactions between marine brines and basin sediments. Chemical Geology **203**(3-4): 225–236.

Bottomley, D.J., Katz, A., Chan, L., Starinsky, A., Douglas, M., Clark, I., et Raven, K. 1999. The origin and evolution of Canadian Shield brines: evaporation or freezing of seawater? New lithium isotope and geochemical evidence from the Slave craton. Chemical Geology **155**(3-4): 295–320.

Bouchard, R., Dion, D., et Tavenas, F. 1983. Origine de la préconsolidation des argiles du Saguenay, Québec. Canadian Geotechnical Journal **20**(2): 315–328.

Boucher, C., Pinti, D.L., Roy, M., Castro, M.C., Cloutier, V., Blanchette, D., Larocque, M., Hall, C.M., Wen, T., et Sano, Y. 2015. Groundwater age investigation of eskers in the Amos region, Quebec, Canada. Journal of Hydrology **524**: 1–14.

Boulton, G., Gustafson, G., Schelkes, K., Casanova, J., et Moren, L. 2001. Paleohydrogeology and geoforecasting for performance assessment in geosphere repositories for radioactive waste disposal (Pagepa). Directorate-General for Research, European Commission. Final report 1018-5593.

Boumaiza, L., Stotler, R., et Frape, S. 2024. A review of the major chemical and isotopic characteristics of groundwater in crystalline rocks of the Canadian Shield. Chemical Geology: 122366.

Brady, P., Lopez, C., et Sassani, D. 2019. Granite hydrolysis to form deep brines. Energies **12**(11): 2180.

Campbell, A.G., Cartwright, I., Webb, J.A., Cendon, D.I., et Currell, M.J. 2025. Using geochemical and geophysical data to characterise inter-aquifer connectivity and impacts on shallow aquifers and groundwater dependent ecosystems. Applied Geochemistry **178**: 106217.

Carpenter, A.B., Trout, M.L., et Pickett, E.E. 1974. Preliminary report on the origin and chemical evolution of lead-and zinc-rich oil field brines in central Mississippi. Economic Geology **69**(8): 1191–1206.

Casanova, J., Négrel, P., et Blomqvist, R. 2005. Boron isotope fractionation in groundwaters as an indicator of past permafrost conditions in the fractured crystalline bedrock of the fennoscandian shield. Water Research **39**(2-3): 362–370.

Chan, L.-H., Starinsky, A., et Katz, A. 2002. The behavior of lithium and its isotopes in oilfield brines: evidence from the Heletz-Kokhav field, Israel. Geochimica et Cosmochimica Acta **66**(4): 615–623.

Chandra, S., Auken, E., Maurya, P.K., Ahmed, S., et Verma, S.K. 2019. Large scale mapping of fractures and groundwater pathways in crystalline hardrock by AEM. Scientific Reports **9**(1): 398.

Chesnaux, R., Rafini, S., et Elliott, A.-P. 2012. A numerical investigation to illustrate the consequences of hydraulic connections between granular and fractured-rock aquifers. Hydrogeology Journal **20**(8): 1669–1680.

Clark, I.D., Douglas, M., Raven, K., et Bottomley, D. 2000. Recharge and preservation of Laurentide glacial melt water in the Canadian Shield. Groundwater **38**(5): 735–742.

Clarke, W.B., Jenkins, W., et Top, Z. 1976. Determination of tritium by mass spectrometric measurement of 3He. The International Journal of Applied Radiation and Isotopes **27**(9): 515–522.

Cloutier, V., Lefebvre, R., Savard, M., et Therrien, R. 2004. Groundwater origin and geochemical processes in the Basses-Laurentides sedimentary rock aquifer system, St. Lawrence Lowlands, Quebec, Canada. *Sous la direction de*. *Dans* Proceedings, 57th Canadian Geotechnical Conference and 5th Joint CGS/IAH Conference, pp. 18–25.

Connolly, C.A., Walter, L.M., Baadsgaard, H., et Longstaffe, F.J. 1990. Origin and evolution of formation waters, Alberta Basin, Western Canada Sedimentary Basin. II. Isotope systematics and water mixing. Applied Geochemistry **5**(4): 397–413.

Dellinger, M., Hardisty, D.S., Planavsky, N.J., Gill, B.C., Kalderon-Asael, B., Asael, D., Croissant, T., Swart, P.K., et West, A.J. 2020. The effects of diagenesis on lithium isotope ratios of shallow marine carbonates. American Journal of Science **320**(2): 150–184.

Desbiens, S., et Lespérance, P.J. 1989. Stratigraphy of the Ordovician of the Lac Saint-Jean and Chicoutimi outliers, Quebec. Canadian Journal of Earth Sciences **26**(6): 1185–1202.

Dessureault, R. 1975. Hydrogeologie du Lac Saint-Jean. Partie Nord-Est. Ministère des Richesses Naturelles du Québec. Rapport hydrogéologique No. HG7. pp. 1–90.

Douglas, M., Clark, I., Raven, K., et Bottomley, D. 2000. Groundwater mixing dynamics at a Canadian Shield mine. Journal of Hydrology **235**(1-2): 88–103.

Edwards, C.T., Saltzman, M.R., Leslie, S.A., Bergström, S.M., Sedlacek, A.R., Howard, A., Bauer, J.A., Sweet, W.C., et Young, S.A. 2015. Strontium isotope (87Sr/86Sr) stratigraphy of Ordovician bulk carbonate: Implications for preservation of primary seawater values. Bulletin **127**(9-10): 1275–1289.

Eggenkamp, H., et Coleman, M.L. 2009. The effect of aqueous diffusion on the fractionation of chlorine and bromine stable isotopes. Geochimica et Cosmochimica Acta **73**(12): 3539–3548.

Eggenkamp, H., Louvat, P., Agrinier, P., Bonifacie, M., Bekker, A., Krupenik, V., Griffioen, J., Horita, J., Brocks, J., et Bagheri, R. 2019. The bromine and chlorine isotope composition of primary halite deposits and their significance for the secular isotope composition of seawater. Geochimica et Cosmochimica Acta **264**: 13–29.

Folk, R.L., et Land, L.S. 1975. Mg/Ca ratio and salinity: two controls over crystallization of dolomite. AAPG Bulletin **59**(1): 60–68.

Frape, S., Blyth, A., Blomqvist, R., McNutt, R., et Gascoyne, M. 2003. Deep fluids in the continents: II. Crystalline rocks. Treatise on Geochemistry **5**: 605.

Frape, S., et Fritz, P. 1987. Geochemical trends for groundwaters from the Canadian Shield. Geological Association of Canada-Special Paper **33**: 19–38.

Frape, S., Fritz, P., et McNutt, R.t. 1984. Water-rock interaction and chemistry of groundwaters from the Canadian Shield. Geochimica et Cosmochimica Acta **48**(8): 1617–1627.

Galloway, D.L. 2010. The complex future of hydrogeology. Hydrogeology Journal **18**(4): 807–810.

Gao, G., et Land, L.S. 1991. Geochemistry of Cambro-Ordovician Arbuckle limestone, Oklahoma: Implications for diagenetic δ18O alteration and secular δ13C and 87Sr86Sr variation. Geochimica et Cosmochimica Acta **55**(10): 2911–2920.

Gimeno, M.J., Tullborg, E.-L., Nilsson, A.-C., Auqué, L.F., et Nilsson, L. 2023. Hydrogeochemical characterisation of the groundwater in the crystalline basement of Forsmark, the selected area for the geological nuclear repositories in Sweden. Journal of Hydrology **624**: 129818.

Goldberg, E., Broecker, W., Gross, M., et Turekian, K. 1971. Radioactivity in the marine environment. National Academy of Science, Washington, DC **137**.

Greene, S., Battye, N., Clark, I., Kotzer, T., et Bottomley, D. 2008. Canadian Shield brine from the Con Mine, Yellowknife, NT, Canada: Noble gas evidence for an evaporated Palaeozoic seawater origin mixed with glacial meltwater and Holocene recharge. Geochimica et Cosmochimica Acta **72**(16): 4008–4019.

Hanor, J.S. 1994. Origin of saline fluids in sedimentary basins. Geological Society, London, Special Publications **78**(1): 151–174.

Hébert, C., et Van Breemen, O. 2004. Mesoproterozoic basement of the Lac St. Jean Anorthosite Suite and younger Grenvillian intrusions in the Saguenay region, Québec: structural relationships and U-Pb geochronology. *Dans* Proterozoic tectonic evolution of the Grenville orogen in North America. *Sous la direction de* L.C. R. P. Tollo, J. M. McLelland & M. J. Bartholomew (Eds.). Geological Society of America. pp. 65–80.

Hobbs, M.Y., Frape, S.K., Shouakar-Stash, O., et Kennell, L.R. 2011. Regional Hydrogeochemistry – Southern Ontario. Nuclear Waste Management Organization. NWMO DGR-TR-2011-12. p. 156.

Holland, G., Sherwood-Lollar, B., Li, L., Lacrampe-Couloume, G., Slater, G., et Ballentine, C. 2013. Deep fracture fluids isolated in the crust since the Precambrian era. Nature **497**(7449): 357–360.

Jiang, W., Sheng, Y., Wang, G., Shi, Z., Liu, F., Zhang, J., et Chen, D. 2022. Cl, Br, B, Li, and noble gases isotopes to study the origin and evolution of deep groundwater in sedimentary basins: a review. Environmental Chemistry Letters: 1–32.

Kaufmann, R.S., Frape, S., McNutt, R., et Eastoe, C. 1993. Chlorine stable isotope distribution of Michigan Basin formation waters. Applied Geochemistry **8**(4): 403–407.

Kharaka, Y.K., et Hanor, J. 2003. Deep fluids in the continents: I. Sedimentary basins. Treatise on Geochemistry **5**: 605.

Laaksoharju, M., Skaarman, C., Smellie, J., et Nilsson, A. 1995. Groundwater sampling and chemical characterisation of the Laxemar deep borehole KLX02. Swedish Nuclear Fuel and Waste Management Co.

Lamontagne, M., et Brouillette, P. 2022. Faults and lineaments of the Quebec City, Charlevoix and Saguenay–Lac-St-Jean regions, Québec. Geological Survey of Canada. Open File 8826. p. 38.

Laurin, A., et Sharma, K. 1975. Mistassini, Péribonka, Saguenay rivers area: Grenville 1965–1967. Ministère des Richesses naturelles, Direction générale des Mines, Service de l'Exploration géologique. Rapport géologique No. 161. p. 89.

Lefebvre, R., Ballard, J.-M., Carrier, M.-A., Vigneault, H., Beaudry, C., Berthot, L., Légaré-Couture, G., Parent, M., Laurencelle, M., et Malet, X. 2015. Portrait des ressources en eau souterraine en Chaudière-Appalaches, Québec, Canada: Rapport final (version révisée).

Lemieux, J.M., Sudicky, E.A., Peltier, W.R., et Tarasov, L. 2008b. Simulating the impact of glaciations on continental groundwater flow systems: 1. Relevant processes and model formulation. Journal of Geophysical Research: Earth Surface **113**(F3).

Liu, H., Giroux, B., Harris, L.B., Quenette, S.M., et Mansour, J. 2018. Numerical analysis of the role of radiogenic basement on temperature distribution in the St. Lawrence Lowlands, Québec. Geothermal Energy **6**(1): 30.

McDonough, L.K., Meredith, K.T., Nikagolla, C., et Banati, R.B. 2021. The influence of water–rock interactions on household well water in an area of high prevalence chronic kidney disease of unknown aetiology (CKDu). NPJ Clean Water **4**(1): 2.

McIntosh, J., Schlegel, M., et Person, M. 2012. Glacial impacts on hydrologic processes in sedimentary basins: evidence from natural tracer studies. Geofluids **12**(1): 7–21.

McNutt, R.H., Frape, S.K., Fritz, P., Jones, M.G., et MacDonald, I.M. 1990. The 87Sr86Sr values of Canadian Shield brines and fracture minerals with applications to groundwater mixing, fracture history, and geochronology. Geochimica et Cosmochimica Acta **54**(1): 205–215.

Méjean, P., Pinti, D.L., Kagoshima, T., Roulleau, E., Demarets, L., Poirier, A., Takahata, N., Sano, Y., et Larocque, M. 2020. Mantle helium in Southern Quebec groundwater: A possible fossil record of the New England hotspot. Earth and Planetary Science Letters **545**: 116352.

Meyzonnat, G., Musy, S., Corcho-Alvarado, J., Barbecot, F., Pinti, D., Purtschert, R., Lauzon, J.-M., et McCormack, R. 2023. Age distribution of groundwater in fractured aquifers of the St. Lawrence Lowlands (Canada) determined by environmental tracers (3H/3He, 85Kr, SF6, CFC-12, 14C). Hydrogeology Journal **31**(8): 2139–2157.

Millot, R., Vigier, N., et Gaillardet, J. 2010. Behaviour of lithium and its isotopes during weathering in the Mackenzie Basin, Canada. Geochimica et Cosmochimica Acta **74**(14): 3897–3912.

Montcoudiol, N., Molson, J., Lemieux, J.-M., et Cloutier, V. 2015. A conceptual model for groundwater flow and geochemical evolution in the southern Outaouais Region, Québec, Canada. Applied Geochemistry **58**: 62–77.

Ngombe, O.G., Walter, J., Chesnaux, R., et Molson, J. 2024. Application of hierarchical cluster analysis and principal component analysis to identify compositional trends of brine in crystalline basements and sedimentary basins. Applied Geochemistry: 106030.

Ngombe, O.G.D., Walter, J., Molson, J., et Chesnaux, R. 2025. Numerical modeling and isotopic evidence of upwelling and mixing of deep, old groundwater with shallow fresh groundwater within the Grenville Province of the Canadian Shield. Hydrogeology Journal. doi: 10.1007/s10040-025-02914-2.

Oviedo, M.J., Raymond, J., Blessent, D., et Larmagnat, S. 2025. Numerical assessment of the geothermal resource potential of the Charlevoix meteorite impact crater, Canada. Geothermics **127**: 103243.

Person, M., McIntosh, J., Bense, V., et Remenda, V. 2007. Pleistocene hydrology of North America: The role of ice sheets in reorganizing groundwater flow systems. Reviews of Geophysics **45**(3).

Pinti, D.L. 2025. Earth's exhale: Geochemistry. Nature Geoscience: 1–2.

Pinti, D.L., Béland-Otis, C., Tremblay, A., Castro, M.C., Hall, C.M., Marcil, J.-S., Lavoie, J.-Y., et Lapointe, R. 2011. Fossil brines preserved in the St-Lawrence Lowlands, Québec, Canada as revealed by their chemistry and noble gas isotopes. Geochimica et Cosmochimica Acta **75**(15): 4228–4243.

Pinti, D.L., Larocque, M., Méjean, P., Saby, M., Hernández-Hernández, M.A., Gagné, S., Roulleau, E., Sano, Y., Castro, M.C., et Matsumoto, T. 2022. Regional-scale distribution of helium isotopes in aquifers: how informative are they as groundwater tracers and chronometers? Water **14**(12): 1940.

Qing, H., Barnes, C.R., Buhl, D., et Veizer, J. 1998. The strontium isotopic composition of Ordovician and Silurian brachiopods and conodonts: relationships to geological events and implications for coeval seawater. Geochimica et Cosmochimica Acta **62**(10): 1721–1733.

Ring, S.J., Henehan, M.J., Blukis, R., et von Blanckenburg, F. 2025. Adsorption pathways of boron on clay and their implications for boron cycling on land and in the ocean. Geochimica et Cosmochimica Acta **389**: 74–83.

Rittenhouse, G. 1967. Bromine in oil-field waters and its use in determining possibilities of origin of these waters. AAPG Bulletin **51**(12): 2430–2440.

Rouleau, A., Daigneault, R., Walter, J., Germaneau, D., Tremblay, M.L., et Lambert, M. 2013. Résultats du programme d'acquisition de connaissances sur les eaux souterraines de la région Saguenay-Lac-Saint-Jean (Results of the groundwater knowledge acquisition programme in the Saguenay-Lac-Saint-Jean region). Ministère du Développement durable, de l'Environnement et de la Lutte contre les changements climatiques (Ministry of Sustainable Development, Environment and the Fight Against Climate Change), MDDELCC p. 248.

Roy, D.W., Beaudoin, G., Leduc, É., Rouleau, A., Walter, J., Chesnaux, R., et Cousineau, P.A. 2011. Isostasie postglaciaire différentielle au Lac-Saint-Jean (Québec) et implications sur la qualité de l'eau souterraine. Geohydro 2011, Québec.

Saby, M., Larocque, M., Pinti, D.L., Barbecot, F., Sano, Y., et Castro, M.C. 2016. Linking groundwater quality to residence times and regional geology in the St. Lawrence Lowlands, southern Quebec, Canada. Applied geochemistry **65**: 1–13.

Shouakar-Stash, O., Alexeev, S., Frape, S., Alexeeva, L., et Drimmie, R. 2007. Geochemistry and stable isotopic signatures, including chlorine and bromine isotopes, of the deep groundwaters of the Siberian Platform, Russia. Applied Geochemistry **22**(3): 589–605.

Snee, L.W. 2002. Argon thermochronology of mineral deposits; a review of analytical methods, formulations, and selected applications. Geological Survey (U.S.). Bulletin No. 2194. p. 39.

Spivack, A., et Edmond, J. 1987. Boron isotope exchange between seawater and the oceanic crust. Geochimica et Cosmochimica Acta **51**(5): 1033–1043.

Stanienda-Pilecki, K.J. 2023. Crystals structures of carbonate phases with Mg in Triassic rocks, mineral formation and transitions. Scientific Reports **13**(1): 18759.

Stotler, R.L., Frape, S.K., et Shouakar-Stash, O. 2010. An isotopic survey of δ81Br and δ37Cl of dissolved halides in the Canadian and Fennoscandian Shields. Chemical Geology **274**(1-2): 38–55.

Suckow, A. 2014. The age of groundwater–Definitions, models and why we do not need this term. Applied Geochemistry **50**: 222–230.

Taylor, S., Campbell, I., McCulloch, M., et McLennan, S. 1984. A lower crustal origin for massif-type anorthosites. Nature **311**(5984): 372–374.

Torgersen, T., Drenkard, S., Stute, M., Schlosser, P., et Shapiro, A. 1995. Mantle helium in ground waters of eastern North America: Time and space constraints on sources. Geology **23**(8): 675–678.

Torgersen, T., et Jenkins, W. 1982. Helium isotopes in geothermal systems: Iceland, the geysers, raft river and steamboat springs. Geochimica et Cosmochimica Acta **46**(5): 739–748.

Tóth, J. 1978. Gravity-induced cross-formational flow of formation fluids, red earth region, Alberta, Canada: Analysis, patterns, and evolution. Water Resources Research **14**(5): 805–843.

Tremblay, G. 1971. Structures sédimentaires dans les dépôts meubles, Saguenay-Lac-Saint-Jean, Québec. Cahiers de Géographie du Québec **15**(36): 537–546.

Tremblay, R., Walter, J., Chesnaux, R., et Boumaiza, L. 2021. Investigating the potential role of geological context on groundwater quality: a case study of the Grenville and St. Lawrence Platform Geological Provinces in Quebec, Canada. Geosciences **11**(12): 503.

Tyne, R., Broadley, M., Bekaert, D., Barry, P., Warr, O., Langman, J., Musan, I., Jenkins, W., et Seltzer, A. 2025. Passive degassing of lithospheric volatiles recorded in shallow young groundwater. Nature Geoscience: 1–6.

Veizer, J. 1989. Strontium isotopes in seawater through time. Annual Review of Earth and Planetary Sciences, Vol. 17, p. 141 **17**: 141.

Vengosh, A. 2003. 9.09-Salinization and Saline Environments In: Editors-in-Chief: Heinrich D. Holland, Karl K. Turekian (Eds.), Treatise on Geochemistry. Pergamon, Oxford.

Vengosh, A., Gill, J., Lee Davisson, M., et Bryant Hudson, G. 2002. A multi-isotope (B, Sr, O, H, and C) and age dating (3H–3He and 14C) study of groundwater from Salinas Valley, California: Hydrochemistry, dynamics, and contamination processes. Water Resources Research **38**(1): 9–1–9–17.

Vengosh, A., Starinsky, A., Kolodny, Y., Chivas, A.R., et Raab, M. 1992. Boron isotope variations during fractional evaporation of sea water: New constraints on the marine vs. nonmarine debate. Geology **20**(9): 799–802.

Walter, J. 2010. Les eaux souterraines à salinité élevée autour du lac Saint-Jean, Québec: origines et incidences. Mémoire de maîtrise, Sciences de la Terre et de l'Atmosphèree, Université du Québec à Chicoutimi, Québec, Canada.

Walter, J., Chesnaux, R., Boumaiza, L., Brindha, K., et Regenspurg, S. 2023. Conceptual model for the chemical evolution of groundwater in a region of the Canadian Precambrian shield covered by soft Quaternary deposit of glacial and marine origin. Applied Geochemistry **150**: 105574.

Walter, J., Chesnaux, R., Cloutier, V., et Gaboury, D. 2017. The influence of water/rock− water/clay interactions and mixing in the salinization processes of groundwater. Journal of Hydrology: Regional Studies **13**: 168–188.

Walter, J., Chesnaux, R., Gaboury, D., et Cloutier, V. 2019. Subsampling of regional-scale database for improving multivariate analysis interpretation of groundwater chemical evolution and ion sources. Geosciences **9**(3): 139.

Walter, J., Rouleau, A., Chesnaux, R., Lambert, M., et Daigneault, R. 2018. Characterization of general and singular features of major aquifer systems in the Saguenay-Lac-Saint-Jean region. Canadian Water Resources Journal/Revue Canadienne des Ressources Hydriques **43**(2): 75–91.

Walter, J., Rouleau, A., Clark, I.D., et Guha, J. 2006. A first investigation of groundwater geochemistry in the crystalline bedrock around lake Saint-Jean, Québec. 59th Canadian Geotechnical Conference and 7th Joint CGS/IAH-CNC Groundwater Specialty Conference - Sea to Sky Geotechnique 2006, Fairmont Hotel, Vancouver, British Columbia, Canada, October 1–4, 2006, X-CD Technologies Incorporated, pp. 1553–1560.

Warr, O., B, S.L., Fellowes, J., Sutcliffe, C.N., McDermott, J.M., Holland, G., Mabry, J.C., et Ballentine, C.J. 2018. Tracing ancient hydrogeological fracture network age and compartmentalisation using noble gases. Geochimica et Cosmochimica Acta **222**: 340–362.

Warr, O., Ballentine, C., Onstott, T., Nisson, D., Kieft, T., Hillegonds, D., et Sherwood Lollar, B. 2022. 86Kr excess and other noble gases identify a billion-year-old radiogenically-enriched groundwater system. Nature Communications **13**(1): 3768.

Warr, O., Giunta, T., Onstott, T.C., Kieft, T.L., Harris, R.L., Nisson, D.M., et B, S.L. 2021. The role of low-temperature 18O exchange in the isotopic evolution of deep subsurface fluids. Chemical Geology **561**: 120027.

Wavrant, L.-M., Sappin, A.-A., Beland, C.M.J., Chartier-Montreuil, W., Fleury, F., Zhao, P., Beaudoin, G., Barnes, S.-J., Cheng, L., Chouteau, M., Constantin, M., Dare, S., Dupuis, C., Stevenson, R., et Williams-Jones. 2017. Projet terres rares au Québec. Ministère de l'Énergie et des Ressources Naturelles, Québec. No. MB 2017-17. p. 123.

Xiao, J., Xiao, Y.k., Jin, Z.d., He, M.y., et Liu, C.q. 2013. Boron isotope variations and its geochemical application in nature. Australian Journal of Earth Sciences **60**(4): 431–447.

Chapitre 5 : DISCUSSION ET PERSPECTIVES DE RECHERCHE

5.1. Introduction

Cette section vise tout d'abord à synthétiser les principales contributions de ce projet doctoral en établissant des liens entre les résultats issus des différents articles, afin de montrer comment ils apportent des éléments de réponse à la problématique de recherche. La présente section a aussi pour objectif de discuter des principaux résultats au regard de la littérature existante, des limites et de la portée de l'étude en faisant une analyse autocritique des conclusions du projet, et d'énoncer les perspectives de recherche du projet doctoral. La première partie se concentre sur la compréhension des écoulements profonds et le rôle des structures géologiques et de la topographie comme vecteurs hydrauliques des saumures profondes en contexte de graben. La deuxième partie met l'accent sur la compréhension de l'évolution géochimique des saumures continentales en fonction du contexte géologique (sédimentaire et cristallin) et de la paléohydrogéologie, discute des processus hydrogéochimiques impliqués et de la connectivité hydraulique entre les réservoirs profonds et les aquifères de subsurface. La troisième partie a permis de discuter des marqueurs géochimiques développés dans le cadre de ce projet de recherche.

5.2. Contribution 1 : Topographie et failles comme vecteurs hydrauliques des saumures continentales

5.2.1. Contrôle de la topographie sur l'écoulement

Dans le cadre de ce projet de recherche, les simulations numériques 2D de l'écoulement et de l'âge de l'eau souterraine ont été développées pour analyser la distribution spatiale des voies d'écoulement des eaux souterraines profondes et leur relation avec la subsurface. Le modèle, développé dans cette étude, couvre une section longitudinale de 56.3 km de long sur 5.4 km de profondeur. La structure hydrostratigraphique a été simplifiée en trois couches de socle rocheux, mettant en évidence les aspects régionaux de l'écoulement des eaux souterraines et de l'âge. La valeur moyenne calculée du taux de recharge du roc fracturé (environ 3 mm/an) à partir du modèle numérique d'écoulement est cohérent avec les valeurs calculées dans l'aquifère fracturé du seuil de Kenogami dans la région d'étude (Chesnaux, 2013).

Afin d'isoler les effets des conditions de surface et de mieux comprendre les mécanismes hydrodynamiques profonds en l'absence de structures complexes, une simulation de référence a été réalisée. Ce cas de base, considéré comme conservateur, n'a pas inclus de système de failles dans sa configuration. Le résultat de la simulation de l'écoulement en régime permanent démontre que les caractéristiques topographiques jouent un rôle significatif dans le contrôle des régimes d'écoulement, générant des systèmes locaux, intermédiaires et régionaux. Le rôle de la topographie sur l'écoulement et la hiérarchisation des cellules d'écoulement ont largement été documentés dans la littérature (Tóth, 1963; Dong et Gao, 2022). Toutefois, dans la région d'étude, la simulation sans failles met en évidence l'effet sur l'écoulement du fort contraste topographique entre les hautes terres et les basses terres induit par la topographie en graben de la région étudiée. À l'échelle locale, la simulation a montré que la zone de rupture de pente (interfaces hautes terres – basses terres) génère une zone de recharge locale à proximité de la marge aval du lac Brûlé (Figure 2-5), tandis que sa marge amont se comporte comme une zone de décharge intermédiaire. L'interface hautes terres - basses terres favorise également un gradient hydraulique élevé, et donc un écoulement rapide et un court temps de résidence, expliquant des points de résurgence observés sur des falaises près des murs nord et sud du graben par exemple (Rouleau et al., 2013). À plus grande échelle, cette observation met en lumière l'importance de la distance horizontale entre les zones de recharge et de décharge dans la remontée des eaux souterraines. En effet, la réduction de la distance horizontale entre les hautes terres et les basses terres (caractéristique des topographies en graben comme dans la région d'étude), favorise l'augmentation du gradient hydraulique, et donc de la vitesse et de l'intensité de la remontée des flux. Le chapitre 2 montre également que des charges hydrauliques suffisamment élevées sont maintenus à des profondeurs significatives, notamment sous les zones de basse altitude comme le Lac Saint-Jean, expliquant la remontée des eaux souterraines profondes. Ainsi, le Lac Saint-Jean a été identifié comme la zone de décharge régionale. Il est intéressant de noter que l'eau la plus salée (~30 g/L) identifiée à ce jour dans la région est localisée près du Lac Saint-Jean (~20 m de distance). À l'échelle régionale, ce cas de base met surtout en évidence la dépendance de l'écoulement aux gradients de charge hydraulique imposés à la surface, car la

simulation n’a pas inclus de puits de pompage, de flux imposés aux limites du modèle, ou d’effet de densité.

Bien que le modèle numérique d’écoulement fournisse un aperçu des mécanismes hydrodynamiques clés, la simplification du modèle conceptuel restreint la portée de ses conclusions. À la différence d’un écoulement dépendant principalement de la topographie, l’effet de densité élevée des saumures (non pris en compte dans cette étude) dû à leur concentration importante en TSD (~300 g/L), pourrait les maintenir immobile en profondeur (Neretnieks, 2024). Négliger la densité constitue une limite importante de l’étude. Comme le montre le Chapitre 4, la glaciation Wisconsinienne a modifié la chimie des eaux anciennes. Selon Lemieux et al. (2008a), la pression accrue de la glace et de l’eau de fonte augmente la charge hydraulique, allant jusqu’à 3 000 m, lesquelles sont maintenues jusqu’à une profondeur de 1 500 m. La persistance de ces charges élevées en profondeur après le retrait de la calotte glaciaire, alors que la charge en surface revient rapidement à des valeurs proches de l’équilibre, indique l’existence d’un gradient hydraulique ascendant favorable à la remontée d’eaux souterraines profondes et anciennes. Ainsi, ignorer la charge glaciaire, les surpressions transitoires et l’injection d’eaux de fonte peut biaiser fortement les âges simulés, réorganiser les trajectoires d’écoulement et modifier des signatures de long temps de résidence (gaz nobles, isotopes). En l'absence d'hétérogénéité structurale ou d'autres apports pourront favoriser la remontée des fluides profonds, le cas de base met en évidence le mécanisme hydrodynamique de fond qui régit les écoulements profonds en contexte de graben et la localisation des zones de résurgences (lacs et rivières).

5.2.2. Simulation de l’âge des eaux souterraines

Concernant l'âge des eaux souterraines, les simulations révèlent une augmentation progressive de l'âge avec la profondeur cohérente avec la littérature (Section 1.2.2.3). Les aquifères peu profonds sont caractérisés par des eaux jeunes (quelques jours à 100 ans). Les âges maximaux atteignent plus de 200 Ma le long des limites inférieures du modèle, avec un maximum de 338.4 Ma dans le cas de base. Ces échelles de temps sont cohérentes avec les observations faites dans les mines profondes dans le Bouclier Canadien (Bottomley et al., 1984; Holland et al., 2013; Warr et al., 2018). L'étude montre que sans structures de failles, la topographie régionale peut induire une

remontée des eaux anciennes, mais généralement limitée aux principales zones de décharge de surface et à des profondeurs supérieures à 400 – 500 m.

Toutefois, entre 1 et 3 km de profondeur dans le modèle numérique, les âges simulés (~1-25 Ma) restent 10 à 100 fois plus jeunes que ceux inférés des gaz rares dans la littérature (Holland et al., 2013; Warr et al., 2018). Cet écart indique des processus non représentés ou simplifiés. Le manque de connaissance des paramètres hydrauliques en profondeur pourrait conduire à une surestimation de la conductivité hydraulique en profondeur d'un ou deux ordres de grandeur et donc à une sous-estimation de l'âge simulé. Ceci a été confirmé par des tests de sensibilité. En diminuant la conductivité hydraulique d'un ordre de grandeur (K_{Px} = 4.3 × 10^{-12} m/s), l'âge simulé entre 1 et 3 km de profondeur a atteint entre 10 à 250 Ma. Par ailleurs, l'hypothèse d'une densité uniforme dans l'étude est aussi une limite importante, empêchant le modèle de reproduire les conditions observées en profondeur dans le Bouclier Canadien et entraînant une sous-estimation des âges simulés de l'eau souterraine profonde. Bien que nos paramètres de dispersivité soient cohérents avec des études menées dans des contextes géologiques similaires à la région d'étude (Montcoudiol et al., 2017; Janos et al., 2018), les incertitudes concernant ces paramètres peuvent également avoir comme effet numérique de rajeunir l'eau ancienne par le mélange avec l'eau plus jeune (Molson et Frind, 2012). Par exemple, en diminuant la dispersivité transversale (α_T^H et α_T^V), l'âge de l'eau en profondeur augmentait considérablement. Pour $\alpha_T^H = \alpha_T^V$ = 0.02 m (Molson et Frind, 2012), l'âge simulé en profondeur augmentait jusqu'à ~444 Ma, représentant un âge approximativement 100 Ma plus vieux que celui du cas de base. De plus, notre modèle numérique suppose un milieu poreux équivalent basé sur un réseau de fractures bien développé, ce qui peut rendre difficile la reproduction des âges des saumures profondes dérivées des gaz rares. Cette approche couramment utilisée pour la modélisation à l'échelle régionale met également en lumière deux courants de pensées concernant la circulation des fluides profonds. D'après l'étude de Warr et al. (2018) l'identification de fluides d'âges distincts provenant de réseaux de fractures compartimentés et hydrauliquement isolés les uns des autres suggère que ces fluides ne participent pas aux systèmes d'écoulement régionaux. Toutefois, un modèle à double porosité avec écoulement régional peut aussi expliquer les observations de Warr et al. (2018). Ce type de modèle distingue deux réservoirs interconnectés :

généralement les fractures (chemins rapides) et la matrice rocheuse (plus lente) (Hermans et al., 2023). Dans un cadre à grande échelle, cela permet de rendre compte des effets de séparation entre zones actives et zones confinées (Chung et al., 2017; Snowdon et al., 2021). Dans cette perspective, la Figure 2-5 met en évidence, à titre illustratif, des zones de stagnation en profondeur (~5 km), précisément entre 20 km et 30 km de distance horizontale ou encore à l'extrême droite du modèle numérique. Bien que ce résultat découle d'un modèle simplifié en milieu poreux équivalent, il suggère que des volumes d'eau peuvent demeurer faiblement renouvelés, voire quasi piégés, même dans le cadre d'un système d'écoulement régional continu (continuum hydraulique). Cette observation invite toutefois à replacer ces résultats dans une dynamique évolutive à long terme. Dans la région du SLSJ, l'exhumation post-orogénique du socle grenvillien, associée à l'érosion de plusieurs kilomètres de roches profondes aujourd'hui affleurantes (Rivers et al., 1989; Rouleau et al., 2013), a probablement entraîné une évolution des contraintes lithostatiques et des gradients hydrauliques profonds au cours du temps géologique. Il est ainsi plausible que des volumes d'eau anciennement situés à grande profondeur et faiblement renouvelés aient été progressivement exhumés et se retrouvent aujourd'hui à des profondeurs relatives plus faibles. Cette hypothèse soulève la question de la capacité des milieux cristallins à conserver des fluides très anciens malgré les réorganisations tectoniques et topographiques successives.

5.2.3. Failles du graben du Saguenay : chemins préférentiels de fluides profonds

Les signatures isotopiques (Chapitre 3 et Chapitre 4) de certaines eaux saumâtres collectées dans le roc fracturé peu profond à proximité de failles majeures de la région révèlent un temps de résidence pouvant atteindre plusieurs centaines de millions d'années, similaire aux âges simulés numériquement en profondeur dans cette étude (cas de base). On y mesure, en outre, une concentration en hélium parmi les plus élevées jamais enregistrées dans les aquifères du Québec (Section 4.7.4). Cette observation suggère qu'une partie de l'eau est demeurée à des profondeurs importantes pendant des centaines de millions d'années, accumulant des quantités substantielles d'hélium crustal radiogénique. De plus, les signatures hydrogéochimiques radiogéniques de $^{87}Sr/^{86}Sr$ et $^{40}Ar^*$ dans l'aquifère peu profond du SLSJ à proximité des failles du graben confirment clairement la présence en subsurface de saumures Précambriennes ayant circulé ou interagi avec des fluides

situés entre 7.5 et 12.5 km sous la surface. Ainsi, un test paramétrique a permis d'analyser numériquement les perturbations hydrauliques dans le système d'écoulement induites par les structures géologiques (failles) et d'évaluer leurs rôles comme chemins préférentiels pour la migration verticale des fluides profonds.

Concernant les failles du Graben du Saguenay, elles ont été inférées à partir de la morphologie du terrain bien que leurs déplacements ne soient pas directement observables en surface. Elles ont été modélisées comme des conduits ou des barrières hydrauliques dans divers scénarios numériques. Ces comportements hydrauliques des failles a été mis en évidence dans plusieurs études (Bense et Person, 2006; Lapperre et al., 2019). Les résultats des tests paramétriques montrent systématiquement que l'intégration de ces structures accentue la migration des eaux souterraines profondes vers la surface, en concentrant les flux le long de chemins préférentiels. Les failles créées des zones où la conductivité hydraulique est significativement différente de l'encaissant, avec le cœur de la faille moins perméable et les zones endommagées plus perméables. Dans tous les scénarios, les eaux profondes empruntent les voies les plus perméables, i.e. vers le haut le long de la zone endommagée plus perméable. Les scénarios les plus complexes de failles conduits-barrières (où le cœur de la faille est peu perméable et la zone endommagée très perméable) révèlent le potentiel maximal de remontée des eaux profondes et anciennes, atteignant des âges allant jusqu'à 1.23 Ga sous le Lac Saint-Jean. Les scénarios où les failles sont très perméables permettent aux eaux souterraines récentes de pénétrer plus profondément dans le substrat rocheux, créant ainsi une zone de mélange. Cette observation n'est pas un cas isolé, elle a aussi été démontrée dans une étude menée au Québec (Janos et al., 2018) et dans des aquifères sédimentaires siliciclastiques (Bense et Person, 2006). Toutefois, il est important de noter que l'étude paramétrique du rôle des failles est avant tout théorique, en raison du manque de connaissance sur les propriétés hydromécaniques des failles du Graben du Saguenay. L'étude permet néanmoins de mettre en évidence le rôle des failles dans la perturbation des systèmes d'écoulement et dans la remontée des fluides profonds.

Notre étude démontre la plausibilité hydraulique d'une remontée d'eaux profondes vers les zones de décharge, processus accentué par les failles du graben, renforçant le modèle conceptuel

hydrogéochimique proposé par Walter et al. (2023). De plus, les traceurs isotopiques et les gaz rares appuient un mélange d'eau météorique avec une saumure ayant circulée profondément dans la croûte, avec des âges simulés similaires à ceux identifiés dans la littérature. Toutefois, les simplifications du modèle numérique limitent la portée prédictive locale des résultats. Les résultats numériques doivent donc être lus comme des ordres de grandeur régionaux et des mécanismes plausibles, utiles pour hiérarchiser les zones susceptibles à la remontée des eaux souterraines profondes et à alimenter le débat concernant la circulation des fluides profonds.

Les réponses acquises dans cette section de l'étude doctorale ouvrent la voie à de nouvelles questions nécessitant de futures investigations, telles que :

- Comprendre l'impact de la dernière glaciation sur la dynamique des écoulements profonds dans la région d'étude : identifier la profondeur et l'empreinte spatiale de l'infiltration sous-glaciaire Wisconsinienne; comprendre l'effet du rebond isostatique post-glaciaire sur l'écoulement des eaux souterraines; évaluer le rôle du pergélisol sur la connectivité hydraulique et les temps de réponse du système hydrogéologique en pression; et caractériser l'ouverture transitoire des failles et ses effets sur la perméabilité et les flux.
- Tester l'hypothèse de la remontée des saumures profondes sous l'effet d'un gradient de densité, en utilisant une approche multi-continuum/DFN (réseau de fractures discrètes). L'approche multi-continuum traitant séparément les fractures et la matrice, ainsi que leurs interactions, permettra d'évaluer l'effet de la densité des saumures dans la dynamique des écoulements dans un milieu fracturé hétérogène complexe.
- Comprendre l'influence des variations topographiques à l'échelle des temps géologiques sur les écoulements profonds et la préservation des fluides anciens. Le modèle numérique présenté dans cette étude s'est basé sur la topographie actuelle. Or, la littérature montre que la topographie contrôle l'organisation des systèmes d'écoulement (local, intermédiaire, régional) et donc que des changements de la paléo-topographie de surface à long terme peuvent réorienter les circulations profondes (Tóth, 1999). Il est donc pertinent d'examiner comment les effets du poids lithostatique associé aux phases d'exhumation et d'érosion de l'Orogène grenvillienne, les cycles glaciaires-interglaciaires et les variations du niveau marin

ont pu modifier les gradients hydrauliques, les pressions de pores et, in fine, la capacité des milieux cristallins à conserver des fluides très anciens.

5.3. Contribution 2 : Modèle géochimique de l'évolution naturelle des eaux souterraines

5.3.1. Trajectoires d'évolution des saumures continentales profondes

Sur la base d'une compilation mondiale de 308 échantillons de saumures continentales profondes, le Chapitre 3 compare, au sein d'une même population statistique, l'évolution des saumures provenant des bassins sédimentaires et des socles cristallins. Plusieurs études décrivent séparément la trajectoire d'évolution des saumures sédimentaires, dominée par la dissolution ou la précipitation de la halite (Rittenhouse, 1967; Kharaka et Hanor, 2003; Yardley, 2013), et celle des saumures cristallines, contrôlée par l'hydrolyse des silicates (Bucher et Stober, 2000; Frape et al., 2003). Toutefois, à notre connaissance, peu d'études comme la nôtre, proposent une analyse statistique combinée de ces deux principaux réservoirs de saumures à l'échelle mondiale. Ainsi, en combinant plusieurs outils statistiques (cf Chapitre 3), l'étude montre que les deux types de saumures convergent vers un membre Ca-Cl riche en Br^- et Sr^{2+} par des trajectoires d'évolution distinctes. Ces trajectoires d'évolution ont été décrites par deux équations linéaires : Cl/Br = 103 + Na/Br (concentration en mg/L) qui traduit le contrôle des processus de dissolution/précipitation de la halite sur les saumures sédimentaires et les saumures cristallines sont décrites par l'équation [Ca] = –1610 + 0.4 [Cl] (concentration en mg/L), qui caractérise l'hydrolyse des silicates et la formation d'argiles hydratées. Ces équations linéaires fournissent un référentiel quantitatif permettant de positionner rapidement un échantillon le long d'une trajectoire d'évolution. L'étude montre également que les saumures sédimentaires sont enrichies en $\delta^{18}O$ et $\delta^{2}H$, reflétant l'évaporation, tandis que leurs ratios $^{87}Sr/^{86}Sr$ (médiane = 0.7087) sont similaires aux évaporites datant du Paléozoïque. Alors que les saumures cristallines présentent un appauvrissement en $\delta^{18}O$ et un enrichissement en $\delta^{2}H$, indiquant des interactions sur de longues échelles de temps (> 100 Ma), tandis que le ratio $^{87}Sr/^{86}Sr$ (médiane = 0.7142) est similaire aux roches silicatées radiogéniques des Bouclier anciens.

5.3.2. Connectivité hydraulique entre les réservoirs et le rôle de la paléohydrogéologie dans l'évolution géochimique

L'approche multi-traceurs appliquée au Chapitre 4 a permis l'identification des pôles compositionnels régionaux et l'évaluation de la connectivité hydraulique entre les réservoirs de la région d'étude. Ces résultats révèlent trois sources distinctes de salinité dans le roc fracturé peu profond au SLSJ: (1) une source marine holocène associée à l'intrusion postglaciaire de la mer Laflamme et partiellement modifiée par des interactions avec des argiles marines. Ceci a mis en évidence une connexion hydraulique roc-argile, appuyant ainsi les conclusions des études de Chesnaux et Elliott (2011) et Chesnaux et al. (2012) dans la région d'étude; (2) une saumure marine Paléozoïque résultant de l'évaporation de la mer Ordovicienne et piégée dans les calcaires Ordoviciens; et (3) une saumure du Bouclier Précambrien (> 100 Ma), associée aux roches du Bouclier Canadien résultant de longues interactions entre l'eau et la roche, et contenant 1 à 5 % d'hélium mantellique provenant directement du manteau lithosphérique sub-continental (MLSC). La présence des saumures profondes du Bouclier Précambrien à de faibles profondeurs met en évidence la connectivité hydraulique entre les aquifères de subsurface et les environnements profonds. L'étude confirme également, pour la première fois au SLSJ, la présence d'eau du Wisconsinien datant d'environ 8,225 à 25,500 ans BP. Les valeurs élevées de $\delta^{81}Br$, $\delta^{11}B$ et $\delta^{7}Li$ observées dans les saumures marines Paléozoïques et Précambriennes du Bouclier indiquent des modifications importantes de leur évolution chimique par des processus de cryo-concentration au cours de la dernière glaciation. La compréhension de l'évolution hydraulique et hydrogéochimique à travers le temps (Chapitre 2 et Chapitre 3), associée à l'approche multi-traceurs (Chapitre 4), a permis de vérifier quantitativement l'aspect hydraulique, de préciser les pôles compositionnels régionaux afin de proposer un modèle conceptuel d'évolution hydrogéologique pour le SLSJ (Figure 4-9).

Bien que l'élaboration d'un modèle hydrogéologique affiné pour le SLSJ réponde d'abord à un objectif régional, plusieurs enseignements sont généralisables et ont un intérêt pour la science fondamentale. D'une part, l'association de traceurs géochimiques indiquant des systèmes profonds (~7.5-12.5 km) identifiés en subsurface (<100 m) et des failles du graben agissant comme vecteurs hydrauliques suggèrent l'existence de connexions ponctuelles entre réservoirs profonds et aquifères

de surface. Cette connaissance peut être généralisée à des contextes similaires, i.e. configuration en graben. Sans pour autant quantifier l'ampleur précise, ce projet doctoral met également en lumière l'impact important de la dernière glaciation sur le système hydrogéologique actuel. La mise en évidence de l'influence des eaux paléo-glaciaires au SLSJ s'inscrit dans un cadre plus large, puisque de nombreux travaux ont déjà démontré l'impact de la dernière glaciation sur les systèmes hydrogéologiques (McIntosh et Walter, 2005; Lemieux et al., 2008b; Gimeno et al., 2023). Aussi, il est intéressant de noter que de nos jours, de plus en plus d'études au Québec identifient des traces d'eau datant de la dernière période glaciaire (Boucher et al., 2015; Meyzonnat et al., 2023). Cette étude (Chapitre 4) nuance l'idée simpliste selon laquelle la salinité augmente nécessairement avec l'âge des eaux souterraines, et met en évidence la diversité des processus qui régissent l'évolution de la chimie des eaux souterraines à travers le temps. Concernant les gaz rares, la thèse, en cohérence avec l'étude de Tyne et al. (2025), soutient l'hypothèse que le dégazage diffusif de l'hélium mantellique provenant du MLSC à travers la croûte continentale contribue de manière plus significative qu'attendu au bilan régional d'hélium. Cette conclusion demeure toutefois dépendante des incertitudes sur les flux, la perméabilité effective des zones de faille et la part relative des contributions crustales versus MLSC. La notion du dégazage de l'hélium mantellique souligne également la problématique concernant la datation des eaux souterraines à l'aide des gaz rares tel que l'hélium, en particulier dans des contextes similaires à la région étudiée. Les processus à l'origine des saumures des boucliers continentaux, tel que l'évaporation ou la cryo-concentration de l'eau de mer ancienne, l'interaction roche-roche, le lessivage d'inclusions fluides (Frape et Fritz, 1987; Nordstrom et al., 1989; Herut et al., 1990; Bottomley et al., 1999), jusqu'à nos jours ne fait pas consensus dans la communauté scientifique. En proposant un mélange entre une saumures contrôlée par l'hydrolyse des silicates et la formation d'argiles hydratés et une eau paléo-glaciaire concentrée par cryo-concentration, ce projet de recherche contribue au débat concernant les processus de salinisation à l'origine des saumures du Bouclier Canadien. De manière générale, ce projet doctoral apporte des éléments importants pour mieux comprendre la paléohydrogéologie des socles cristallins fracturés, en particulier les interactions entre les processus géochimiques profonds,

les climats glaciaires anciens, les multiples intrusions marines du passé et la dynamique des eaux souterraines dans des systèmes hydrogéologiques complexes à l'échelle mondiale.

Toutefois, les interprétations faites sur l'aspect géochimique de cette étude sont également sujettes à la nuance. Bien que les données géochimiques fournissent des résultats bien documentés par la littérature, la représentativité des échantillons tant à l'échelle locale (n = 14) qu'à l'échelle mondiale (surreprésentation du Bouclier Canadien) représente une limite de l'étude. Les inférences sur la connectivité profonde, l'empreinte glaciaire et le bilan d'hélium (MLSC vs roche) restent étayées par des indicateurs indirects (traceurs hydrogéochimiques, structures de failles du graben, contraintes de modélisation), par des données géochimiques des roches tirées de la littérature, et par des observations ponctuelles. À la lumière des résultats de ce projet de recherche, nous ne sommes toujours pas capables de trancher de façon claire sur une origine marine ou non-marine des saumures continentales, en particulier celles du Bouclier Canadien. En effet, d'après plusieurs sources dans la littérature (ex : Savoye, 1998), l'interaction intense eau-roche a tendance à effacer la signature initiale de l'eau (eau de mer ou eau météoritique). Toutefois, ce projet doctoral permet de distinguer des sources ayant une composante marine (saumures sédimentaires), des saumures ne montrant pas de signature marine mais une composante crustale claire. Par conséquent, la généralisation des interprétations géochimiques doit se faire avec prudence, en privilégiant les contextes géologiques analogues au SLSJ et en reconnaissant les marges d'incertitude sur les profondeurs effectives de circulation des eaux souterraines, les temps de résidence et la part relative des sources de salinisation. Par ailleurs, les limites et incertitudes présenter dans cette section, ouvrent la voie à des études additionnelles, telles que :

- L'analyse et la compilation des signatures géochimiques des roches de la région pour une meilleure caractérisation hydrogéochimique des pôles compositionnels régionaux et une meilleure compréhension du rôle du contexte géologique.
- La détermination de l'âge des saumures Précambriennes en prenant en compte l'origine des gaz rares (crustale vs MLSC), tel que l'hélium, et le mélanges de plusieurs sources d'eau d'âge et de composition distinctes.

- Analyser les inclusions fluides et les minéraux témoins des circulations anciennes pour reconstituer, du Précambrien au sub-actuel, l'histoire des flux profonds de la région d'étude, puis proposer des modèles qualitatifs et quantitatifs d'écoulement (fluide–roche ou fluide-fluide). Ceci est particulièrement pertinent en l'absence de forages profonds.

5.4. Contribution 3 : Marqueurs géochimiques de l'évolution des saumures continentales

L'intégration des données locales du SLSJ (n = 14) et d'une compilation internationale de saumures continentales (n = 308) a permis d'identifier un ensemble cohérent de marqueurs géochimiques discriminant à la fois l'origine lithologique et l'histoire temporelle des saumures continentales. Les saumures sédimentaires comme les environnements marins (ex : eau de mer, sédiments marins) sont caractérisées par une covariance avec les paramètres Na^+, K^+, Mg^{2+} et SO_4^{2-}, alors que les saumures cristallines sont caractérisées par une covariance avec les paramètres Br^-, Sr^{2+}, et Ca^{2+}. Ces observations ont été mises en évidence dans plusieurs études telles que Gimeno et al. (2023) dans le Bouclier Fennoscandien ou Walter et al. (2017) dans la région d'étude (Bouclier Canadien). Au-delà de ces covariances déjà bien documentées, l'apport majeur de ce travail réside dans l'introduction de nouveaux ratios élémentaires, à notre connaissance, auparavant très peu exploités dans un même cadre d'analyse. Ces traceurs servent de marqueurs discriminatoires entre les saumures des environnements sédimentaires et cristallins. Les résultats montrent que les saumures issues d'environnements cristallins présentent systématiquement des valeurs B/Br et Li/Br inférieures à 0.01, tandis que celles issues d'environnements sédimentaires dépassent ce seuil. Cette distinction reflète des régimes d'altération et des conditions géothermiques contrastés. Dans les roches cristallines, l'hydrolyse des silicates et l'adsorption du B^{3+} et du Li^+ sur les argiles hydratées nouvellement formées conduisent à des rapports B/Br et Li/Br faibles. Alors que dans les environnements sédimentaires, la dissolution/précipitation des évaporites et les interactions avec des minéraux riches en B^{3+} et Li^+ conduisent à des rapports plus élevés.

La faible incorporation du Br^- en solution dans la phase solide (Kloppmann et al., 2011) en fait un bon traceur de temps de résidence, tel que mis en évidence dans ce projet de doctorat. Ainsi, les ratios B/Br et Li/Br associés aux isotopes de lithium, de bore et de brome ont également permis

de mettre en évidence la contribution d'eau de fonte datant de la dernière glaciation et des processus de cryo-concentration (Chapitre 4).

En hydrogéochimie, les études traitent généralement du ratio Rb/Sr dans les minéraux constitutifs des roches afin d'expliquer les variations $^{87}Sr/^{86}Sr$ dans l'eau souterraine (Négrel et al., 2001), très peu en tant qu'indicateur de saumures cristallines. McNutt et al. (1990) mentionnent que le ratio Rb/Sr des saumures cristallines sont faibles sans pourtant y attribuer de valeur seuil. Dans ce projet doctoral, le ratio Rb/Sr < 0.001 associé au ratio isotopique $^{87}Sr/^{86}Sr$ a permis de discriminer les sources de saumures crustales des autres sources (Chapitre 4). La Figure 5-1 présente les données des eaux saumâtres d'origine Précambrienne (Chapitre 4), les eaux souterraines du Bouclier Canadien en Abitibi (dont certains ont été classés comme saumures cristallines au Chapitre 3), ainsi que les saumures sédimentaires (Pauwels et al., 1993). Il est intéressant de noter que les échantillons d'origine marine et sédimentaire se distinguent clairement des saumures provenant du socle cristallin. La bonne corrélation entre le ratio Rb/Sr et le TSD pour les eaux du bouclier suggère que le ratio Rb/Sr peut constituer un bon indicateur de l'évolution chimique des eaux souterraines vers des saumures cristallines.

Les grandes bases de données géochimiques à l'échelle régionale n'incluent généralement pas de données isotopiques. En leur absence, les ratios Li/Br, B/Br et Rb/Sr constituent des indicateurs intéressants pour mieux comprendre l'évolution de la chimie des eaux souterraines et distinguer les sources de salinité selon le contexte géologique. Toutefois, la compréhension approfondie des processus contrôlant la variabilité et la modification de ces ratios est nécessaire. Afin de développer des outils d'interprétations robuste, il est nécessaire de comprendre les cinétiques de réaction eau-roche et explorer les relations entre les éléments mineurs et traces, en particulier Br^-, Sr^{2+}, Li^+, Rb^+ et B^{3+} à l'aide d'une approche expérimental-modélisation géochimique. La bonne application des traceurs tels que Li/Br, B/Br ou Rb/Sr à l'ensemble des données (locales et mondiales) met en évidence un ensemble de processus communs directement liés au contexte géologique durant les interactions eau-roche. Comprendre l'origine et l'évolution de ces éléments permettra de développer de nouveaux modèles géologiques pour les fluides profonds à l'interface socle-couverture.

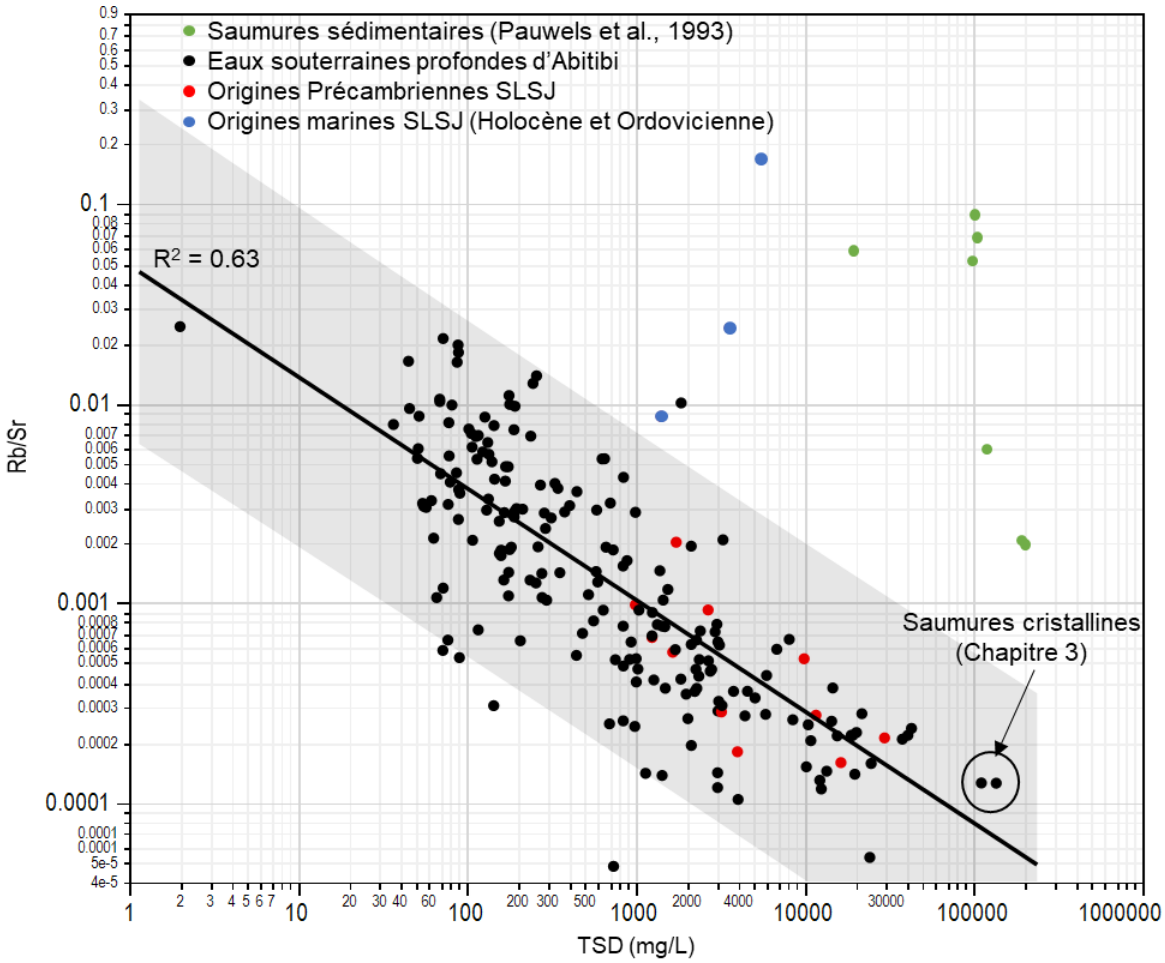

Figure 5-1 : Graphique montrant la répartition et les origines des échantillons d'eaux selon le diagramme log-log Rb/Sr (en mg/L) vs. TSD (total des solides dissous). Ligne noire – droite de régression linéaire. Zone ombrée – intervalle de prédiction avec un niveau de confiance de 95% calculé sur les données provenant des eaux souterraines profondes d'Abitibi dans le Bouclier Canadien (ANNEXE VIII, Richard et al. (2024)) et des eaux saumâtres du SLSJ d'origine Précambrienne.

Chapitre 6 : CONCLUSION

La compréhension des processus hydrogéochimiques qui contrôlent l'évolution des eaux souterraines constitue un préalable scientifique essentiel à la protection de cette ressource face aux pressions croissantes du changement climatique et de l'intensification des usages. C'est dans cette perspective que s'inscrit le présent projet doctoral, intégré au programme d'envergure initié par Walter (2018) qui vise à approfondir la connaissance de la dynamique hydrogéochimique d'un territoire. L'attention particulière a été portée à la salinisation continentale au Saguenay-Lac-Saint-Jean, considéré comme laboratoire naturel à l'étude. L'objectif général du projet doctoral était d'explorer les conditions de migration des eaux souterraines profondes vers la surface, ainsi que de comprendre l'évolution des saumures continentales en fonction du contexte géologique (sédimentaire et cristallin) et de la paléohydrogéologie régionale. Pour ce faire, l'approche méthodologique a combiné (1) la modélisation numérique de l'écoulement et du transport advectif-dispersif de l'âge; (2) les analyses statistiques (analyse hiérarchique en grappe, analyse en composante principale et tests non-paramétriques) sur une compilation mondiale de saumures continentales; et (3) les analyses multi-traceurs sur des eaux saumâtres prélevées dans le roc fracturé de la région étudiée.

La réponse synthétique à la question de recherche peut se formuler ainsi : À l'échelle régionale, la topographie en graben hiérarchise les cellules d'écoulement et permet sous-condition (nappe imposée et limites latérales à flux nul), dans les principales zones de décharge (lacs, rivières), la remontée de vieilles eaux en l'absence même de failles ; l'intégration de failles joue un rôle conduit-barrière, accentuant la remontée verticale et créant des zones de mélange avec des eaux plus jeunes ; sur le plan géochimique, les ratios Li/Br, B/Br et Rb/Sr ont permis de discriminer les saumures sédimentaires des saumures cristallines ; l'évolution des saumures sédimentaires est contrôlée par les processus de dissolution/précipitation de la halite tandis que les saumures cristallines par l'hydrolyse des silicates et la formations d'argiles hydratés. Malgré les processus différents, l'évolution des saumures continentales tend à converger vers un membre Ca-Cl riche en Br^- et Sr^{2+} ; cette évolution des saumures cristallines et sédimentaire a également été observée dans la région

étudiée. On y retrouve précisément en subsurface, des vestiges de la mer Laflamme, et de saumures sédimentaires liées à la mer à l'Ordovicien, des traces d'eau sous-glaciaire datant du Wisconsinien et les évidences de saumures cristallines profondes (entre 7.5 à 12.5 km). L'ensemble renforce un modèle conceptuel hydrogéologique régional où topographie et structures profondes contrôlent la circulation, tandis que la signature chimique retrace l'héritage des interactions eau-roche et l'histoire hydrogéologique de la région.

Toutefois, les limites et incertitudes concernant la modélisation numérique d'écoulement et la représentativité des données géochimiques restreindre la portée des conclusions de l'étude. Ces dernières doivent donc être lues comme un cadre général, offrant un aperçu : 1) des mécanismes hydrodynamiques qui gouvernent les eaux souterraines profondes ; 2) des profils d'âge avec la profondeur ; 3) du rôle des failles comme vecteur hydraulique des saumures continentales profondes ; 4) de la diversité des processus hydrogéochimiques et d'origines de salinité en contexte de bouclier continental ; 5) des marqueurs géochimiques de l'origine de la salinité. Les résultats de cette thèse sont utiles pour hiérarchiser les zones à risque de salinisation (zones de résurgence situées près des systèmes des failles) et pour alimenter le débat sur les processus de salinisation des saumures continentales profondes et sur la circulation des fluides profond en contexte de graben. Le modèle numérique développer dans le cadre de ce projet de recherche sert de base au développement de modèles plus complexe, reflétant les nombreux mécanismes qui contrôlent les écoulements des fluides, en particulier dans les environnements profonds. En termes de marqueurs géochimiques, la suite logique de cette étude, est de préciser les cinétiques de réaction contrôlant les variations de ces éléments lors des interactions eau-roche via la combinaison d'essais expérimentaux d'interaction eau-roche et de modélisation hydrogéochimique. Pour l'UQAC, le développement de connaissances en hydrogéochimie quantitative, en complément du centre d'expertise déjà bien établi en hydraulique des aquifères, favorisera la mise sur pied de nouvelles collaborations nationales et internationales fructueuses. Les outils d'interprétation élaborés dans le cadre de ce projet doctoral visent, à terme, à produire des indices de vulnérabilité, à cartographier les menaces liées à la salinisation et à anticiper les problèmes qui en découlent, afin de soutenir les décideurs régionaux dans la définition des politiques et dans la gestion de l'eau.

Chapitre 7 : LISTE DE RÉFÉRENCES

Abascal, E., Gómez-Coma, L., Ortiz, I., et Ortiz, A. 2022. Global diagnosis of nitrate pollution in groundwater and review of removal technologies. Science of the Total Environment **810**: 152233.

Abhervé, R. 2019. Effet de la résolution topographique des modèles hydrogéologiques sur l'estimation des débits de base des rivières et des temps de résidence de l'eau souterraine (Effect of the topographic resolution of hydrogeological models on the estimation of base flows in rivers and groundwater residence times). Mémoire de maîtrise, Centre Eau Terre et Environnement, Université de Rennes 1, Rennes, France.

Abi, A., Walter, J., Saeidi, A., et Chesnaux, R. 2022. A cluster-based multiparametric similarity test for the compartmentalization of crystalline rocks into structural domains. Quarterly Journal of Engineering Geology and Hydrogeology **55**(3): qjegh2021–2136.

Achtziger-Zupančič, P., Loew, S., et Mariethoz, G. 2017. A new global database to improve predictions of permeability distribution in crystalline rocks at site scale. Journal of Geophysical Research: Solid Earth **122**(5): 3513–3539.

Adombi, A.V.D.P., Chesnaux, R., Boucher, M.-A., Braun, M., et Lavoie, J. 2024. A causal physics-informed deep learning formulation for groundwater flow modeling and climate change effect analysis. Journal of Hydrology **637**: 131370.

Aggarwal, P.K., Araguas-Araguas, L., Choudhry, M., van Duren, M., et Froehlich, K. 2014. Lower groundwater 14C age by atmospheric CO2 uptake during sampling and analysis. Ground Water **52**(1): 20–24. doi: https://doi.org/10.1111/gwat.12110.

Al Radi, M., Adil Al-Isawi, O., Abdelghafar, A.A., Fayez Abu Qiyas, A., AlMallahi, M., Khanafer, K., et Assad, M.E.H. 2022. Recent progress, economic potential, and environmental benefits of mineral recovery geothermal brine treatment systems. Arabian Journal of Geosciences **15**(9): 832.

Allen, D.M., et Nott, A.H. 2021. How important are those fracture zones? Scale dependent characteristics revealed through field studies and an integrated hydrological model of a mountain headwater catchment. Frontiers in Water **3**: 767399.

André, L., Rabemanana, V., et Vuataz, F.-D. 2006. Influence of water–rock interactions on fracture permeability of the deep reservoir at Soultz-sous-Forêts, France. Geothermics **35**(5-6): 507–531.

Appelo, C., et Postma, D. 2005. Geochemistry. Groundwater and Pollution **536**.

Araoka, D., Kawahata, H., Takagi, T., Watanabe, Y., Nishimura, K., et Nishio, Y. 2014. Lithium and strontium isotopic systematics in playas in Nevada, USA: constraints on the origin of lithium. Mineralium Deposita **49**(3): 371–379.

Aslannezhad, M., Ali, M., Kalantariasl, A., Sayyafzadeh, M., You, Z., Iglauer, S., et Keshavarz, A. 2023. A review of hydrogen/rock/brine interaction: Implications for Hydrogen Geo-storage. Progress in Energy and Combustion Science **95**: 101066.

Bachu, S. 1999. Regional-scale geothermal and hydrodynamic regimes in the Alberta basin: A synthesis. *Dans* Geothermics in basin analysis. Springer. pp. 81–98.

Bagheri, R., Nadri, A., Raeisi, E., Eggenkamp, H., Kazemi, G., et Montaseri, A. 2014. Hydrochemical and isotopic (δ18O, δ2H, 87Sr/86Sr, δ37Cl and δ81Br) evidence for the origin of saline formation water in a gas reservoir. Chemical Geology **384**: 62–75.

Ballentine, C., Mazurek, M., et Gautschi, A. 1994. Thermal constraints on crustal rare gas release and migration: Evidence from Alpine fluid inclusions. Geochimica et Cosmochimica Acta **58**(20): 4333–4348.

Ballentine, C.J., et Burnard, P.G. 2002. Production, release and transport of noble gases in the continental crust. Reviews in Mineralogy and Geochemistry **47**(1): 481–538.

Banks, D., et Frengstad, B. 2006. Evolution of groundwater chemical composition by plagioclase hydrolysis in Norwegian anorthosites. Geochimica et Cosmochimica Acta **70**(6): 1337–1355.

Barth, S. 1993. Boron isotope variations in nature: a synthesis. Geologische Rundschau **82**: 640–651.

Beaucaire, C., et Michard, G. 1982. Origin of dissolved minor elements (Li, Rb, Sr, Ba) in superficial waters in a granitic area. Geochemical Journal **16**(5): 247–258.

Bein, A., et Arad, A. 1992. Formation of saline groundwaters in the Baltic region through freezing of seawater during glacial periods. Journal of Hydrology **140**(1-4): 75–87.

Bennett, P.C., Hiebert, F.K., et Rogers, J.R. 2000. Microbial control of mineral–groundwater equilibria: Macroscale to microscale. Hydrogeology Journal **8**(1): 47–62.

Bense, V., Gleeson, T., Loveless, S., Bour, O., et Scibek, J. 2013. Fault zone hydrogeology. Earth-Science Reviews **127**: 171–192.

Bense, V., et Person, M. 2006. Faults as conduit-barrier systems to fluid flow in siliciclastic sedimentary aquifers. Water Resources Research **42**(5).

Bhattacherjee, R., Botchway, K., Pashin, J.C., Chakraborty, G., et Bikkina, P. 2023. Machine learning-based prediction of CO2 fugacity coefficients: Application to estimation of CO2 solubility in aqueous brines as a function of pressure, temperature, and salinity. International Journal of Greenhouse Gas Control **128**: 103971.

Birkle, P., García, B.M., et Padrón, C.M.M. 2009. Origin and evolution of formation water at the Jujo–Tecominoacán oil reservoir, Gulf of Mexico. Part 1: chemical evolution and water–rock interaction. Applied Geochemistry **24**(4): 543–554.

Bishop, B.A., et Robbins, L.J. 2024. In-Situ Water-Rock Interactions as the Source of Brine-Hosted Lithium: Implications for Developing a Deposit Model. Geoconvention, Calgary, Canada, 17–19 June 2024, p. 4.

Bjørlykke, K. 2015. Subsurface water and fluid flow in sedimentary basins. Springer. pp. 279–300.

Blake, R., et Walter, L. 1999. Kinetics of feldspar and quartz dissolution at 70–80 C and near-neutral pH: effects of organic acids and NaCl. Geochimica et Cosmochimica Acta **63**(13-14): 2043–2059.

Blomqvist, R. 1999. Hydrogeochemistry of deep groundwaters in the central part of the Fennoscandian Shield. Geological Survey of Finland. GTK-YST-101.

Bockgård, N. 2004. Groundwater recharge in crystalline bedrock: processes, estimation, and modelling. Doctoral dissertation, Faculty of Science and Technology, Acta Universitatis Upsaliensis, Uppsala, Swedish.

Boschetti, T. 2013. Oxygen isotope equilibrium in sulfate–water systems: A revision of geothermometric applications in low-enthalpy systems. Journal of Geochemical Exploration **124**: 92–100.

Bottomley, D., Ross, J., et Clarke, W. 1984. Helium and neon isotope geochemistry of some ground waters from the Canadian Precambrian Shield. Geochimica et Cosmochimica Acta **48**(10): 1973–1985.

Bottomley, D.J., et Clark, I.D. 2004. Potassium and boron co-depletion in Canadian Shield brines: evidence for diagenetic interactions between marine brines and basin sediments. Chemical Geology **203**(3-4): 225–236.

Bottomley, D.J., Conrad Gregoire, D., et Raven, K.G. 1994. Saline ground waters and brines in the Canadian Shield: Geochemical and isotopic evidence for a residual evaporite brine component. Geochimica et Cosmochimica Acta **58**(5): 1483–1498. doi: 10.1016/0016-7037(94)90551-7.

Bottomley, D.J., Katz, A., Chan, L., Starinsky, A., Douglas, M., Clark, I., et Raven, K. 1999. The origin and evolution of Canadian Shield brines: evaporation or freezing of seawater? New lithium isotope and geochemical evidence from the Slave craton. Chemical Geology **155**(3-4): 295–320.

Bouchard, R., Dion, D., et Tavenas, F. 1983. Origine de la préconsolidation des argiles du Saguenay, Québec. Canadian Geotechnical Journal **20**(2): 315–328.

Boucher, C., Pinti, D.L., Roy, M., Castro, M.C., Cloutier, V., Blanchette, D., Larocque, M., Hall, C.M., Wen, T., et Sano, Y. 2015. Groundwater age investigation of eskers in the Amos region, Quebec, Canada. Journal of Hydrology **524**: 1–14.

Boulton, G., Gustafson, G., Schelkes, K., Casanova, J., et Moren, L. 2001. Paleohydrogeology and geoforecasting for performance assessment in geosphere repositories for radioactive waste disposal (Pagepa). Directorate-General for Research, European Commission. Final report 1018-5593.

Boumaiza, L., Stotler, R., et Frape, S. 2024. A review of the major chemical and isotopic characteristics of groundwater in crystalline rocks of the Canadian Shield. Chemical Geology: 122366.

Boumaiza, L., Walter, J., Chesnaux, R., Lambert, M., Jha, M.K., Wanke, H., Brookfield, A., Batelaan, O., Galvão, P., et Laftouhi, N.E. 2022a. Groundwater recharge over the past 100 years: Regional spatiotemporal assessment and climate change impact over the Saguenay-Lac-Saint-Jean region, Canada. Hydrological Processes **36**(3): e14526.

Boumaiza, L., Walter, J., Chesnaux, R., Stotler, R.L., Wen, T., Johannesson, K.H., Brindha, K., et Huneau, F. 2022b. Chloride-salinity as indicator of the chemical composition of groundwater: empirical predictive model based on aquifers in Southern Quebec, Canada. Environmental Science and Pollution Research **29**(39): 59414–59432.

Bowles, M.W., Mogollón, J.M., Kasten, S., Zabel, M., et Hinrichs, K.-U. 2014. Global rates of marine sulfate reduction and implications for sub–sea-floor metabolic activities. Science **344**(6186): 889–891.

Brady, P., Lopez, C., et Sassani, D. 2019. Granite hydrolysis to form deep brines. Energies **12**(11): 2180.

Brown, P.J., Vannucci, M., et Fearn, T. 1998. Multivariate Bayesian variable selection and prediction. Journal of the Royal Statistical Society: Series B (Statistical Methodology) **60**(3): 627–641.

Bucher, K., et Stober, I. 2000. The composition of groundwater in the continental crystalline crust. *Dans* Hydrogeology of Crystalline Rocks. Springer. pp. 141–175.

Bucher, K., et Stober, I. 2010. Fluids in the upper continental crust. Geofluids **10**(1-2): 241–253.

Bungum, H., et Eldholm, O. 2022. The conundrums of the postglacial tectonic response of the Fennoscandian and Canadian Shields. Earth-Science Reviews: 104146.

Caine, J.S. 2006. Questa baseline and premining ground-water quality investigation 18. Characterization of brittle structures in the Questa Caldera and their potential influence on bedrock groundwater flow, Red River Valley, New Mexico. USGS Numbered Series. 2330-7102.

Campbell, A.G., Cartwright, I., Webb, J.A., Cendon, D.I., et Currell, M.J. 2025. Using geochemical and geophysical data to characterise inter-aquifer connectivity and impacts on shallow aquifers and groundwater dependent ecosystems. Applied Geochemistry **178**: 106217.

Carpenter, A.B., Trout, M.L., et Pickett, E.E. 1974. Preliminary report on the origin and chemical evolution of lead-and zinc-rich oil field brines in central Mississippi. Economic Geology **69**(8): 1191–1206.

Cartaud, F. 2004. Modélisation des écoulements dans les interfaces des barrières d'étanchéité composites d'installation de stockage de déchets (Flow modelling in the interfaces of composite sealing barriers in waste storage facilities). Thèse de doctorat, Hydrologie et Hydrogéologie Quantitative, École Nationale Supérieure des Mines de Paris, Paris, France.

Casanova, J., Négrel, P., et Blomqvist, R. 2005. Boron isotope fractionation in groundwaters as an indicator of past permafrost conditions in the fractured crystalline bedrock of the fennoscandian shield. Water Research **39**(2-3): 362–370.

Casanova, J., Négrel, P., Petelet-giraud, E., Brach, M., Bourguignon, A., et Millot, R. 2004. Projet PALÉOHYD II Paléohydrologie et géoprospective: modèles conceptuels et processus d'acquisition de la chimie des eaux dans les massifs granitiques: BRGM. Rapport BRGM/RP-53469-FR. 124 p. 98 ill.

Chan, L.-H., Starinsky, A., et Katz, A. 2002. The behavior of lithium and its isotopes in oilfield brines: evidence from the Heletz-Kokhav field, Israel. Geochimica et Cosmochimica Acta **66**(4): 615–623.

Chandra, S., Auken, E., Maurya, P.K., Ahmed, S., et Verma, S.K. 2019. Large scale mapping of fractures and groundwater pathways in crystalline hardrock by AEM. Scientific Reports **9**(1): 398.

Chebotarev, I. 1955. Metamorphism of natural waters in the crust of weathering—1. Geochimica et Cosmochimica Acta **8**(1-2): 22–48.

Chesnaux, R. 2013. Regional recharge assessment in the crystalline bedrock aquifer of the Kenogami Uplands, Canada. Hydrological Sciences Journal **58**(2): 421–436.

Chesnaux, R., et Elliott, A.-P. 2011. Demonstrating evidence of hydraulic connections between granular aquifers and fractured rock aquifers. *Sous la direction de*. *Dans* Proceedings of GeoHydro 2011, Joint meeting of the Canadian quaternary association and the Canadian chapter of the International Association of Hydrogeologists, pp. 28–31.

Chesnaux, R., Rafini, S., et Elliott, A.-P. 2012. A numerical investigation to illustrate the consequences of hydraulic connections between granular and fractured-rock aquifers. Hydrogeology Journal **20**(8): 1669–1680.

Chung, E.T., Efendiev, Y., Leung, T., et Vasilyeva, M. 2017. Coupling of multiscale and multi-continuum approaches. GEM - International Journal on Geomathematics **8**(1): 9–41. doi: 10.1007/s13137-017-0093-8.

Clark, I.D., Al, T., Jensen, M., Kennell, L., Mazurek, M., Mohapatra, R., et Raven, K. 2013. Paleozoic-aged brine and authigenic helium preserved in an Ordovician shale aquiclude. Geology **41**(9): 951–954.

Clark, I.D., Douglas, M., Raven, K., et Bottomley, D. 2000. Recharge and preservation of Laurentide glacial melt water in the Canadian Shield. Groundwater **38**(5): 735–742.

Clark, I.D., et Fritz, P. 1997. Environmental isotopes in hydrogeology. CRC Press.

Clarke, W.B., Jenkins, W., et Top, Z. 1976. Determination of tritium by mass spectrometric measurement of 3He. The International Journal of Applied Radiation and Isotopes **27**(9): 515–522.

Clauser, C., et Huenges, E. 1995. Thermal conductivity of rocks and minerals. Rock Physics and Phase Relations: A Handbook of Physical Constants **3**: 105–126.

Cloutier, V., Lefebvre, R., Savard, M., et Therrien, R. 2004. Groundwater origin and geochemical processes in the Basses-Laurentides sedimentary rock aquifer system, St. Lawrence Lowlands, Quebec, Canada. *Sous la direction de*. *Dans* Proceedings, 57th Canadian Geotechnical Conference and 5th Joint CGS/IAH Conference, pp. 18–25.

Cloutier, V., Lefebvre, R., Therrien, R., et Savard, M.M. 2008. Multivariate statistical analysis of geochemical data as indicative of the hydrogeochemical evolution of groundwater in a sedimentary rock aquifer system. Journal of Hydrology **353**(3-4): 294–313.

Collins, A. 1975. Geochemistry of oilfield waters. Elsevier Scientific Publishing Company, Amsterdam.

Connolly, C.A., Walter, L.M., Baadsgaard, H., et Longstaffe, F.J. 1990. Origin and evolution of formation waters, Alberta Basin, Western Canada Sedimentary Basin. II. Isotope systematics and water mixing. Applied Geochemistry **5**(4): 397–413.

Cortecci, G., Dinelli, E., Bolognesi, L., Boschetti, T., et Ferrara, G. 2001. Chemical and isotopic compositions of water and dissolved sulfate from shallow wells on Vulcano Island, Aeolian Archipelago, Italy. Geothermics **30**(1): 69–91.

Craig, H. 1961. Isotopic variations in meteoric waters. Science **133**(3465): 1702–1703.

Daus, A., Frind, E., et Sudicky, E. 1985. Comparative error analysis in finite element formulations of the advection-dispersion equation. Advances in Water Resources **8**(2): 86–95.

Dellinger, M., Hardisty, D.S., Planavsky, N.J., Gill, B.C., Kalderon-Asael, B., Asael, D., Croissant, T., Swart, P.K., et West, A.J. 2020. The effects of diagenesis on lithium isotope ratios of shallow marine carbonates. American Journal of Science **320**(2): 150–184.

Desbarats, A. 2002. A lumped-parameter model of groundwater influx to a mine adit in mountainous terrain. Water Resources Research **38**(11): 38–31–38–11.

Desbiens, S., et Lespérance, P.J. 1989. Stratigraphy of the Ordovician of the Lac Saint-Jean and Chicoutimi outliers, Quebec. Canadian Journal of Earth Sciences **26**(6): 1185–1202.

Dessureault, R. 1975. Hydrogeologie du Lac Saint-Jean. Partie Nord-Est. Ministère des Richesses Naturelles du Québec. Rapport hydrogéologique No. HG7. pp. 1–90.

Dewey, J., Kiseeva, E.S., Pearce, J., et Robb, L. 2021. Precambrian tectonic evolution of Earth: an outline. South African Journal of Geology 2021 **124**(1): 141–162.

Di Leo, G., et Sardanelli, F. 2020. Statistical significance: p value, 0.05 threshold, and applications to radiomics—reasons for a conservative approach. European Radiology Experimental **4**(1): 1–8.

Domenico, P.A. 1972. Concepts and models in groundwater hydrology. McGraw Hill.

Dong, H., et Gao, Z. 2022. Theoretical progress of groundwater chemical evolution based on tóthian theory: A review. Frontiers in Marine Science **9**: 972426.

Douglas, M., Clark, I., Raven, K., et Bottomley, D. 2000. Groundwater mixing dynamics at a Canadian Shield mine. Journal of Hydrology **235**(1-2): 88–103.

Downing, R., Edmunds, W., et Gale, I. 1987. Regional groundwater flow in sedimentary basins in the UK. Geological Society, London, Special Publications **34**(1): 105–125.

Du Berger, R., Roy, D.W., Lamontagne, M., Woussen, G., North, R.G., et Wetmiller, R.J. 1991. The Saguenay (Quebec) earthquake of November 25, 1988: seismologic data and geologic setting. Tectonophysics **186**(1-2): 59–74.

Dugamin, E.J., Cathelineau, M., Boiron, M.-C., Richard, A., et Despinois, F. 2023. Lithium enrichment processes in sedimentary formation waters. Chemical Geology **635**: 121626.

Dyke, A.S., et Prest, V.K. 1987. Late Wisconsinan and Holocene history of the Laurentide ice sheet. Géographie Physique et Quaternaire **41**(2): 237–263.

Edmunds, W., Andrews, J., Burgess, W., Kay, R., et Lee, D. 1984. The evolution of saline and thermal groundwaters in the Carnmenellis granite. Mineralogical Magazine **48**(348): 407–424.

Edmunds, W., Guendouz, A., Mamou, A., Moulla, A., Shand, P., et Zouari, K. 2003. Groundwater evolution in the Continental Intercalaire aquifer of southern Algeria and Tunisia: trace element and isotopic indicators. Applied Geochemistry **18**(6): 805–822.

Edwards, C.T., Saltzman, M.R., Leslie, S.A., Bergström, S.M., Sedlacek, A.R., Howard, A., Bauer, J.A., Sweet, W.C., et Young, S.A. 2015. Strontium isotope (87Sr/86Sr) stratigraphy of Ordovician bulk carbonate: Implications for preservation of primary seawater values. Bulletin **127**(9-10): 1275–1289.

Eggenkamp, H., et Coleman, M.L. 2009. The effect of aqueous diffusion on the fractionation of chlorine and bromine stable isotopes. Geochimica et Cosmochimica Acta **73**(12): 3539–3548.

Eggenkamp, H., Louvat, P., Agrinier, P., Bonifacie, M., Bekker, A., Krupenik, V., Griffioen, J., Horita, J., Brocks, J., et Bagheri, R. 2019. The bromine and chlorine isotope composition of primary halite deposits and their significance for the secular isotope composition of seawater. Geochimica et Cosmochimica Acta **264**: 13–29.

Farnham, I.M., Singh, A.K., Stetzenbach, K.J., et Johannesson, K.H. 2002. Treatment of nondetects in multivariate analysis of groundwater geochemistry data. Chemometrics and Intelligent Laboratory Systems **60**(1-2): 265–281.

Farvolden, R., Pfannkuch, O., Pearson, R., et Fritz, P. 1988. The Geology of North America, The Geological Society of America, 19th edition: Chapter 15 Region 12, Precambrian Shield. Hydrogeology **O-2**: 101–114.

Ferguson, G., McIntosh, J., Warr, O., et Sherwood Lollar, B. 2023. The low permeability of the Earth's Precambrian crust. Communications Earth & Environment **4**(1): 323.

Ferguson, G., McIntosh, J.C., Warr, O., Sherwood Lollar, B., Ballentine, C.J., Famiglietti, J.S., Kim, J.H., Michalski, J.R., Mustard, J.F., et Tarnas, J. 2021. Crustal groundwater volumes greater than previously thought. Geophysical Research Letters **48**(16): e2021GL093549.

Folk, R.L., et Land, L.S. 1975. Mg/Ca ratio and salinity: two controls over crystallization of dolomite. AAPG Bulletin **59**(1): 60–68.

Frampton, A. 2025. Flow channelling and variability in transit times and tortuosity in a fractured rock model with small scale heterogeneity. Advances in Geosciences **65**: 149–158.

Frape, S., Blyth, A., Blomqvist, R., McNutt, R., et Gascoyne, M. 2003. Deep fluids in the continents: II. Crystalline rocks. Treatise on Geochemistry **5**: 605.

Frape, S., et Fritz, P. 1982. The chemistry and isotopic composition of saline groundwaters from the Sudbury Basin, Ontario. Canadian Journal of Earth Sciences **19**(4): 645–661.

Frape, S., et Fritz, P. 1987. Geochemical trends for groundwaters from the Canadian Shield. Geological Association of Canada-Special Paper **33**: 19–38.

Frape, S., Fritz, P., et McNutt, R.t. 1984. Water-rock interaction and chemistry of groundwaters from the Canadian Shield. Geochimica et Cosmochimica Acta **48**(8): 1617–1627.

Freeze, R.A., et Cherry, J.A. 1979. Groundwater Prentice-Hall Inc. Eaglewood Cliffs, NJ.

Frost, C.D., et Toner, R.N. 2004. Strontium isotopic identification of water-rock interaction and ground water mixing. Groundwater **42**(3): 418–432.

Galloway, D.L. 2010. The complex future of hydrogeology. Hydrogeology Journal **18**(4): 807–810.

Gao, G., et Land, L.S. 1991. Geochemistry of Cambro-Ordovician Arbuckle limestone, Oklahoma: Implications for diagenetic δ18O alteration and secular δ13C and 87Sr86Sr variation. Geochimica et Cosmochimica Acta **55**(10): 2911–2920.

Gascoyne, M., et Kamineni, D. 1994. The hydrogeochemistry of fractured plutonic rocks in the Canadian Shield. Applied Hydrogeology **2**(2): 43–49.

Gerber, C., Vaikmäe, R., Aeschbach, W., Babre, A., Jiang, W., Leuenberger, M., Lu, Z.-T., Mokrik, R., Müller, P., et Raidla, V. 2017. Using 81Kr and noble gases to characterize and date groundwater and brines in the Baltic Artesian Basin on the one-million-year timescale. Geochimica et Cosmochimica Acta **205**: 187–210.

Gimeno, M.J., Auqué, L.F., Acero, P., et Gómez, J.B. 2014. Hydrogeochemical characterisation and modelling of groundwaters in a potential geological repository for spent nuclear fuel in crystalline rocks (Laxemar, Sweden). Applied Geochemistry **45**: 50–71.

Gimeno, M.J., Auque, L.F., Gomez, J.B., et Acero, P. 2009. Water-rock interaction modelling and uncertainties of mixing modelling. SDM-Site Laxemar. Swedish Nuclear Fuel and Waste Management Co. SKB R-08-110.

Gimeno, M.J., Tullborg, E.-L., Nilsson, A.-C., Auqué, L.F., et Nilsson, L. 2023. Hydrogeochemical characterisation of the groundwater in the crystalline basement of Forsmark, the selected area for the geological nuclear repositories in Sweden. Journal of Hydrology **624**: 129818.

Goldberg, E., Broecker, W., Gross, M., et Turekian, K. 1971. Radioactivity in the marine environment. National Academy of Science, Washington, DC **137**.

Goode, D.J. 1996. Direct simulation of groundwater age. Water Resources Research **32**(2): 289–296.

Grasby, S.E., Jessop, A., Kelman, M., Ko, M., Chen, Z., Allen, D., Bell, S., Ferguson, G., Majorowicz, J., et Moore, M. 2011. Geothermal energy resource potential of Canada. Geological Survey of Canada. 6914. p. 283.

Greene, S., Battye, N., Clark, I., Kotzer, T., et Bottomley, D. 2008. Canadian Shield brine from the Con Mine, Yellowknife, NT, Canada: Noble gas evidence for an evaporated Palaeozoic seawater origin mixed with glacial meltwater and Holocene recharge. Geochimica et Cosmochimica Acta **72**(16): 4008–4019.

Grenthe, I., Stumm, W., Laaksuharju, M., Nilsson, A., et Wikberg, P. 1992. Redox potentials and redox reactions in deep groundwater systems. Chemical Geology **98**(1-2): 131–150.

Guha, J., et Kanwar, R. 1987. Vug brines-fluid inclusions: a key to the understanding of secondary gold enrichment processes and the evolution of deep brines in the Canadian Shield. *Dans* Saline water and gases in crystalline rocks. Ottawa: Geological Association of Canada Special Paper. pp. 95–101.

Güler, C., Thyne, G.D., McCray, J.E., et Turner, K.A. 2002. Evaluation of graphical and multivariate statistical methods for classification of water chemistry data. Hydrogeology Journal **10**(4): 455–474.

Hanor, J.S. 1994. Origin of saline fluids in sedimentary basins. Geological Society, London, Special Publications **78**(1): 151–174.

Hébert, C., Cadieux, A.-M., et Breemen, O.v. 2005. Temporal evolution and nature of Ti Fe P mineralization in the anorthosite mangerite charnockite granite (AMCG) suites of the south-central Grenville Province, Saguenay Lac St. Jean area, Quebec, Canada. Canadian Journal of Earth Sciences **42**(10): 1865–1880.

Hébert, C., et Lacoste, P. 1998. Géologie de la région de Jonquière-Chicoutimi Ministère des Ressources naturelles du Québec. . RG 97-08. p. 32.

Hébert, C., et Van Breemen, O. 2004. Mesoproterozoic basement of the Lac St. Jean Anorthosite Suite and younger Grenvillian intrusions in the Saguenay region, Québec: structural relationships and U-Pb geochronology. *Dans* Proterozoic tectonic evolution of the Grenville orogen in North America. *Sous la direction de* L.C. R. P. Tollo, J. M. McLelland & M. J. Bartholomew (Eds.). Geological Society of America. pp. 65–80.

Hebig, K.H., Ito, N., Scheytt, T., et Marui, A. 2012. Deep groundwater research with focus on Germany. Hydrogeology Journal **20**(2): 227.

Helgeson, H.C. 1978. Summary and critique of the thermodynamic properties of rock-forming minerals. American Journal of Science, A **278**: 1–229.

Hermans, T., Goderniaux, P., Jougnot, D., Fleckenstein, J.H., Brunner, P., Nguyen, F., Linde, N., Huisman, J.A., Bour, O., Alvis, J.L., Hoffmann, R., Palacios, A., Cooke, A.K., Á, P.-Á., Blazevic, L.,

Pouladi, B., Haruzi, P., Visentini, A.F., Nogueira, G.E.H., Tirado-Conde, J., Looms, M.C., Kenshilikova, M., Davy, P., et Borgne, T.L. 2023. Advancing measurements and representations of subsurface heterogeneity and dynamic processes: towards 4D hydrogeology Hydrology and Earth System Sciences **27**: 255–287. Disponible à http://dx.doi.org/10.5194/hess-27-255-2023 [cité.

Herut, B., Starinsky, A., Katz, A., et Bein, A. 1990. The role of seawater freezing in the formation of subsurface brines. Geochimica et Cosmochimica Acta **54**(1): 13–21.

Hiscock, K.M., et Bense, V.F. 2014. Hydrogeology: principles and practice. John Wiley & Sons éd. Wiley-Blackwell, Chichester, United Kingdom.

Hobbs, M.Y., Frape, S.K., Shouakar-Stash, O., et Kennell, L.R. 2011. Regional Hydrogeochemistry – Southern Ontario. Nuclear Waste Management Organization. NWMO DGR-TR-2011-12. p. 156.

Holland, G., Sherwood-Lollar, B., Li, L., Lacrampe-Couloume, G., Slater, G., et Ballentine, C. 2013. Deep fracture fluids isolated in the crust since the Precambrian era. Nature **497**(7449): 357–360.

Houyun, S., Xiaoming, S., Xiaofeng, W., Ziran, C., Wei, L., Xingkai, H., Xia, L., Zhiqiang, Y., et Wenbo, L. 2022. Formation mechanism of metasilicate mineral water in Chengde, Hebei Province: Evidence from rock weathering and water-rock interaction. Geology in China **49**(4): 1088–1113.

Hoyer, M., Kummer, N.-A., et Merkel, B. 2015. Sorption of lithium on bentonite, kaolin and zeolite. Geosciences **5**(2): 127–140.

Hsissou, Y., Mudry, J., Mania, J., Bouchaou, L., et Chauve, P. 1999. Utilisation du rapport Br/Cl pour déterminer l'origine de la salinité des eaux souterraines: exemple de la plaine du Souss (Maroc). Comptes Rendus de l'Académie des Sciences-Series IIA-Earth and Planetary Science **328**(6): 381–386.

Hu, R., et Walsh, S.D. 2022. The Role of Heterogeneity on Deformation and Flow in Fractured Coal Slopes. Minerals **12**(10): 1297.

Huet, M., Chesnaux, R., Boucher, M.-A., et Poirier, C. 2016. Comparing various approaches for assessing groundwater recharge at a regional scale in the Canadian Shield. Hydrological Sciences Journal **61**(12): 2267–2283.

Hutcheon, I. 2000. Principles of diagenesis and what drives mineral change. Fluids and Basin Evolution **28**: 93–114.

Janos, D., Molson, J., et Lefebvre, R. 2018. Regional groundwater flow dynamics and residence times in Chaudière-Appalaches, Québec, Canada: Insights from numerical simulations. Canadian Water Resources Journal/Revue Canadienne des Ressources Hydriques **43**(2): 214–239.

Jiang, W., Sheng, Y., Wang, G., Shi, Z., Liu, F., Zhang, J., et Chen, D. 2022. Cl, Br, B, Li, and noble gases isotopes to study the origin and evolution of deep groundwater in sedimentary basins: a review. Environmental Chemistry Letters: 1–32.

Jiang, X.W., Wan, L., Wang, X.S., Ge, S., et Liu, J. 2009. Effect of exponential decay in hydraulic conductivity with depth on regional groundwater flow. Geophysical Research Letters **36**(24).

Jones, B., et Deocampo, D. 2003. Geochemistry of saline lakes. Treatise on Geochemistry **5**: 605.

Kaiser, H.F. 1960. The application of electronic computers to factor analysis. Educational and Psychological Measurement **20**(1): 141–151.

Kaleem, M., Naseem, S., Bashir, E., Shahab, B., et Rafique, T. 2021. Discrete geochemical behavior of Sr and Ba in the groundwater of Southern Mor Range, Balochistan, a tracer for igneous and sedimentary rocks weathering and related environmental issues. Applied Geochemistry **130**: 104996.

Kaufmann, R.S., Frape, S., McNutt, R., et Eastoe, C. 1993. Chlorine stable isotope distribution of Michigan Basin formation waters. Applied Geochemistry **8**(4): 403–407.

Kelly, W.C., Rye, R.O., et Livnat, A. 1986. Saline minewaters of the Keweenaw Peninsula, northern Michigan; their nature, origin, and relation to similar deep waters in Precambrian crystalline rocks of the Canadian Shield. American Journal of Science **286**(4): 281–308.

Kharaka, Y., Maest, A., Carothers, W., Law, L., Lamothe, P., et Fries, T. 1987. Geochemistry of metal-rich brines from central Mississippi Salt Dome basin, USA. Applied Geochemistry **2**(5-6): 543–561.

Kharaka, Y.K., et Berry, F.A. 1973. Simultaneous flow of water and solutes through geological membranes—I. Experimental investigation. Geochimica et Cosmochimica Acta **37**(12): 2577–2603. doi: https://doi.org/10.1016/0016-7037(73)90267-6.

Kharaka, Y.K., et Dorsey, N.S. 2005. Environmental issues of petroleum exploration and production: Introduction. Environmental Geosciences **12**(2): 61–63.

Kharaka, Y.K., et Hanor, J. 2003. Deep fluids in the continents: I. Sedimentary basins. Treatise on Geochemistry **5**: 605.

Kim, J.-H., Bailey, L., Noyes, C., Tyne, R.L., Ballentine, C.J., Person, M., Ma, L., Barton, M., Barton, I., et Reiners, P.W. 2022. Hydrogeochemical evolution of formation waters responsible for sandstone bleaching and ore mineralization in the Paradox Basin, Colorado Plateau, USA. Bulletin **134**(9-10): 2589–2610.

Kısakűrek, B., James, R.H., et Harris, N.B. 2005. Li and δ7Li in Himalayan rivers: proxies for silicate weathering? Earth and Planetary Science Letters **237**(3-4): 387–401.

Kloppmann, W., Bourhane, A., et Asfirane, F. 2011. Méthodologie de diagnostic de l'origine de la salinité des masses d'eau. BRGM. p. 129.

Kuchling, K., Chorley, D., et Zawadzki, W. 2000. Hydrogeological modeling of mining operations at the Diavik Diamonds project. Proceedings of the Sixth International Symposium on Environmental Issues and Management of Waste in Energy and Mineral Production. Taylor and Francis, Calgary, Alberta, 30 May–2 June, pp. pp 1–8.

Kukkonen, I., et Peltonen, P. 1999. Xenolith-controlled geotherm for the central Fennoscandian Shield: implications for lithosphere–asthenosphere relations. Tectonophysics **304**(4): 301–315.

Laaksoharju, M., Skaarman, C., Smellie, J., et Nilsson, A. 1995. Groundwater sampling and chemical characterisation of the Laxemar deep borehole KLX02. Swedish Nuclear Fuel and Waste Management Co.

Laaksoharju, M., Tullborg, E.-L., Wikberg, P., Wallin, B., et Smellie, J. 1999. Hydrogeochemical conditions and evolution at the Äspö HRL, Sweden. Applied Geochemistry **14**(7): 835–859.

Lamontagne, M., et Brouillette, P. 2022. Faults and lineaments of the Quebec City, Charlevoix and Saguenay–Lac-St-Jean regions, Québec. Geological Survey of Canada. Open File 8826. p. 38.

Land, L., et Macpherson, G. 1992. Geothermometry from brine analyses: lessons from the Gulf Coast, USA. Applied Geochemistry **7**(4): 333–340.

Lapperre, R.E., Kasse, C., Bense, V.F., Woolderink, H.A., et Van Balen, R.T. 2019. An overview of fault zone permeabilities and groundwater level steps in the Roer Valley Rift System. Netherlands Journal of Geosciences **98**: e5.

LaSalle, P., et Tremblay, G. 1978. Dépôts meubles Saguenay-Lac-Saint-Jean. Québec (Province), Direction générale de la recherche géologique et minérale. RG191. p. 61.

Laurin, A., et Sharma, K. 1975. Mistassini, Péribonka, Saguenay rivers area: Grenville 1965–1967. Ministère des Richesses naturelles, Direction générale des Mines, Service de l'Exploration géologique. Rapport géologique No. 161. p. 89.

Le Chatelier, H.L. 1884. A general statement of the laws of chemical equilibrium. Comptes Rendus **99**: 786–789.

Le Roux, G.I., Laverret, E., et Shotyk, W. 2006. Fate of calcite, apatite and feldspars in an ombrotrophic peat bog, Black Forest, Germany. Journal of the Geological Society **163**(4): 641–646.

Lefebvre, R., Ballard, J.-M., Carrier, M.-A., Vigneault, H., Beaudry, C., Berthot, L., Légaré-Couture, G., Parent, M., Laurencelle, M., et Malet, X. 2015. Portrait des ressources en eau souterraine en Chaudière-Appalaches, Québec, Canada: Rapport final (version révisée).

Lemieux, J.M., Sudicky, E., Peltier, W., et Tarasov, L. 2008a. Simulating the impact of glaciations on continental groundwater flow systems: 2. Model application to the Wisconsinian glaciation over the Canadian landscape. Journal of Geophysical Research: Earth Surface **113**(F3).

Lemieux, J.M., Sudicky, E.A., Peltier, W.R., et Tarasov, L. 2008b. Simulating the impact of glaciations on continental groundwater flow systems: 1. Relevant processes and model formulation. Journal of Geophysical Research: Earth Surface **113**(F3).

Li, C., Gao, X., Li, S., et Bundschuh, J. 2020. A review of the distribution, sources, genesis, and environmental concerns of salinity in groundwater. Environmental Science and Pollution Research: 1–18.

Li, K., Cai, C., Tan, X., Jiang, H., et Fan, J. 2022. Massive dolomitization driven by MgSO4-rich seawater and its effects on thermochemical sulfate reduction, Upper Permian Changxing Formation, northeastern Sichuan, China. Energy Exploration & Exploitation **40**(5): 1315–1343.

Lichtner, P.C., Kelkar, S., et Robinson, B. 2002. New form of dispersion tensor for axisymmetric porous media with implementation in particle tracking. Water Resources Research **38**(8): 21–21–21–16.

Liu, H., Giroux, B., Harris, L.B., Quenette, S.M., et Mansour, J. 2018. Numerical analysis of the role of radiogenic basement on temperature distribution in the St. Lawrence Lowlands, Québec. Geothermal Energy **6**(1): 30.

Llewellyn, G.T. 2014. Evidence and mechanisms for Appalachian Basin brine migration into shallow aquifers in NE Pennsylvania, USA. Hydrogeology Journal **22**(5): 1055.

Lucas, Y., Schmitt, A., Chabaux, F., Clément, A., Fritz, B., Elsass, P., et Durand, S. 2010. Geochemical tracing and hydrogeochemical modelling of water–rock interactions during salinization of alluvial groundwater (Upper Rhine Valley, France). Applied Geochemistry **25**(11): 1644–1663.

McCaffrey, M., Lazar, B., et Holland, H. 1987. The evaporation path of seawater and the coprecipitation of Br (super-) and K (super+) with halite. Journal of Sedimentary Research **57**(5): 928–937.

McCallum, J.L., Dogramaci, S., Bai, A., Cook, P.G., Engdahl, N.B., Simmons, C.T., Skrzypek, G., et Grierson, P.F. 2020. Assessing temporal changes in groundwater recharge using spatial variations in groundwater ages. Water Resources Research **56**(8): e2020WR027240.

McDonough, L.K., Meredith, K.T., Nikagolla, C., et Banati, R.B. 2021. The influence of water–rock interactions on household well water in an area of high prevalence chronic kidney disease of unknown aetiology (CKDu). NPJ Clean Water **4**(1): 2.

McIntosh, J., Schlegel, M., et Person, M. 2012. Glacial impacts on hydrologic processes in sedimentary basins: evidence from natural tracer studies. Geofluids **12**(1): 7–21.

McIntosh, J., et Walter, L. 2005. Volumetrically significant recharge of Pleistocene glacial meltwaters into epicratonic basins: Constraints imposed by solute mass balances. Chemical Geology **222**(3-4): 292–309.

McIntosh, J.C., et Ferguson, G. 2021. Deep meteoric water circulation in Earth's crust. Geophysical Research Letters **48**(5): e2020GL090461.

McKight, P.E., et Najab, J. 2010. Kruskal-wallis test. The Corsini Encyclopedia of Psychology: 1–1.

McNutt, R.H., Frape, S.K., et Fritz, P. 1984. Strontium isotopic composition of some brines from the Precambrian Shield of Canada. Chemical Geology **46**(3): 205–215.

McNutt, R.H., Frape, S.K., Fritz, P., Jones, M.G., et MacDonald, I.M. 1990. The 87Sr86Sr values of Canadian Shield brines and fracture minerals with applications to groundwater mixing, fracture history, and geochronology. Geochimica et Cosmochimica Acta **54**(1): 205–215.

Méjean, P., Pinti, D.L., Kagoshima, T., Roulleau, E., Demarets, L., Poirier, A., Takahata, N., Sano, Y., et Larocque, M. 2020. Mantle helium in Southern Quebec groundwater: A possible fossil record of the New England hotspot. Earth and Planetary Science Letters **545**: 116352.

Meyzonnat, G., Musy, S., Corcho-Alvarado, J., Barbecot, F., Pinti, D., Purtschert, R., Lauzon, J.-M., et McCormack, R. 2023. Age distribution of groundwater in fractured aquifers of the St. Lawrence Lowlands (Canada) determined by environmental tracers (3H/3He, 85Kr, SF6, CFC-12, 14C). Hydrogeology Journal **31**(8): 2139–2157.

Millot, R., Vigier, N., et Gaillardet, J. 2010. Behaviour of lithium and its isotopes during weathering in the Mackenzie Basin, Canada. Geochimica et Cosmochimica Acta **74**(14): 3897–3912.

Mizutani, S. 1970. Silica minerals in the early stage of diagenesis. Sedimentology **15**(3-4): 419–436.

Molofsky, L.J. 2023. Isotopic Insights into Water of Condensation, Cross-Formation Water Flow, and Natural Hydrocarbon Migration in Sedimentary Basins. Doctoral dissertation, Geological Sciences The University of Texas at El Paso, Texas, United States.

Molson, J., et Frind, E. 2012. On the use of mean groundwater age, life expectancy and capture probability for defining aquifer vulnerability and time-of-travel zones for source water protection. Journal of Contaminant Hydrology **127**(1-4): 76–87.

Molson, J., et Frind, E. 2023. FLONET/TR2, user guide version 6.0; a two-dimensional simulator for groundwater flownets, contaminant transport and residence time. *Dans* Université Laval and University of Waterloo.

Montcoudiol, N., Molson, J., et Lemieux, J.-M. 2017. Numerical modelling in support of a conceptual model for groundwater flow and geochemical evolution in the southern Outaouais Region, Quebec,

Canada. Canadian Water Resources Journal/Revue Canadienne des Ressources Hydriques **43**(2): 240–261.

Montcoudiol, N., Molson, J., Lemieux, J.-M., et Cloutier, V. 2015. A conceptual model for groundwater flow and geochemical evolution in the southern Outaouais Region, Québec, Canada. Applied Geochemistry **58**: 62–77.

Morales-Arredondo, J., Hernández, M.A., Cuellar-Ramírez, E., Morton-Bermea, O., et Ortega-Gutiérrez, J. 2022. Hydrogeochemical behavior of Ba, B, Rb, and Sr in an urban aquifer located in central Mexico and its environmental implications. Journal of South American Earth Sciences **116**: 103870.

Morgan, A.L.F. 2018a. Low temperature geothermal resources in abandoned mines of the Canadian Shield: a case study in the Chapais and Chibougamau area, Québec, Canada.

Morgan, A.L.F. 2018b. Low temperature geothermal resources in abandoned mines of the Canadian Shield: a case study in the Chapais and Chibougamau area, Québec, Canada. Master's Thesis, Department of Engineering, Reykjavík University, Reykjavik, Islande.

Moussaoui, I., Rosa, E., Cloutier, V., Neculita, C.M., et Dassi, L. 2023. Chemical and isotopic evaluation of groundwater salinization processes in the Djebeniana coastal aquifer, Tunisia. Applied Geochemistry **149**: 105555.

Nagaraju, P., Ray, L., Ravi, G., Akkiraju, V.V., et Roy, S. 2012. Geothermal investigations in the Upper Vindhyan sedimentary rocks of Shivpuri area, central India. Journal of the Geological Society of India **80**: 39–47.

Négrel, P. 1999. Geochemical study of a granitic area–the Margeride Mountains, France: chemical element behavior and 87Sr/86Sr constraints. Aquatic Geochemistry **5**: 125–165.

Négrel, P., Casanova, J., et Aranyossy, J.-F. 2001. Strontium isotope systematics used to decipher the origin of groundwaters sampled from granitoids: the Vienne Case (France). Chemical Geology **177**(3-4): 287–308.

Négrel, P., Lemiere, B., Machard de Grammont, H., Billaud, P., et Sengupta, B. 2007. Hydrogeochemical processes, mixing and isotope tracing in hard rock aquifers and surface waters from the Subarnarekha River Basin,(east Singhbhum District, Jharkhand State, India). Hydrogeology Journal **15**: 1535–1552.

Neretnieks, I. 2024. Saline groundwaters counteract up-flow of contaminants-implications for radionuclide repositories? Journal of Contaminant Hydrology **262**: 104309.

Neuzil, C.E., et Person, M. 2017. Reexamining ultrafiltration and solute transport in groundwater. Water Resources Research **53**(6): 4922–4941.

Ngombe, O.G., Walter, J., Chesnaux, R., et Molson, J. 2024. Application of hierarchical cluster analysis and principal component analysis to identify compositional trends of brine in crystalline basements and sedimentary basins. Applied Geochemistry: 106030.

Ngombe, O.G.D., Walter, J., Molson, J., et Chesnaux, R. 2025. Numerical modeling and isotopic evidence of upwelling and mixing of deep, old groundwater with shallow fresh groundwater within the Grenville Province of the Canadian Shield. Hydrogeology Journal. doi: 10.1007/s10040-025-02914-2.

Nisson, D., Kieft, T., Drake, H., Warr, O., Lollar, B.S., Ogasawara, H., Perl, S., Friefeld, B., Castillo, J., et Whitehouse, M.J. 2023. Hydrogeochemical and isotopic signatures elucidate deep subsurface hypersaline brine formation through radiolysis driven water-rock interaction. Geochimica et Cosmochimica Acta **340**: 65–84.

Nisson, D.M. 2023. Hydrogeochemical Support for Microbial Habitability in an Ancient, Hypersaline, Thermal, and Radiogenic Subsurface Brine in South Africa. Doctoral dissertation, Department of Geosciences, Princeton University, New Jersey, United States.

Norden, B., et Fröster, A. 2006. Thermal conductivity and radiogenic heat production of sedimentary and magmatic rocks in the Northeast German Basin. AAPG Bulletin **90**(6): 939–962.

Nordström, D., Andrews, J., Carlsson, L., Fontes, J.-C., Frits, P., Moser, H., et Olsson, T. 1985. Hydrogeological and hydrogeochemical investigations in boreholes-final report of the phase I geochemical investigations of the Stripa groundwaters. Swedish Nuclear Fuel and Waste Management Co.

Nordstrom, D., et Ball, J.W. 1989. Mineral saturation states in natural waters and their sensitivity to thermodynamic and analytic errors. Etat de saturation des minéraux dans les eaux naturelles et sensibilité des tests aux données thermodynamiques et aux erreurs analytiques. Sciences Géologiques, Bulletins et Mémoires **42**(4): 269–280.

Nordstrom, D.K., Ball, J.W., Donahoe, R.J., et Whittemore, D. 1989. Groundwater chemistry and water-rock interactions at Stripa. Geochimica et Cosmochimica Acta **53**(8): 1727–1740.

Normani, S., et Sykes, J. 2012. Paleohydrogeologic simulations of Laurentide ice-sheet history on groundwater at the eastern flank of the Michigan Basin. Geofluids **12**(1): 97–122.

Nurmi, P.A., Kukkonen, I.T., et Lahermo, P.W. 1988. Geochemistry and origin of saline groundwaters in the Fennoscandian Shield. Applied Geochemistry **3**(2): 185–203.

Oviedo, M.J., Raymond, J., Blessent, D., et Larmagnat, S. 2025. Numerical assessment of the geothermal resource potential of the Charlevoix meteorite impact crater, Canada. Geothermics **127**: 103243.

Papizadeh, M., Roayaei Ardakani, M., Fakour, H., Ghaderi, G., et Firouzei, Y. 2017. Microbio-ecology and hydro-geochemistry of saline sulfur springs of Ghale-Madreseh, Khuzestan, Iran. Pollution **3**(4): 623–637.

Patchett, P., Embry, A., Ross, G., Beauchamp, B., Harrison, J., Mayr, U., Isachsen, C., Rosenberg, E., et Spence, G. 2004. Sedimentary cover of the Canadian Shield through Mesozoic time reflected by Nd isotopic and geochemical results for the Sverdrup Basin, Arctic Canada. The Journal of Geology **112**(1): 39–57.

Pauwels, H., Fouillac, C., et Fouillac, A.-M. 1993. Chemistry and isotopes of deep geothermal saline fluids in the Upper Rhine Graben: Origin of compounds and water-rock interactions. Geochimica et Cosmochimica Acta **57**(12): 2737–2749.

Peiffer, L., Taran, Y., Lounejeva, E., Solís-Pichardo, G., Rouwet, D., et Bernard-Romero, R. 2011. Tracing thermal aquifers of El Chichón volcano–hydrothermal system (México) with 87Sr/86Sr, Ca/Sr and REE. Journal of Volcanology and Geothermal Research **205**(3-4): 55–66.

Perri, F. 2020. Chemical weathering of crystalline rocks in contrasting climatic conditions using geochemical proxies: an overview. Palaeogeography, Palaeoclimatology, Palaeoecology **556**: 109873.

Person, M., McIntosh, J., Bense, V., et Remenda, V. 2007. Pleistocene hydrology of North America: The role of ice sheets in reorganizing groundwater flow systems. Reviews of Geophysics **45**(3).

Person, M.A., et Sazeed, N. 2022. Continental Brackish Groundwater Resources. *Dans* Unconventional Water Resources. Springer. pp. 111–128.

Pinti, D.L. 2025. Earth's exhale: Geochemistry. Nature Geoscience: 1–2.

Pinti, D.L., Béland-Otis, C., Tremblay, A., Castro, M.C., Hall, C.M., Marcil, J.-S., Lavoie, J.-Y., et Lapointe, R. 2011. Fossil brines preserved in the St-Lawrence Lowlands, Québec, Canada as revealed by their chemistry and noble gas isotopes. Geochimica et Cosmochimica Acta **75**(15): 4228–4243.

Pinti, D.L., Larocque, M., Méjean, P., Saby, M., Hernández-Hernández, M.A., Gagné, S., Roulleau, E., Sano, Y., Castro, M.C., et Matsumoto, T. 2022. Regional-scale distribution of helium isotopes in aquifers: how informative are they as groundwater tracers and chronometers? Water **14**(12): 1940.

Plummer, L.N. 1988. A computer program incorporating Pitzer's equations for calculation of geochemical reactions in brines. Department of the Interior, US Geological Survey.

Pohlert, T. 2016. Non-parametric trend tests and change-point detection. CC BY-ND **4**.

Pohlert, T. 2020. Non-Parametric Trend Tests and Change-Point Detection. 1.1.6. R Foundation for Statistical Computing, Vienna, Austria. https://CRAN.R-project.org/package=trend.

Qi, H., Ma, C., He, Z., Hu, X., et Gao, L. 2019. Lithium and its isotopes as tracers of groundwater salinization: a study in the southern coastal plain of Laizhou Bay, China. Science of The Total Environment **650**: 878–890.

Qian, K., Sun, H., Li, J., et Xie, X. 2023. Strontium isotopes as tracers for water-rocks interactions of groundwater to delineate iodine enrichment in aquifer of Datong Basin, northern China. Applied Geochemistry **158**: 105783.

Qing, H., Barnes, C.R., Buhl, D., et Veizer, J. 1998. The strontium isotopic composition of Ordovician and Silurian brachiopods and conodonts: relationships to geological events and implications for coeval seawater. Geochimica et Cosmochimica Acta **62**(10): 1721–1733.

Raposo, J., Molinero, J., et Dafonte, J. 2012. Parameterization and quantification of recharge in crystalline fractured bedrocks in Galicia-Costa (NW Spain). Hydrology and Earth System Sciences **16**(6): 1667–1683.

Reimann, C., et Filzmoser, P. 2000. Normal and lognormal data distribution in geochemistry: Death of a myth. Consequences for the statistical treatment of geochemical and environmental data. Environmental Geology **39**(9).

Richard, D., Rafini, S., et Walter, J. 2024. Natural metal contents and influence of salinization in deep Canadian Shield groundwater: Base level versus mineral deposit enrichment halos. Applied Geochemistry **170**: 106078.

Richard, S., Chesnaux, R., et Rouleau, A. 2011. Estimating the hydraulic properties of aquifers from specific capacity data: Saguenay-Lac-Saint-Jean, Quebec. *Sous la direction de*. *Dans* Proceedings of GeoHydro 2011, Joint Meeting of the Canadian Quaternary Association and the Canadian Chapter of the International Association of Hydrogeologists, Canada, pp. 28–31.

Richard, S.K., Chesnaux, R., Rouleau, A., et Coupe, R.H. 2016. Estimating the reliability of aquifer transmissivity values obtained from specific capacity tests: examples from the Saguenay-Lac-Saint-Jean aquifers, Canada. Hydrological Sciences Journal **61**(1): 173–185.

Ring, S.J., Henehan, M.J., Blukis, R., et von Blanckenburg, F. 2025. Adsorption pathways of boron on clay and their implications for boron cycling on land and in the ocean. Geochimica et Cosmochimica Acta **389**: 74–83.

Rittenhouse, G. 1967. Bromine in oil-field waters and its use in determining possibilities of origin of these waters. AAPG Bulletin **51**(12): 2430–2440.

Rivers, T., Martignole, J., Gower, C., et Davidson, A. 1989. New tectonic divisions of the Grenville Province, southeast Canadian Shield. Tectonics **8**(1): 63–84.

Rouleau, A., Daigneault, R., Walter, J., Germaneau, D., Tremblay, M.L., et Lambert, M. 2013. Résultats du programme d'acquisition de connaissances sur les eaux souterraines de la région Saguenay-Lac-Saint-Jean (Results of the groundwater knowledge acquisition programme in the Saguenay-Lac-Saint-Jean region). Ministère du Développement durable, de l'Environnement et de la Lutte contre les changements climatiques (Ministry of Sustainable Development, Environment and the Fight Against Climate Change), MDDELCC p. 248.

Roy, D., Schmitt, L., Woussen, G., et DuBerger, R. 1993. Lineaments from airborne SAR images and the 1988 Saguenay earthquake, Quebec, Canada. Photogrammetric Engineering and Remote Sensing **59**(8): 1299–1305.

Roy, D.W., Beaudoin, G., Leduc, É., Rouleau, A., Walter, J., Chesnaux, R., et Cousineau, P.A. 2011. Isostasie postglaciaire différentielle au Lac-Saint-Jean (Québec) et implications sur la qualité de l'eau souterraine. Geohydro 2011, Québec.

Ruppel, S.C., Jones, R.H., Breton, C.L., et Kane, J.A. 2005. Preparation of maps depicting geothermal gradient and Precambrian structure in the Permian basin. USGS Order(04CRSA0834).

Saby, M., Larocque, M., Pinti, D.L., Barbecot, F., Sano, Y., et Castro, M.C. 2016. Linking groundwater quality to residence times and regional geology in the St. Lawrence Lowlands, southern Quebec, Canada. Applied geochemistry **65**: 1–13.

Sall, J., Stephens, M.L., Lehman, A., et Loring, S. 2017. JMP start statistics: a guide to statistics and data analysis using JMP. 6 éd. SAS Institute Inc., Cary, North Carolina, United States.

Savoye, S. 1998. Origine de la salinité des eaux souterraines en milieu granitique: identification et caractérisation des sources de chlorure. Thèse de doctorat, Terre, océan, espace, Paris 11, Paris, France.

Shand, P., Darbyshire, D.F., Love, A.J., et Edmunds, W.M. 2009. Sr isotopes in natural waters: Applications to source characterisation and water–rock interaction in contrasting landscapes. Applied Geochemistry **24**(4): 574–586.

Sharqawy, M.H., Lienhard, J.H., et Zubair, S.M. 2010. Thermophysical properties of seawater: a review of existing correlations and data. Desalination and water treatment **16**(1-3): 354–380.

Sherwood-Lollar, B., Heuer, V.B., McDermott, J., Tille, S., Warr, O., Moran, J., Telling, J., et Hinrichs, K.-U. 2021. A window into the abiotic carbon cycle–Acetate and formate in fracture waters in 2.7 billion year-old host rocks of the Canadian Shield. Geochimica et Cosmochimica Acta **294**: 295–314.

Shouakar-Stash, O., Alexeev, S., Frape, S., Alexeeva, L., et Drimmie, R. 2007. Geochemistry and stable isotopic signatures, including chlorine and bromine isotopes, of the deep groundwaters of the Siberian Platform, Russia. Applied Geochemistry **22**(3): 589–605.

Snee, L.W. 2002. Argon thermochronology of mineral deposits; a review of analytical methods, formulations, and selected applications. Geological Survey (U.S.). Bulletin No. 2194. p. 39.

Snowdon, A.P., Normani, S.D., et Sykes, J.F. 2021. Analysis of crystalline rock permeability versus depth in a Canadian Precambrian rock setting. Journal of Geophysical Research: Solid Earth **126**(5): e2020JB020998.

Spivack, A., et Edmond, J. 1987. Boron isotope exchange between seawater and the oceanic crust. Geochimica et Cosmochimica Acta **51**(5): 1033–1043.

Stalder, H.A., Sicher, V., et Lussmann, L. 1980. Die Mineralien des Gotthardbahntunnels und des Gotthardstrassentunnels. Verlag nicht ermittelbar.

Stanienda-Pilecki, K.J. 2023. Crystals structures of carbonate phases with Mg in Triassic rocks, mineral formation and transitions. Scientific Reports **13**(1): 18759.

Starn, J.J., Kauffman, L.J., et Feinstein, D.T. 2023. Groundwater residence times in glacial aquifers—A new general simulation-model approach compared to conventional inset models. US Geological Survey. 2328-0328.

Steuber, T. 1999. Isotopic and chemical intra-shell variations in low-Mg calcite of rudist bivalves (Mollusca-Hippuritacea): disequilibrium fractionations and late Cretaceous seasonality. International Journal of Earth Sciences **88**: 551–570.

Stevenson, D., Kozak, E., Davison, C., Gascoyne, M., et Broadfoot, R. 1996. Hydrogeologic characteristics of domains of sparsely fractured rock in the granitic Lac du Bonnet Batholith, Southeastern Manitoba, Canada. Atomic Energy of Canada Limited Report.

Stober, I., et Bucher, K. 1999. Deep groundwater in the crystalline basement of the Black Forest region. Applied Geochemistry **14**(2): 237–254.

Stober, I., et Bucher, K. 2007. Hydraulic properties of the crystalline basement. Hydrogeology Journal **15**: 213–224.

Stotler, R.L., Frape, S.K., et Shouakar-Stash, O. 2010. An isotopic survey of δ81Br and δ37Cl of dissolved halides in the Canadian and Fennoscandian Shields. Chemical Geology **274**(1-2): 38–55.

Stueber, A.M., Saller, A.H., et Ishida, H. 1998. Origin, migration, and mixing of brines in the Permian basin: geochemical evidence from the eastern central basin platform, Texas. AAPG Bulletin **82**(9): 1652–1672.

Suckow, A. 2014. The age of groundwater–Definitions, models and why we do not need this term. Applied Geochemistry **50**: 222–230.

Taylor, S., Campbell, I., McCulloch, M., et McLennan, S. 1984. A lower crustal origin for massif-type anorthosites. Nature **311**(5984): 372–374.

Teiber, H., Marks, M.A., Wenzel, T., Siebel, W., Altherr, R., et Markl, G. 2014. The distribution of halogens (F, Cl, Br) in granitoid rocks. Chemical Geology **374**: 92–109.

Tellam, J.H. 1995. Hydrochemistry of the saline groundwaters of the lower Mersey Basin Permo-Triassic sandstone aquifer, UK. Journal of Hydrology **165**(1-4): 45–84.

Thorne, G. 2004. Hydrological processes in Precambrian Shield catchments of southeastern Manitoba. *Sous la direction de*. *Dans* AGU Spring Meeting Abstracts, pp. H53E–02.

Torgersen, T., Drenkard, S., Stute, M., Schlosser, P., et Shapiro, A. 1995. Mantle helium in ground waters of eastern North America: Time and space constraints on sources. Geology **23**(8): 675–678.

Torgersen, T., et Jenkins, W. 1982. Helium isotopes in geothermal systems: Iceland, the geysers, raft river and steamboat springs. Geochimica et Cosmochimica Acta **46**(5): 739–748.

Tóth, J. 1963. A theoretical analysis of groundwater flow in small drainage basins. Journal of Geophysical Research **68**(16): 4795–4812.

Tóth, J. 1978. Gravity-induced cross-formational flow of formation fluids, red earth region, Alberta, Canada: Analysis, patterns, and evolution. Water Resources Research **14**(5): 805–843.

Tóth, J. 1999. Groundwater as a geologic agent: an overview of the causes, processes, and manifestations. Hydrogeology Journal **7**(1): 1–14.

Tremblay, G. 1971. Structures sédimentaires dans les dépôts meubles, Saguenay-Lac-Saint-Jean, Québec. Cahiers de Géographie du Québec **15**(36): 537–546.

Tremblay, R., Walter, J., Chesnaux, R., et Boumaiza, L. 2021. Investigating the potential role of geological context on groundwater quality: a case study of the Grenville and St. Lawrence Platform Geological Provinces in Quebec, Canada. Geosciences **11**(12): 503.

Trudel, C., et Malo, M. 1993. Analyses des contraintes par méthodes graphiques dans une zone de coulissage: exemple de la région de Matapédia, Gaspésie, Appalaches du Québec. Canadian Journal of Earth Sciences **30**(3): 591–602.

Tyne, R., Broadley, M., Bekaert, D., Barry, P., Warr, O., Langman, J., Musan, I., Jenkins, W., et Seltzer, A. 2025. Passive degassing of lithospheric volatiles recorded in shallow young groundwater. Nature Geoscience: 1–6.

Veizer, J. 1989. Strontium isotopes in seawater through time. Annual Review of Earth and Planetary Sciences, Vol. 17, p. 141 **17**: 141.

Vengosh, A. 2003. 9.09-Salinization and Saline Environments In: Editors-in-Chief: Heinrich D. Holland, Karl K. Turekian (Eds.), Treatise on Geochemistry. Pergamon, Oxford.

Vengosh, A., Gill, J., Lee Davisson, M., et Bryant Hudson, G. 2002. A multi-isotope (B, Sr, O, H, and C) and age dating (3H–3He and 14C) study of groundwater from Salinas Valley, California: Hydrochemistry, dynamics, and contamination processes. Water Resources Research **38**(1): 9–1–9–17.

Vengosh, A., Starinsky, A., Kolodny, Y., Chivas, A.R., et Raab, M. 1992. Boron isotope variations during fractional evaporation of sea water: New constraints on the marine vs. nonmarine debate. Geology **20**(9): 799–802.

Vosteen, H.-D., et Schellschmidt, R. 2003. Influence of temperature on thermal conductivity, thermal capacity and thermal diffusivity for different types of rock. Physics and Chemistry of the Earth, Parts a/b/c **28**(9-11): 499–509.

Vovk, I. 1981. Radiolytic model of formation of composition of brines in crystalline basement of the shields. Geokhimiya(4): 467–480.

Walter, J. 2010. Les eaux souterraines à salinité élevée autour du lac Saint-Jean, Québec: origines et incidences. Mémoire de maîtrise, Sciences de la Terre et de l'Atmosphèree, Université du Québec à Chicoutimi, Québec, Canada.

Walter, J., Chesnaux, R., Boumaiza, L., Brindha, K., et Regenspurg, S. 2023. Conceptual model for the chemical evolution of groundwater in a region of the Canadian Precambrian shield covered by soft Quaternary deposit of glacial and marine origin. Applied Geochemistry **150**: 105574.

Walter, J., Chesnaux, R., Cloutier, V., et Gaboury, D. 2017. The influence of water/rock− water/clay interactions and mixing in the salinization processes of groundwater. Journal of Hydrology: Regional Studies **13**: 168–188.

Walter, J., Chesnaux, R., Gaboury, D., et Cloutier, V. 2019. Subsampling of regional-scale database for improving multivariate analysis interpretation of groundwater chemical evolution and ion sources. Geosciences **9**(3): 139.

Walter, J., Rouleau, A., Chesnaux, R., Lambert, M., et Daigneault, R. 2018. Characterization of general and singular features of major aquifer systems in the Saguenay-Lac-Saint-Jean region. Canadian Water Resources Journal/Revue Canadienne des Ressources Hydriques **43**(2): 75–91.

Walter, J., Rouleau, A., Clark, I.D., et Guha, J. 2006. A first investigation of groundwater geochemistry in the crystalline bedrock around lake Saint-Jean, Québec. 59th Canadian Geotechnical Conference and 7th Joint CGS/IAH-CNC Groundwater Specialty Conference - Sea to Sky Geotechnique 2006, Fairmont Hotel, Vancouver, British Columbia, Canada, October 1–4, 2006, X-CD Technologies Incorporated, pp. 1553–1560.

Wark, D.A., et Watson, E.B. 2006. TitaniQ: a titanium-in-quartz geothermometer. Contributions to Mineralogy and Petrology **152**(6): 743–754.

Warner, N.R., Jackson, R.B., Darrah, T.H., Osborn, S.G., Down, A., Zhao, K., White, A., et Vengosh, A. 2012. Geochemical evidence for possible natural migration of Marcellus Formation brine to shallow aquifers in Pennsylvania. Proceedings of the National Academy of Sciences **109**(30): 11961–11966.

Warr, O., B, S.L., Fellowes, J., Sutcliffe, C.N., McDermott, J.M., Holland, G., Mabry, J.C., et Ballentine, C.J. 2018. Tracing ancient hydrogeological fracture network age and compartmentalisation using noble gases. Geochimica et Cosmochimica Acta **222**: 340–362.

Warr, O., Ballentine, C., Onstott, T., Nisson, D., Kieft, T., Hillegonds, D., et Sherwood Lollar, B. 2022. 86Kr excess and other noble gases identify a billion-year-old radiogenically-enriched groundwater system. Nature Communications **13**(1): 3768.

Warr, O., Giunta, T., Onstott, T.C., Kieft, T.L., Harris, R.L., Nisson, D.M., et B, S.L. 2021. The role of low-temperature 18O exchange in the isotopic evolution of deep subsurface fluids. Chemical Geology **561**: 120027.

Wavrant, L.-M., Sappin, A.-A., Beland, C.M.J., Chartier-Montreuil, W., Fleury, F., Zhao, P., Beaudoin, G., Barnes, S.-J., Cheng, L., Chouteau, M., Constantin, M., Dare, S., Dupuis, C., Stevenson, R., et Williams-Jones. 2017. Projet terres rares au Québec. Ministère de l'Énergie et des Ressources Naturelles, Québec. No. MB 2017-17. p. 123.

Welch, L., et Allen, D. 2014. Hydraulic conductivity characteristics in mountains and implications for conceptualizing bedrock groundwater flow. Hydrogeology Journal **22**(5): 1003.

White, A.F., Bullen, T.D., Schulz, M.S., Blum, A.E., Huntington, T.G., et Peters, N.E. 2001. Differential rates of feldspar weathering in granitic regoliths. Geochimica et Cosmochimica Acta **65**(6): 847–869.

Williams, L.B., Elliott, W.C., et Hervig, R.L. 2015. Tracing hydrocarbons in gas shale using lithium and boron isotopes: Denver Basin USA, Wattenberg Gas Field. Chemical Geology **417**: 404–413.

Xiao, J., Xiao, Y.k., Jin, Z.d., He, M.y., et Liu, C.q. 2013. Boron isotope variations and its geochemical application in nature. Australian Journal of Earth Sciences **60**(4): 431–447.

Xie, Y., Liu, G., Chen, Y., Yang, M., Xia, C., et Huang, X. 2022a. The effects of temperature, pressure and concentration on the hydraulic conductivity of deep groundwater-bearing layers. Hydrogeology Journal **30**(4): 1295–1313.

Xie, Y., Love, A.J., Simmons, C.T., Costar, A., et Wu, J. 2022b. Groundwater age persistence in topography-driven groundwater flow over paleohydrogeologic time scales. Geology **50**(6): 731–735.

Yan, K., Wang, C., Chen, R., Liu, C., Wang, J., Yu, X., Shen, L., Li, R., Zhou, Y., et Zhou, Q. 2023. Origin and evolution of deep lithium-rich brines in the southwest Jianghan Basin, central China: Evidence from hydrochemistry and stable isotopes. Journal of Hydrology **626**: 130163.

Yang, N., Su, C., Liu, W., et Zhao, L. 2022. Occurrences and mechanisms of strontium-rich groundwater in Xinglong County, northern China: insight from hydrogeological and hydrogeochemical evidence. Hydrogeology Journal **30**(7): 2043–2057.

Yardley, B.W. 2013. The chemical composition of metasomatic fluids in the crust. *Dans* Metasomatism and the chemical transformation of rock. Springer. pp. 17–51.

Yardley, B.W., et Bodnar, R.J. 2014. Fluids in the continental crust. Geochemical Perspectives **3**(1): 1–2.

Yeomans, K.A., et Golder, P.A. 1982. The Guttman-Kaiser criterion as a predictor of the number of common factors. The Statistician: 221–229.

Yu, X., Liu, C., Wang, C., Wang, J., Li, Q., et Meng, L. 2022. Origin of Li brine-type deposits in the Cretaceous gypsum-bearing formation of the Jitai Basin, South China: Constraints from geochemistry and H, O, Li, B, and Sr isotopes. Applied Geochemistry **139**: 105257.

Yu, X., Wang, C., Huang, H., et Yan, K. 2024. Origin of lithium in oilfield brines in continental petroliferous basin: Insights from Li and Sr isotopes in the Jianghan Basin, central China. Marine and Petroleum Geology **160**: 106576.

Zhang, X., Jiao, J.J., et Guo, W. 2022. How Does Topography Control Topography-Driven Groundwater Flow? Geophysical Research Letters **49**(20): e2022GL101005.

Zuddas, P. 2010. Water–rock interaction processes seen through thermodynamics. Elements **6**(5): 305–308.

Chapitre 8 : ANNEXES

ANNEXE I : Modèle numérique conventionnel d'écoulement et d'âge de l'eau souterraine

Context

The top surface watertable boundary condition plays a critical role in numerical simulations of groundwater flow. In the presented model, the watertable was assigned as a Dirichlet (Type-1) boundary based on interpolated heads from the regional piezometry within the fractured rock aquifer. For simplicity, shallow alluvial deposits were not included. Computed recharge across the watertable was checked for realism and compared well with other estimates. The numerical modelling developed in this study aims to investigate whether a gravity flow model alone could explain deep Precambrian Shield brine upwelling, and, to assess the role of the graben faults as preferential pathways for deep groundwater to migrate toward the surface using a parametric study (see the main manuscript for details). Our non-conventional approach by applying a fixed watertable, allows us to observe directly the intrinsic effects of the graben faults on groundwater flow with realistic results. Here, in ANNEXE I, a comparison is provided using a more conventional approach of applying recharge across the watertable while fixing heads only at specific surface water control points. In this approach, the upper part of the mesh is also allowed to deform to the watertable shape.

Conventional regional groundwater flow model

The conventional model presented here applies fixed watertable elevations at specific surface water control points at streams, rivers and lakes, with imposed recharge elsewhere, and includes surficial deposits and limestone. At the model surface, applied recharge varied from 3 to 50 mm/yr where the watertable lay within the fractured rock. The calibration curve is presented in Figure 8-1. The minimum and maximum differences between observed and simulated heads were 6.91 m and 28.4 m, respectively, with a root mean square error (RMSE) of 5.05 m. Thus, in relation to the overall head difference across the model domain (280 m), the 2 % error remains well below the accepted error of 5% (30 m in this case), as defined by Anderson et al. (2015). As a comparison, the present modelling approach and the simplified case (presented in the main manuscript) showed similar results on the regional scale (Figure 8-2).

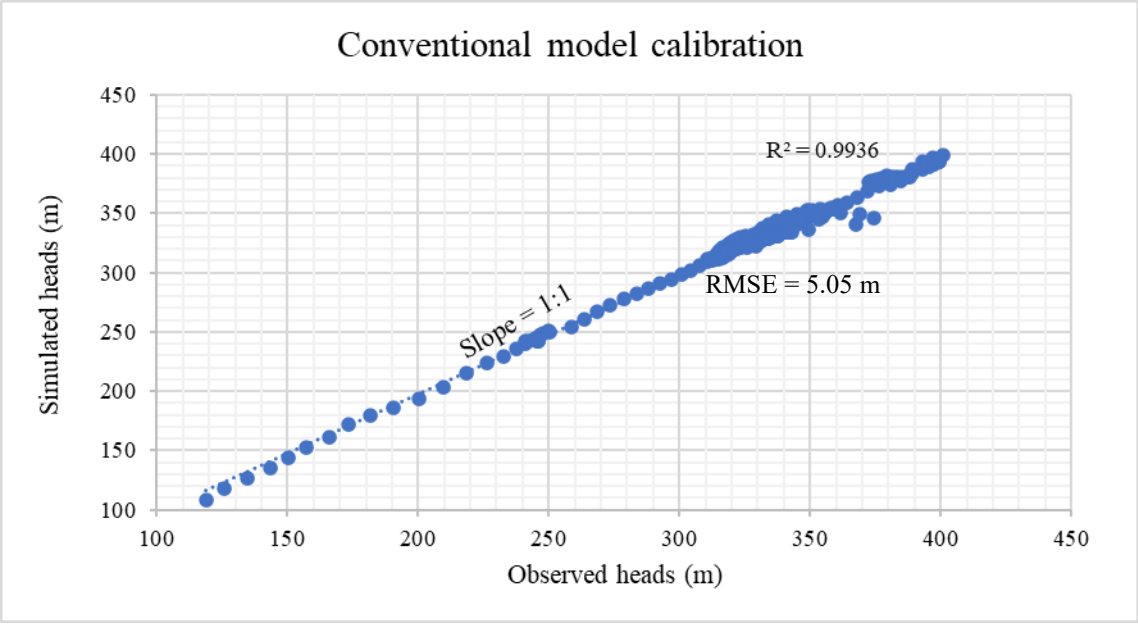

Figure 8-1: Model calibration. Observed heads against simulated heads.

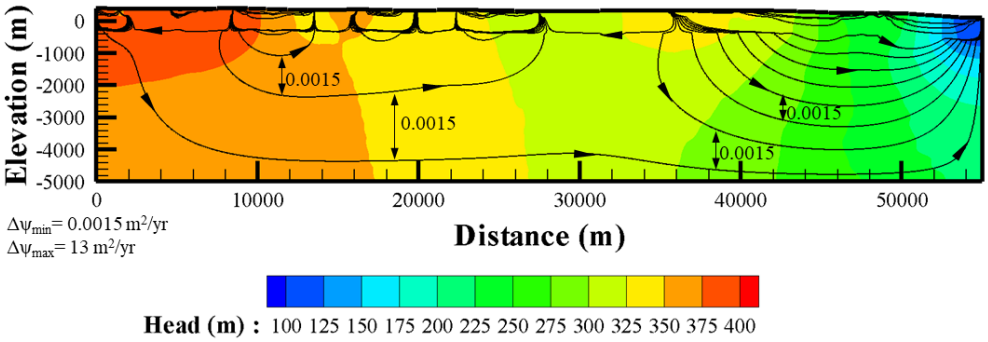

Figure 8-2: Calibrated steady-state flow model showing hydraulic heads and streamline distribution. Numerical labels identify specific stream function intervals in m^2/yr.

ANNEXE II : Base de données complète des échantillons des saumures continentales tirées de la littérature – Fichier Excel

ANNEXE III : Lithologie des socles cristallins et des bassins sédimentaires – Fichier Excel

ANNEXE IV : Groupes des échantillons générés par l'analyse hiérarchique en grappe – Fichier Excel

ANNEXE V : Graphiques des indices de saturation et résultats des tests statistiques

Results of saturation indexes

Figure 8-3 (a and b) shows the saturation states of sedimentary brines with respect to sylvite and carnallite. The plot shows that sylvite and carnallite contribute to the salinization processes of sedbrine. Dissolution of sylvite and carnallite contributes to K^+ dissolve content in sedbrine.

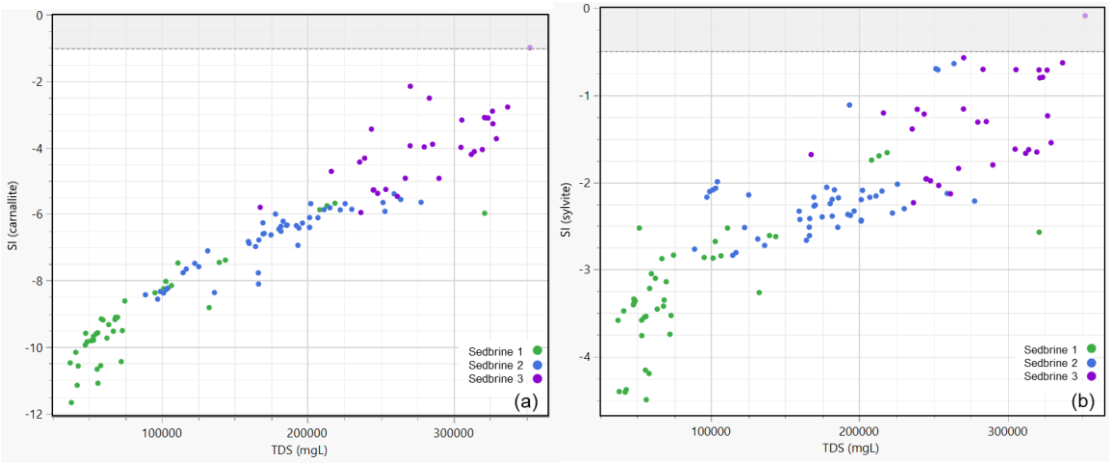

Figure 8-3: Saturation state of sedimentary brine with respect to (a) carnallite, and (b) sylvite. The dashed area corresponds to the equilibrium state and the analytical errors. The overall uncertainty is ± 0.5 units.

Figure 8-4 shows log-log plot of SO_4^{2-} vs Ca^{2+} concentrations. The plot shows increase of Ca^{2+} and decrease of SO_4^{2-} sedbrine clusters content.

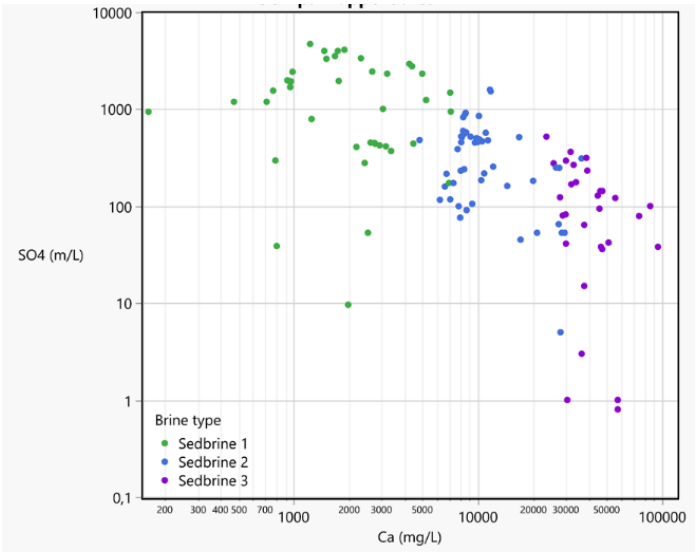

Figure 8-4 : log-log plot of SO_4^{2-} vs Ca^{2+} concentrations (in mg/L).

Statistical test results

Correlation matrix

The correlation matrix of each dataset from which principal components were extracted is presented in Tableau 8-1.

Tableau 8-1: Correlation matrix for all dataset

	Na^+							
Mg^{2+}	0.44	**Mg^{2+}**						
K^+	0.64	0.41	**K^+**					
Ca^{2+}	-0.03	0.01	0.11	**Ca^{2+}**				
Cl^-	0.59	0.28	0.53	0.68	**Cl^-**			
Sr^{2+}	0.21	0.20	0.33	0.88	0.73	**Sr^{2+}**		
SO_4^{2-}	0.17	-0.07	0.07	-0.44	-0.19	-0.40	**SO_4^{2-}**	
Br^-	0.16	0.29	0.24	0.86	0.75	0.89	-0.34	**Br^-**

Loading matrix

Tableau 8-2 presents chemical element coefficients in loading matrix for Components 1 and 2 as obtained by Principal Component Analysis (PCA). The results show that Component 1 separates chemical elements in two parts in loadings matrix: positive coefficients (Na^+, K^+, Mg^{2+}, Ca^{2+}, Sr^{2+}, Br^-, Cl^-) and negative coefficient SO_4^{2-}. While Component 2 separates chemical elements in two parts in loadings matrix: positive coefficients (Na^+, K^+, Mg^{2+}, SO_4^{2-}) and negative coefficients (Ca^{2+}, Sr^{2+}, Br^-).

Tableau 8-2: Loading matrix for Components 1 and 2 as obtained by PCA

Chemical elements	Component 1	Component 2
Na^+	0.44	0.79
Mg^{2+}	0.39	0.52
K^+	0.51	0.66
Ca^{2+}	0.83	-0.49
Cl^-	0.90	0.18
Sr^{2+}	0.92	-0.24
SO_4^{2-}	-0.39	0.51
Br^-	0.91	-0.24

Tableau 8-3 shows statistical summary of several ratios of shieldbrine clusters. These ratios were used in the study to discuss salinization processes of shieldbrine clusters.

Tableau 8-3: Statistical summary of shieldbrine clusters ratios

Analysis columns	Cluster 1			Cluster 4		
	N	Med	%. err. std	N	Med	%. err. std
Ca/Sr	44	50.30	12.00	37	46.80	3.04
Br/Cl	44	0.01	3.86	37	0.01	5.16
K/Cl	44	0.001	10.80	37	0.002	9.67
Na/Cl	44	0.20	5.90	37	0.20	5.00
Sr/Cl	44	0.01	7.30	37	0.01	3.65
B/Br	16	0.003	13.80	11	0.002	9.44
Li/Br	20	0.001	30.80	20	0.0008	17.60
Na/Ca	44	0.50	10.80	37	0.40	6.21

ANNEXE VI : Résultats des indices de saturation calculées à partir des résultats de l'analyse hiérarchique en grappe – Fichier Excel

ANNEXE VII Données géochimiques des échantillons des eaux saumâtres collectées dans le roc fracturé de la région du Saguenay-Lac-Saint-Jean

Context:
This document compiles all geochemical data from the study covering the period from 2021 to 2023.

Tableau 8-4: Results of major, minor and trace elements for all samples

Parameter	Samples						
	S1	S2	S3	S4	S5	S6	S7
Water type	Ca-Na-Cl	Ca-Cl	Ca-Na-Cl	Na-Cl	Na-Cl	Ca-Cl	Ca-Na-Cl
T (°C)	7.5	14.4	7.7	7.8	8.8	8.5	10.75
Eh (mV)	260	288	318	305	321	307	293
pH	7.83	7.36	6.6	9.59	7.35	7.67	7.71
TSD (g/L)	2.67	16.35	1.65	5.51	9.90	3.99	3.21
B (mg/L)	0.55	1.1	0.76	0.68	0.46	0.1	0.55
Ba (mg/L)	0.10	14.7	0.05	0.002	0.10	0.06	0.58
HCO_3 (mg/L)	71.37	40.50	13.42	192.76	28.18	62.95	89.91
Br (mg/L)	17.9	138	12.3	14.7	34.4	18.2	16.3
Ca (g/L)	0.45	3.81	0.27	0.01	0.68	0.72	0.54
Cl (g/L)	1.52	10.3	1.01	3	6.52	2.26	1.86
Li (µg/L)	30.1	100	26.5	38.8	163	16.9	13.6
Mg (mg/L)	60.1	378	34.7	143	190	75.5	47.8
K (mg/L)	7.47	9.97	4.3	61.9	14.4	6.2	3.79
Rb (µg/L)	12.6	20.2	4.09	12.6	19.2	7.7	6.05
Si (mg/L)	5.35	5	0.82	0.5	3.7	4.89	7.1
Na (g/L)	0.47	1.81	0.32	1.92	1.98	0.71	0.62
Sr (mg/L)	13.6	127	7.19	0.075	36.4	42.7	21.2
SO_4 (mg/L)	94.2	6	1.5	189	490	151	40.7

*S1, S2, S3, S5, S6, S7, S8, S9, S10, S13 – collected in LSJAS,
S4, S11, S12, S14 – collected in Ordovician limestones.

Tableau 8-4 (suite)

Parameters	Samples						
	S8	S9	S10	S11	S12	S13	S14
Water type	Na-Cl	Na-Cl	Ca-Na-Cl	Na-Cl	Na-Cl	Na-Cl	Ca-Cl
T (°C)	9.5	10.3	7.3	10.1	10.7	7.5	7.9
Eh (mV)	280	292	293	289	305	274	130
pH	8.39	7.93	7.12	7.99	7.75	8.3	6.77
TSD (g/L)	0.99	1.41	11.63	3.58	1.73	1.24	29.63

B (mg/L)	0.44	0.1	1	4.34	3.19	0.45	1.23
Ba (mg/L)	0.02	0.26	0.05	0.06	1.12	4.77	1
HCO_3 (mg/L)	219.6	323.3	14.52	463.6	456.28	137.86	35.62
Br (mg/L)	4.61	0.5	51.3	28.1	10.6	7.48	297
Ca (g/L)	0.06	0.15	1.92	0.006	0.11	0.12	8.35
Cl (g/L)	0.39	0.56	6.66	1.75	0.7	0.66	18.8
Li (µg/L)	37.4	10	100	751	440	30.6	468
Mg (mg/L)	14.6	13.9	176	3.87	75.1	23.6	374
K (mg/L)	3.44	6.9	8.98	24.5	34.4	3.53	40.6
Rb (µg/L)	2.36	5.26	20	16.9	24.7	3.57	47.4
Si (mg/L)	5.82	5.53	6.78	3.62	3.7	5.8	5
Na (g/L)	0.26	0.33	2.35	1.33	0.35	0.29	1.85
Sr (mg/L)	2.4	0.61	72.7	0.7	12.2	5.29	224
SO_4 (mg/L)	40	24.2	502	3	1.5	9.71	182

Tableau 8-5: Results of chemical elements presented as ratios of element for all samples

Samples	Ca/Sr	Ca/Mg	Cl/Br	B/Br × 10^3	B/Cl × 10^3	Rb/Sr × 10^3	Li/Br × 10^3
S1	33.09	7.49	84.92	30.73	0.36	0.93	1.68
S2	30.00	10.08	74.64	7.97	0.11	0.16	0.72
S3	37.41	7.75	82.11	61.95	0.75	0.57	2.15
S4	70.68	0.04	204.08	45.99	0.23	168.67	2.64
S5	18.57	3.56	189.53	13.49	0.07	0.53	4.74
S6	16.81	9.51	124.18	5.49	0.04	0.18	0.93
S7	25.61	11.36	114.11	33.99	0.30	0.29	0.83
S8	26.88	4.42	84.16	95.44	1.13	0.98	8.11
S9	250	10.94	1126.00	200.00	0.18	8.65	20
S10	26.41	10.91	129.82	19.49	0.15	0.28	1.95
S11	9.12	1.66	62.28	154.45	2.48	24.01	26.73
S12	9.18	1.49	66.23	300.94	4.54	2.02	41.51
S13	22.68	5.08	88.77	60.70	0.68	0.67	4.09
S14	37.28	22.33	63.30	4.14	0.07	0.21	1.58

*S1, S2, S3, S5, S6, S7, S8, S9, S10, S13 – collected in LSJAS,
S4, S11, S12, S14 – collected in Ordovician limestones.

Tableau 8-6: Isotopic results of all samples.

Samples	$^{87}Sr/^{86}Sr$	2ε	δ^7Li (‰)	Stdv	$\delta^{11}B$ (‰)	Stdv	$\delta^{37}Cl$ (‰)	Stdv	$\delta^{81}Br$ (‰)	Repeat
S1	0.70827	0.000015	29.82	0.73	26.86	0.55	-0.1	0.15	1.35	0.09
S2	0.70709	0.000016	27.6	1.07	27.73	0.64	-0.09	0.15	1.16	0.05
S3	0.70801	0.000015	30.65	0.79	26.3	0.6	-0.16	0.1	1.16	0.14
S4	0.71126	0.000011	31.38	0.78	37.49	0.66	-0.05	0.17	0.8	0.09
S5	0.70712	0.000015	34.99	0.85	35.65	0.77	-0.35	0.12	0.59	0.11
S6	0.70775	0.000015	35.57	0.77	24.48	0.63	-0.35	0.16	1.36	0.1

S7	0.70779	0.000011	47.74	0.64	36.34	0.57	0.27	0.13	1.41	0.1
S8	0.7074	0.000015	47.9	0.88	28	0.62	0.04	0.17	1.55	0.12
S9	0.71015	0.000015	23.51	0.85	1.96	0.87	-0.2	0.11	n.d.	n.d.
S10	0.70759	0.000015	31.14	0.88	28.68	0.63	-0.13	0.12	0.84	0.1
S11	0.70863	0.000015	25.4	0.93	41.37	0.57	-0.42	0.18	1.6	0.17
S12	0.70864	0.000015	31.25	0.91	42.03	0.65	0.41	0.15	1.8	0.1
S13	0.70809	0.000011	31.69	0.74	37.04	0.63	0.36	0.17	1.44	0.07
S14	0.70939	0.000015	30.54	0.94	40.9	0.61	-0.42	0.1	1.17	0.03

S1, S2, S3, S5, S6, S7, S8, S9, S10, S13 – collected in LSJAS,
S4, S11, S12, S14 – collected in Ordovician limestones.
n.d. – not determined.

Tableau 8-6 (suite)

Samples	$^{14}C^*$ (pmC)	1σ error	$^{14}C^*$ Age (BP)	1σ error	$\delta^{13}C$ (‰)	Repeat	HCO_3 (mg/L)
S1	n.d.	n.d.	n.d.	n.d.	-11.57	-11.54	71.37
S2	**21.22**	**0.13**	**12,453**	**49**	-16.23	n.d.	**40.5**
S3	n.d.	n.d.	n.d.	n.d.	-11.23	-10.95	13.42
S4	**30.22**	**0.12**	**9,613**	**32**	-12.87	n.d.	**192.76**
S5	**70.64**	**0.22**	**2,792**	**25**	-13.11	n.d.	**28.18**
S6	n.d.	n.d.	n.d.	n.d.	-17.36	-17.43	62.95
S7	n.d.	n.d.	n.d.	n.d.	-20.2	n.d.	89.91
S8	n.d.	n.d.	n.d.	n.d.	-15.47	n.d.	219.6
S9	n.d.	n.d.	n.d.	n.d.	-16.93	n.d.	323.3
S10	**35.92**	**0.24**	**8,225**	**54**	-16.26	n.d.	**14.52**
S11	n.d.	n.d.	n.d.	n.d.	12.71	12.61	463.6
S12	n.d.	n.d.	n.d.	n.d.	9.11	n.d.	456.28
S13	n.d.	n.d.	n.d.	n.d.	-13.87	n.d.	137.86
S14	**4.18**	**0.046**	**25,504**	**96**	-9.6	n.d.	**35.62**

* Renormalized to -25 ‰ using provided $\delta^{13}C$ values.

Tableau 8-7: Results of noble gases of brackish groundwater samples

Samples	**^{4}He**	**±**	**R/R_a**	**±**	**$^4He/^{20}Ne$**	**±**	**$^{20}Ne/^{22}Ne$**	**±**	**$^{21}Ne/^{22}Ne$**	**±**
S2	7.5E-05	1.5E-06	0.341	0.013	379.2	22.8	10.72	0.03	0.0305	0
S4	1E-05	2.1E-07	0.115	0.006	9.14	0.55	11.12	0.01	0.0309	0
S5	2.3E-05	4.6E-07	0.642	0.014	0.84	0.05	11.11	0.01	0.0308	0
S8	0.00133	2.7E-05	0.188	0.006	2716	163	10.55	0.01	0.0301	0.0001
S9	1.1E-07	2.2E-09	0.981	0.063	0.66	0.04	9.8	0.02	0.029	0
S10	8.2E-06	1.7E-07	0.473	0.013	1.37	0.08	10.06	0.01	0.0293	0.0001
S11-a	7.2E-07	1.4E-08	0.12	0.006	8.28	0.5	9.82	0.01	0.0285	0.0002
S11-b	n.d.	n.d.	n.d.	n.d.	n.d.	n.d.	9.6	0.02	0.0282	0
S12	6.8E-07	1.4E-08	0.142	0.005	4.62	0.28	10.01	0.02	0.0292	0
S13	0.00271	5.4E-05	0.31	0.01	6261	376	9.96	0	0.0293	0
S14-a	0.17	0.0034	0.136	0.004	767935	46076	9.76	0	0.03	0.0001
S14-b	0.0107	0.00022	0.161	0.011	23449	1407	9.95	0.02	0.0298	0.0005

* all noble gases in cm^3STP/g_{H2O}.
R/R_a - where R = $^3He/^4He$ normalized to atmospheric air ratio (R_a=1.384E-06).
n.d. – not determined

Tableau 8-7 (suite)

Samples	$^{40}Ar/^{36}Ar$	±	$^{38}Ar/^{36}Ar$	±
S2	297	0.5	0.1823	0.001
S4	279.2	0.6	0.184	0.0012
S5	n.d.	n.d.	n.d.	n.d.
S8	280.9	0.5	0.185	0.0009
S9	288.7	0.7	0.1839	0.0015
S10	261.5	2.7	0.18	0.0048
S11-a	n.d.	n.d.	n.d.	n.d.
S11-b	297	0.5	0.1823	0.001
S12	276.8	0.9	0.1797	0.0015
S13	297.8	0.6	0.1852	0.0008
S14-a	355.6	0.7	0.1893	0.0011
S14-b	341.7	0.8	0.1907	0.0011

ANNEXE VIII : Données hydrogéochimiques des eaux souterraines profondes d'Abitibi.

References	Sample_id	TSD (mg/L)	Rb/Sr
Richard et al., 2024	DANIEL 25	160.54	0.0018
Richard et al., 2024	DANIEL 25	145.36	0.0042
Richard et al., 2024	DANIEL 25	68.83	0.0106
Richard et al., 2024	DANIEL 25	6 820.93	0.0006
Richard et al., 2024	DANIEL 25	1 490.52	0.0004
Richard et al., 2024	DANIEL 25	2 356.71	0.0004
Richard et al., 2024	DANIEL 25	2 264.11	0.0005
Richard et al., 2024	DANIEL 25	4 572.56	0.0004
Richard et al., 2024	DANIEL 25	4 419.34	0.0003
Richard et al., 2024	DANIEL 25	3 230.09	0.0003
Richard et al., 2024	DANIEL 25	3 089.58	0.0003
Richard et al., 2024	DANIEL 25	3 118.52	0.0006
Richard et al., 2024	DANIEL 25	2 281.50	0.0007
Richard et al., 2024	DANIEL 25	2 805.79	0.0005
Richard et al., 2024	DANIEL 25	178.74	0.0099
Richard et al., 2024	DANIEL 25	1 274.92	0.0004
Richard et al., 2024	DANIEL 25	842.98	0.0043
Richard et al., 2024	DANIEL 25	651.35	0.0053
Richard et al., 2024	DANIEL 25	630.16	0.0053
Richard et al., 2024	DANIEL 25	732.92	0.0019
Richard et al., 2024	DANIEL 25	154.90	0.0026
Richard et al., 2024	DANIEL 25	2.00	0.0244
Richard et al., 2024	DANIEL 25	178.47	0.0019
Richard et al., 2024	DANIEL 25	2 370.06	0.0005
Richard et al., 2024	DANIEL 25	1 338.13	0.0008
Richard et al., 2024	DANIEL 25	3 055.87	0.0006
Richard et al., 2024	DANIEL 25	2 940.29	0.0007
Richard et al., 2024	DANIEL 25	196.10	0.0030
Richard et al., 2024	DANIEL 25	640.03	0.0009
Richard et al., 2024	DANIEL 25	885.14	0.0016
Richard et al., 2024	DANIEL 25	1 448.85	0.0010
Richard et al., 2024	DANIEL 25	935.46	0.0006
Richard et al., 2024	DANIEL 25	262.99	0.0019
Richard et al., 2024	DANIEL 25	5 855.88	0.0003
Richard et al., 2024	DANIEL 25	295.59	0.0010
Richard et al., 2024	DANIEL 25	3 041.27	0.0001
Richard et al., 2024	DANIEL 25	4 022.80	0.0001
Richard et al., 2024	DANIEL 25	3 043.87	0.0001
Richard et al., 2024	DANIEL 25	378.13	0.0029
Richard et al., 2024	DANIEL 25	166.14	0.0029
Richard et al., 2024	DANIEL 25	593.60	0.0013

Richard et al., 2024	DANIEL 25	2 123.93	0.0019
Richard et al., 2024	DANIEL 25	14 630.77	0.0004
Richard et al., 2024	DANIEL 25	169.04	0.0048
Richard et al., 2024	DANIEL 25	177.08	0.0110
Richard et al., 2024	DANIEL 25	191.96	0.0097
Richard et al., 2024	DANIEL 25	20 199.28	0.0002
Richard et al., 2024	DANIEL 25	238.15	0.0069
Richard et al., 2024	DANIEL 25	1 384.84	0.0015
Richard et al., 2024	DANIEL 25	257.67	0.0138
Richard et al., 2024	DANIEL 25	1 250.31	0.0009
Richard et al., 2024	DANIEL 25	2 124.91	0.0006
Richard et al., 2024	DANIEL 25	1 981.91	0.0004
Richard et al., 2024	DANIEL 25	1 244.67	0.0007
Richard et al., 2024	DANIEL 25	2 402.68	0.0007
Richard et al., 2024	DANIEL 25	3 014.14	0.0008
Richard et al., 2024	DANIEL 25	189.38	0.0074
Richard et al., 2024	DANIEL 25	482.09	0.0007
Richard et al., 2024	DANIEL 25	840.03	0.0003
Richard et al., 2024	DANIEL 25	2 126.70	0.0002
Richard et al., 2024	DANIEL 25	278.00	0.0011
Richard et al., 2024	DANIEL 25	696.54	0.0002
Richard et al., 2024	DANIEL 25	1 139.50	0.0001
Richard et al., 2024	DANIEL 25	1 428.04	0.0001
Richard et al., 2024	DANIEL 25	155.19	0.0018
Richard et al., 2024	DANIEL 25	158.76	0.0018
Richard et al., 2024	DANIEL 25	158.82	0.0017
Richard et al., 2024	DANIEL 25	443.90	0.0005
Richard et al., 2024	DANIEL 25	992.70	0.0029
Richard et al., 2024	DANIEL 25	190.46	0.0029
Richard et al., 2024	DANIEL 25	182.66	0.0019
Richard et al., 2024	DANIEL 25	164.96	0.0013
Richard et al., 2024	DANIEL 25	176.18	0.0014
Richard et al., 2024	DANIEL 25	175.02	0.0048
Richard et al., 2024	DANIEL 25	189.83	0.0027
Richard et al., 2024	WINDFALL	2 290.04	0.0004
Richard et al., 2024	WINDFALL	2 751.17	0.0005
Richard et al., 2024	WINDFALL	5 931.10	0.0004
Richard et al., 2024	WINDFALL	63.36	0.0021
Richard et al., 2024	WINDFALL	13 467.27	0.0001
Richard et al., 2024	WINDFALL	10 206.00	0.0002
Richard et al., 2024	WINDFALL	1 844.35	0.0004
Richard et al., 2024	WINDFALL	24 688.39	0.0002
Richard et al., 2024	WINDFALL	76.94	0.0007

Richard et al., 2024	WINDFALL	66.03	0.0011
Richard et al., 2024	WINDFALL	838.98	0.0015
Richard et al., 2024	WINDFALL	110 914.67	0.0001
Richard et al., 2024	WINDFALL	135 849.17	0.0001
Richard et al., 2024	WINDFALL	8 482.72	0.0003
Richard et al., 2024	WINDFALL	14 397.87	0.0003
Richard et al., 2024	WINDFALL	21 765.06	0.0003
Richard et al., 2024	WINDFALL	10 472.14	0.0002
Richard et al., 2024	WINDFALL	107.07	0.0061
Richard et al., 2024	WINDFALL	2 028.40	0.0003
Richard et al., 2024	WINDFALL	235.94	0.0013
Richard et al., 2024	WINDFALL	71.83	0.0006
Richard et al., 2024	WINDFALL	736.39	0.0000
Richard et al., 2024	WINDFALL	206.62	0.0006
Richard et al., 2024	WINDFALL	1 544.26	0.0012
Richard et al., 2024	WINDFALL	3 780.91	0.0004
Richard et al., 2024	WINDFALL	116.34	0.0007
Richard et al., 2024	WINDFALL	560.85	0.0008
Richard et al., 2024	WINDFALL	78.23	0.0055
Richard et al., 2024	WINDFALL	580.67	0.0014
Richard et al., 2024	WINDFALL	1 709.85	0.0006
Richard et al., 2024	WINDFALL	140.27	0.0051
Richard et al., 2024	WINDFALL	81.30	0.0099
Richard et al., 2024	WINDFALL	90.05	0.0005
Richard et al., 2024	WINDFALL	175.81	0.0011
Richard et al., 2024	WINDFALL	276.94	0.0014
Richard et al., 2024	WINDFALL	255.58	0.0013
Richard et al., 2024	PASCALIS	523.19	0.0011
Richard et al., 2024	PASCALIS	446.74	0.0036
Richard et al., 2024	PASCALIS	271.73	0.0039
Richard et al., 2024	PASCALIS	57.23	0.0030
Richard et al., 2024	PASCALIS	50.81	0.0053
Richard et al., 2024	PASCALIS	168.36	0.0041
Richard et al., 2024	PASCALIS	331.15	0.0040
Richard et al., 2024	PASCALIS	585.07	0.0029
Richard et al., 2024	PASCALIS	589.71	0.0029
Richard et al., 2024	PASCALIS	79.39	0.0040
Richard et al., 2024	PASCALIS	291.01	0.0024
Richard et al., 2024	PASCALIS	1 004.02	0.0004
Richard et al., 2024	PASCALIS	213.07	0.0030
Richard et al., 2024	PASCALIS	88.86	0.0181
Richard et al., 2024	PASCALIS	88.38	0.0197
Richard et al., 2024	PASCALIS	87.24	0.0162

Richard et al., 2024	PASCALIS	86.46	0.0045
Richard et al., 2024	PASCALIS	90.63	0.0036
Richard et al., 2024	PASCALIS	755.13	0.0005
Richard et al., 2024	WINDFALL	839.23	0.0008
Richard et al., 2024	WINDFALL	1 002.00	0.0005
Richard et al., 2024	WINDFALL	916.55	0.0005
Richard et al., 2024	WINDFALL	72.12	0.0213
Richard et al., 2024	WINDFALL	143.70	0.0003
Richard et al., 2024	WINDFALL	88.80	0.0026
Richard et al., 2024	WINDFALL	77.93	0.0080
Richard et al., 2024	WINDFALL	55.32	0.0031
Richard et al., 2024	WINDFALL	102.37	0.0075
Richard et al., 2024	WINDFALL	45.61	0.0095
Richard et al., 2024	TRIANGLE	245.49	0.0127
Richard et al., 2024	TRIANGLE	123.65	0.0057
Richard et al., 2024	TRIANGLE	983.54	0.0002
Richard et al., 2024	TRIANGLE	114.49	0.0053
Richard et al., 2024	TRIANGLE	704.59	0.0032
Richard et al., 2024	TRIANGLE	68.86	0.0103
Richard et al., 2024	TRIANGLE	69.67	0.0045
Richard et al., 2024	FENELON	15 537.43	0.0002
Richard et al., 2024	FENELON	18 828.91	0.0002
Richard et al., 2024	FENELON	19 135.87	0.0002
Richard et al., 2024	FENELON	1 481.30	0.0008
Richard et al., 2024	FENELON	1 426.70	0.0008
Richard et al., 2024	FENELON	107.75	0.0021
Richard et al., 2024	FENELON	105.91	0.0071
Richard et al., 2024	FENELON	132.41	0.0064
Richard et al., 2024	FENELON	112.63	0.0069
Richard et al., 2024	FENELON	5 070.85	0.0003
Richard et al., 2024	FENELON	10 846.23	0.0002
Richard et al., 2024	FENELON	314.86	0.0027
Richard et al., 2024	FENELON	286.65	0.0028
Richard et al., 2024	FENELON	1 040.95	0.0009
Richard et al., 2024	FENELON	354.09	0.0014
Richard et al., 2024	FENELON	116.40	0.0069
Richard et al., 2024	FENELON	265.57	0.0019
Richard et al., 2024	FENELON	130.43	0.0029
Richard et al., 2024	FENELON	404.69	0.0031
Richard et al., 2024	FENELON	140.25	0.0051
Richard et al., 2024	FENELON	344.69	0.0038
Richard et al., 2024	FENELON	134.65	0.0056
Richard et al., 2024	FENELON	664.52	0.0019

Richard et al., 2024	FENELON	2 684.81	0.0005
Richard et al., 2024	FENELON	51.35	0.0060
Richard et al., 2024	WINDFALL2021	127.48	0.0086
Richard et al., 2024	WINDFALL2021	144.28	0.0078
Richard et al., 2024	WINDFALL2021	44.95	0.0163
Richard et al., 2024	WINDFALL2021	54.52	0.0032
Richard et al., 2024	WINDFALL2021	1 026.26	0.0005
Richard et al., 2024	WINDFALL2021	2 231.04	0.0004
Richard et al., 2024	WINDFALL2021	24 219.09	0.0001
Richard et al., 2024	WINDFALL2021	#DIV/0!	0.0033
Richard et al., 2024	WINDFALL2021	61.45	0.0012
Richard et al., 2024	WINDFALL2021	72.14	0.0031
Richard et al., 2024	WINDFALL2021	77.25	0.0079
Richard et al., 2024	WINDFALL2021	36.62	0.0033
Richard et al., 2024	WINDFALL2021	133.70	0.0001
Richard et al., 2024	WINDFALL2021	12 513.04	0.0001
Richard et al., 2024	WINDFALL2021	12 262.98	0.0101
Richard et al., 2024	WINDFALL2021	1 850.75	0.0021
Richard et al., 2024	WINDFALL2021	3 273.44	0.0007
Richard et al., 2024	WINDFALL2021	8 080.07	0.0003
Richard et al., 2024	WINDFALL2021	3 057.13	0.0005
Richard et al., 2024	WINDFALL2021	841.46	0.0002
Richard et al., 2024	WINDFALL2021	37 773.28	0.0001
Richard et al., 2024	WINDFALL2021	19 760.16	0.0002
Richard et al., 2024	WINDFALL2021	40 724.05	0.0002
Richard et al., 2024	WINDFALL2021	42 764.48	0.0037
Richard et al., 2024	WINDFALL2021	89.11	0.0087
Pauwels et al., 1993	GPKI KS228	51.92	0.0523
Pauwels et al., 1993	4616	98 434.28	0.0886
Pauwels et al., 1993	Cronenbourg	95 132.23	0.0716
Pauwels et al., 1993	B2460	97 328.17	0.0020
Pauwels et al., 1993	B2535	97 710.20	0.0021
Pauwels et al., 1993	GB1	101 189.00	0.0059
Pauwels et al., 1993	Merckwiller/les hélions	102 294.09	0.0627

* Ratio in mg/L.

ANNEXE IX : GeoMontreal 2024

Communication orale présentées lors de la conférence de géotechnique et d'hydrogéologie – GeoMontreal 2024, Montréal, Canada, du 15 au 18 septembre 2024.

Résumé soumis :

APPLICATION DE L'ANALYSE HIÉRARCHIQUE EN GRAPPES ET DE L'ANALYSE EN COMPOSANTES PRINCIPALES POUR IDENTIFIER L'ÉVOLUTION DE LA COMPOSITION CHIMIQUE DES SAUMURES CRISTALLINES ET SÉDIMENTAIRES

Othniel G.D. Ngombe[1,3]*, Julien Walter[1,3], Romain Chesnaux[1,3], John Molson[2]
[1] Département des Sciences appliquées, Université du Québec à Chicoutimi, Saguenay, Québec, G7H 2B1, Canada
[2] Département de géologie et de génie géologique, Université Laval, Québec, Québec, G1V 0A6, Canada
[3] Centre d'études sur les ressources minérales, Groupe de recherche Risque Ressource Eau, Université du Québec à Chicoutimi, Saguenay, Québec, G7H 2B1, Canada

RÉSUMÉ

La présente étude identifie des tendances différentes dans les signatures géochimiques des saumures profondes provenant des socles cristallins et des bassins sédimentaires. Pour ce faire, un modèle hydrogéochimique conceptuel décrivant l'évolution des saumures cristallines et sédimentaires a été développé à l'aide des analyses en éléments majeurs, mineurs et isotopiques. L'approche statistique appliquée par l'utilisation combinée de l'Analyse Hiérarchique en Grappes et de l'Analyse en Composantes Principales a permis d'identifier les trajectoires d'évolution des eaux souterraines vers les saumures cristallines et sédimentaires. Cette approche statistique se base sur l'analyse de 308 échantillons de saumure tirés de la littérature et prend en compte huit éléments chimiques : le sodium, le magnésium, le potassium, le calcium, le strontium, le chlore, le sulfate et le brome. À partir de ces données, deux voies d'évolution de la salinité vers des saumures communes de type Ca-Cl sont dérivées : (1) l'évolution des saumures cristallines, qui tend de l'eau de recharge à la saumure par l'hydratation des silicates. Cette évolution est caractérisée par l'équation linéaire Ca = -1610 + 0.4*Cl; (2) l'évolution des saumures sédimentaires, qui tend de l'eau de recharge à la saumure par la dissolution et la précipitation de l'halite, est décrite par une autre équation linéaire, Cl/Br = 103 + Na/Br. L'étude discute également des différences dans les isotopes stables de l'eau et dans les concentrations de lithium et de bore qui reflètent directement les divers processus dépendant de la température qui contrôlent l'évolution des saumures sédimentaires et cristallines. Ce sont ces différences qui ont conduit à la mise au point d'un outil graphique discriminant basé sur les rapports B/Br et Li/Br. Cet outil graphique permet de distinguer les saumures cristallines, dont les rapports B/Br et Li/Br sont inférieurs à 0,01, des saumures sédimentaires, dont les rapports sont supérieurs à 0,01. Nos résultats améliorent notre compréhension de l'évolution des saumures de la croûte profonde par le biais de l'interaction saumure-roche.

ANNEXE X : GAG-MAC-IAH-CNC Ottawa 2025

Communication orale présentée lors du congrès GAC-MAC-IAH-CNC Ottawa 2025, du 11 au 14 mai 2025.

Résumé soumis :

A Numerical Modelling and Isotopic Analysis to Investigate Upwelling and Mixing of Deep, Old Groundwater with Shallow Water Within the Grenville Province of the Canadian Shield

GAC-MAC-IAH-CNC 2025
OTTAWA

Shallow brackish groundwater is a significant issue affecting water supplies in the Saguenay–Lac-Saint-Jean region of Quebec, Canada. Recently (2023), a highly saline groundwater sample in the region, with a total dissolved solids concentration of approximately 30 g/L, was identified in a 45 m deep well within fractured bedrock. To investigate the origin of this anomaly, isotope analyses alongside two-dimensional numerical simulations of groundwater flow and advective-dispersive age transport were conducted. Furthermore, the influence of the Saguenay Graben faults on the upward migration of deep brine was assessed. The results of the isotope analyses ($\delta^{18}O$ and $\delta^{2}H$ and $^{87}Sr/^{86}Sr$) suggest that brackish groundwater from the fractured bedrock in the region is a mix between meteoric water and deep Precambrian Shield brine, which has experienced intense water-rock interaction over geological timescales. Our numerical simulations explored the hydrodynamic conditions under which deep groundwater upwelling could occur and offer insights into deep groundwater time scales and age patterns in the study area. The numerical flow simulations suggest that, under the imposed boundary conditions, vertical hydraulic gradients can sustain the upward flow of deep groundwater. However, regional flow is less significant in comparison to local flow systems which dilute the upwelling brine. The simulated ages of deep groundwater on the order of hundreds of millions of years are consistent with some ages of deep Precambrian Shield brines identified elsewhere in the Canadian Shield. Parametric tests suggest that graben faults facilitate the upwelling of groundwater and act as preferential pathways for deep, ancient groundwater. This paper provides a detailed view of the mixing processes between deep, old groundwater and shallow, fresh groundwater in Saguenay-Lac-Saint-Jean region. Moreover, our study highlights the influence of topography and geological structures on groundwater flow regimes and chemical evolution.